

UNIVERSIDADE FEDERAL DO RIO GRANDE DO SUL
INSTITUTO DE INFORMÁTICA
PROGRAMA DE PÓS-GRADUAÇÃO EM MICROELETRÔNICA

LEONARDO BARLETTE DE MORAES

**Schmitt Trigger Dimensioning Under
Variability and Voltage Scaling for
Minimum Energy Operation**

Thesis presented in partial fulfillment
of the requirements for the degree of
Master of Microelectronics

Advisor: Prof. Dr. Ricardo Reis
Coadvisor: Profa. Dra. Cristina Meinhardt

Porto Alegre
June 2020

CIP — CATALOGING-IN-PUBLICATION

de Moraes, Leonardo Barlette

Schmitt Trigger Dimensioning Under Variability and Voltage Scaling for Minimum Energy Operation / Leonardo Barlette de Moraes. – Porto Alegre: PGMICRO da UFRGS, 2020.

161 f.: il.

Thesis (Master) – Universidade Federal do Rio Grande do Sul. Programa de Pós-Graduação em Microeletrônica, Porto Alegre, BR-RS, 2020. Advisor: Ricardo Reis; Coadvisor: Cristina Meinhardt.

1. Process Variability. 2. FinFET. 3. Energy. 4. Schmitt Trigger. 5. Full Adder. 6. Microelectronics. I. Reis, Ricardo. II. Meinhardt, Cristina. III. Título.

UNIVERSIDADE FEDERAL DO RIO GRANDE DO SUL

Reitor: Prof. Rui Vicente Oppermann

Vice-Reitora: Prof.^a Jane Fraga Tutikian

Pró-Reitor de Pós-Graduação: Prof. Celso Giannetti Loureiro Chaves

Diretora do Instituto de Informática: Prof.^a Carla Maria Dal Sasso Freitas

Coordenador do PGMICRO: Prof. Tiago Roberto Balen

Bibliotecária-chefe do Instituto de Informática: Beatriz Regina Bastos Haro

LIST OF ABBREVIATIONS AND ACRONYMS

IoT	Internet of Things
CMOS	Complementary Metal Oxide Semiconductor
ULP	Ultra Low Power
FinFET	Fin Field Effect Transistor
SCE	Short Channel Effect
RDF	Random Dopant Fluctuation
ST	Schmitt Trigger
FA	Full Adder
V_T	Threshold Voltage
NBTI	Negative Bias Temperature Instability
HCI	Hot Carrier Injection
CMP	Chemical-Mechanical Polishing
LER	Line-Edge Roughness
WF	Work Function
FET	Field Effect Transistor
MOSFET	Metal Oxide Semiconductor Field Effect Transistor
PVT	Process Voltage and Temperature
WID	Within-Die
SIMD	Single Instruction Multiple Data
PDP	Power Delay Product
TGA	Transmission Gate Adder
TFA	Transmission Function Adder
CPL	Complementary Pass Transistor Logic
CNFET	Carbon Nanotube Field Effect Transistor

FDSOI	Fully Depleted Silicon On Insulator
OTS	Optimal Transistor Sizing
L	Gate Length
W_{FIN}	Fin Width
H_{FIN}	Fin Height
T_{OX}	Oxide Thickness
SOI	Silicon On Insulator
WFF	Work Function Fluctuation
SRAM	Static Random Access Memory
GOBD	Gate Oxide Break Down
ECC	Error Correcting Code
SNM	Static Noise Margin
UDSM	Ultra-Deep Sub-Micron
VTC	Voltage Transfer Curve
DRC	Design Rule Checking
LVS	Layout Versus Schematic
EDA	Electronic Design Automation
PDK	Process Design Kit
ASAP	Arizona State Predictive PDK
FEOL	Front End Of Line
MOL	Middle End Of Line
BEOL	Back End Of Line
SDT	Source-Drain Trench
LIG	Local-Interconnect Gate
LISD	Local-Interconnect Source-Drain
V0	Via 0

M1 Metal 1
M2 Metal 2
MC Monte Carlo
EDP Energy Deviation Product
TIST Triple-Inverter ST
SIG Stacked-Inverter Gate

LIST OF FIGURES

Figure 2.1 Levels of abstraction from a ideal transistor concept towards a realistic and "atomistic" device concept. (a) Depicts a the current approach of semiconductor device simulation, with continuous dopant charge and smooth boundaries. (b) Depicts a 20-nm MOSFET, with less than 50 Si atoms along the channel. RDF, interface roughness and LER introduce considerable intrinsic parameter fluctuation. (c) Depicts a 4-nm MOSFET, with less than 10 Si atoms along the channel.	21
Figure 2.2 Above, structural comparison between (a) planar MOSFET and (b) FinFET transistors. Below, structural comparison between (a) bulk and (b) SOI FinFETs.....	25
Figure 2.3 Metal fabrication ideal and real aspects.....	26
Figure 2.4 Electrostatic potential in a generic 30-nm MOSFET with the surface potential shown below. The metal gate has two grains with the grain boundary diagonally across the channel.	26
 Figure 3.1 ST inverter leakage suppression (LOTZE; MANOLI, 2017).	32
Figure 3.2 Modified TIST schematic (RABAЕY; CHANDRAKASAN; NIKOLIC, 2002)	33
Figure 3.3 SIG schematic (BOSE; JOHNSTON, 2018)	34
Figure 3.4 LPST Inverter from Dokania and Islam (2015).....	34
 Figure 4.1 Design flow of the experiments.	37
Figure 4.2 TIST schematic, to the left, and smallest 2:1 and 3:1 designs, to the right..	38
Figure 4.3 Technology layers and 3-fins transistors 6T ST layout	39
Figure 4.4 1 to 5 fins (left to the right) traditional CMOS inverter layout comparison .	40
Figure 4.5 1 to 5 fins (left to the right) ST layout comparison.	41
Figure 4.6 1 to 5 fins (left to the right) SIG layout comparison.....	42
Figure 4.7 From the left to the right, 2, 4 and 6 maximum fins TIST layout comparison.	43
Figure 4.8 TAP-Cell Layout.....	44
Figure 4.9 Original and modified Low Power STs (LPST) side-by-side.....	45
Figure 4.10 Noise margins measurements.	46
Figure 4.11 Test-bench.....	47
Figure 4.12 Full Adders with internal inverters to be replaced highlighted. Transmission Gate Adder (a), Transmission Function Adder (b), Mirror CMOS Adder (c) and Hybrid Full Adder (d).	48
Figure 4.13 Test-bench for the Full Adders simulation.	49
 Figure 5.1 Frequency decrease over variability scaling for each design.....	53
Figure 5.2 Propagation times deviation for each design in relation to the WFF level considering all scenarios.	54
Figure 5.3 Energy increase for each WFF level step.	56
Figure 5.4 Energy measures in function of the supply voltage for each design.	57
Figure 5.5 Layout comparison for each scenario considering the energy metrics for the inverter.....	59
Figure 5.6 Layout comparison for each scenario considering the energy metrics for the ST.	60
Figure 5.7 Layout comparison for each scenario considering the energy metrics for the SIG.	60

Figure 5.8 Layout comparison for each scenario considering the energy metrics for the TIST at 2:1 proportion.	60
Figure 5.9 Layout comparison for each scenario considering the energy metrics for the TIST at 3:1 proportion.	61
Figure 5.10 Low energy layouts energy metrics comparison for each design.	62
Figure 5.11 High robustness layouts energy metrics comparison for each design.	62
Figure 5.12 CB layouts energy metrics comparison for each design.	63
Figure 5.13 Energy consumption and energy consumption deviations difference between the cost-benefit and low energy layouts.	64
Figure 5.14 Energy consumption and energy consumption deviations difference between the cost-benefit and high robustness layouts.	64
Figure 5.15 Dynamic (on) current average measures through supply voltage and WFF scaling.	66
Figure 5.16 Dynamic (on) current normalized standard deviations through supply voltage and WFF scaling.	66
Figure 5.17 Static (off) current average measures through supply voltage and WFF scaling.	67
Figure 5.18 Static (off) current normalized standard deviations through supply voltage and WFF scaling.	67
Figure 5.19 Average on and off-current increase over all designs through variability scaling. The scaling is normalized in relation to the 1% WFF level measures.	68
Figure 5.20 Current ratio (left) and current ratio deviation (right) design comparison across variability scaling.	68
Figure 5.21 Average on and off-current normalized deviation over all designs through variability scaling. The marked line is related to the on-current normalized deviations (left axis) while the bars are related to the off-current normalized deviation (right axis).	69
Figure 5.22 Output gain value across voltage scaling.	71
Figure 5.23 Voltage Transfer Curve slopes through supply voltage scaling for each design.	71
Figure 5.24 Voltage Transfer Curves for all designs at 0.1V.	72
Figure 5.25 Voltage Transfer Curves for all designs at 0.7V.	72
Figure 5.26 Design hysteresis ratio comparison (left) and hysteresis ratio normalized deviation (right), across variability scaling.	73
Figure 5.27 Hysteresis curves for all designs at nominal supply voltage.	74
Figure 5.28 Design hysteresis ratios comparison across supply voltage scaling.	74
Figure 5.29 Energy measures distribution for the inverter at different levels of variability and supply voltage.	76
 Figure 6.1 Average delay measures for nominal operation and their respective normalized deviation (variability sensitivity).	80
Figure 6.2 Average energy measures for nominal operation and their respective normalized deviation (variability sensitivity).	80
Figure 6.3 Average delay measures for near-threshold operation and their respective normalized deviation (variability sensitivity).	81
Figure 6.4 Average energy measures for near-threshold operation and their respective normalized deviation (variability sensitivity).	81
 Figure B.1 1 fin inverter layout. Height (H): 270nm, Width (W): 162nm, Area (A): 43,740nm ²	98
Figure B.2 2 fins inverter layout. H: 270nm, W: 162nm, A: 43,740nm ²	99

Figure B.3 3 fins inverter layout. H: 270nm, W: 162nm, A: 43,740nm ² .	100
Figure B.4 4 fins inverter layout. H: 324nm, W: 162nm, A: 52,488nm ² .	101
Figure B.5 5 fins inverter layout. H: 378nm, W: 162nm, A: 61,236nm ² .	102
Figure B.6 1 fin ST layout. H: 270nm, W: 378nm, A: 102,060nm ² .	103
Figure B.7 2 fins ST layout. H: 270nm, W: 378nm, A: 102,060nm ² .	104
Figure B.8 3 fins ST layout. H: 270nm, W: 378nm, A: 102,060nm ² .	105
Figure B.9 4 fins ST layout. H: 324nm, W: 378nm, A: 122,472nm ² .	106
Figure B.10 5 fins ST layout. H: 378nm, W: 378nm, A: 142,884nm ² .	107
Figure B.11 1 fin SIG layout. H: 270nm, W: 378nm, A: 102,060nm ² .	108
Figure B.12 2 fins SIG layout. H: 270nm, W: 378nm, A: 102,060nm ² .	109
Figure B.13 3 fins SIG layout. H: 270nm, W: 378nm, A: 102,060nm ² .	110
Figure B.14 4 fins SIG layout. H: 324nm, W: 378nm, A: 122,472nm ² .	111
Figure B.15 5 fins SIG layout. H: 378nm, W: 378nm, A: 142,884nm ² .	112
Figure B.16 2 fin max., proportion 2:1 TIST layout. H: 270nm, W: 270nm, A: 72,900nm ² .	113
Figure B.17 3 fin max., proportion 3:1 TIST layout. H: 270nm, W: 270nm, A: 72,900nm ² .	114
Figure B.18 4 fin max., proportion 2:1 TIST layout. H: 324nm, W: 270nm, A: 87,480nm ² .	115
Figure B.19 6 fin max., proportion 3:1 TIST layout. H: 432nm, W: 270nm, A: 116,640nm ² .	116
Figure B.20 6 fin max., proportion 2:1 TIST layout. H: 432nm, W: 270nm, A: 116,640nm ² .	117
Figure C.1 Traditional Mirror Full Adder layout. The image is rotated 90° anti-clockwise.	119
Figure C.2 Mirror Full Adder layout with internal inverters replaced by ST1. The image is rotated 90° anti-clockwise.	120
Figure C.3 Mirror Full Adder layout with internal inverters replaced by ST2. The image is rotated 90° anti-clockwise.	121
Figure C.4 Traditional Transmission Full Adder layout. The image is rotated 90° anti-clockwise.	122
Figure C.5 Transmission Full Adder layout with internal inverters replaced by ST1. The image is rotated 90° anti-clockwise.	123
Figure C.6 Transmission Full Adder layout with internal inverters replaced by ST2. The image is rotated 90° anti-clockwise.	124
Figure C.7 Traditional Transmission Gate Adder layout. The image is rotated 90° anti-clockwise.	125
Figure C.8 Transmission Gate Adder layout with internal inverters replaced by ST1. The image is rotated 90° anti-clockwise.	126
Figure C.9 Transmission Gate Adder layout with internal inverters replaced by ST2. The image is rotated 90° anti-clockwise.	127
Figure C.10 Traditional Hybrid Full Adder layout. The image is rotated 90° anti-clockwise.	128
Figure C.11 Hybrid Full Adder layout with internal inverters replaced by ST1. The image is rotated 90° anti-clockwise.	129
Figure C.12 Hybrid Full Adder layout with internal inverters replaced by ST2. The image is rotated 90° anti-clockwise.	130
Figure D.1 Inverter energy measures distribution operating at 0.2V.	132
Figure D.2 Inverter energy measures distribution operating at 0.4V.	133

Figure D.3 Inverter energy measures distribution operating at 0.7V.	134
Figure D.4 Inverter energy measures dispersion operating at 0.2V.	135
Figure D.5 Inverter energy measures dispersion operating at 0.4V.	136
Figure D.6 Inverter energy measures dispersion operating at 0.7V.	137
Figure D.7 ST energy measures distribution operating at 0.2V.	138
Figure D.8 ST energy measures distribution operating at 0.4V.	139
Figure D.9 ST energy measures distribution operating at 0.7V.	140
Figure D.10 ST energy measures dispersion operating at 0.2V.	141
Figure D.11 ST energy measures dispersion operating at 0.4V.	142
Figure D.12 ST energy measures dispersion operating at 0.7V.	143
Figure D.13 SIG energy measures distribution operating at 0.2V.	144
Figure D.14 SIG energy measures distribution operating at 0.4V.	145
Figure D.15 SIG energy measures distribution operating at 0.7V.	146
Figure D.16 SIG energy measures dispersion operating at 0.2V.	147
Figure D.17 SIG energy measures dispersion operating at 0.4V.	148
Figure D.18 SIG energy measures dispersion operating at 0.7V.	149
Figure D.19 TIST 2:1 energy measures distribution operating at 0.2V.	150
Figure D.20 TIST 2:1 energy measures distribution operating at 0.4V.	151
Figure D.21 TIST 2:1 energy measures distribution operating at 0.7V.	152
Figure D.22 TIST 2:1 energy measures dispersion operating at 0.2V.	153
Figure D.23 TIST 2:1 energy measures dispersion operating at 0.4V.	154
Figure D.24 TIST 2:1 energy measures dispersion operating at 0.7V.	155
Figure D.25 TIST 3:1 energy measures distribution operating at 0.2V.	156
Figure D.26 TIST 3:1 energy measures distribution operating at 0.4V.	157
Figure D.27 TIST 3:1 energy measures distribution operating at 0.7V.	158
Figure D.28 TIST 3:1 energy measures dispersion operating at 0.2V.	159
Figure D.29 TIST 3:1 energy measures dispersion operating at 0.4V.	160
Figure D.30 TIST 3:1 energy measures dispersion operating at 0.7V.	161

ABSTRACT

Technology scaling alongside the increasing process variability impact in modern technology nodes are the main reasons to control deviations over metrics in IC nanometer designs. Also, given the increasing set of devices working in battery-oriented environments, energy consumption should be minimal and the operation regime reliable. Schmitt Triggers are traditionally used for noise immunity enhancement, and have been recently applied to mitigate radiation effects and process variability impact. However, Schmitt Trigger operation at the nominal voltage introduces higher power consumption, in comparison to an inverter, making the application of Schmitt Trigger in ultra low power applications difficult. Thus, this work main contribution is to trace the relationship between transistor sizing, supply voltage, and process variability to get a low energy consumption circuit while still keeping low levels of deviations due to the impact of process-induced variability. The results are extracted from three different designs of inverters. All simulations are performed upon the extracted layouts design at 7-nm with the FinFET technology. Each layout presents a different number of fins, where each simulation presents a different level of variability and supply voltage. Amongst the several metrics considered - propagation times, energy, hysteresis interval, current ratios, voltage gains, and slopes - the energy is the prioritized metrics with an analysis considering different kinds of applications - low energy, low sensibility, and cost-benefit - being performed. Given so, it is shown that a cost-benefit analysis can highlight sets of sizing and supply voltage where it can provide a 37.51% decrease on energy consumption while only increasing its sensibility by 7.42%. Furthermore, it is presented that the dependence of supply voltage and sensibility to process variability is not directly related, with slight decreases in the supply voltages bringing better results. Considering the average measures, the inverter is still the fastest and most energy-efficient circuit, presenting the highest performance, lowest energy consumption, and smallest area. Although, when comparing noise immunity characteristics, the 6-Transistor Schmitt Trigger presents the highest noise margins and slopes, with higher current ratios, and gains. The TIST designs present the highest current ratios, gains, and hysteresis ratios. The improvements, although, do not come without respective increases in propagations times, energy consumption, and area.

Keywords: Process Variability. FinFET. Energy. Schmitt Trigger. Full Adder. Microelectronics.

Dimensionamento de inversores sob influência de variabilidade de processo e diminuição da tensão de alimentação para operação com consumo mínimo.

RESUMO

A miniaturização da tecnologia de transistores, juntamente com o crescente impacto da variabilidade de processo nos nodos tecnológicos modernos são a principal razão para o esforço da indústria em investir nos métodos para controle dos efeitos de variabilidade nas métricas dos circuitos integrados. Além disso, dado o crescimento exponencial do número de aplicações dependentes de bateria, o consumo de energia deve-se manter mínimo e o regime de operação estável. Circuitos *Schmitt Trigger* são tradicionalmente aplicados para melhora da resistência de circuitos integrados ao ruído e foram recentemente aplicados para mitigar os efeitos da radiação e do impacto da variabilidade. Contudo, a operação de *Schmitt Triggers* em tensão nominal introduz alto consumo de potência, tornando a adoção de *Schmitt Triggers* em cenários de ultra baixa potência, difícil. Assim, a principal contribuição deste trabalho é traçar a relação entre dimensionamento dos transistores, tensão de alimentação e variabilidade de processo, para alcançar o menor possível consumo de energia, mas mantendo a robustez aos efeitos de variabilidade em níveis aceitáveis. Os resultados são extraídos de três tipos de inversores, entre eles *Schmitt Triggers*. Todas as simulações são realizadas considerando os leiautes extraídos projetados em 7nm com a tecnologia de transistores FinFET. Cada leiaute apresenta um numero diferente de *fins*, onde cada simulação apresenta um nível diferente de variabilidade de processo e tensão de alimentação. Entre diversas métricas consideradas - tempos de propagação, energia, intervalo de histerese, razões entre as correntes dinâmica e estática, ganhos de tensão e inclinação dos sinais - as medidas de energia são priorizadas, com uma análise considerando diferentes tipos de aplicações - baixa energia, máxima robustez e custo-benefício. A partir dos resultados, é demonstrado que uma análise de custo-benefício pode destacar conjuntos de dimensionamentos e tensões de alimentação que podem prover uma redução de até 37.51% no consumo de energia com um aumento de somente 7.42% na sensibilidade aos efeitos de variabilidade. Além disso, é demonstrado que a dependência da tensão de alimentação e a robustez aos efeitos da variabilidade de processo não é direta, com pequenas diminuições na tensão de alimentação resultando em ganhos na robustez. Nas medidas médias das métricas, o inversor tradicional ainda é o circuito mais rápido e mais energéticamente eficiente, apresentando o melhor desempenho, menor consumo de

energia e menor área. Porém, quando comparando características que provêem imuidade ao ruído, o *Schmitt Trigger* de seis transistores apresentou as maiores margens de ruído, com maiores razões das correntes e ganhos. Já o circuito TIST apresentou as maiores razões entre correntes, ganhos e intervalos de histerese. Entretanto, estas melhorias não vem sem as respectivas penalidades nos tempos de propagação, consumo de energia e área.

Palavras-chave: Variabilidade de Processo, FinFET, Energia, *Schmitt Trigger*, Somadores Completos, Microeletrônica.

CONTENTS

1 INTRODUCTION.....	14
2 PROCESS VARIABILITY EFFECTS ON FINFET TECHNOLOGY	18
2.1 FinFET Technology.....	24
3 CONSIDERED DESIGNS TO COPE WITH VARIABILITY.....	29
3.1 ST Topologies and alternatives	29
3.2 Evaluated Circuits.....	31
3.2.1 Traditional 6T ST.....	31
3.2.2 Three Inverter Schmitt Trigger (TIST)	32
3.2.3 Stacked Inverter Gate (SIG).....	33
3.2.4 Low Power Schmitt Trigger (LPST).....	34
4 METHODOLOGY	36
4.1 Layout Design.....	37
4.2 Electrical Simulation	45
4.2.1 Inverters evaluation	46
4.2.2 ST technique on Full Adders	47
5 EVALUATION OF ST CIRCUITS AND ALTERNATIVES	51
5.1 Non-viable scenarios and Frequencies	51
5.2 Propagation Times	54
5.3 Energy Consumption and Deviation	55
5.4 Current Ratios.....	65
5.5 Static Noise Margins	69
5.6 Output Gains and Slopes.....	70
5.7 Hysteresis	72
5.8 Measures Distribution	75
6 FULL ADDERS	77
6.1 Nominal Operation	77
6.2 Near-Threshold Operation.....	77
6.3 Penalties	79
7 CONCLUSIONS	82
7.1 Future Works.....	86
REFERENCES.....	87
ANNEX A — PUBLICATIONS	95
A.1 Published.....	95
A.2 Co-author	95
A.3 Submitted and Accepted.....	95
A.4 Book Chapter (to be published).....	95
A.5 In Proceedings	96
ANNEX B — INVERTER DESIGNS LAYOUTS	97
ANNEX C — FULL ADDERS	118
ANNEX D — ENERGY MEASURES DISTRIBUTIONS	131

1 INTRODUCTION

Technology scaling, as stated by Moore where the number of transistors in a chip should double at about every two years, is a major factor in the ascendance of Integrated Circuits (ICs), providing higher transistor densities and voltage scaling due to the miniaturization of gate dimensions, internal capacitances and resistances. Such improvements provided the IC designers with plenty processing power per area unit of a chip and energy efficiency, making it the perfect combination for the usage of ICs in mobile applications (ISLAM et al., 2010).

As devices shrank, several transistor characteristic became severe problems for the modern semiconductor industry, alongside some new challenges. As transistors got smaller, the supply voltage decreased as well, to accomodate appropriate currents to an evermore smaller channel. Although, as the supply voltage decreases the noise margins got narrower, with the smaller currents, and capacitances curbing the circuit ability to mask the transients caused by external noise and radiation (ABBAS et al., 2015).

Furthermore, variations into the device's geometrical and electrical parameters were always a reality, introducing minor, if not negligible, variations into the circuits behavior. Even though, those geometrical variations did not scale down at the same rate as the devices. It has gotten increasingly difficult to produce further smaller light waves to correctly print such small patterns. Additionally, modern devices are so close to the atomic limit, that even variations in the scale of few units to few hundreds of atoms can exert influence into the device behavior, decreasing yield (ABBAS et al., 2015).

One of the many categories of systems which emerged from the technology scaling is The Internet of Things (IoT) which turned out to be one of the major mainstream trends, shaping technology development and the industry. The IoT concept englobes the shift from an internet which is used to interconnect end-user devices to, nowadays, interconnect physical objects that communicate with each other and/or with humans (MIORANDI et al., 2012). The IoT rise, alongside battery technology improvements, has provided us with portable, powerful and useful equipment for our daily routine, with wireless communication making information available anytime and anywhere (MANOLI, 2010).

IoT devices have been applied in many different scenarios, from improving building maintenance, to sensing remote areas for environmental observation and even in cars, for better safety and comfort. However, while many devices have to be connected to the power grid, sensor nodes are expected to be self-sufficient. Additionally, batter-

ies, the traditional means of powering self-sufficient systems, need to be replaced and/or charged, which means maintenance must be frequently performed (BLEITNER et al., 2018). Given that, energy harvesting in combination with rechargeable batteries has become a viable way to alleviate the power source and consumption dilemma (MANOLI, 2010).

Energy harvesting makes use of readily available power sources in the vicinity as for example motion or vibration induced kinetic energy, solar and electromagnetic or temperature gradients. A number of viable solutions are already present on the market, like self powered wireless light switches and electro-magnetic generators, which converts vibrations available in industrial plants for powering wireless monitoring sensors (MANOLI, 2010) (BLEITNER et al., 2018). Although, regardless of the sensors power supply, it will be always restricted by its power budget, with devices which are able to perform their functionality under heavy power constraints being essential for IoT. In traditional Complementary Metal Oxide Semiconductor (CMOS) circuit design aimed at Ultra Low Power (ULP) applications, the ideal circuit is the one that performs a given task or functionality while consuming the least amount of energy. Such circuits are achieved under transistor sizing and supply voltage tuning, and are technology and application-dependent.

Nevertheless, the performance of a system operating in its minimum energy per operation point may exceed the power budget of a given application. For example, with an application such as presented in (FOJTIK et al., 2013), where the device is only active once per hour, about 80% of its power consumption is due to standby power. In such a case, the minimization of energy-per-operation seems to be suboptimal in comparison to an idle power minimization kind-of solution. The minimization of supply voltage brings advantage for certain energy harvesting approaches such as thermo-electric. Such harvesting technique can result in DC voltage levels from tens to even hundreds of milivolts (KHAN; DAHIYA; LORENZELLI, 2014).

One of the industry responses to the challenges related to the improvements in the semiconductor industry is the Fin Field Effect Transistor (FinFET) Technology. FinFET devices present superior channel control due to the reduced Short Channel Effects (SCE) and low (if none) Random Dopant Fluctuation (RDF) effect due to the fully depleted channel (FARKHANI et al., 2014). Although, at deep technology nodes, variability is, still, one of the most challenging factors, including on FinFET devices. Variability introduces geometrical inconsistencies which changes the circuits behavior in comparison

to the final manufactured product. Such changes influence the circuits metrics, hastening its degradation and deviating from its correct operation regime (ABBAS et al., 2015) (NASSIF, 2008).

Due to the energy constraints of low power applications and the variability impact on recent nodes, the Schmitt Trigger (ST) circuit has been pointed as an alternative. The classical ST has been employed as a key element for several ULP circuits (KULKARNI; KIM; ROY, 2007; HAYS, 2012; MELEK et al., 2017; LOTZE; MANOLI, 2017). For variability mitigation, mainly attenuating the deviation on the power consumption, and replacing internal inverters on more complex circuits (DOKANIA; ISLAM, 2015) where spreads in major metrics were successfully limited. Also, the same experiment was executed at electrical and layout levels considering FinFET technology, and showed a considerable decrease in overall variability impact on metrics (TOLEDO et al., 2018; MORAES et al., 2018). However, with a considerable increase in delay and power consumption.

Given all the laid concepts, this work has two main objectives:

1) to identify an appropriate layout, considering transistor sizing, and supply voltage to achieve the most appropriate design for a set of applications. The considered circuits will be the traditional 6T ST, Stacked Inverter Gate (SIG), Triple Inverter Schmitt Trigger (TIST) and, for the sake of comparison, a traditional inverter. Multiple levels of process variability will be considered. Therefore, depending on manufacturability quality, different recommended layouts and supply voltages can arise.

2) to apply the ST technique into circuits. In this work, the Full Adder circuit is adopted as a case-study. The technique consists of the replacement of the FAs internal inverters with the respective STs. The considered FAs will be: the Mirror FA, the Transmission Function Adder (TFA), the Transmission Gate Adder (TGA) and Hybrid FA. The two applied STs are the traditional 6T ST and a low-power back-gating-based ST (LPST). The LPST was chosen for demonstrating good results at (DOKANIA; ISLAM, 2015). Due to technology restrictions, the LPST design had to be modified, given so, the 6T ST was chosen, to provide a reference for comparison and showing desirable results in sub-threshold applications (LOTZE; MANOLI, 2017). All layouts will be designs with a fixed number of transistors and two levels of supply voltages. All simulations will be performed at the same level of process variability.

For both analysis it will be considered the means, standard deviations and normalized standard deviations for the energy and propagation time measures. Specifically for the first analysis, the means, standard deviations and normalized standard deviations will

be calculated for further metrics: on and off currents, current ratios and hysteresis interval (when applicable). The output curve slopes and voltage gain will be presented, as well.

This work is divided into five further sections: Variability Effects on FinFET Technology, where a theoretical foundation about variability is laid with several related works about mitigating its impact in the characteristics of FinFET devices and how process variability presents itself in the device. A section about the considered circuits will explain their functionality and applications. The Methodology Section will explain the experimental setup which will be employed to generate the results. A Results Section is present, showing the extracted measures and related analysis. Lastly, there are a Conclusions and Future Work sections.

2 PROCESS VARIABILITY EFFECTS ON FINFET TECHNOLOGY

According to the ITRS Roadmap (BLISH et al., 2003), reliability will become one of the major challenges for the semiconductor industry. The device scaling combined with the adoption of new materials are the source of the increasing yield loss and reliability problems (GIELEN et al., 2008).

As process technology scaling advanced, decreasing the transistor dimensions, the ratio between device size and atom-size have been decreasing as well. Multiple techniques have been developed to reduce the loss of precision due to the manufacturing process at different end-of-lines. However, as the quantum-mechanical limit approaches, manufacturing-induced imprecision impact rises (ASENOV, 1999) (NEUBERGER; WIRTH; REIS, 2014).

Variability consists of characteristic deviations, internal or external to the circuit, which can determine its operational features and can be divided in two types concerning its effects, local and global, and three subtypes of variability causes (Environmental, Manufacturing, and Reliability). The general classification can be divided as:

- Global (Inter-die):

Global variations are related to the difference in parameter value across identical dies (whether those dies are in the same wafer, on different wafer, in different lots, or even in different fabrication plants).

- Local (Intra-die):

Occurs spatially within one chip. It can have a variety of sources, depending on physics of the manufacturing process.

These two types of effects are submitted to 3 subtypes of variability causes:

- Environmental:

Mostly external to the circuit, englobes variations in the power supply voltage and temperature. Voltage drops mainly occur due to abrupt changes in the switching activity, inducing large current transients in the system both locally or globally across the die. Local temperature within the die can cause variations in the device mobility and threshold voltages (V_T), and wire resistance. It is highly design dependent with timing constants similar to clock frequency (NASSIF, 2008) (BERNSTEIN et al., 2006). The intra-die factors include local effects caused by the chip operation such as device voltage variations due to IR drops and ground bounce, delay and slew

variations due to crosstalk, input pin capacitance deviations due to slew and state dependency, and differences in temperature inside the chip.

- Reliability:

Related to the aging process of the circuit, occurring during its day-to-day operation. Two of the main phenomena are electromigration, due to high enough current densities causing the gradual movement of metal ions due to the electron-ion momentum transfer (YOUNG; CHRISTOU, 1994) (POSSE; SAPATNEKAR; REIS, 2016) and Hot Carrier Injection (HCI) trapping electrons on oxide which degrades n-MOSFET on-current (TAKEDA; SUZUKI, 1983) (NASSIF, 2008) (BERNSTEIN et al., 2006). The intra-die phenomena is mainly represented by the effects of the phenomenon like Negative Bias Temperature Instability (NBTI) which mines the performance of p-channel due to the weakening of Si-H bonds in the oxide generating of interface states and trapping positive charges while the device is operating (WANG et al., 2008).

- Manufacturing:

Defined by device and interconnect geometry variations due to design dependency as well as random material variations. Interconnect width and spacing variations occur mainly due to photolithographic and etch dependencies. Those deviations will impact the interconnect parasitics, resulting in performance and signal degradation. An example is the Chemical-Mechanical Polishing (CMP) relationship between the thickness of the metal and the layout feature density (STINE; BONING; CHUNG, 1997). Random material variations consist of atomic-level deviations between devices (even when they are identical in layout and geometry) inside the chip. Overall, devices and interconnects will have fully correlated random components, which mean each random component will influence devices and interconnections equally (DIETRICH; HAASE, 2011).

Fig. 2.1, depicts the transistor intrinsic variability and different levels of abstraction, where from left to right it is shown a typical ideal transistor, a more realistic transistor with variations in its geometrical and electrical parameter, and the atomic-level limit at which we find the transistors in the most modern technologies, where a single atom can make a difference, respectively. These deviations appear in dopant profiles, thickness variations, and Line-Edge Roughness (LER). Dopant fluctuations are the main cause to V_T variations (ASENOV et al., 2003), with the removal of doping from the channel contributing for the V_T variation reduction, introducing

Table 2.1: Impact of variability on performance and power.

Property	Ease of measuring	Variability	Effects of variability	Effect of missing specification
Performance	Medium	Medium: up to 60%	L, W, R, C, V_T , μ	Slower product, yield, timing error
Leakage Power	Easy	Large: up to 148%	L, V_T , μ , t_{ox}	Shorter battery life, yield, heat
Dynamic Power	Difficult	Workload dependent	C, α	Shorter battery life, heat

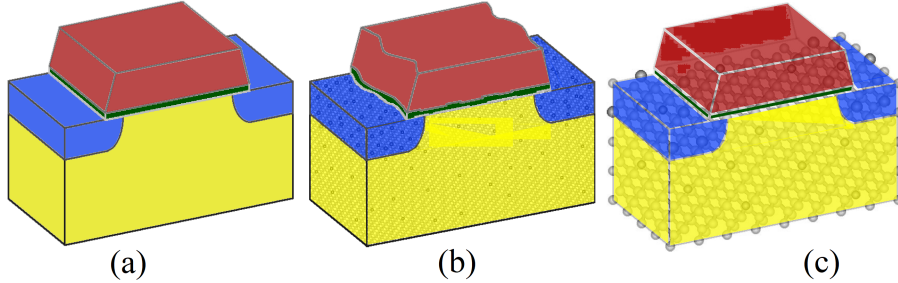
Source: Rahimi, Benini and Gupta (2016)

the necessity to set the V_T by gate-metal Work Function (WF) or by biased back gate (FRANK et al., 2001; WONG et al., 1999).

Fluctuations in doping levels and device features cause variations in the source/drain regions, which affects the overlap capacitance and the source resistance (FRANK; WONG, 2000). LER arises from variations in the total number of incident photons during lithography. Such roughness introduction into the polygons geometry may determine the effective gate width as one moves along the x axis of a Field Effect Transistor (FET) (BRUNNER, 2003). Another source of random device variability rises from the atomic-scale oxide thickness variation. It can introduce variations in the V_T (ASENOV et al., 2003), in the oxide tunneling current, and may cause mobility degradation due to the potential variation across the Metal Oxide Semiconductor FET (MOSFET) channel (BERNSTEIN et al., 2006). The manufacturing factor influencing at intra-die level comprises of geometric and parameter variations in the device and the interconnect derived from the manufacturing process. *Film Thickness* and *Channel Length* variations can result in systematic (not random) differences in V_T and leakage currents between chips in the same wafer. Additionally, deviations in the width in the lower layers of metal due to the congestion and proximity between layers and defects of lithographic nature can impact line resistance as well coupling capacitance. This type of variation is caused by the manufacturing steps: rapid thermal annealing (the wafer is rapidly heated up and cooled down to trigger additional chemical reactions within the photoresist) - with an uneven temperature accross the wafer and by-reticle variability can contribute due to changes in the focus as the mask is stepped across the wafer in the photolithography process - the focus can suffer deviations due to exposure tool lens astigmatisms or by wafer nonplanarity (BERNSTEIN et al., 2006; QIAN, 2015).

Table 2.1 presents the effects of variability and the impact on design, where L and W are the channel length and width, R and C are the parasitic resistances and capacitances, V_T is the threshold voltage, μ is the semiconductor electron mobility, t_{ox} corresponds to the oxide thickness, and α , the ratio between the transistor collector and emitter currents.

Figure 2.1: Levels of abstraction from a ideal transistor concept towards a realistic and "atomistic" device concept. (a) Depicts a the current approach of semiconductor device simulation, with continuous dopant charge and smooth boundaries. (b) Depicts a 20-nm MOSFET, with less than 50 Si atoms along the channel. RDF, interface roughness and LER introduce considerable intrinsic parameter fluctuation. (c) Depicts a 4-nm MOSFET, with less than 10 Si atoms along the channel.



Source: Asenov et al. (2003)

The impact on power is particularly challenging, since its variability is either large, though easy to measure, or difficult to measure, being dependent on workload. And both types of power variability (related to dynamic or leakage, power) have as a consequence shorter battery life and heat, apart from yield.

As a way to handle timing errors due to variations in the path delay, circuit designers commonly add safety timing margins to the voltage and/or the clock frequency (guardband). Such practice leads to overly conservative designs due to the guardband overlapping and accumulation in the ever increasing multi-corner analysis (AUSTIN et al., 2005).

In (JEONG; KAHNG; SAMADI, 2009) the impact of each individual variability source: Process, Voltage and Temperature (PVT) is quantified concerning a standard inverter cell through electrical simulations. A 1.8x delay variations was observed, with 1.46x, 1.25x and 0.97x coming from the process, voltage and temperature variations, respectively. Under the same operation conditions and smaller supply voltages for a 80-core Intel processor, it was observed a normalized deviation of 5.93%, 6.37% and 8.64% for 1.2V (nominal), 0.9V, and 0.8V, respectively. The lowering from 1.2V to 0.8V increases the critical path variability up to 45% (DIGHE et al., 2011).

Near-threshold operation has become a popular technique to achieve energy-efficient digital circuits. Although, operating at low voltages exacerbates the effects of delay variations (JEON et al., 2012; DRESLINSKI et al., 2010; RITHE et al., 2011; KAKOEE; LOI; BENINI, 2012; PAWLOWSKI et al., 2012). The measurement of Within-Die (WID) delay was performed for a 45nm Single Instruction Multiple Data (SIMD) processor, showing that reducing V_{DD} from 1.0V to 0.53V increases delay variation by 6x (PAWLOWSKI

et al., 2012).

Given the increase in performance variation, there is the need for mitigation methods to make the design resilient to timing errors, especially for circuits at low voltage operation regimes. There are several approaches to how and when errors should be manipulated as well as their abstraction levels. Among the steps there are: Predicting and Preventing, Detecting and Correcting, and Accepting. And among the abstraction levels there are Application Algorithm, Software, Architecture and Circuit. Since this work aims to investigate variability impact at layout level, some circuit-level techniques will be explained next with higher level techniques being thoroughly explained at (RAHIMI; BENINI; GUPTA, 2016).

Tuning CMOS knobs consists of several approaches to tune electrical characteristics (e.g., power and delay) of circuit by interfering with the body bias supply voltage and clock frequency, for example. Forward body biasing reduces the V_T (improving performance and increasing leakage power) while reverse body bias increases the V_T (reducing performance and leakage power). Given so, a slow circuit block can have its performance improved upon forward body biasing while a leaky circuit can be reverse body biased. Additionally, voltage and/or the circuit's frequency can be tuned to compensate variations (DIGHE et al., 2011; TSCHANZ et al., 2002; BORKAR et al., 2004).

There are topology changes employed during design time, using CAD optimizations to enhance the circuit resiliency against timing errors. Due to the general presence of clusters of critical paths in circuits, some approaches focus on uncertainty-aware circuit optimizations (BAI; VISWESWARIAH; STRENSKI, 2002). Optimization such as upsizing and downsizing of gates, use of multiple V_T cells, and restructuration of the path delay distribution (KAHNG et al., 2010).

Lastly, asynchronous circuits have been proposed since there is no need for a clock signal to determine a starting time for computation. In (CHANG et al., 2013) both versions (synchronous and asynchronous) of 8051 microcontroller are designed. When PVT and workload variations are introduced, the synchronous version required 4x, 1.5x, and 2x delay margins while the asynchronous version operated at nominal performance.

In order to mitigate variability impact, many works try to indicate the most robust design for a given type of circuit. For example, in (DOKANIA; IMRAN; ISLAM, 2013) twelve different FA topologies are analyzed considering delay, power and Power-Delay-Product (PDP) variability. It is used a 16nm bulk CMOS technology node in SPICE simulations with PVT variability being considered and Monte Carlo simulations performed.

The authors concluded that Cell A, CLRCL and Cell B FAs presented the best results for all three metrics (Delay, Power and PDP).

In (AMES et al., 2016) the effects of PVT variability in different FA designs are investigated. The simulations of the circuits are performed using SPICE and a bulk CMOS 32nm node technology. This work presented the TGA and TFA acceptable behavior under PVT variability with the lowest power consumption sensibility amongst the tested FAs.

In (ISLAM; HASAN, 2011) various popular 1-bit digital summing circuits functionality and robustness are analyzed in light of PVT variations with the best FA being simulated in Carbon Nanotube Field Effect Transistor (CNFET) technology for comparison with the bulk CMOS version. The simulations are carried at the 22nm bulk CMOS and CNFET technology node at electrical level. Its results show that the TGA has the strongest PVT variability robustness and its CNFET version provides over 3x, 1.14x and 1.1x less propagation delay, power dissipation and energy delay product (EDP) variations, respectively. This work does not consider the total power consumption of each FA separately.

Some articles analyze the adoption of new technologies: (GUDURI; ISLAM, 2015) proposes a hybrid of bulk CMOS and CNFET FA at 16nm in deep subthreshold operation region for ULP applications simulated in SPICE which showed some improvement over its bulk CMOS FA counterpart achieving 5% and 1% improvement in power, power-delay and energy-delay products and their variability, respectively. In (ISLAM; AKRAM; HASAN, 2011) a new subthreshold-FinFET FA is proposed and compared over multiple FAs showing huge metric improvements provided by the FinFET technology up to 2.22x improvement in power variability. It was simulated in 32nm predictive technology model on SPICE.

It is notable that none of these works consider the layout in its simulations and do not address any novel general technique which can be applied to a range of different types of circuits. Although, some works introduce novel designs.

(FEDERSPIEL et al., 2012) presents reliability comparison between 28nm bulk CMOS and Fully Depleted Silicon On Insulator (FDSOI) technologies at layout level, with FDSOI showing 32% improved performance, 40% reduced power consumption and improved matching, with its intrinsic reliability behavior similar to 28nm bulk at the device level. (ALIOTO; PALUMBO, 2007) presents a study about the delay variability caused by supply variations in the TGA. The experiments were performed at 90nm and 180nm bulk CMOS Technology in Spectre at layout level. It showed that lower supply

voltages bring more delay variability to the circuit with the TGA presenting worse results 15% (25%) for the 90 nm (180 nm) in comparison to static logic.

Some works focus on evaluating techniques: In (MORAES et al., 2018a) three transistor sizing techniques are applied on a set of cells and their impact on variability robustness is analyzed. The simulations were performed considering a 14nm FinFET technology using a SPICE tool. The authors concluded that the Optimized Transistor Sizing (OTS) technique has the best ratio between nominal PDP and PDP under process variability. (AHMADI; ALIZADEH; FOROUZANDEH, 2016) introduces a new technique to improve the performance of digital circuits in the presence of variations. It consists of a hybrid of two former methods to prevent errors due to delay variations. The simulations were performed with a 45nm predictive technology and applied on ITC'99 and ISCAS'89 benchmarks circuits. The results show that the hybrid technique can tolerate process variations up to 27.3% better than previous state-of-the-art techniques.

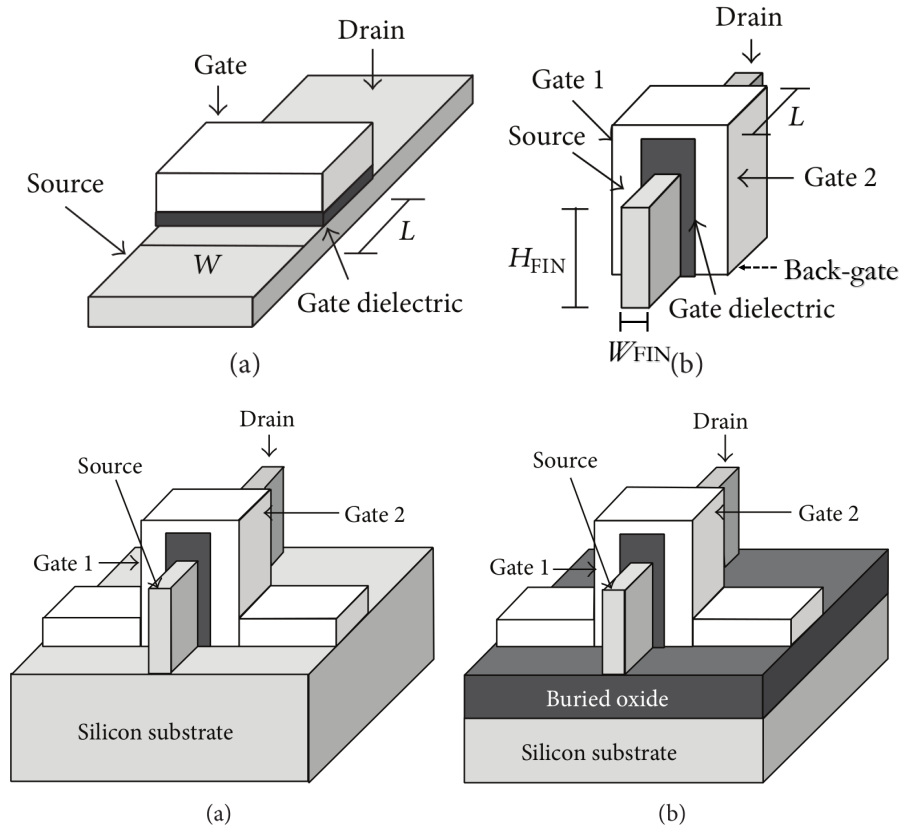
2.1 FinFET Technology

The Fin Field Effect Transistor (FinFET), and new commercial transistor technologies, have been developed for the mitigation of Short-Channel Effects and remains as one promising new technology for variability mitigation. The FinFET main geometric parameters are the gate length (L or L_G), fin width (W_{FIN} , T_{FIN} or T_{SI}), fin height (H_{FIN}) and Oxide Thickness (T_{OX}). FinFET transistors can be built on a traditional bulk or on a Silicon on Insulator (SOI) substrate with a conducting channel that rises above the level of the insulator, creating a thin silicon structure, the gate, as shown in Figures 2.2. FinFET devices can be shorted-gate (3 gate nodes) or independent-gate (4 gate nodes). The shorted gate model is similar to the traditional MOSFET given that the front-gate and back-gate are connected and controlled by the gate signal. The independent gate has 4 nodes, making possible to connect the front and back gate to different voltage values.

The channel being surrounded from three dimensions by the gate results in a superior control, reduced SCE and RDF effect due to the fully depleted channel that causes less sensitivity to process variations (TAUR; NING, 2013). FinFETs also present relative immunity to gate LER, a major source of variability in planar nanoscale FETs (KING, 2005). The disadvantage over bulk MOSFETs is the harder manufacturing process due to difficulty in the lithography steps as it is increasingly difficult to print small patterns, the increased variability impact due to the further miniaturization of dimensions, in com-

Figure 2.2: Above, structural comparison between (a) planar MOSFET and (b) FinFET transistors.

Below, structural comparison between (a) bulk and (b) SOI FinFETs.



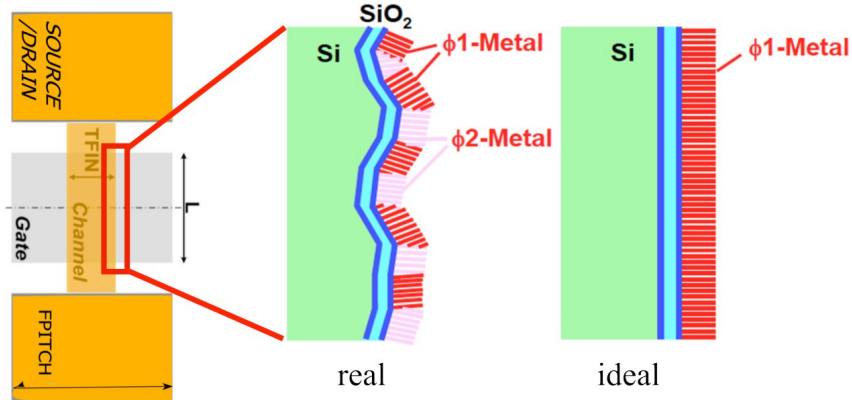
Source: Bhattacharya and Jha (2014)

parison to bulk MOSFET and a more costly manufacturing process due to the need of techniques to address the manufacturing imprecision and, in the case of SOI FinFET, to change the CMOS substrate process to support a SOI substrate manufacturing process (KING, 2005) (MANOJ et al., 2007).

Given the elevated levels of gate leakage due to the scaling down of the gate oxide, insulating materials with higher dielectric constant (high-k) have been introduced. Although, with the high-k dielectric adoption, challenges such as Fermi level pinning (HOBBS et al., 2004) and phonon scattering (GUSEV; NARAYANAN; FRANK, 2006) rised, being necessary the replacement of the traditional polysilicon gate electrode by a metal gate electrode (GUSEV et al., 2001; DATTA et al., 2003).

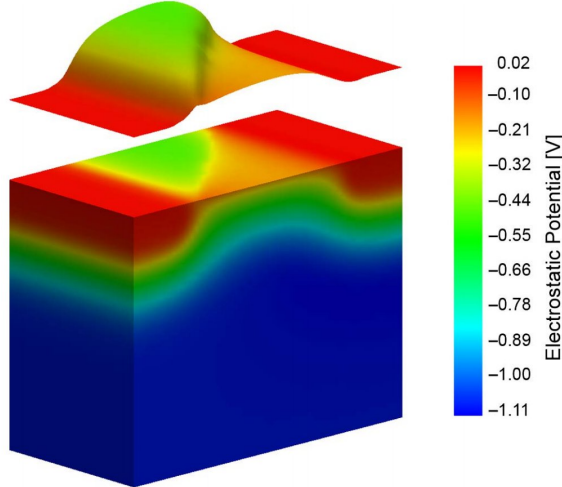
In the bulk FET devices in nanotechnologies, the variations in the gate length was the dominant parameter related to I_{ON} deviations due to the RDF effects. Although, as a results of the shapes of the fin-like structures in FinFET, the channel is prefered to be low-doped to minimize threshold voltage variations. Given so, threshold voltage is mainly set

Figure 2.3: Metal fabrication ideal and real aspects.



Source: Meinhardt, Zimpeck and Reis (2014)

Figure 2.4: Electrostatic potential in a generic 30-nm MOSFET with the surface potential shown below. The metal gate has two grains with the grain boundary diagonally across the channel.



Source: Brown et al. (2010)

by the workfunction.

Metals exist *in natura* in the form of crystals where each atom has several bonds with adjacent atoms. Although, due to defects and disorientations, several crystals are formed, with "grain boundaries" between regions of regularity (crystal grains) in the metal (DADGOUR; DE; BANERJEE, 2008), as shown in Fig. 2.3. The electrostatic potential (e.g. V_T) varies depending on each grain boundary, as shown in Fig. 2.4. At Table 2.2 a example of possible orientation, probability and WF is given. Between several technology nodes - FD-SOI, Bulk and FinFET - the latter showed the lowest V_T variation due to the much larger gate area (DADGOUR; DE; BANERJEE, 2008).

The WFF impact can be better understood when considering the equation 2.1, where the threshold voltage for multigate devices is expressed. Additionally, the fermi

Table 2.2

Orientation	Probability	Work Function
<200>	60%	4.6 eV
<111>	40%	4.4 eV

Source: Brown et al. (2010)

potential for the P-type silicon is given by equation 2.2 (COLINGE et al., 2008).

The effects of Q_D and Q_{SS} onto the threshold voltage (V_{th}) are almost negligible compared to f_f , in ultrathin body and lightly doped devices, like the FinFET. Additionally, V_{in} is the additional surface potential to $2f_f$, of ultrathin body devices, that is needed to accumulate enough inversion charges into the channel region of the transistor to reach the threshold point (MUSTAFA; BHAT; BEIGH, 2013).

$$V_{th} = f_{ms} + 2f_f + \frac{Q_D}{C_{ox}} - \frac{Q_{SS}}{C_{ox}} + V_{in} \quad (2.1)$$

where:

Q_{SS} = charge in the gate dielectric

C_{ox} = gate capacitance

Q_D = depletion charge in the channel

f_{ms} = work-function difference between the gate electrode and the semiconductor

f_f = fermi-potential

$$f_f = \frac{kT}{q} \ln \frac{N_A}{n_i} \quad (2.2)$$

where:

N_A = acceptor concentration

n_i = intrinsic carrier concentration

Several works analyze the FinFET reliability. It is shown in (MEINHARDT; ZIMPECK; REIS, 2014) the major influence that WF Fluctuations (WFF) exercise over V_T variations of several standard cells. In addition, in (WANG et al., 2011) it was shown the high correlation between the I_{ON} and I_{OFF} currents and V_T fluctuations due to the granularity of the metal gate.

In (ZHANG et al., 2017) the modeling of the reliability degradation of a FinFET-based Static Random Access Memory (SRAM) is shown. It is concluded that the probability of failure due to NBTI and Gate Oxide Break Down (GOBD) is relatively lower in comparison to HCl-induced failures. They also show the improvement of lifetime due to Error-Correcting Code (ECC) memory.

In (HARRINGTON et al., 2018) it is shown, at 14/16nm fabricated bulk FinFET technology, that for high energy charged particles, the drive current is the dominant factor to the transient fault pulse width and cross-section. And low energy particles have a greater dependence on secondary transistor and circuit design factors (number of fins, transistor arrangement, etc).

In (REN et al., 2018) the HCI effect is analyzed in pass-gate FinFET transistors. The tests were executed using a commercial FinFET technology showing a 50% chance of errors due to HCI in pass-gate transistors. In (XIONG; BOKOR, 2003) a analysis of the sensitivity of double-gate and FinFET devices to process variations is shown. It is concluded that for 20nm FinFET devices large channel doping concentration is necessary to obtain suitable values of V_T if heavily doped polysilicon gates are used. Due to the small volume of the channel doping will bring unacceptable V_T fluctuations. Given that, heavily doped polysilicon may not be a viable choice with the work function adjustment being a better approach.

In (LIAO et al., 2008) an investigation on reliability characteristics of NMOS and PMOS FinFETs is conducted. Based on fabricated FinFETs transistor with 17-27 nm width, it was shown that the life-time of FinFET is very dependable of its dimensions. The predicted lifetime for a 50nm gate length NMOS FinFET was 133 years, for the first HCI event. While a 27nm fin-width PMOS FinFET showed 26.84 years of lifetime which is reduced to 2.76 years when reducing its fin-width from 27 to 17 nm for a NBTI event, showing the huge reliability challenge introduced by technology scaling.

Given all the works trying to characterize the impact of variability in FinFET devices, and developing methods to tackle this problem, at several levels of abstraction, the FinFET variability challenge is kept as an open problem. This work aims to assess whether there are inverter circuits applicable for replacing the traditional inverter, presenting better results in relation to the impact of process variability, while maintaining low energy consumption.

3 CONSIDERED DESIGNS TO COPE WITH VARIABILITY

This work selected 4 inverter alternative circuits based in recent literature, to evaluate their effectiveness in diminishing the impact of variability into metrics.

Schmitt Triggers are commonly used as internal circuits on systems to provide enhanced noise tolerance and robustness against random variations in the input waveforms. On a typical input (non-ST), its binary value will switch at the same point on the rising and falling edges. With a slow rising edge, the input will change near the threshold point. When the switching occurs, it will require current from the supply source. With current being pushed from the supply, it can cause a voltage drop across the circuit causing a shift in the threshold voltage.

If the threshold shifts, it will cross the input causing it to switch again. It can go indefinitely causing oscillation. The same thing can happen if there is noise on the input. STs are applied in these cases to filter noise introducing superior and inferior threshold voltages. STs circuits present a hysteresis characteristic. This hysteresis exists in the presence of two switching V_T . If the input level is within the hysteresis region, the ST shall not switch. Such characteristic gives a higher static noise margin (SNM) in comparison to traditional inverters, ensuring a high noise immunity.

Variations in physical parameters became alarming at ultra-deep sub-micron (UDSM) nodes because the node scaling was accompanied by a supply voltage scaling, making the circuits more susceptible to noise and electromagnetic interference due to the deterioration in SNM (PAL; ISLAM, 2018). Given that, this work explores four types of inverters, where three of them are considered STs given their hysteresis characteristic.

3.1 ST Topologies and alternatives

A variety of CMOS STs have been proposed and implemented over the years based on different requirements. A higher performance ST is proposed in (STEYAERT; SANSEN, 1986) where, by a different design, a smaller load capacitor value is achieved, decreasing the slew rate of the ST internal node. In (PFISTER, 1992) a ST with a programmable hysteresis is proposed. The programmable hysteresis is achieved by adding a P and N transistors in series with the 6T ST P_F and N_F transistors, respectively, both receiving the same gate signal. (KIM; KIH; KIM, 1993) proposes a 10T ST which its hysteresis interval does not depend on transistors width/length ratios being, consequently,

more robust to process variations.

A low-power ST is proposed at (AL-SARAWI, 2002) with low short circuit current achieved by the presence of only one path to each power rail, being recommended for low power, and very low frequency applications. In (PEDRONI, 2005) proposes a low-power ST by having only one transistor transmitting (at stable output values), considerably reducing power consumption. STs can be optimised by adequate dimensioning as well as stated in (TACHE et al., 2018) where the OTS technique presented the best metrics for low power applications, in accordance to (MORAES et al., 2018a).

In (SHAH et al., 2020) a voltage-booster is applied in the traditional 6T ST to replace its pull up network and reduce the number of PMOS transistor to only one. This replacement makes it less vulnerable to the effects of NBTI, which severely affects PMOS devices. It was simulated on 32 nm bulk CMOS technology and was revealed to present an almost negligible delay shift of 0.47%, with the traditional 6T ST and CMOS inverter presenting 7.2% and 5.32% shifts, after three years of simulated NBTI stress, respectively. Furthermore, it presented an improved sensitivity against charged particles of 62.48% and 55.10% against the CMOS inverter and 6T ST, respectively. And finally, it presented 168.68% less deviations in comparison to the CMOS inverter considering process variability. It is important, though, to highlight its 4.315x higher leakage power and potential higher area, given finfet technology restrictions considering the higher number of NMOS transistors (5) in comparison to the traditional 6T ST (3).

In (DOKANIA; ISLAM, 2015) a novel technique based on the replacement of FA's internal inverters with low voltage STs for PVT variability robustness improvement is originally introduced and applied on seven different FA designs. The simulations were performed using the 16nm bulk CMOS predictive technology model in SPICE. It presented significant variability improvement up to 4.8x in PDP. Although, the improvements occur at the cost of an increase in the area and power dissipation of each design. This technique is tested in several works: in (TOLEDO; ZIMPECK; MEINHARDT, 2016) the ST technique is applied on four FAs. It presented promising results regarding the power deviation due to the process variability with a decrease up to 79% with a drawback of a significant increase in average energy consumption. The simulations were performed with the 16nm technology predictive technology model in SPICE.

In (AHMAD et al., 2016) it is presented a novel Schmitt-trigger-based single-ended 11 Transistor SRAM cell. It analyses its performance against seven different SRAM topologies. The novel cell showed the least energy consumption per operation

with the smallest leakage power and a 6.9x higher I_{ON}/I_{OFF} ratio. Further PVT variability simulations confirmed the robustness of the design regarding read and write operation. The simulations were carried in 22nm predictive technology using SPICE. (MOGHAD-DAM; MOAIYERI; ESHGHI, 2017) presents a ST buffer using CNFET. It was evaluated against other two buffers and showed, on average, 68% higher critical charge and 53% lower energy consumption and a huge gain considering PVT variability robustness. The simulations were carried in 16nm Stanford CNFET model using SPICE. Lastly, in our previous work (MORAES et al., 2018), the ST technique is evaluated considering 4 different FAs layouts at 7nm FinFET. 64.74% and 66.6% reduction in delay and power deviation was achieved.

3.2 Evaluated Circuits

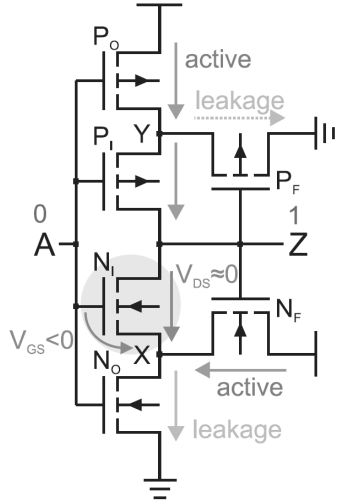
Several circuits were chosen to be analyzed as alternatives to mitigate the effects of process variability. Simulations considering several supply voltage levels, transistor sizing, and level of process variability will be carried out upon the considered designs, and their results are compared, to indicate the most appropriate design for each type of application and priority. The following circuits are considered:

3.2.1 Traditional 6T ST

The 6T traditional ST main feature is the presence of P_F and N_F devices as shown in Fig. 3.1 (DOKI, 1984). These transistors are responsible for a feedback system. For example, if the output is in a high level, the N_F is on, pulling the node X to a high potential, and forcing the drain-source voltage of transistor N_I almost zero and its gate-source voltage into the negative region. This kind of arrangement reduces the leakage current N_I exponentially, increasing the on-to-off current ratio, and minimizing the output degradation (LOTZE; MANOLI, 2017).

The main effect of process variability is a shift on the voltage transfer curve (VTC) due to the threshold voltage variation. Usually, the input voltage, where a device starts delivering current, is directly dependent on the V_T . Thus, the variability impact on VTC is reduced in the ST as a result of the high influence of the gate-source voltage of the inner transistor (N_I and P_I) over its switching point (LOTZE; MANOLI, 2017).

Figure 3.1: ST inverter leakage suppression (LOTZE; MANOLI, 2017).



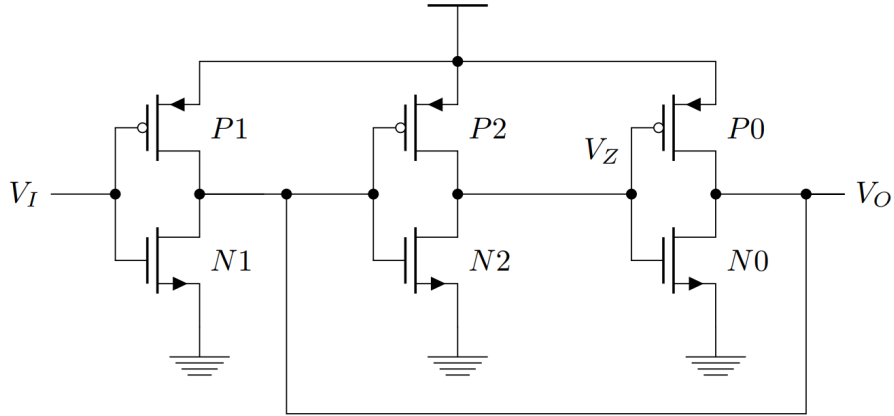
The 6T ST was chosen due to promising results at (LOTZE; MANOLI, 2017), where a ST-based 8x8 multiplier was presented, with the ST greatly improving the on-to-off current ratio. In (KULKARNI; KIM; ROY, 2007) a SRAM based on 6T ST is proposed working at 160mV and showing improvements of both robustness and static noise margins in comparison to a traditional inverter-based solution.

3.2.2 Three Inverter Schmitt Trigger (TIST)

The TIST, shown in Fig. 3.2 is a ST implementation, most common in textbooks. It has been mostly unexplored for low power applications. It consists of a CMOS inverter followed by a latch. The idea behind this circuit is related to the switching threshold of a CMOS inverter being determined by the ratio between NMOS and PMOS transistors (k_n/k_p). Increasing the ratio results in a reduction of the threshold and vice-versa. Adapting the ratio depending upon the direction of the transition results in a shift in the switching threshold, characterizing a hysteresis effect. This effect is achieved with a feedback mechanism, as the previous design. For example, when the input signal is low (zero) the P_2 and P_0 are conducting, while the N_2 and N_0 are off.

As the input goes high (one) with P_1 shutting down and N_1 start conducting. As the input to the latch start discharging P_2 and P_0 will start conducting at the same time, changing the ratio between the number of parallel PMOS/NMOS transistor conducting and effectively changing the ratio. The same dynamic occurs when changing the input from a high value to a low value, just inverting the transistors from PMOS to NMOS and vice-versa. The brief ratio change is enough for decreasing the switching threshold for

Figure 3.2: Modified TIST schematic (RABAEY; CHANDRAKASAN; NIKOLIC, 2002)



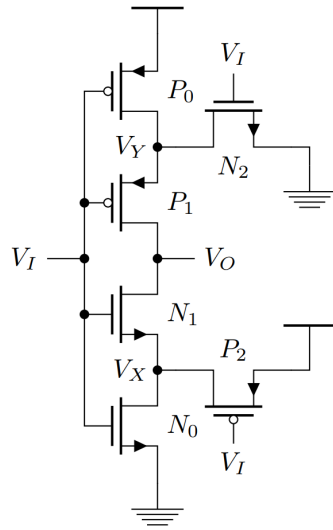
the appearance of hysteresis. The TIST in this work has been modified to turn it into an inverter. The original TIST is shown in (RABAEY; CHANDRAKASAN; NIKOLIC, 2002).

According to (FERNANDES, 2019), the TIST is able to provide hysteresis from a supply voltage as low as the classical inverter unity gain. However, for higher supply voltages, the hysteresis interval will grow excessively to a point where the cell locks itself in a random state (low or high), which cannot be changed. Furthermore, it was shown that the hysteresis interval and the minimum supply voltage for it to appear greatly benefit from increasing the ratio between the latch and inverter transistors. Given so, to tackle some of that problem, the inverter transistors were sized with a higher number of fins in comparison to the latch. Still, it shows the TIST viability to work at sub 100mV supply voltages, which will be explored in future works.

3.2.3 Stacked Inverter Gate (SIG)

SIG, shown in Fig. 3.3, is a circuit composed of unbalanced inverters without positive feedback, referred to as stacked, or redundant, inverters. It presented improvements over the CMOS inverter regarding voltage gains (BOSE; JOHNSTON, 2018; LUO et al., 2017). Originally, it was applied on replacing the inverter of a ring-oscillator working at a sub-50mV supply voltage, presenting 30% higher gains, claiming that energy harvesting techniques based on the body-to-ambient temperature gradient can leverage such oscillator to achieve self-startup.

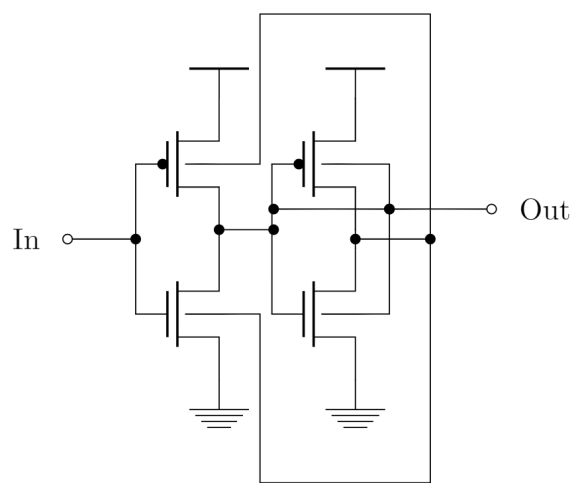
Figure 3.3: SIG schematic (BOSE; JOHNSTON, 2018)



3.2.4 Low Power Schmitt Trigger (LPST)

The following circuit is not compared to the previous ones, although being applied on the following analysis considering the replacement of FAs internal inverters. It was not applied in the comparison between inverter circuits due to technology restrictions, which did not permit to connect the NMOS devices back-gates to specific nodes. The LPST inverter circuit used in this work was inspired by (ZHANG; SRIVASTAVA; AJMERA, 2003) and modified in (DOKANIA; ISLAM, 2015) to achieve the desired inverting characteristic, as shown in Figure 3.4.

Figure 3.4: LPST Inverter from Dokania and Islam (2015)



It is designed for operation at a supply voltage of 0.4V to achieve low power consumption, and consists of the junction of two inverters where the output from the second one will be the bulk for the first one. On previous work (MORAES et al., 2018), the

Table 3.1: Each design number of transistors and main characteristic, advertised by respective works.

Design	# Transistors	Main characteristic
INV	2	-
ST	6	Hysteresis
SIG	6	Higher gains, ULP
TIST	6	Hysteresis
LPST	4	Hysteresis, LP

LPST was applied on Full Adders, presenting up to 37.38% decrease on energy deviations at nominal level supply voltage and 66.59% for near-threshold operation (0.4V). In this design a dynamic body-bias technique is applied through a feedback mechanism to a standard CMOS inverter circuit, thus allowing a change in the threshold voltages of two MOSFETs, implying a change in the switching voltage. In order to provide an overview, the number of transistor and main characteristic for each design are highlighted at Table 3.1.

4 METHODOLOGY

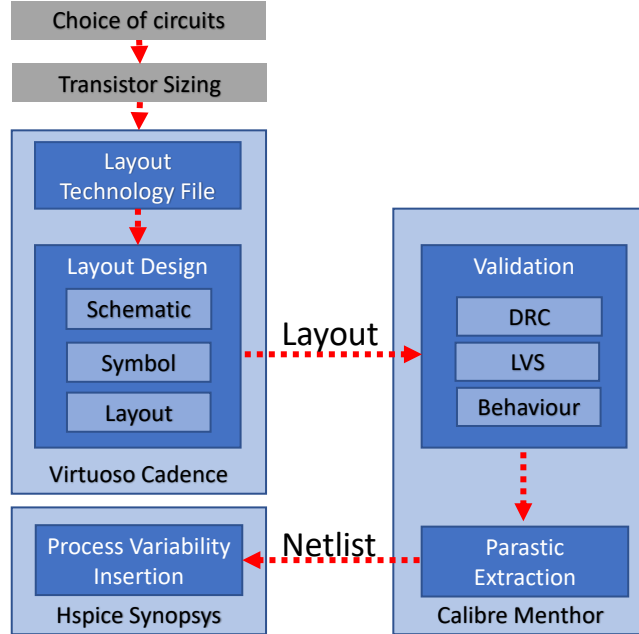
To provide an extensive exploration of the process variability effects on the circuits characteristics, this work evaluates:

- 1) 4 inverter circuits. The traditional CMOS inverter, the 6T ST, the SIG, and TIST, operating at multiple combinations of supply voltages. The supply voltage range will start from 0.1V to 0.7V (nominal) in 100mV steps;
- 2) the influence of the transistor sizing where all transistors have the same number of fins (except for the TIST), ranging from 1 fin to 5 fins, increasing the number of fins one-by-one;
- 3) the impact of these parameters on the maximum achievable frequency within a failure threshold of 10% of the 2000 Monte Carlo simulations;
- 4) the impact of different levels of process variability (WFF) from 1% to 5% in steps of 1%. This variations is inserted into the simulations following gaussian distribution;
- 5) as a case-study to show the potential of these circuits as a technique to mitigate process variability effects.

The design flow is shown at Figure 4.1. The design was divided into two main steps: the layout design and electrical simulations. After finishing the layout design process, each layout passed through validation which consisted of a Design Rule Checking (DRC) to detect if the layout obeys the technology geometry restrictions and layer rules, Layout Versus Schematic (LVS) where the schematic and the layout extracted netlists are compared to detect their equivalence (same nodes and nets) and a Behavioral test, to observe if the circuit works as expected.

The transistor sizing exploration evaluate layouts from 1 to 5 fins through 1-fin steps for the CMOS inverter, the traditional ST and the SIG. The TIST did not present an adequate behaviour with its P and N devices presenting the same number of fins, with its output value getting stuck. Thus, for the TIST, a different approach was adopted. The TIST consists of a traditional inverter (transistors P_1 and N_1) followed by a latch (transistors P_0 , P_2 , N_0 and N_2), given so, the inverter transistors were resized following a proportion between their size and the size of the latch transistors. It was adopted two proportions: 2:1 and 3:1, resulting in five different layouts. Three layouts follow a 2:1 proportion with the inverter transistors containing 2, 4, and 6 fins and the latch transistors containing 1, 2, and 3 fins, respectively. Two layouts follow a 3:1 proportion with the

Figure 4.1: Design flow of the experiments.



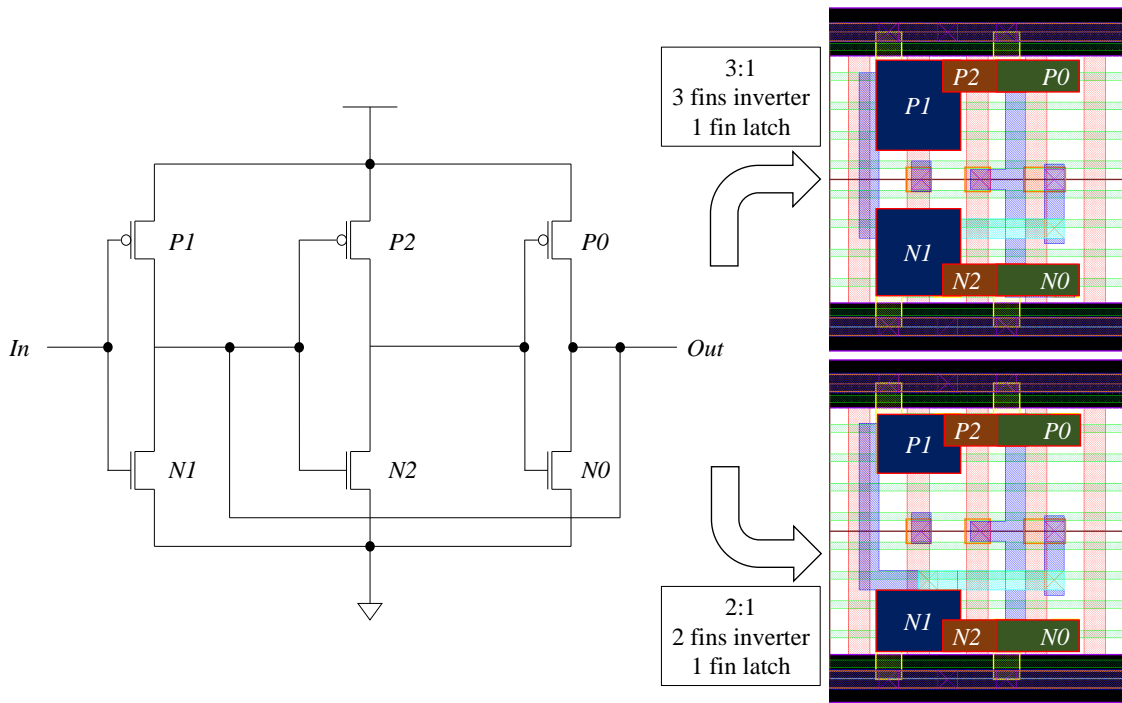
Source: From the author.

ST transistors containing 3 and 6 fins, and the latch transistors containing 1 and 2 fins, respectively. For the sake of simplicity TIST layouts will be referred to as TIST2F1F, TIST4F2F, TIST6F3F, TIST3F1F and TIST6F2F. With such sizing, the TIST worked properly in a higher number of cases, with near-threshold voltage operations presenting the highest number of failures. Fig. 4.2 presents the TIST circuit with the smallest 2:1 and 3:1 proportion designs, with each transistor mapped.

4.1 Layout Design

All circuits were designed using the Virtuoso Electronic Design Automation (EDA) tool from Cadence® with the process design kit (PDK) of 7-nm FinFET of Arizona State Predictive PDK (ASAP7) from the Arizona State University in partnership with ARM (CLARK et al., 2016). It is the only open-source and free 7-nm PDK available for academic use. This PDK was chosen due to realistic design conjecture regarding the current design competencies. FinFET technologies present the width quantization aspect (ALIOTO; CONSOLI; PALUMBO, 2015a). With a 27nm fin pitch, high-density layout is achieved with 3-fins transistors. Otherwise, for a higher fin count, there is a lower density and routing complexity (CHAVA et al., 2015). The main PDK rules and lithography assumptions considered in this work are shown in Table I. To exemplify the PDK layers,

Figure 4.2: TIST schematic, to the left, and smallest 2:1 and 3:1 designs, to the right.



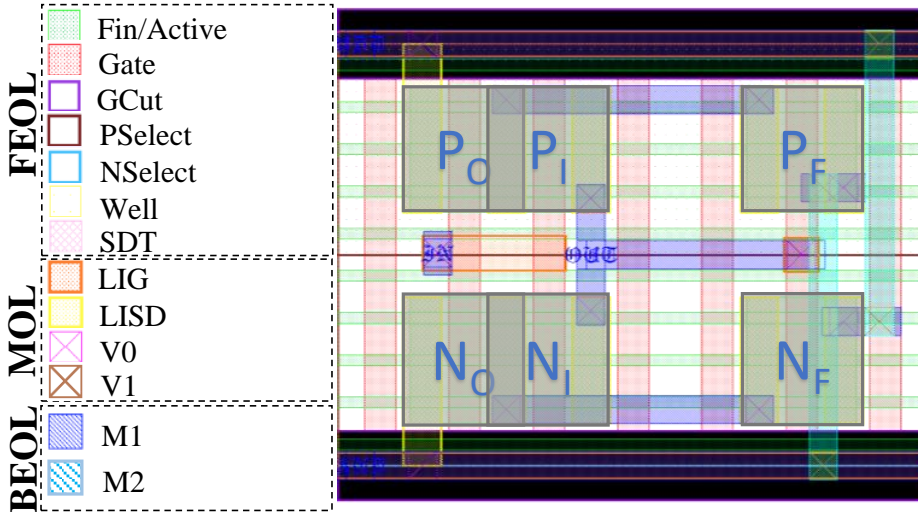
Source: From the author.

the 3-fins transistors ST is shown in Fig. 4.3. The dimensions and areas related to each layout is shown at Table 4.1. Figs. 4.4, 4.5, 4.6 and 4.7 show comparisons between each circuit layouts. All inverters layouts are shown individually in Annex B, at the end of the document.

Due to technology restriction it is not possible to decrease the cell height when considering layout with a fin count below 3. In the case of the ST, for the layouts with a fin count below 3, M2 was applied to connect the source/drain of the P_F and N_F transistors to the X and Y layout nodes. For the TIST, in layouts with less than 3 fins, M2 was necessary to connect the output signal to the P_2 and N_2 transistors gate. Given the smaller area to work with, it was necessary to apply M2 to respect the M1 spacing rules, bringing to light one of the challenges related to a smaller layout. The M2 usage in those cases will increase the design parasitics from the necessary extra vias connecting M1 and M2.

The ASAP7 PDK contains the manufacturing process composed by front end of line (FEOL), middle of line (MOL) and back end of line (BEOL). The layouts were developed in a continuous diffusion layer with every gate surrounding another gate in the horizontal axis. The Source-Drain Trench (SDT) connects the active area to the LISD layer. The Local-Interconnect Gate (LIG) is applied to connect the gate terminal, and Local-Interconnect Source-Drain (LISD) is used to connect the source and drain of the

Figure 4.3: Technology layers and 3-fins transistors 6T ST layout



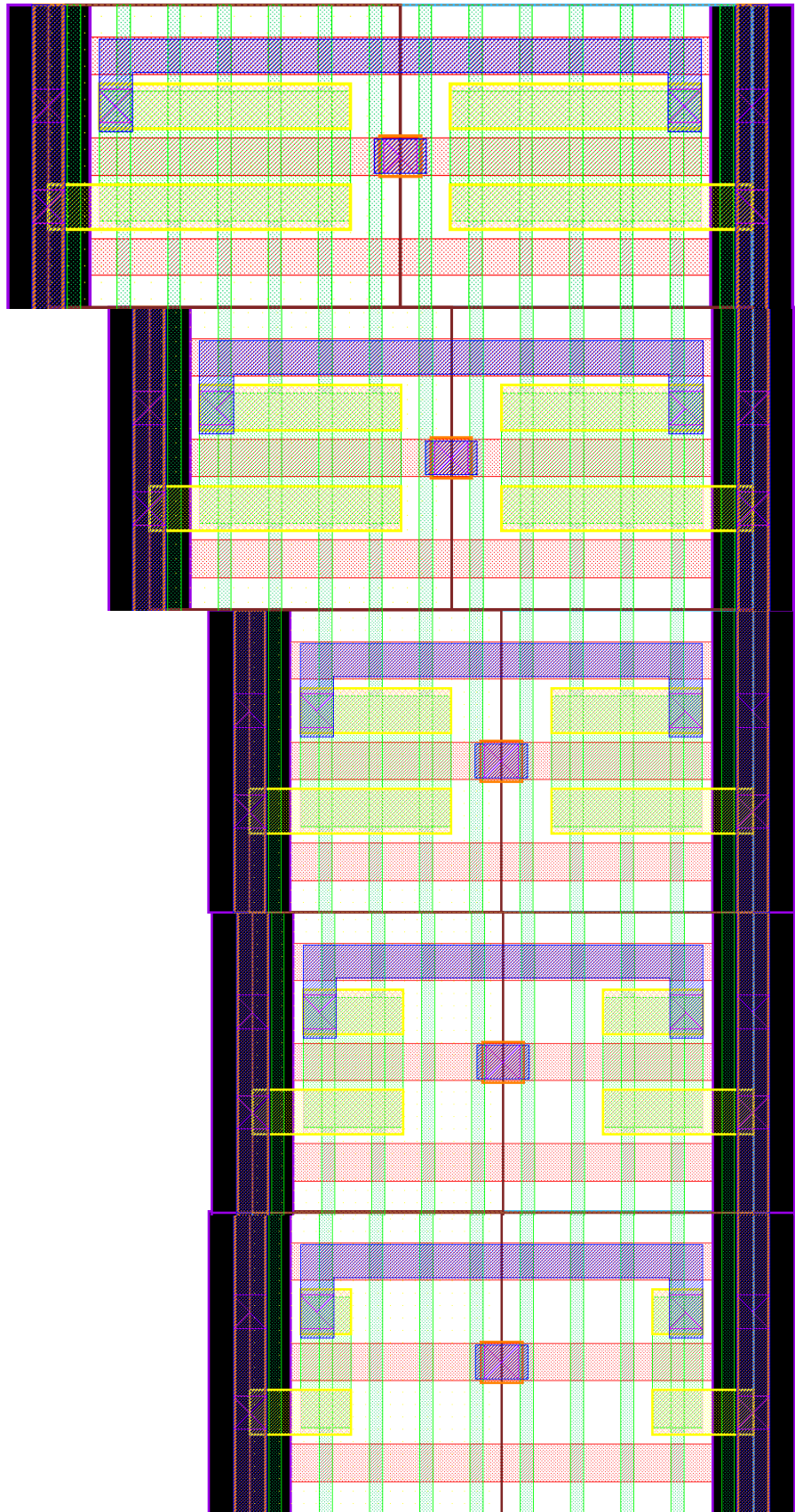
Source: From the author.

Table 4.1: Each layout proportion/maximum number of fins, dimension and area (the TAP-Cell area is not taken into account).

	Layout	Height (nm)	Width (nm)	Area (nm ²)
INV	1 Fin	270	162	43,740
	2 Fins	270	162	43,740
	3 Fins	270	162	43,740
	4 Fins	324	162	52,488
	5 Fins	378	162	61,236
ST	1 Fin	270	378	102,060
	2 Fins	270	378	102,060
	3 Fins	270	378	102,060
	4 Fins	324	378	122,472
	5 Fins	378	378	142,884
SIG	1 Fin	270	378	102,060
	2 Fins	270	378	102,060
	3 Fins	270	378	102,060
	4 Fins	324	378	122,472
	5 Fins	378	378	142,884
TIST	2 Fins : 1 Fin	270	270	72,900
	4 Fins : 2 Fins	324	270	87,480
	6 Fins : 3 Fins	432	270	116,640
	3 Fins : 1 Fin	270	270	72,900
	6 Fins : 2 Fins	432	270	116,640

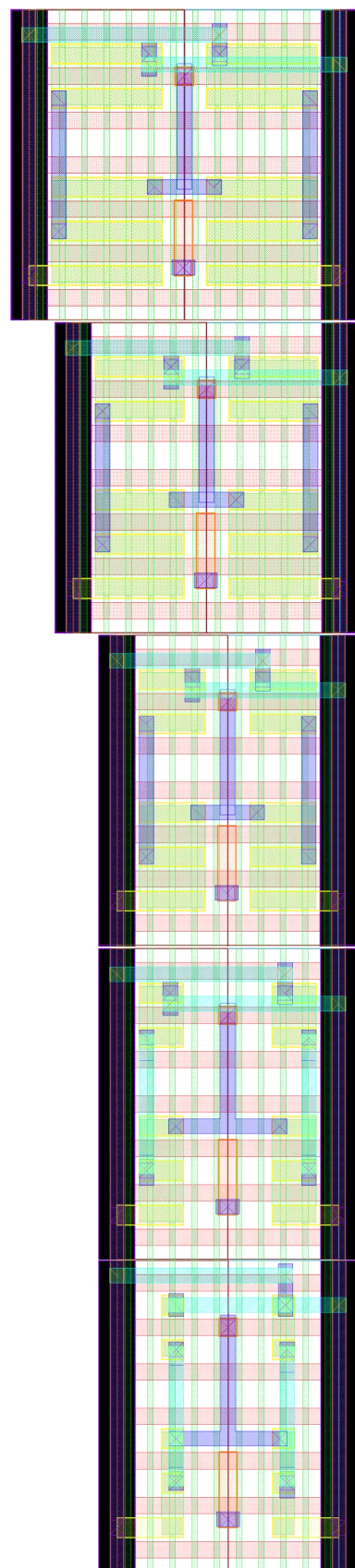
Source: from the author.

Figure 4.4: 1 to 5 fins (left to the right) traditional CMOS inverter layout comparison.



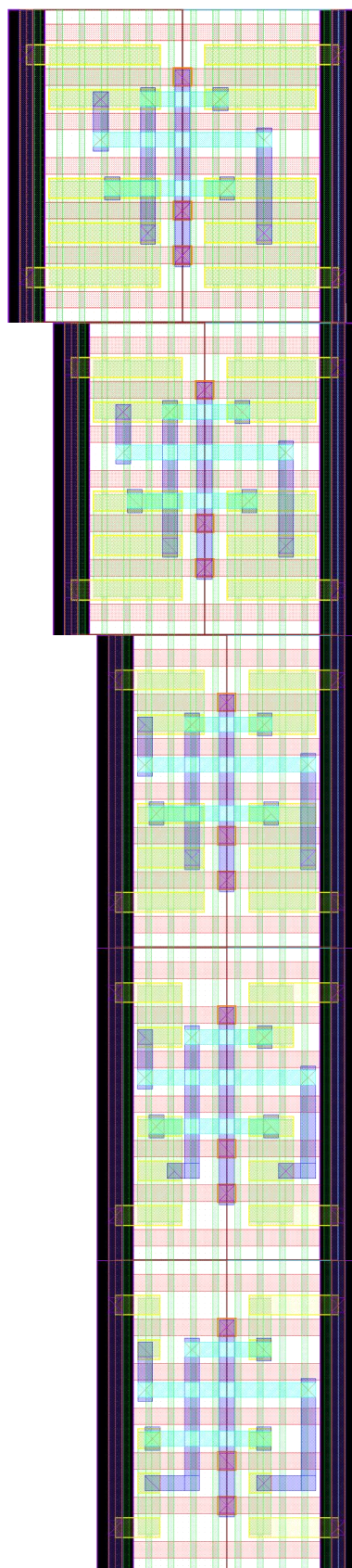
Source: From the author.

Figure 4.5: 1 to 5 fins (left to the right) ST layout comparison.



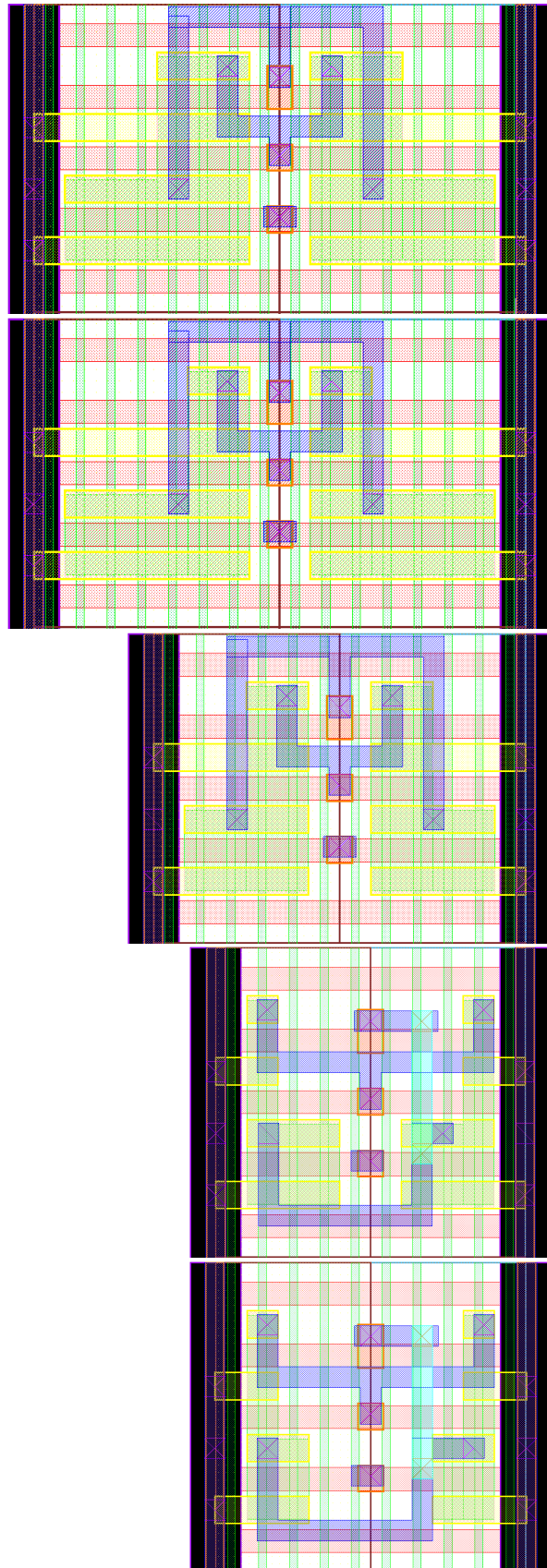
Source: From the author.

Figure 4.6: 1 to 5 fins (left to the right) SIG layout comparison.



Source: From the author.

Figure 4.7: From the left to the right, 2, 4 and 6 maximum fins TIST layout comparison.



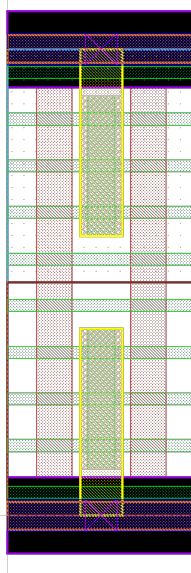
Source: From the author.

Table 4.2: Key layer lithography assumptions, widths and pitches

Layer	Lithography	Width/drawn (nm)	Pitch (nm)
Fin	SAQP	6.5/7	27
Active (horizontal)	EUV	54/16	108
Gate	SADP	21/20	54
SDT/LISD	EUV	25/24	54
LIG	EUV	16/16	54
VIA0-VIA3	EUV	18/18	25
M1-M3	EUV	18/18	36

Source: Clark et al. (2016)

Figure 4.8: TAP-Cell Layout.



Source: From the author.

transistors. The function of Via 0 (V0) is to join the LIG and LISD to the BEOL layers. The Metal 1 (M1) is used for intra-cell routing and short connections. The Metal 2 (M2) was applied to connect the PF and NF drains to ground and source, respectively. To make the back-gate connections, it is necessary a TAP-Cell. It is responsible to connect the NMOS and PMOS back-gates to supply/ground, respectively, being possible to connect the PMOS back-gates to another node. It is a PDK restriction needed for the proper function of the circuit. Its layout has a length of 108nm resulting in an area of $29,160\text{nm}^2$ the 3-fins variant is shown in Figure 4.8. In order to build the back-gate connections present in the LPST, it was necessary the insertion of TAP-Cells, greatly increasing the layouts size.

Furthermore, given the shared well of the NMOS devices, it was not possible to connect each NMOS back-gate to a specific node. Given so, the LPST NMOS transistors back-gates were connected to the ground, as shown in Fig 4.9.

Figure 4.9: Original and modified Low Power STs (LPST) side-by-side

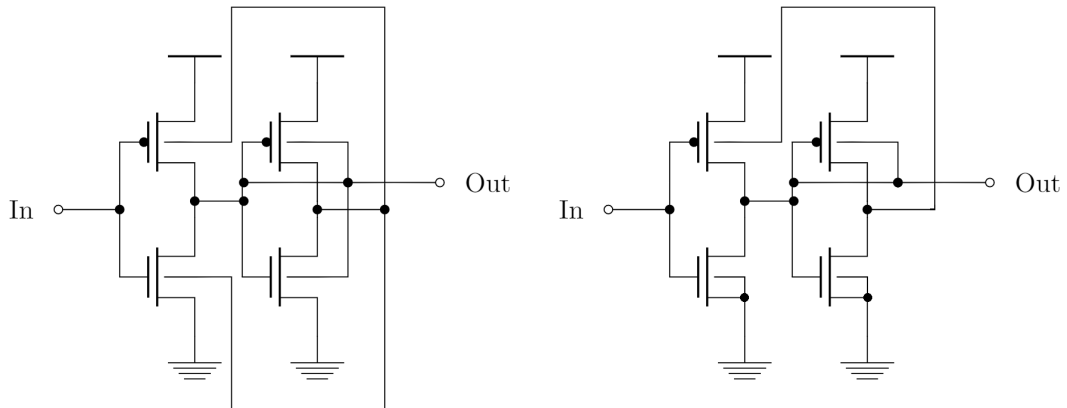


Table 4.3: Parameters applied in the electrical simulations

Parameter	7nm	
Nominal Supply Voltage	0.7 V	
Gate Length (LG)	21nm	
Fin Width (WFIN)	6.5nm	
Fin Height (HFIN)	32nm	
Oxide Thickness (TOX)	2.1nm	
Channel Doping	$1 \times 10^{22} m^{-3}$	
Source/Drain Doping	$2 \times 10^{22} m^{-3}$	
Work Function (eV)	NFET PFET	4.372 4.8108

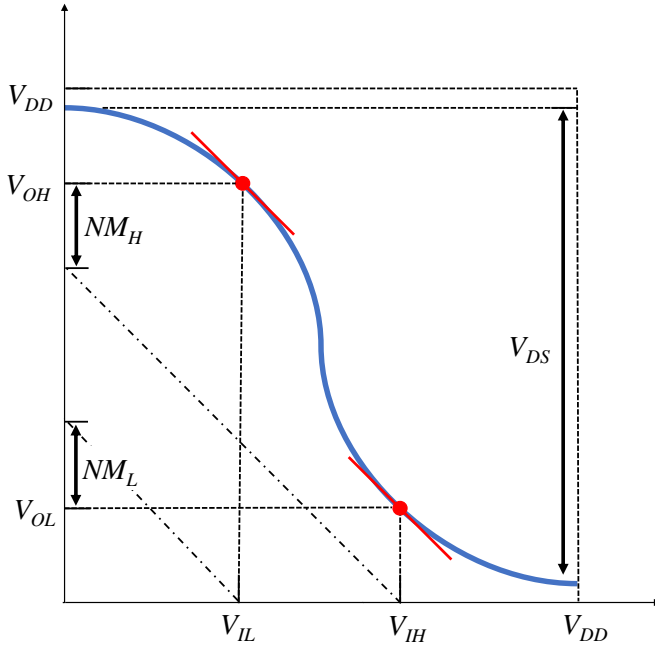
Source: Clark et al. (2016)

4.2 Electrical Simulation

The simulations will be carried out in HSPICE ¹ using the netlist obtained after the physical verification flow and the parasitic capacitances extraction. The deviation on the device geometry impacts the electrical parameter WF causing high fluctuations (MORAES et al., 2018a). It happens due to the orientation of metal grains randomly aligned in FinFET manufacturing process. In this way, WFF represents the most significant variation beyond the other parameters (MEINHARDT; ZIMPECK; REIS, 2014). The process variability evaluation will be taken through 2000 Monte Carlo (MC) simulations (ALIOTO; CONSOLI; PALUMBO, 2015b) varying the WF of devices according to a Gaussian distribution considering a 3σ deviation. The reference values from ASAP7 technology for electrical simulations are shown in Table 4.3.

¹<https://www.synopsys.com/>

Figure 4.10: Noise margins measurements.



Source: Schrom, De and Selberherr (1997).

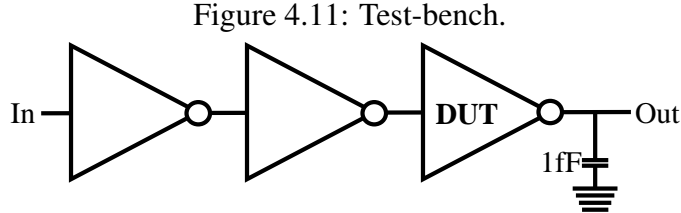
4.2.1 Inverters evaluation

The WFF level for all simulations will range from 1% to 5% with 1% steps on nominal values (NAWAZ et al., 2014). For each step on WF variation, all simulations will be carried from 0.1V to 0.7V supply voltage, with 0.1V steps. For all experiments, it will be observed mean (μ), standard deviation (σ) and normalized standard deviation (σ/μ) for each metric: hysteresis interval, propagation times, energy, and on and off currents. The σ/μ represents the sensibility of the cell to process variability, where the lower it is, highest is the robustness of the circuit to the impact of process variability.

The energy was calculated by integrating the current through time and multiplying by the supply voltage, and the propagation times were calculated by the timing difference between input and output signals to reach 50% of its value ($V_{DD}/2$). Additionally, noise margins, gains and VTC curve slopes will be presented. The noise margins were calculated as shown in Fig. 4.10 where the margin values are extracted from the VTC curve points where the derivative/slope is -1. The slopes were calculated following the equation 4.1, based on Fig. 4.10.

$$\text{Slope} = \frac{V_{OH} - V_{OL}}{V_{IH} - V_{IL}} \quad (4.1)$$

For the maximum frequencies, each time there was 10% or more of failed simu-



Source: From the author.

lations, from the 2000 MC, the frequency was decreased. On the contrary, if there was less than 10% of failures, the frequency was increased. At each increase/decrease the simulations were performed again. The minimum frequency considered for the circuit to be considered functional at determined sizing, supply voltage, and level of variability is 50KHz. This frequency was chosen to save resources and bring a wide frequency range.

For a more realistic test-bench, it will be considered a scenario where the Device Under Test (DUT) receives the signal passing through two inverters in series and having a 1fF output capacitance, as shown in Fig. 4.11. It is essential to consider some details such as: the same supply voltage is applied in the entire testbench, only the DUT suffers from variability, the inverters are the same (3-fins transistors) for all experiments, and they are, like the DUT, simulated from the extracted layout.

4.2.2 ST technique on Full Adders

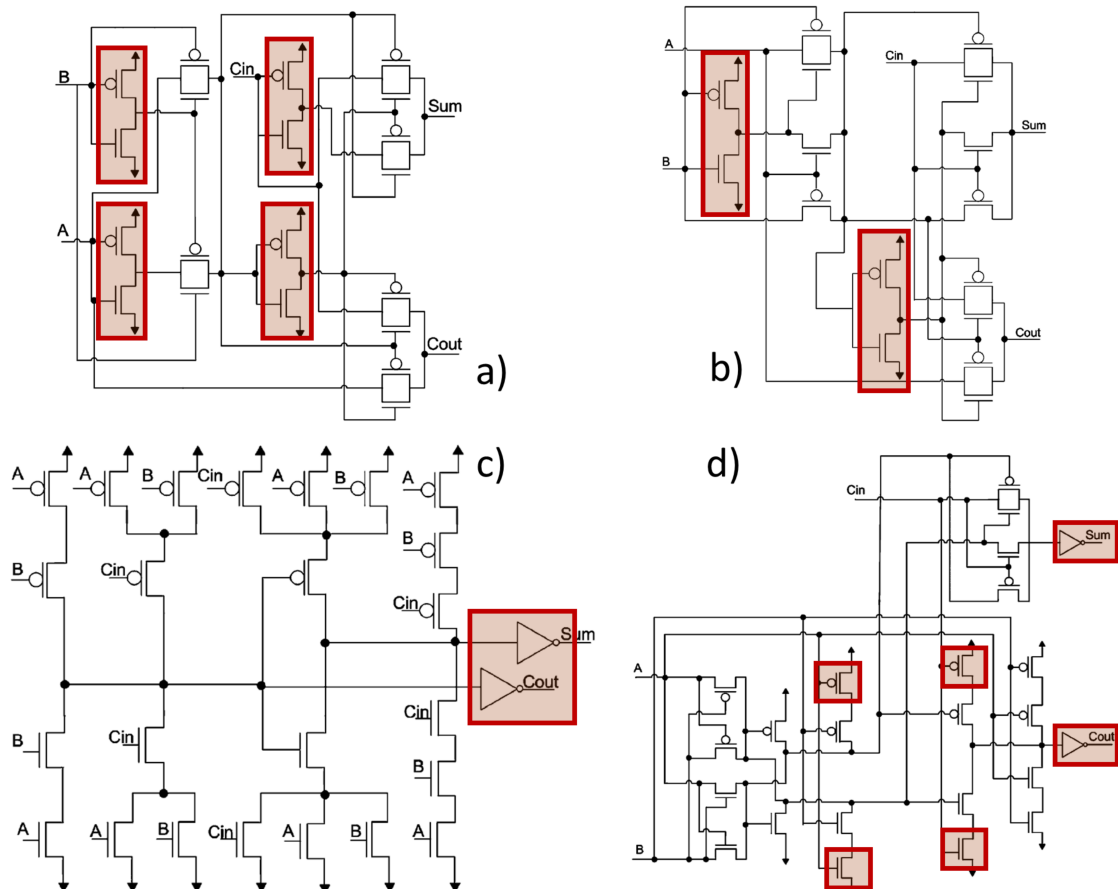
To provide an analysis of the impact of the replacement of FAs internal inverters with STs, it was considered four different types of Full Adders topologies to evaluate their robustness to process variability. In order to analyze such impact:

- 1) All FAs will be analyzed with the same sizing of 3 fins;
- 2) Each FA will have 3 versions: the traditional (internal inverters not replaced), the FA with its internal inverters replaced by LPST, and the FA with its internal inverters replaced by the 6TST.
- 3) It will be considered only one level of variability of 5% WFF, following a Gaussian distribution.
- 4) There will be considered two level of supply voltage: nominal (0.7V) and near-threshold (0.4V).

The Full Adders listed below have been chosen due to their promising results in related and previous works (AMES et al., 2016; DOKANIA; ISLAM, 2015; DOKANIA; IMRAN; ISLAM, 2013; MORAES et al., 2018). All FAs designs are shown in Fig. 4.12:

1. Complementary MOSFET Mirror Adder (Mirror)
2. Transmission Gate Adder (TGA)
3. Transmission Function Adder (TFA)
4. Hybrid Full Adder

Figure 4.12: Full Adders with internal inverters to be replaced highlighted. Transmission Gate Adder (a), Transmission Function Adder (b), Mirror CMOS Adder (c) and Hybrid Full Adder (d).



Source: Toledo, Zimpeck and Meinhardt (2016)

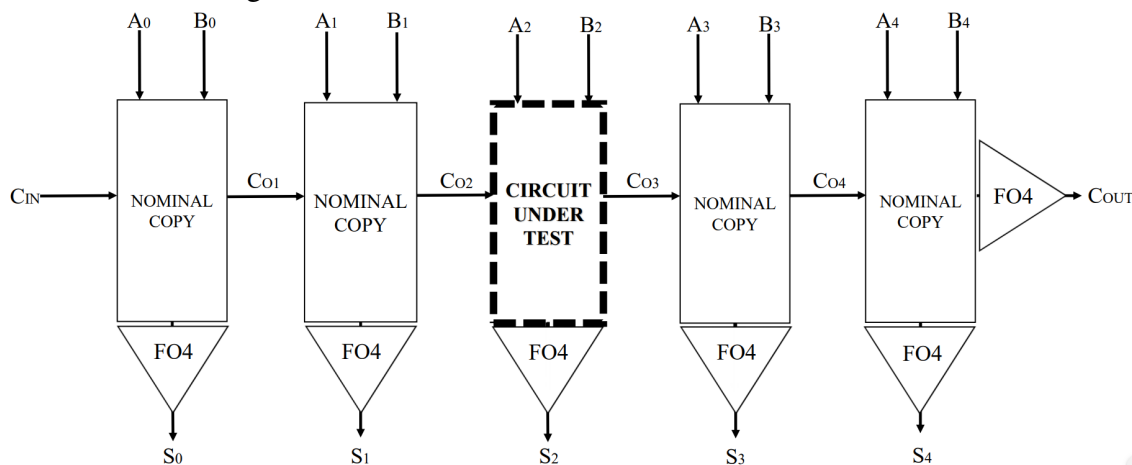
The Mirror Full Adder is considered the most traditional Full Adder topology containing 28 Transistors arranged in a pull-up and pull-down networks, which are logically complementary. It has a full voltage swing and buffered Sum and Cout signal and the advantages of good conductibility and robustness when working with novel technologies and low voltages. However, it has high capacitance because each input is connected to the gate of at least a p-channel metal-oxide-semiconductor (PMOS) and n-channel metal-oxide-semiconductor (NMOS) device additionally, it shows the impact of the pull-up network that makes the circuit slower due to the low mobility of its holes (BECKETT, 2002) (DEVADAS; KISHORE, 2017) (ISLAM; HASAN, 2011).

Transmission Gate Full Adder (WESTE; ESHRAGHIAN, 1985) contains 16 transistors, and is a high speed and low power design. However, shows low driving capability which may be unacceptable in some cases where there is a long chain of full adders due to the increase in delay (ISLAM; HASAN, 2011). The Transmission Function Adder is based on transmission gates as well, containing 20 transistors, working satisfactorily with low voltages but losing performance when cascaded due to the lack of supply/ground contacts and, consequently, driving capability (NAVI et al., 2009). Both TFA and TGA generate the XOR function ($H = A \text{ XOR } B$) followed by an inverter which produces the XNOR function (H'). H and H' are used to control the transmission gates generating the Sum and Cout outputs. The inverter generates delay between H and H' , which will cause the transmission gates to behave as pass transistors, that may introduce glitches and consequently, increase the power consumption of these cells. Additionally, TGA contains three inverters, one more than TFA. The inverters switching introduce more short-circuit power (SHAMS; BAYOUMI, 2000).

Inspired by CMOS and CPL Full Adders architectures, the Hybrid Full Adder (NAVI et al., 2009) contains 26 transistors, with the main advantage of a high output signal and low power properties. Although, the design shows high input capacitance for specific input vectors.

For the simulations concerning the Full Adders, it was considered two levels of supply voltage, near-threshold (0.4V) and nominal (0.7V) and single level of WFF level of 5%. For the metrics, it was considered the mean, standard deviations, and normalized standard deviations for the energy and delay measures. The test-bench applied consists of a 5-bit Ripple Carrier Adder with each output (Sum outputs for each FA and last

Figure 4.13: Test-bench for the Full Adders simulation.



Source: From the author.

Carry Out) connected to a fan-out of 4 inverters, as shown in Fig 4.13. In order to extract the delay and energy measures, an input vector was applied to trigger a pair of transitions (high-to-low and low-to-high) for each output (Sum and Carry Out) in relation to each input (A, B and C).

Each FA area is shown in Table 4.4 where the LPST and traditional 6T ST are renamed as ST1 and ST2, respectively. All FAs layouts were designed with a dense 7.5 M2 (Metal 2) track cell, baseline resulting in a 270nm cell height. This corresponds to three fins for each transistor. All FA layouts are shown in Annex C.

Table 4.4: Each Full Adder area with the ST technique applied where ST1 and ST2 corresponds to the LPST and 6T ST, respectively.

Full Adder	# Transistors	Width (nm)	Area (nm ²)	Ratio
Mirror	28	1,188	320,760	-
Mirror ST1	32	2,808	758,160	2.36
Mirror ST2	36	1,836	495,720	1.55
TGA	20	1,836	495,720	-
TGA ST1	28	5,292	1,428,840	2.88
TGA ST2	36	2,916	787,320	1.59
TFA	16	1,620	437,400	-
TFA ST1	20	3,240	874,800	2.00
TFA ST2	24	2,052	554,040	1.27
HYBRID	26	1,728	466,560	-
HYBRID ST1	34	5,292	1,428,840	3.06
HYBRID ST2	42	2,916	787,320	1.69

Source: from the author.

5 EVALUATION OF ST CIRCUITS AND ALTERNATIVES

The analysis of the behaviour of several inverter under the effects of process variability will be divided in sections concerning the metrics. The first section will be about the maximum frequency reached by each design depending on the supply voltage and the level of process variability and the scenarios, sets of supply voltage and level of variability, at which the frequency did not remain above 50KHz. The second section will lay out the propagation times, since the frequency already gives a good notion about the circuits performance, this section will show the propagation times deviations, presenting each design behavior.

The third section will lay the results concerning the energy consumption and deviation. The designs will be compared to one another and the impact between each supply voltage and number of fins will be considered. Additionally, considering different types of applications - minimum energy, highest robustness, and cost-benefit - different sets of supply voltages and transistor sizing will be recommended for each level of variability, where patterns are identified. The currents and current ratios will be discussed in the forth section, where measures and deviations will be shown, as well the increase scaling through the variability levels. Further on, SNM measures, output gains and slopes, hysteresis, and measures histograms will be discussed at the fifth, sixth, seventh, and eighth sections, respectively.

5.1 Non-viable scenarios and Frequencies

Across the simulations, as the variability level scaled and supply voltage decreased, to maintain the percentage of failures below 10%, the circuits frequency had to be reducted. For the traditional inverter, ST, and SIG, the considered *non-viable* scenarios (when the viable frequency of operation is below or at 50KHz) started to appear at 200mV, for any scenario above 4% WFF, and 100mV for any scenario above 5% WFF.

The TIST presented a particular behavior, with its hysteresis interval growing too large as supply voltages got higher. The TIST got the same subset of *non-viable* scenarios of the previous designs, although due to its hysteresis, sub- to near-threshold supply voltages did not work properly.

The TIST 2:1 designs did not present any viable scenarios at 200mV and 300mV, with only low-variability scenarios (1% and 2% WFF) working at 0.4V and 0.5V. The

Table 5.1: All scenarios frequencies.

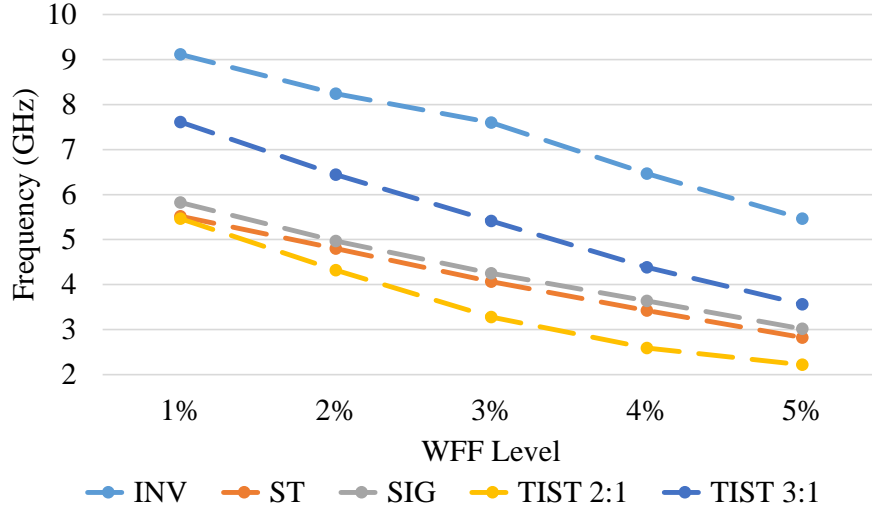
Design	WFF	Supply Voltage (V)						
		0.1	0.2	0.3	0.4	0.5	0.6	0.7
INV	Nom.	6MHz	160.7MHz	2.1GHz	9.42GHz	15.2GHz	20.5GHz	24.5GHz
	1%	2.18MHz	49.4MHz	1.12GHz	6.5GHz	13.6GHz	19.1GHz	23.4GHz
	2%	510KHz	15.4MHz	504MHz	4.95GHz	12GHz	17.9GHz	22.3GHz
	3%	-	4.79MHz	149MHz	4.86GHz	10.3GHz	16.6GHz	21.3GHz
	4%	-	-	47.2MHz	1.77GHz	8GHz	15.1GHz	20.3GHz
	5%	-	-	17.8MHz	360MHz	5.2GHz	13.5GHz	19.2GHz
ST	Nom.	2.35MHz	59.7MHz	1.29GHz	6.84GHz	14.6GHz	21.2GHz	16.7GHz
	1%	930KHz	22MHz	510MHz	3.2GHz	7.8GHz	12GHz	15.1GHz
	2%	192KHz	7.2MHz	210MHz	2.3GHz	6.3GHz	10.7GHz	14.1GHz
	3%	-	2.39MHz	74.2MHz	1.3GHz	5GHz	9GHz	13.1GHz
	4%	-	-	28.4MHz	550MHz	3.7GHz	7.9GHz	1.11GHz
	5%	-	-	4.6MHz	170MHz	2.2GHz	6.7GHz	10.7GHz
SIG	Nom.	2.65MHz	60.8MHz	1.21GHz	6.4GHz	9.84GHz	13.8GHz	17GHz
	1%	1.02MHz	23.8MHz	540MHz	3.5GHz	8.2GHz	12.6GHz	15.9GHz
	2%	268KHz	7.4MHz	216MHz	2.45GHz	6.6GHz	10.7GHz	14.8GHz
	3%	-	2.34MHz	71.4MHz	1.25GHz	5.5GHz	9.7GHz	13.2GHz
	4%	-	-	20.8MHz	540MHz	4GHz	8.5GHz	12.4GHz
	5%	-	-	5MHz	150MHz	2.2GHz	7.3GHz	11.5GHz
TIST 2:1	Nom.	4.23MHz	90MHz	2.33GHz	3.48GHz	9.65GHz	15.3GHz	19.4GHz
	1%	833KHz	-	-	783MHz	6.37GHz	13.3GHz	17.8GHz
	2%	142KHz	-	-	-	2.86GHz	10.9GHz	16.5GHz
	3%	-	-	-	-	-	8.17GHz	14.8GHz
	4%	-	-	-	-	-	4.93GHz	13.2GHz
	5%	-	-	-	-	-	4.33GHz	11.2GHz
TIST 3:1	Nom.	5.18MHz	118MHz	2.8GHz	10.5GHz	13.3GHz	18.7GHz	22.6GHz
	1%	1.3MHz	5.5MHz	175MHz	3.3GHz	11.2GHz	17.3GHz	21.3GHz
	2%	275KHz	-	-	600MHz	8.51GHz	15.7GHz	20.3GHz
	3%	-	-	-	-	5GHz	13.9GHz	19GHz
	4%	-	-	-	-	1.1GHz	11.8GHz	17.8GHz
	5%	-	-	-	-	-	8.65GHz	16.3GHz

TIST 3:1 designs presented a slight improvement with viable scenarios at 200mV and 300mV at 1% WFF. For 0.4V and 0.5V the TIST 3:1 presented to be more viable, although not working at high to medium level of variability (3% 5% WFF). The frequencies for each scenarios are shown at Table 5.1.

Comparing each circuit frequencies to the inverter, it can be noted the fairly lower frequencies of the ST, SIG, TIST 2:1 designs. On average, those designs maximum frequencies stayed at about half the inverter frequency (47.61%, 50.5%, and 49.71%, respectively). The TIST 3:1, due to its wider transistors, capable of higher currents, less resistance, and lower hysteresis (as will be shown further on) presented on average 65.72% of the inverter frequencies. The difference between the other designs and the traditional inverter is higher at near and sub-threshold supply voltages.

The decrease in the operating frequencies of the inverters, in comparison to the traditional CMOS inverter is mainly due to the hysteresis effects of the ST and TIST

Figure 5.1: Frequency decrease over variability scaling for each design.



Source: From the author.

designs and the higher parasitics present in designs with a higher number of transistors, vias, and wire length.

Furthermore, the frequencies decrease over variability level scaling is due to the effects of threshold voltage variations into the circuits behavior. There are scenarios where, due to variability, the threshold voltage will increase, making the transistor switching process slower. Given so, the frequency at which the circuit is working must englobe the worst-case scenarios.

A robust design must maintain its frequency level as high as possible even as variability arises. For this reason, considering the impact of variability on the frequency retention, the inverter, ST, SIG, TIST 2:1, and TIST 3:1 presented 40.03%, 48.81%, 48.2%, 59.4%, and 53.17% average frequency decrease. The decrease is calculated comparing a best-case scenario (1% WFF) with a worst case scenario (5% WFF) circuit frequency at the same supply voltage. The frequency decrease over the variability levels is shown at Fig. 5.1.

When isolating the influence of the number of fins and supply voltage over the frequency behavior over variability, it can be observed clear advantages for sizings above 1 fin and supply voltages above 300mV. From 1 fin to 2 fins it was observed an increase of 10.62% over frequency retention, although above 2 fins, the increase on retention for each extra fin kept steady at 0.77%. For the supply voltage, each 100mV increase from 0.1V to 0.3V increased the frequency retention by 3.66%, while each 100mV increase from 0.3V to 0.7V improved the frequency retention by 13.79%, on average. Given so, if performance is a priority, the number of fins should be kept above 2, and if trying to

improve robustness, the increase of supply voltage from 100mV to 300mV will not provide considerable gains.

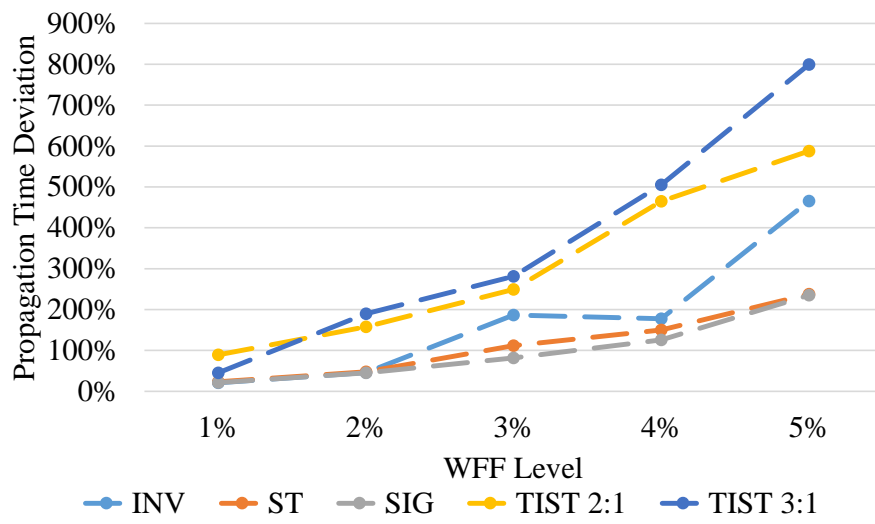
5.2 Propagation Times

Related to the frequencies, the propagation times will deviate according to the threshold voltages variations and its effects into the currents. Propagation times deviations will directly influence the circuit frequency, increasing the time guardband necessary to include the worst cases at the circuit frequency.

Given so, propagation times deviations for each design, in comparison to the inverter was 36.36% and 43.21% lower, for the ST and SIG, while the TIST 2:1 and 3:1 designs presented 72.89% and 103.26% higher deviations, as shown in Fig. 5.2. These results are calculated considering the normalized deviation for all scenarios, even the ones where the design did not work properly, to not deflate the results for the TIST designs.

Calculating the average normalized deviations only considering the cases where each design works properly puts the inverter at the lowest normalized deviation while the ST, SIG, TIST 2:1, and TIST 3:1 presented 8.54%, 7.04%, 146.15%, and 36.28% higher sensitivities. By calculating the average normalized deviation this way, a fair comparison can be made between designs, given that only the subset of scenarios where all designs work is considered.

Figure 5.2: Propagation times deviation for each design in relation to the WFF level considering all scenarios.



Source: From the author.

5.3 Energy Consumption and Deviation

For a circuit operating on a battery-oriented application or even, making use of energy harvesting methods to power itself up, the energy consumption should be stable. Deviation in energy consumption will influence the device battery-life and even leave energy-harvesting circuits non-operational. In addition, the energy consumption absolute value should be as minimal as possible, to preserve battery lifetime and make energy-harvesting methods feasible.

Among the considered inverter designs, when comparing average energy consumption measures for the scenarios where each design worked properly, the ST and SIG presented 173.07% and 50.74% higher energy consumptions than the inverter, while the TIST 2:1 and 3:1 designs presented 480.68% and 310.83% increases. With energy being a factor of propagation times (and consequently the frequency) and power drawn from the supply rails, there are factors that will specifically influence the circuit propagation times or the power consumption. Influencing the propagation times, there is the transistor count, increasing the circuits parasitics which increases its time to properly charge/discharge its signal and, for the circuits that present it, the hysteresis effects will make the circuit take longer to change its output value, decreasing its frequency. And influencing the power consumption, a by-product of how much current is being drawn from the supply rail.

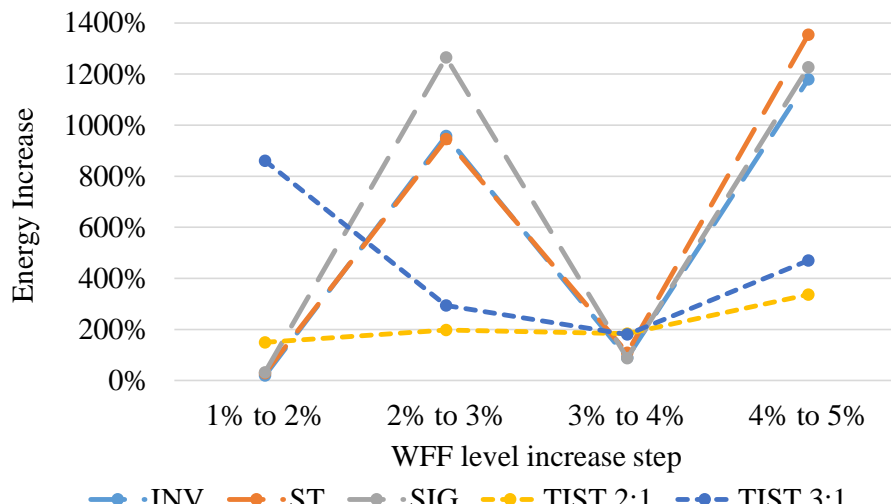
When comparing the average energy consumption measures for all scenarios, in comparison to the inverter, the ST and SIG presented 174.21% and 95.84% higher energy consumption, while the TIST 2:1 and 3:1 designs presented 1303.38% and 993.77% increases. This result shows the much higher impact of variability in the cases where the circuits could not work at the minimum frequency of 50KHz, for the SIG and TISTS designs. Given the larger transistor count, the hysteresis effect, and the number of paths from source to ground, it is expected an ascending increase from the inverter, SIG, ST and TIST designs energy consumption.

Isolating each variable, the impact of each extra fin start from a maximum of 145.75% increase from 1 to 2 fins to 18.7% from 4 to 5 fins, with diminishing energy increases alongside the number of fins. The higher increase at a lower number of fins is due to the higher relative increase in transistor area, given that from 1 to 2 fins the area is doubled, while from 4 to 5 fins the area increases by 25%, with the SIG presenting the lowest increase overall.

Considering each level of variability, in average, there was a maximum energy

increase of 652.86%. Although, this result is inflated due to two peaks in energy increase at 3% and 5% WFF level as shown in Fig. 5.3. Those peaks are due to the increase in non-viable scenarios (cases that present a 10% failure rate of the Monte Carlo simulations at the minimum stipulated frequency) at each of the peaks WFF level. When considering only the viable scenarios, the energy increase for each WFF step is 15.16%, 35.61%, 20.94%, 9.04%, and 7.18% for the inverter, ST, SIG, TIST 2:1 and 3:1, respectively.

Figure 5.3: Energy increase for each WFF level step.



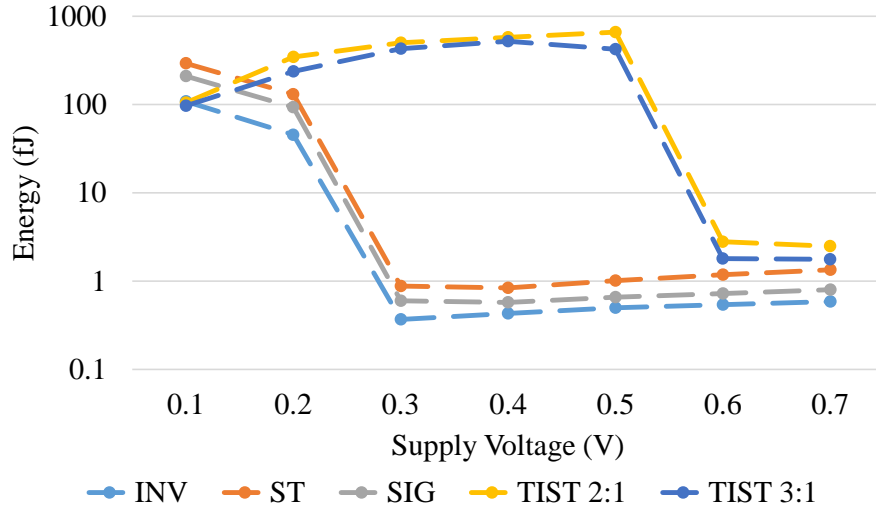
Source: From the author.

The impact of supply voltage on the energy consumption is shown at 5.4. Highlighted in blue, for the inverter, ST, and SIG, and in red, for the TIST 2:1 and 3:1, respectively, are the clusters of scenarios operating at the minimum frequency due to the variability impact. As shown, there are up to 2-order magnitude increases due to the decrease of supply voltage, revealing sub-300mV supply voltage operations to be highly susceptible to the variability effects.

Depending on the focus of the application, there could be several kinds of objectives. Overall, for low power applications, the focus should be on circuit designs directives to achieve circuits with the minimum energy consumption possible. Much of these directives aims the decrease of currents, like the increase of the transistors channel length and the decrease of supply voltages. Although, such techniques will further decrease the circuits robustness to the effects of variability and radiation.

Given so, trying to achieve a balance between given applications three types of analysis were performed, where the most appropriate subset of characteristics involving transistor sizing and supply voltage for each level of process variability is identified for the 1) lowest energy consumption, 2) highest robustness to the effects of process variability

Figure 5.4: Energy measures in function of the supply voltage for each design.



Source: From the author.

and 3) the most Cost-Benefit (CB). The lowest energy layout is identified through the energy measures - product of the supply rail drained current through the simulation and the supply voltage. The higher robustness layout is identified by the lowest normalized standard deviation concerning energy consumption, and the CB layout is identified by the lowest value considering the product between the energy consumption and normalized standard deviation (EDP - Energy Deviation Product). The results are shown at Table 5.2. Some results will show more than one appropriate layout/supply voltage to provide flexibility, considering values up to 5% higher than the minimum considered value.

It is possible to identify patterns concerning the minimum energy and highest robustness layouts. The minimum energy layouts, as a general rule, will contain only few fins, if not only one, and lower supply voltages. Both low values aim to lower currents and increase resistance, therefore decreasing energy consumption. As variability rises, the supply voltage rises as well. That is due to the lower frequencies applied in those scenarios and the consequent increase on propagation times, given that energy is the by-product of power and time. A higher supply voltage will decrease propagation times followed by a decrease on energy consumption. The TIST designs present a steep increase on supply voltage, from 0.1V to 0.6V/0.7V due to the lack of possible mid-term (0.2V to 0.5V) viable scenarios.

The robust layouts present a shift on supply voltage. At low variability scenarios (1% to 3%) the nominal supply voltage will persist at nominal value (0.7V). As the variability level rises, the supply voltage will abruptly fall into near-threshold region (300mV to 400mV) and increase, as the variability level increases as well.

Table 5.2: Recommended layout and supply voltage for each design and variability level.

Design	WFF	Minimum Energy		Highest Robustness		CB	
		Supply (V)	#Fins	Supply (V)	#Fins	Supply (V)	#Fins
INV	1%	0.1	1 or 2	0.7	1	0.7	1
	2%	0.1	1	0.3	4 or 5	0.2	2 to 4
	3%	0.2	1	0.3	5	0.3	3 to 5
	4%	0.3	1 or 2	0.4	5	0.4	5
	5%	0.3	1	0.4	1	0.4	1
ST	1%	0.1	1	0.7	5	0.7	1
	2%	0.2	1	0.7	5	0.7	1
	3%	0.2	1	0.7	4 or 5	0.3	1
	4%	0.3	1	0.4	2	0.4	1 or 2
	5%	0.4	1	0.5	2 to 5	0.5	1 or 2
SIG	1%	0.1	1	0.7	2	0.7	1
	2%	0.2	1	0.3	3 or 4	0.7	1
	3%	0.2	1	0.3	3	0.3	1
	4%	0.3	1	0.4	3	0.4	2 or 3
	5%	0.4	1	0.5	2 or 3	0.5	2
TIST 2:1	1%	0.1	2F1F	0.7	4F2F	0.7	2F1F
	2%	0.1	2F1F	0.6	4F2F	0.6	2F1F
	3%	0.7	2F1F	0.6	2F1F	0.6	2F1F
	4%	0.7	2F1F	0.7	4F2F	0.7	2F1F
	5%	0.7	2F1F	0.7	6F3F	0.7	2F1F
TIST 3:1	1%	0.1	3F1F	0.7	6F2F	0.7	3F1F
	2%	0.1	3F1F	0.7	6F2F or 3F1F	0.7	3F1F
	3%	0.7 or 0.6	3F1F	0.6 or 0.7	6F2F or 3F1F	0.7	3F1F
	4%	0.7 or 0.6	3F1F	0.6	6F2F	0.6	3F1F
	5%	0.7 or 0.6	3F1F	0.6	3F1F	0.6	3F1F

The sudden fall into a near-threshold region can be explained in terms of the transistors current. When the on-current is at the saturation region, it presents an quadratic dependency over the V_T , as shown in equation 5.1, while at the linear region, the on-current presents a linear dependency over the V_T , as shown in equation 5.2 (ZEGHBROECK, 2004). Given so, as the level of variability rises, the transistor will have to fall into linear region operation to decrease the current deviations due to increasingly V_T variability.

$$I_{D,sat} = \frac{\mu_p \cdot C_{ox}}{2} \cdot \frac{W}{L} \cdot (V_{GS} - V_T)^2 \begin{cases} V_{GS} \leq V_T \\ V_{DS} \leq V_{GS} - V_T \end{cases} \quad (5.1)$$

$$I_{D,lin} = \frac{\mu_p \cdot C_{ox}}{2} \cdot \frac{W}{L} \cdot [2 \cdot (V_{GS} - V_T)V_{DS} - V_{DS}^2] \begin{cases} V_{GS} \leq V_T \\ V_{DS} > V_{GS} - V_T \end{cases} \quad (5.2)$$

where:

$I_{D,sat}$ = saturation current

$I_{D,lin}$ = linear current

μ_p = p-material electron mobility

C_{ox} = specific capacitance of the gate

W = transistor width

L = transistor length

V_{GS} = gate-source voltage

V_{DS} = drain-source voltage

V_T = threshold voltage

For the CB layouts, what can be observed is an adoption of supply voltages similar to the high robustness layouts, with an earlier adoption of near-threshold supply voltages, as variability rises, and the adoption of a fin count similar to the low energy layouts, although slightly higher. Energy consumption and deviation comparisons between each recommended layout are shown in Fig. 5.5, Fig. 5.6, Fig. 5.7, Fig. 5.8, and Fig. 5.9. The lines correspond to the energy consumption axis (left), while the bars correspond to the energy deviation axis (right).

Figure 5.5: Layout comparison for each scenario considering the energy metrics for the inverter.

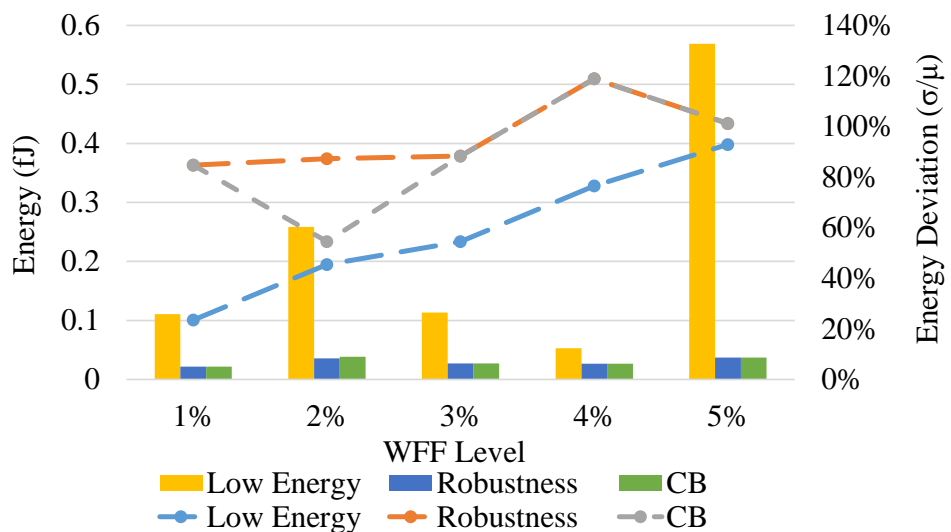


Figure 5.6: Layout comparison for each scenario considering the energy metrics for the ST.

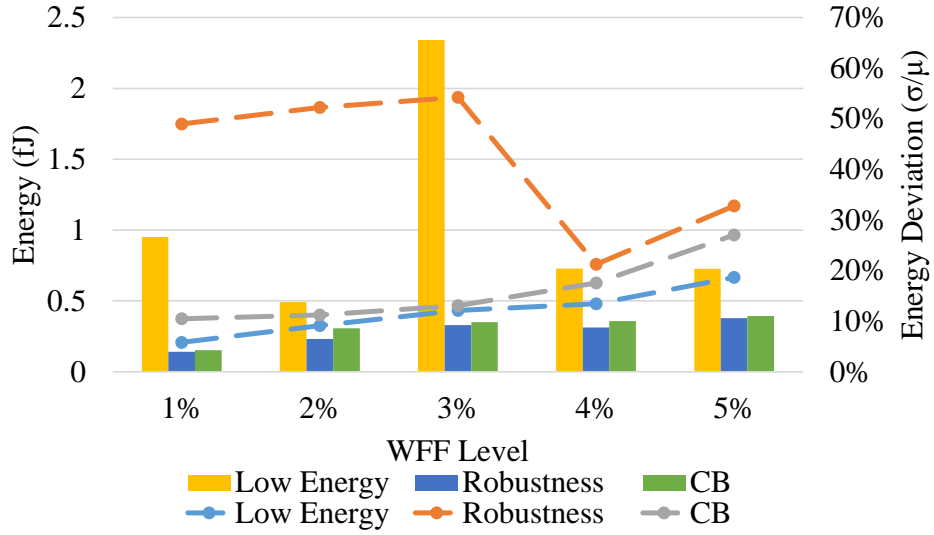


Figure 5.7: Layout comparison for each scenario considering the energy metrics for the SIG.

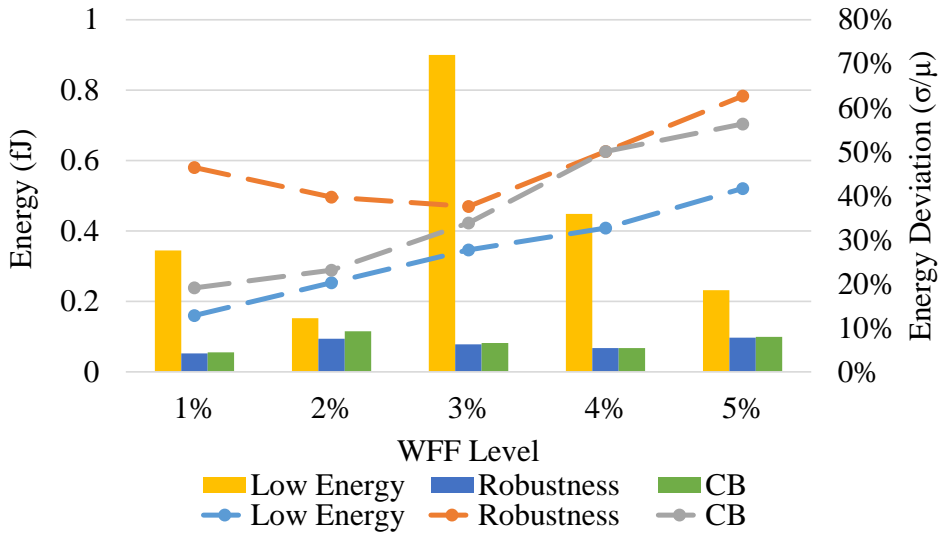


Figure 5.8: Layout comparison for each scenario considering the energy metrics for the TIST at 2:1 proportion.

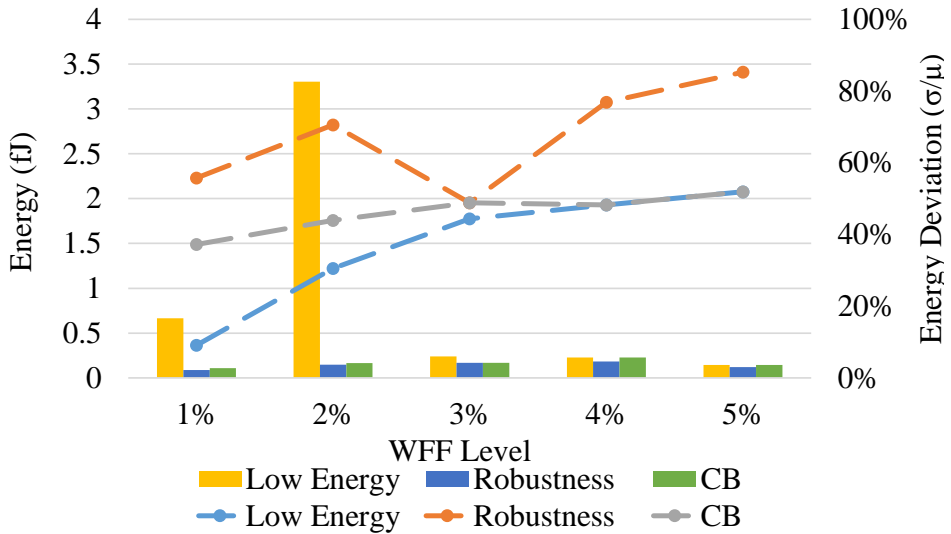
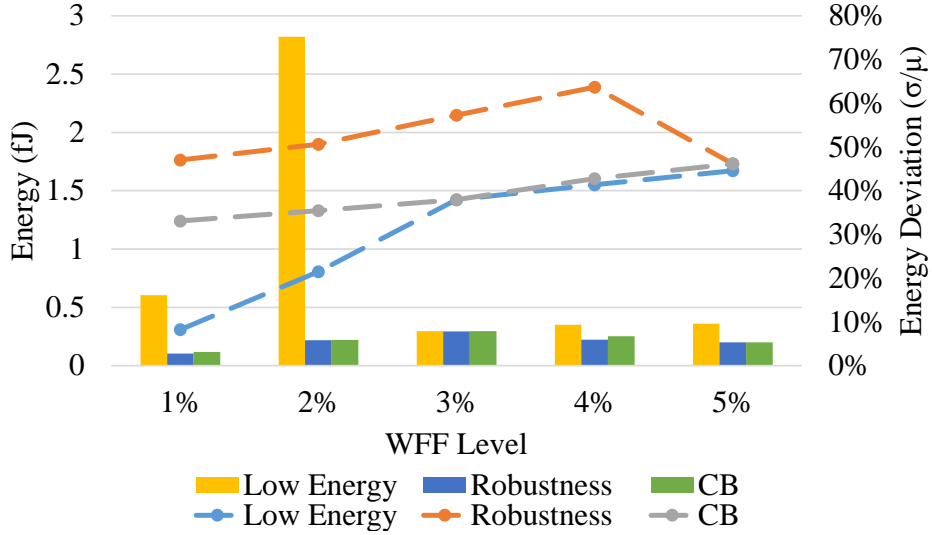


Figure 5.9: Layout comparison for each scenario considering the energy metrics for the TIST at 3:1 proportion.



A further comparison between each design layout is presented in Fig. 5.10, Fig. 5.11, and Fig. 5.12. The lines correspond to the energy consumption axis (left), while the bars correspond to the energy deviation axis (right). Considering the averages, for the low energy layouts, the inverter presented the lowest energy consumption, followed by the SIG (34.61% higher), ST (68.32% higher), TIST 3:1 (358.84% higher) and TIST 2:1 (487% higher), respectively. The TIST layouts, showed the highest robustness, with the 2:1 variants presenting a 22.93% average energy deviation and the 3:1 variants showing a minor increase with its 23.62% average energy deviation. Following the TIST layouts, the ST, SIG and inverter present a 29.34%, 33.25%, and 51.55% energy deviation, respectively. It can be noted that, while the inverter presents the lowest energy consumption it presents the highest energy deviation as well. It is mainly due to its spike on deviation at 5% WFF but even disconsidering this spike, the inverter would show an average deviation of 31.25%, which is still higher than most of the designs.

For the high robustness spectrum, the energy consumption difference between designs follows the same behaviour, although with much broader differences. In comparison to the inverter energy consumption each design presented an average increase of 43.52%, 263.24%, 382.12%, and 555.21%, for the SIG, ST, TIST 3:1, and TIST 2:1, respectively. The deviation metrics presented a similar behaviour as well, although the ST presented the highest deviations. The TIST designs presented the lowest deviations with 3.56%, and 5.55% for the TIST 2:1, and 3:1, respectively. Following, the SIG, inverter, and ST, presented 6.23%, 6.93%, and 7.81% deviations. In this case, the inverter is a strong candidate, with the lowest energy consumption, and acceptable robustness.

Figure 5.10: Low energy layouts energy metrics comparison for each design.

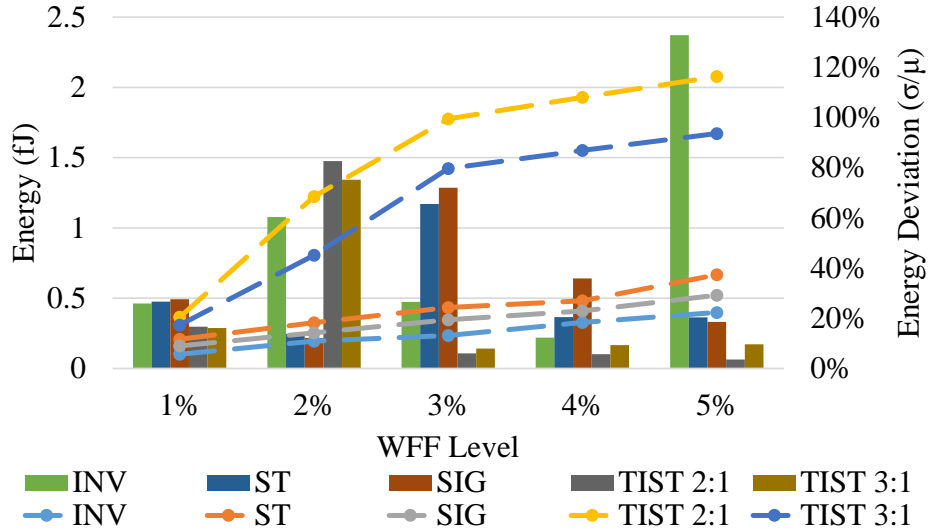
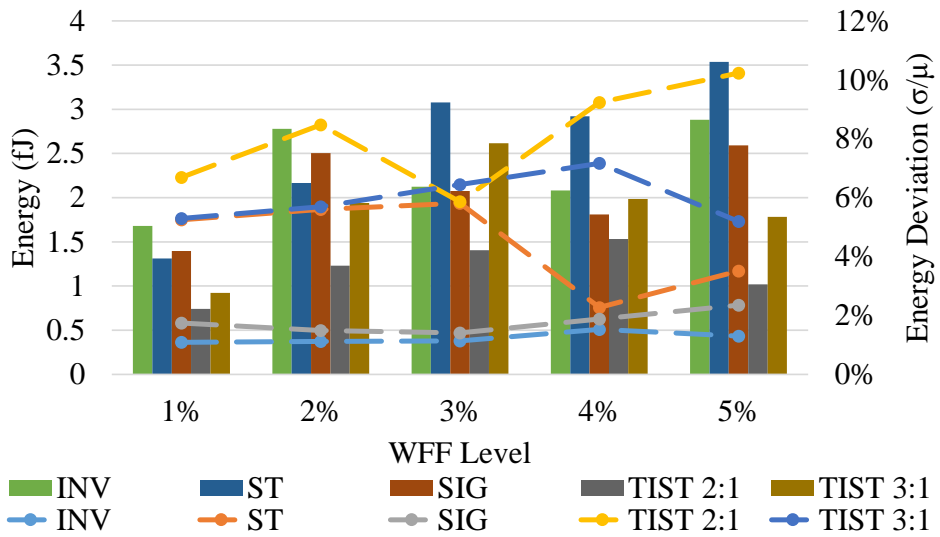


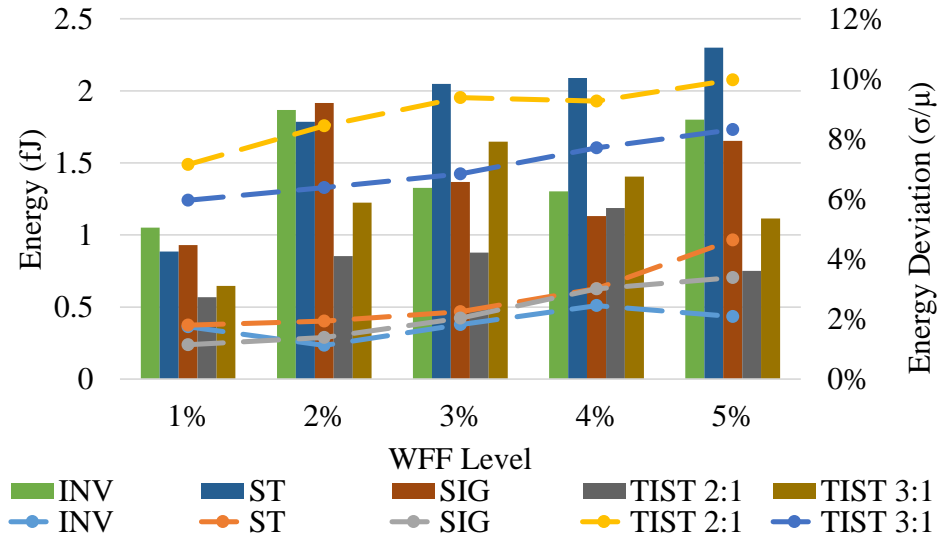
Figure 5.11: High robustness layouts energy metrics comparison for each design.



Lastly, for the CB layouts, the energy consumption scaling through the designs follows the same pattern, although with smaller differences. In comparison to the inverter, the SIG, ST, TIST 3:1, and TIST 2:1 presented average increases of 18.84%, 47.74%, 281.85%, and 379.6%. The TIST designs presented the lowest deviations with 4.07% and 5.8% for the 2:1 and 3:1 proportions, respectively. The SIG, inverter and ST, presented respectively, 6.72%, 7.05%, and 8.74% deviations on energy. In this case, the SIG, presents a higher energy consumption and much bigger layout, it only provides a minor improvement over deviations (4.91%, relative to the inverter). The ST presented higher energy and bigger area as well, with a increase on deviations (1.69%, absolute and 23.97% relative increases, in comparison to the inverter), although it still presents hysteresis. The TIST designs, consume considerably more energy, with less deviation (although, as stated

before, those numbers are deflated), bigger layout area, and less viable scenarios to work with.

Figure 5.12: CB layouts energy metrics comparison for each design.



It is shown that the CB layouts presents similar energy deviations in comparison to the high robustness layouts while maintaining a lower energy consumption, for the ST and SIG, with the exception of the inverter. The inverter presents a high deviation for its minimum energy layout at 5% WFF (1 fin layout with a supply voltage of 0.3V). Although, with a little increase on supply voltage, from 300mV to 400mV, matching the CB layout, the inverter presents a 8.95% increase on energy consumption while decreasing its energy deviation by 93.49%. The ST presented a similar results at 3% WFF where a 100mV increase, from 200mV to 300mV of supply voltage, provided a reduction of 85.01% in energy deviations while increasing the energy consumption by 7.86%. For the SIG, at 3% WFF as well, it was possible to decrease the deviation by 90.88% while increasing the energy consumption by 22.09%, with the same supply voltage increase performed for the ST. Average and maximum differences in energy consumption and deviations between CB, low energy, and high robustness layouts are shown in Fig. 5.13 and Fig. 5.14, respectively.

Figure 5.13: Energy consumption and energy consumption deviations difference between the cost-benefit and low energy layouts.

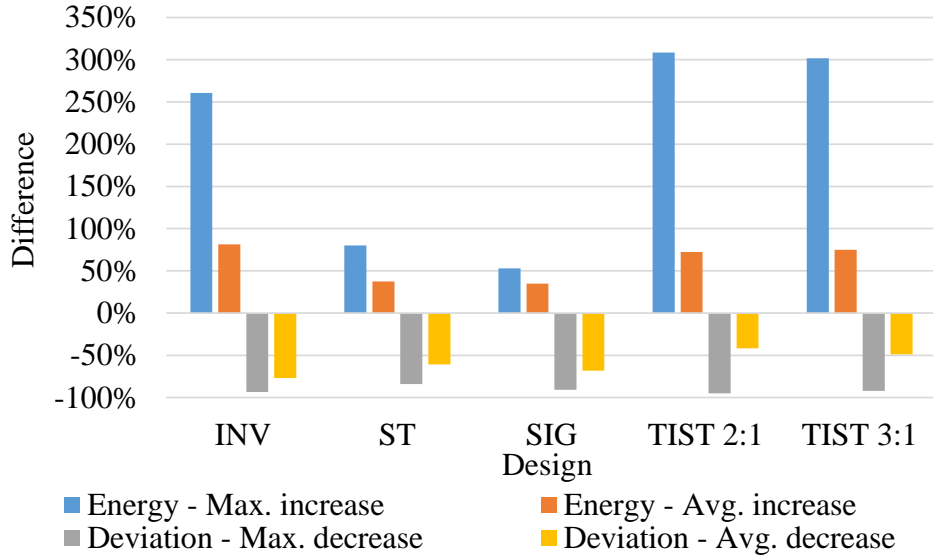
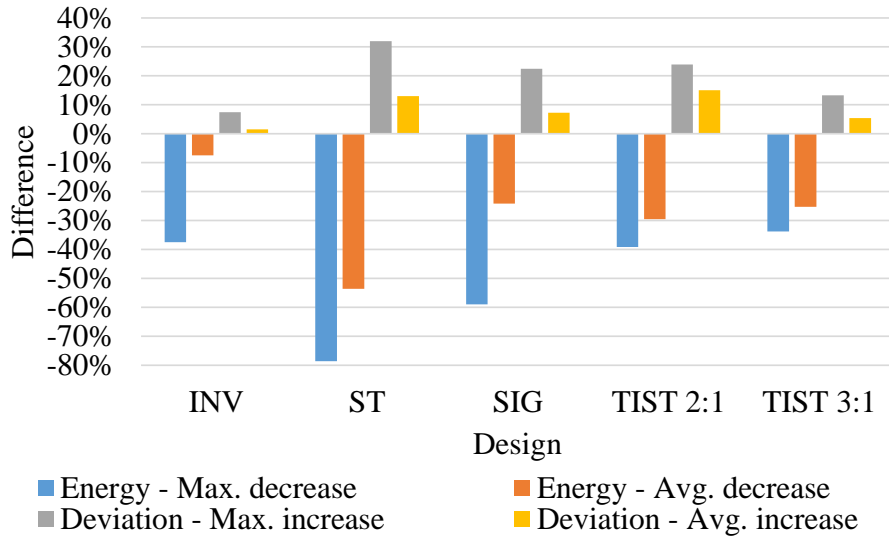


Figure 5.14: Energy consumption and energy consumption deviations difference between the cost-benefit and high robustness layouts.



At the same time, it is important to analyze the drawbacks of a CB approach. The CB layouts for inverter and TIST layouts presented higher increases on energy consumption, in comparison to the ST and SIG designs. Higher average increase is directly related to the shift of a supply voltage from 100mV to 0.7V, at 1% WFF. The supply voltage switch on the inverter is due to the considerable decrease in energy deviation (from 25.83% to 5.04%) of 5.125x, while the energy consumption increased 3.6x. For the TIST the higher energy increases are related to the lack of working scenarios at near-threshold, and the sudden increase in supply voltage, similar to the inverter. When observing the

increases in energy deviations comparing the CB and high robustness layouts, the CB layouts can bring up to 32% increase in energy deviations, although, causing an 79% decrease in energy consumption, highlighting the differences between applications.

5.4 Current Ratios

When considering the impact of process variability into the energy consumption, it will depend of the propagation times and the power consumption, and their respective deviations. Performance and power are highly dependent on the value and stability of the devices currents, either dynamic (on) and static (off). The devices delays are highly dependent on how fast can the circuit switch its value, which is related to the circuit parasitics and its dynamic current. In parallel, the circuit power, being a function of the current and resistances will suffer higher influence from current values and deviations. In order for the circuit to maintain its signals well defined, fast signal value switching, and low static power consumption, it is recommended to maintain the on and off current high and low as possible, respectively. The ideal current setup may be achieved through circuit level methods or the appropriate transistor sizing, where the length and width of the channel will be fine tuned to achieve the highest ratio possible between currents.

In order to more clearly understand the impact of process variability and supply voltage influence on current behaviour, the dynamic and static currents average measures and normalized standard deviations will be explored. The graphs are divided in two parts for each current, with average measures and normalized standard deviations. Fig. 5.15 and Fig. 5.16 present the average values and normalized standard deviations for the dynamic current. It can be observed an exponential and an overall linear dependency over supply voltage and WFF level, respectively, with the current slightly decreasing due to WFF level. Although, when considering sub-200mV supply voltages, the average dynamic current will increase exponentially as variability level scales. This happens due to the higher number of extreme cases where the worst-case measure can be up to 5-orders of magnitude higher than the average. For the normalized standard deviations of the dynamic current, there are exponential dependencies over both variables when considering low supply voltage/high variability level scenarios, with curves presenting a linear behaviour at the remaining scenarios.

Figure 5.15: Dynamic (on) current average measures through supply voltage and WFF scaling.

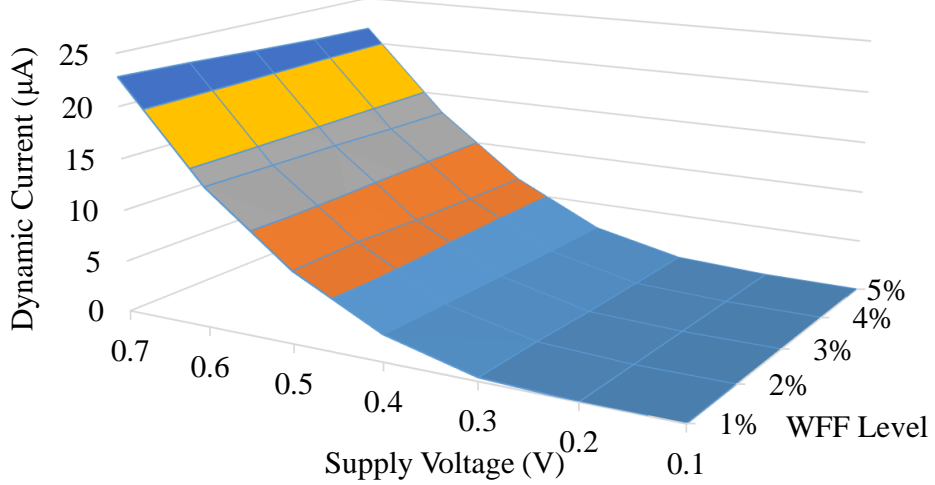


Figure 5.16: Dynamic (on) current normalized standard deviations through supply voltage and WFF scaling.

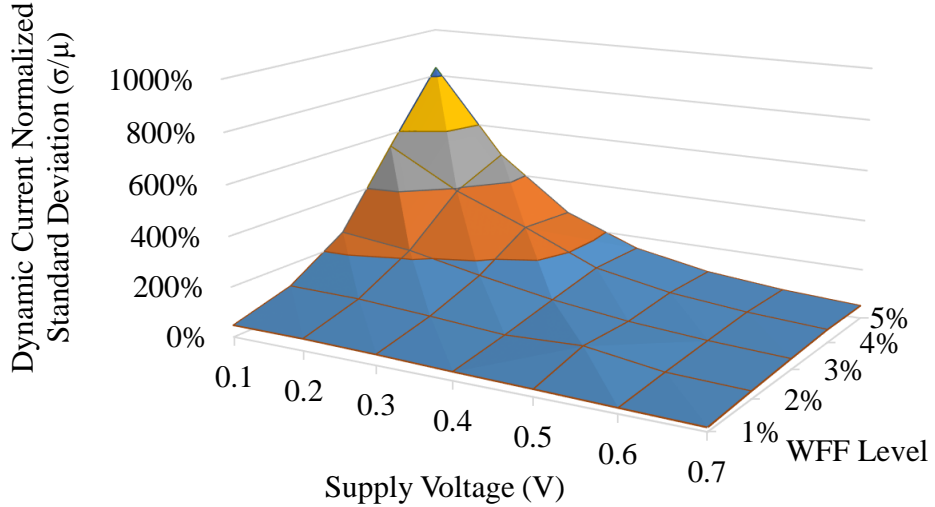


Fig. 5.17 and Fig. 5.18 present the results for the static current. The average measures will exponentially scale due to the process variability level and linearly decrease as the supply voltage scales down. The normalized standard deviations for the static current presents a linear relation with the supply voltage, with a 16% difference between the lowest and highest average normalized deviations, and a exponential dependency over variability level, with averages doubling at each WFF level increase step.

Figure 5.17: Static (off) current average measures through supply voltage and WFF scaling.

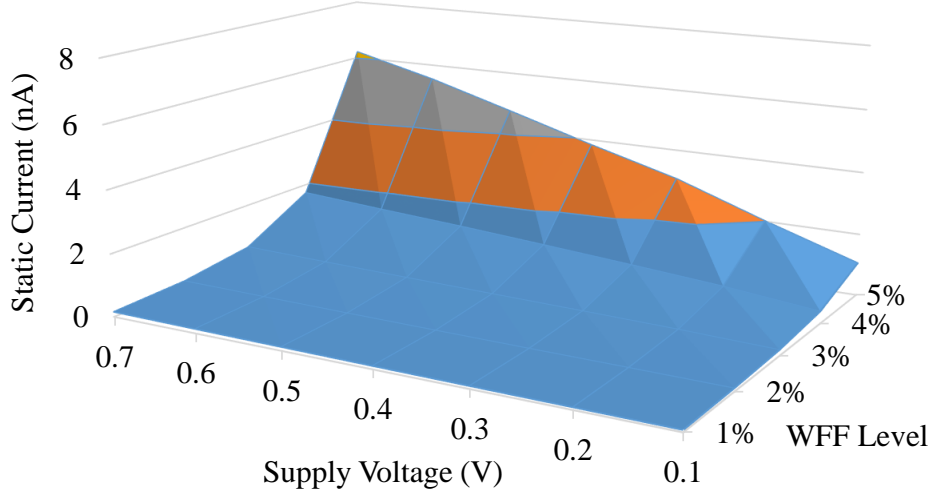
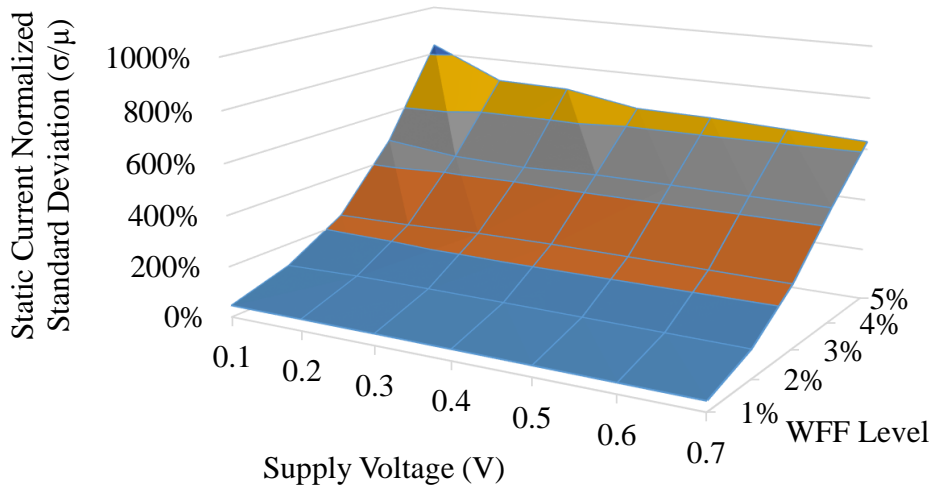


Figure 5.18: Static (off) current normalized standard deviations through supply voltage and WFF scaling.



As shown in Fig. 5.19, due to the linear and exponential dependency of the dynamic and static current measures upon the variability level, the static current presents a much higher scaling factor, in comparison to its counterpart. Given so, the current ratios will present a decrease as the process variability level increases, as shown in Fig. 5.20. Comparing to the inverter, the ST, TIST 2:1, and TIST 3:1 presented, on average, 118.01%, 600.21%, and 468.7% higher ratios. The SIG is the only design which presented a worsening, with a 12.53% lower ratio. While considering deviations into the ratio due to process variability, the ST and SIG presented 11.1% and 6.91% lower deviations, with the TIST 2:1 and 3:1 presenting 49.57% and 42.79% higher deviations, respectively.

Figure 5.19: Average on and off-current increase over all designs through variability scaling. The scaling is normalized in relation to the 1% WFF level measures.

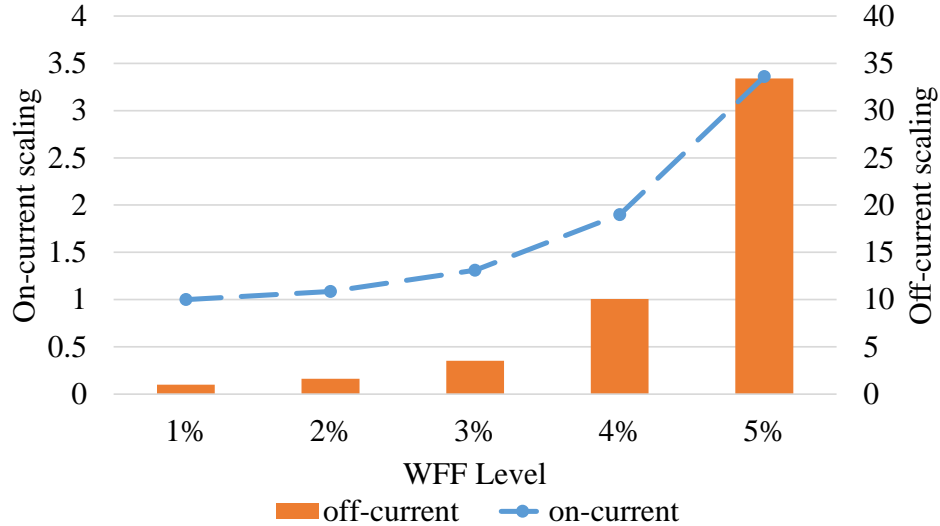
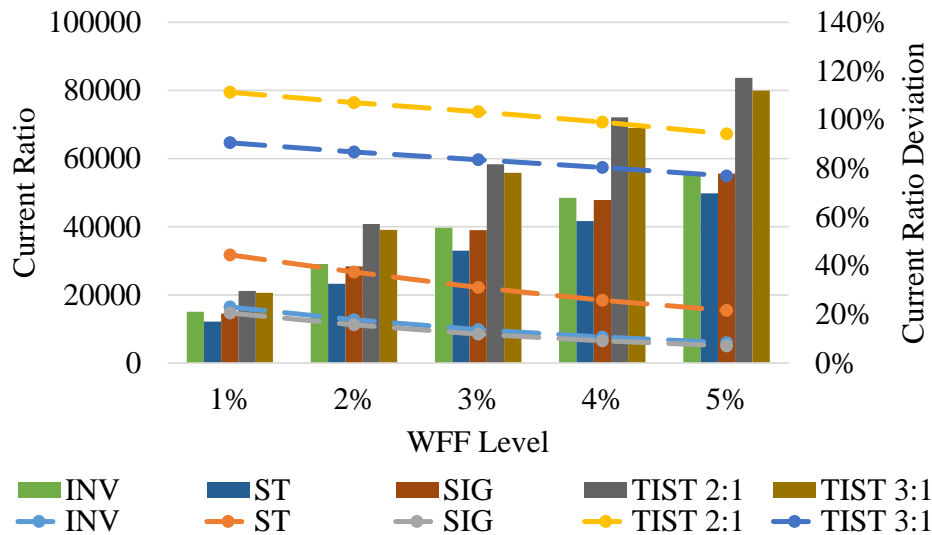
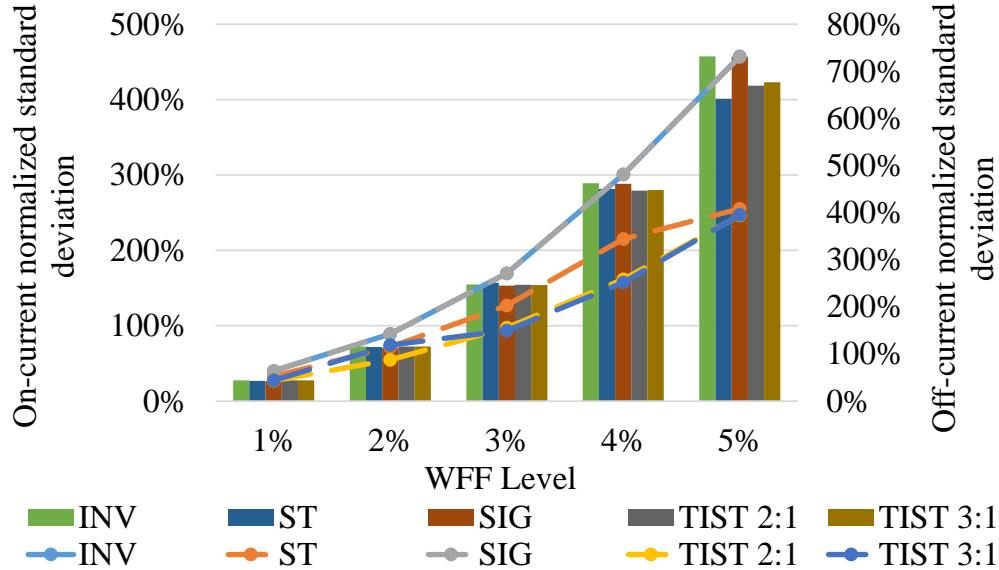


Figure 5.20: Current ratio (left) and current ratio deviation (right) design comparison across variability scaling.



When considering the ratio decrease, the TIST designs presented the lowest decrease, at 15.21%, with the ST, inverter, and SIG presenting much higher losses with 51.44%, 63.59%, 65.54%, respectively. In more depth, as shown in Fig. 5.21, in comparison to the inverter, for the on-current, the ST, TIST 2:1, and TIST 3:1 presented 33.63%, 44.45%, and 43.23% lower normalized deviations, respectively. Meanwhile, for the off-current, the improvements were narrower with a 6.27%, 4.89%, and 4.37% lower off-current normalized deviations for the ST, TIST 2:1 and, TIST 3:1, respectively. The SIG presented little to no improvement, staying below 1% decrease on both deviations. For the off-current measures, in comparison to the inverter, the SIG and ST presented

Figure 5.21: Average on and off-current normalized deviation over all designs through variability scaling. The marked line is related to the on-current normalized deviations (left axis) while the bars are related to the off-current normalized deviation (right axis).



101.03% and 155.69% higher currents, while the TIST 2:1 and 3:1 designs, presented 339.61% and 438.11% increases.

Given all the current-related results, the TIST designs present the lowest deviations for the dynamic current, lowest ratio loss and highest current ratio. The ST showed the lowest deviations for the static current and lowest ratio deviations.

5.5 Static Noise Margins

The SNM of a circuit should be as high as possible to provide more noise tolerance. The noise, is defined by any extraneous voltage amplitude added to the signal in consideration. The circuit noise tolerance is defined by the circuit ability to receive this extraneous voltage amplitude summed with the *noise-free* signal without causing it output voltage to deviate from the allowable logic voltage level. In this case, the SNMs were measures considering each designs VTCs at different supply voltage levels. This characteristic becomes increasingly critical for low power devices, as supply voltage decreases and noise amplitudes which accounted for only a fraction of the device supply voltage, can now be comparable to the total value of the supply voltage.

The evaluation of the SNMs are shown at Table 5.3. The inverter and SIG presented identical SNMs. The TIST designs presented higher SNMs than the inverter and

SIG at sub-threshold levels. The ST presented higher SNMs overall. In comparison to the inverter, SIG, and TIST 3:1 - which presented the same average SNM of 0.164V - the TIST 2:1 presented 2.6% lower SNMs, while the ST showed 17.5% higher SNMs. The ST presents the biggest differences at low supply voltages, with 41.91% and 28.23% higher SNMs at 0.1V and 0.2V, respectively, comparing to the inverter.

Table 5.3: Static Noise Margins for each design as supply voltage scales.

Design	SNM (V)	Supply Voltage (V)						
		0.1	0.2	0.3	0.4	0.5	0.6	0.7
INV	NM_L	0.025	0.074	0.122	0.171	0.217	0.253	0.277
	NM_H	0.025	0.073	0.121	0.169	0.216	0.259	0.299
	Avg.	0.025	0.073	0.122	0.170	0.216	0.256	0.288
SIG	NM_L	0.025	0.074	0.122	0.171	0.217	0.253	0.277
	NM_H	0.025	0.073	0.121	0.169	0.216	0.259	0.299
	Avg.	0.025	0.073	0.122	0.170	0.216	0.256	0.288
ST	NM_L	0.036	0.111	0.178	0.244	0.310	0.376	0.440
	NM_H	0.036	0.077	0.111	0.144	0.178	0.213	0.248
	Avg.	0.036	0.094	0.144	0.194	0.244	0.294	0.344
TIST 2:1	NM_L	0.061	0.161	0.245	0.292	0.319	0.337	0.359
	NM_H	0.014	0.007	0.010	0.038	0.079	0.131	0.189
	Avg.	0.037	0.084	0.128	0.165	0.199	0.234	0.274
TIST 3:1	NM_L	0.051	0.150	0.233	0.277	0.300	0.314	0.341
	NM_H	0.022	0.017	0.022	0.056	0.108	0.173	0.235
	Avg.	0.036	0.084	0.128	0.167	0.204	0.244	0.288

5.6 Output Gains and Slopes

The output gain and slopes will mainly determine how much and how fast the output will change and respond to changes in the input. The gain will measure how much more the output will change its value in comparison to a small change in the input. The slopes will determine how fast the output takes to change its value. A circuit can present a high gain, which means that at a specific point in the VTC curve a small change in the input value is changing the output value drastically. Although, it can present low slope values as well, which means that the time the output takes to change its value is

Figure 5.22: Output gain value across voltage scaling.

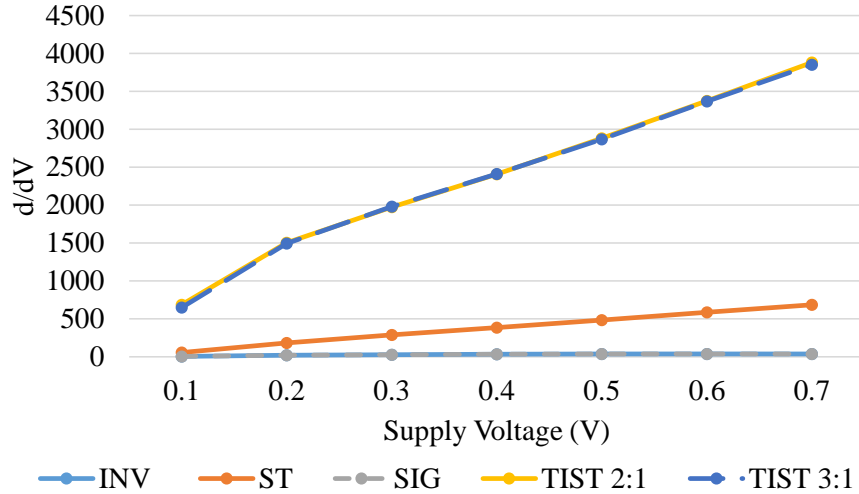
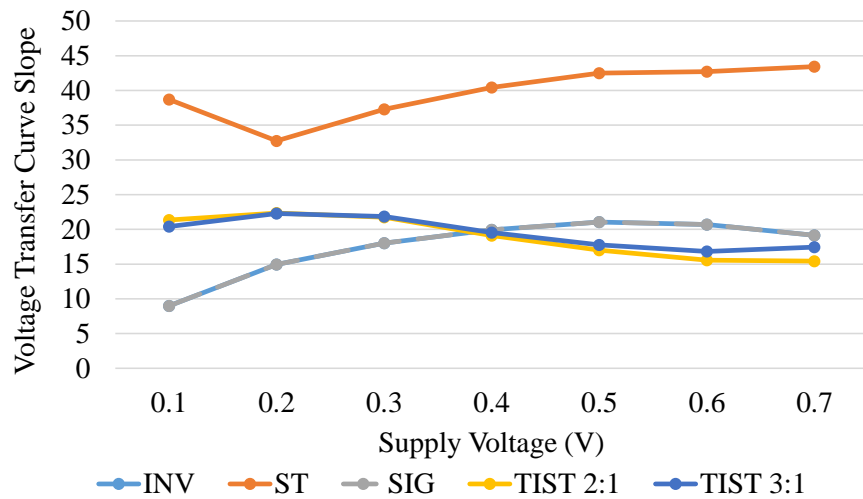


Figure 5.23: Voltage Transfer Curve slopes through supply voltage scaling for each design.



relatively high. In an ideal scenario, the circuit should show both high gains and slopes, making the change of its output as fast as possible, approaching its output signal to an ideal square signal.

It was considered the output gain values for each design, as shown in Fig. 5.22. These measures present the most broader difference across all designs. The TIST and ST designs presented, on average, values up to 8300.60%, and 1246.50% higher, respectively, in comparison to the inverter and SIG designs, which presented the same gains. Furthermore, the curve slope measures are shown in Fig. 5.23, where lower slopes can be observed for the TIST, SIG and inverter designs in comparison to the ST. The ST and TIST designs presented 126.24% and 9.43% higher average slopes, respectively, in com-

parison to the inverter and SIG designs which showed identical measures. Figs. 5.24 and 5.25 show the VTC curves for all designs, all curves were plotted in CScope¹ from DC simulations performed in HSpice. It shows how the TIST although presenting higher gain, present lower slopes, given that it takes more time to properly discharge.

Figure 5.24: Voltage Transfer Curves for all designs at 0.1V.

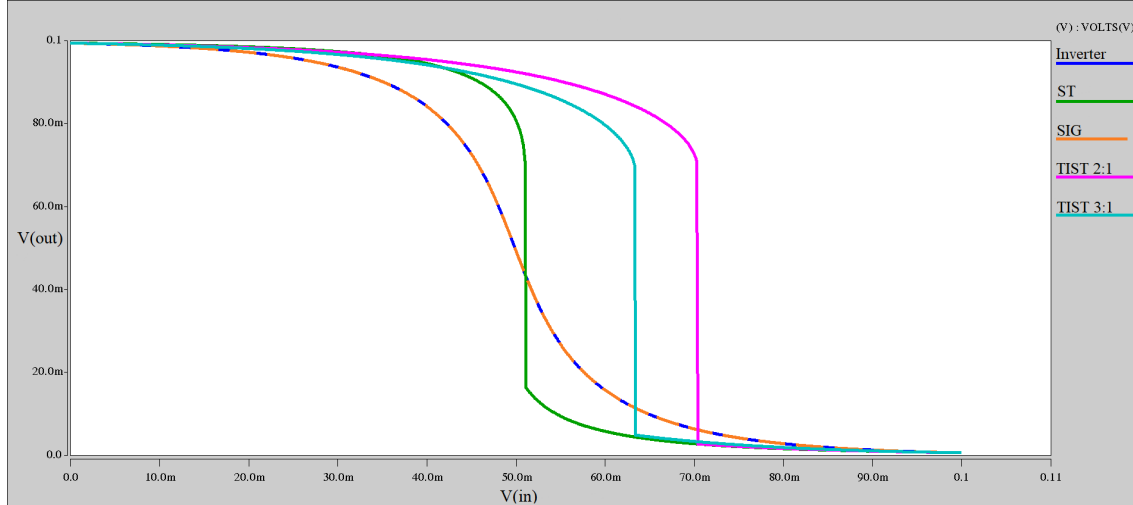
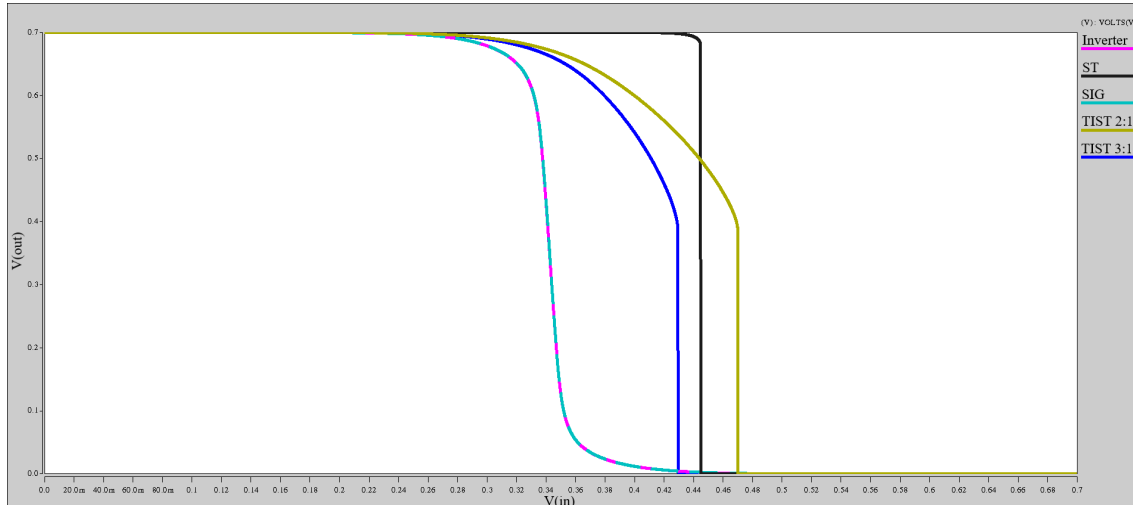


Figure 5.25: Voltage Transfer Curves for all designs at 0.7V.



5.7 Hysteresis

The hysteresis characteristic, for the designs who present it through circuit-level methods, will improve the circuit noise margins through the insertion of upper and lower threshold voltages. The hysteresis does not improve the noise margins through enhancing the signal - by making it closer to an ideal square signal - although, through the two

¹<https://www.synopsys.com/>

threshold voltages, it will make necessary higher noise amplitude to kickoff the value change of the output signal.

The hysteresis ratios measures for all designs, which present hysteresis, are shown in Fig. 5.26. The hysteresis ratio is the ratio between the hysteresis interval (V) and the supply voltage (V), which will result in a percentage of the current supply voltage. Given so, the TIST designs presented higher average ratios of 18.92% and 15.95% for the 2:1 and 3:1 designs, respectively, with the ST presenting an average ratio of 8.62%. It is important to highlight the ratio losses as well, the TIST designs presented ratio decreases up to 14.68% and the ST presented a better response with a 5.68% decrease. The hysteresis curves for all designs at nominal supply voltage are shown in Fig. 5.27. Furthermore, the hysteresis ratios in relation to the supply voltage are shown in Fig. 5.28, it can be observed huge hysteresis intervals for the TIST designs, which are responsible for the circuit failing working at acceptable frequencies.

Figure 5.26: Design hysteresis ratio comparison (left) and hysteresis ratio normalized deviation (right), across variability scaling.

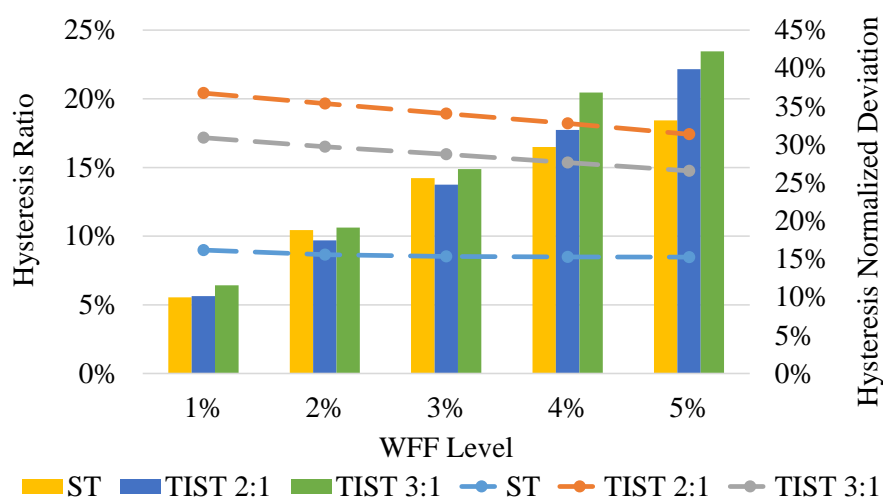


Figure 5.27: Hysteresis curves for all designs at nominal supply voltage.

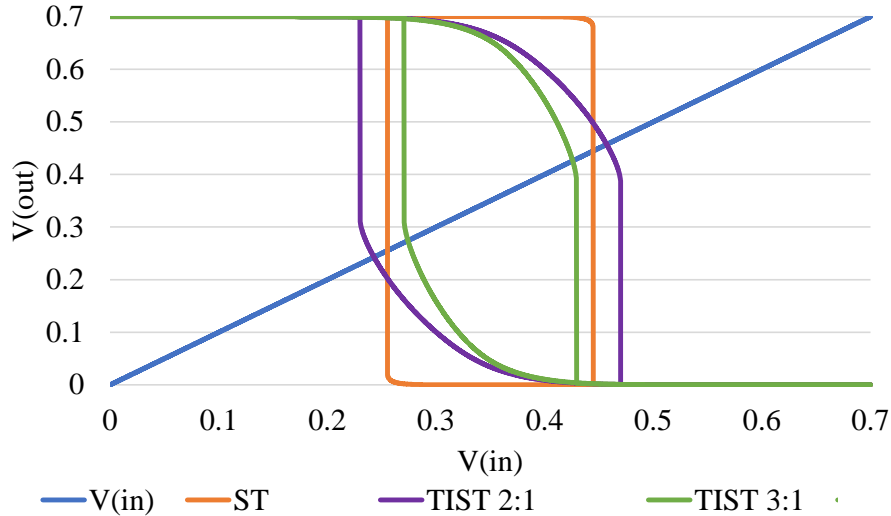
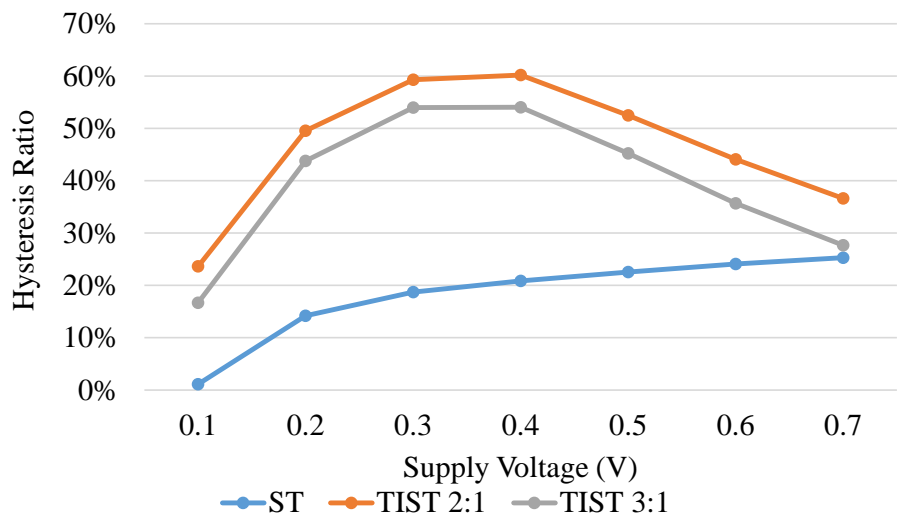


Figure 5.28: Design hysteresis ratios comparison across supply voltage scaling.

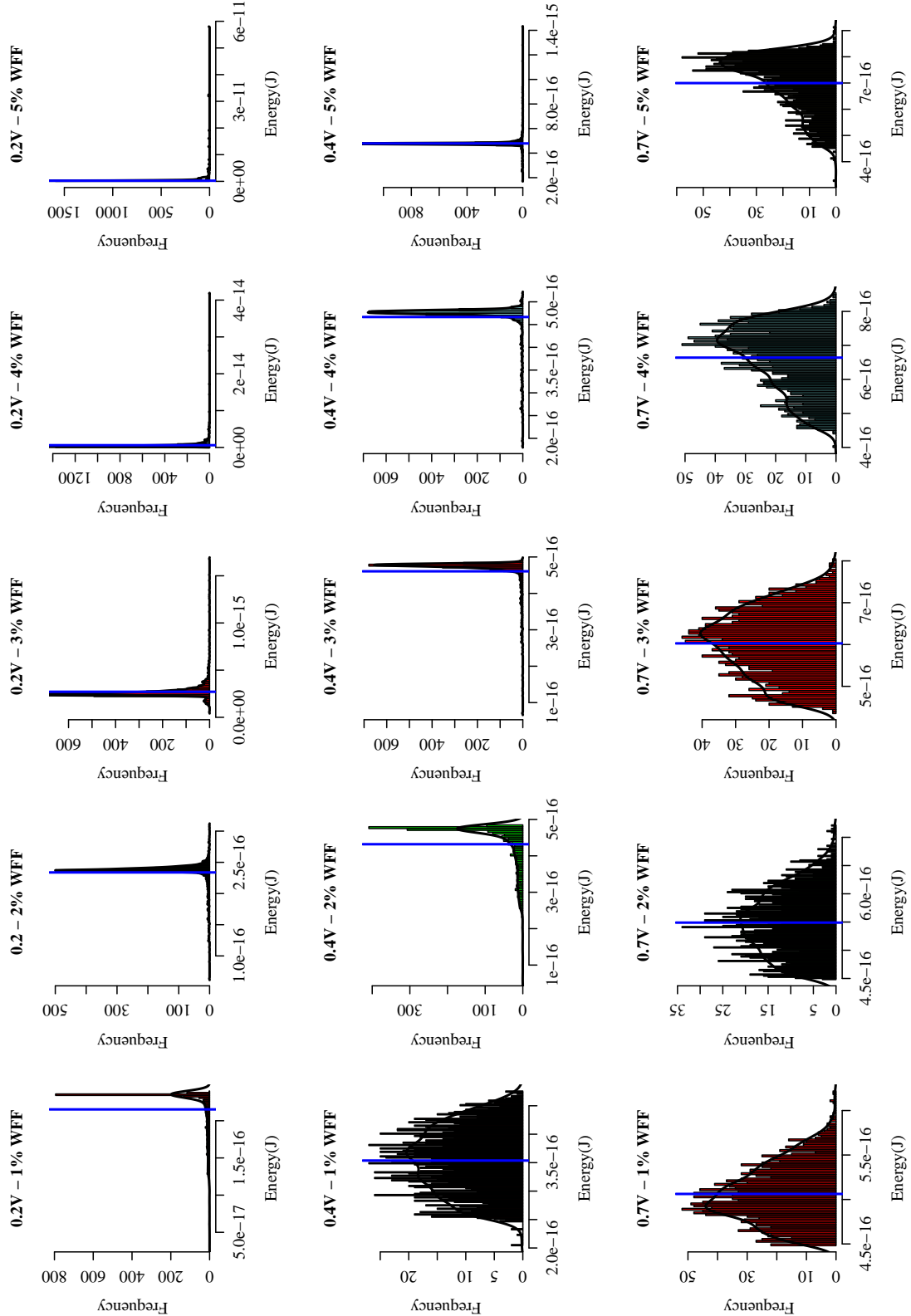


The average hysteresis ratio deviations for each design was 23.44%, 24.83%, and 27.30% for the ST, TIST 2:1 and TIST 3:1. The hysteresis average ratio deviation measures did not present considerable differences between designs, although, at high variability scenarios (5% WFF) the ST presented 16.79% and 21.40% lower deviations, in comparison to the TIST 2:1 and TIST 3:1, respectively.

5.8 Measures Distribution

Fig. 5.29 shows the distribution of the energy metrics for the inverter over all levels of WFF for 0.2V, 0.4V, and 0.7V supply voltages. Each figure presents an histogram of the 2000 simulations with a blue line, indicating where the average energy measure is located at. The black line corresponds to a projection of the local average. For low variability and high supply voltage scenarios it can be observed a normal, or close-to-normal, distribution. At higher variability and lower supply voltages, a right skew can be noted at first, where the majority of the cases stay clustered although, there is a considerable number of cases where the energy is lower than the average. As variability rises even further, the skew direction will shift and take a hard left, with the worst scenarios showing up to 5 orders of magnitude higher than the average. Histograms and dispersion graphs for all designs, are shown in Annex D.

Figure 5.29: Energy measures distribution for the inverter at different levels of variability and supply voltage.



6 FULL ADDERS

The results are divided into two main analyses, with the set of FAs operating at nominal and near-threshold. In both cases, simulations were performed with and without the ST technique. To better present the improvements (positive values) and drawbacks (negative values) of each ST, results also show a comparison (Δ) between the normalized deviation between the traditional and the circuits with the applied technique. For the sake of simplicity the LPST and traditional 6T ST were renamed ST1 and ST2, respectively.

6.1 Nominal Operation

The results concerning propagation times at nominal levels are shown in Table 6.1. It is possible to observe no considerable improvement over variability robustness concerning the propagation times. It can be explained due to the pass-transistor logic present in the TFA, TGA, and Hybrid given further signal degradation as a result of the area and parasitics increase. Furthermore, it can be observed only a slight improvement over the Mirror FA given its mirroring-based logic with many paths to source and ground.

For the energy results, it was observed considerable improvement over robustness in the Mirror, TFA, and TGA, as shown in Table 6.2. There was a considerable worsening over the Hybrid energy robustness. It is mainly due to its number of transistors, which is comparable to the Mirror FA but it is not entirely based on complementary logic, and the four internal inverters replaced, which , further increasing its area and signal degradation. Overall, the traditional TFA presented the best performance and, by far, the lowest energy consumption and energy normalized deviation at nominal operation. However, it presented the highest delay deviations.

6.2 Near-Threshold Operation

At near-threshold operation the noise margins are decreased. Given so, the designs make full use of the higher SNMs of the STs, as shown in Table 6.3. It can be observed a superior robustness improvement with the ST2, given its smaller area, and consequently, lower signal degradation. In the case of the TFA it seems that due to its few paths to source and ground, the higher parasitic capacitance and resistance present in ST2 brings

Table 6.1: Delay measures for nominal voltage operation

FA	ST	Delays							
		SUM				CARRY OUT			
		$\mu(\text{ps})$	$\sigma(\text{ps})$	$\sigma/\mu(\%)$	$\Delta(\%)$	$\mu(\text{ps})$	$\sigma(\text{ps})$	$\sigma/\mu(\%)$	$\Delta(\%)$
Mirror	-	22.83	4.82	20.89	-	22.60	4.39	19.38	-
	ST1	27.38	5.75	20.77	0.54	25.31	4.79	18.87	2.63
	ST2	42.28	8.57	20.23	3.13	41.48	7.96	19.17	1.10
TFA	-	20.76	5.51	30.69	-	19.75	4.70	25.74	-
	ST1	24.24	6.43	31.42	-2.37	22.50	5.51	26.74	-3.86
	ST2	42.36	76.87	126.26	-311.36	26.91	6.86	31.45	-22.18
TGA	-	21.56	4.30	22.36	-	22.96	4.70	20.46	-
	ST1	25.32	5.36	26.42	-18.16	26.39	5.41	20.38	0.37
	ST2	97.92	210.62	102.35	-357.80	32.80	7.85	25.70	-25.63
Hybrid	-	24.02	5.31	21.75	-	23.58	4.89	21.65	-
	ST1	60.96	64.91	92.40	-324.90	42.07	21.84	34.84	-60.90
	ST2	69.68	40.87	50.82	-133.72	72.05	25.81	29.23	-35.00

Table 6.2: Energy measures for nominal voltage operation

FA	ST	Energy							
		SUM				CARRY OUT			
		$\mu(\text{fJ})$	$\sigma(\text{fJ})$	$\sigma/\mu(\%)$	$\Delta(\%)$	$\mu(\text{fJ})$	$\sigma(\text{fJ})$	$\sigma/\mu(\%)$	$\Delta(\%)$
Mirror	-	19.30	3.55	18.35	-	27.30	3.99	14.60	-
	ST1	26.80	4.85	18.10	1.37	37.20	5.54	14.87	-1.84
	ST2	36.50	5.50	15.07	17.87	50.80	6.54	12.87	11.84
TFA	-	4.97	1.27	25.59	-	5.15	0.72	13.91	-
	ST1	10.90	1.46	13.38	47.70	10.80	0.98	9.09	34.68
	ST2	17.00	2.02	11.94	53.35	15.30	2.02	13.21	5.05
TGA	-	14.10	3.81	27.07	-	15.70	4.44	28.20	-
	ST1	24.90	6.33	25.46	5.95	26.40	4.21	15.94	43.48
	ST2	32.40	7.49	23.16	14.44	37.60	7.35	19.53	30.74
Hybrid	-	19.30	4.10	21.26	-	26.30	4.55	17.29	-
	ST1	72.50	37.95	52.34	-146.19	94.60	48.21	50.94	-194.62
	ST2	73.20	21.25	29.05	-36.64	95.20	19.89	20.90	-20.88

higher deviation, with the ST1 presenting better results.

For the energy results, shown in Table 6.4, ST1 showed superior robustness improvement for the TFA and TGA, which can be explained by their pass-transistor based logic and the ST1 smaller parasitics, in comparison to the Mirror and Hybrid FAs which showed no improvement whatsoever.

For the delay results, the Mirror FA showed the lowest means and normalized deviations, which is expected given it is not based on pass-transistor logic, having better driving capabilities. For the energy measures, TFA showed the lowest mean, due to its pass-transistor logic and lower number of transistors. Although, the TFA presented the highest delay normalized deviations. Overall, the TGA showed the lowest normal-

Table 6.3: Delay measures for near-threshold operation

FA	ST	Delays							
		SUM				CARRY OUT			
		$\mu(\text{ps})$	$\sigma(\text{ps})$	$\sigma/\mu(\%)$	$\Delta(\%)$	$\mu(\text{ps})$	$\sigma(\text{ps})$	$\sigma/\mu(\%)$	$\Delta(\%)$
Mirror	-	103.49	63.18	60.95	-	91.62	55.41	59.18	-
	ST1	119.98	67.63	56.09	7.97	115.50	73.68	64.11	-8.32
	ST2	155.58	67.03	42.94	29.55	153.50	68.89	44.86	24.20
TFA	-	122.48	117.46	111.51	-	111.64	186.41	236.88	-
	ST1	142.18	146.61	97.85	12.25	118.26	194.03	242.22	-2.26
	ST2	215.93	222.26	117.29	-5.18	165.48	335.16	273.57	-15.49
TGA	-	130.43	109.19	85.78	-	114.78	130.53	138.93	-
	ST1	122.99	98.03	79.75	7.03	128.98	101.51	88.48	36.32
	ST2	187.84	125.13	70.99	17.25	164.06	109.19	72.68	47.68
Hybrid	-	115.90	83.02	70.57	-	111.92	82.45	74.76	-
	ST1	187.36	143.80	78.99	-11.93	116.02	71.26	61.00	18.41
	ST2	207.00	168.04	72.56	-2.81	167.50	66.72	40.94	45.23

Table 6.4: Energy measures for near-threshold operation

FA	ST	Energy							
		SUM				CARRY OUT			
		$\mu(\text{fJ})$	$\sigma(\text{fJ})$	$\sigma/\mu(\%)$	$\Delta(\%)$	$\mu(\text{fJ})$	$\sigma(\text{fJ})$	$\sigma/\mu(\%)$	$\Delta(\%)$
Mirror	-	10.10	3.04	30.12	-	14.10	2.53	18.00	-
	ST1	13.90	4.05	29.07	3.50	18.60	4.25	22.93	-27.42
	ST2	18.40	4.34	23.60	21.64	25.30	5.73	22.59	-25.53
TFA	-	2.62	0.83	31.49	-	2.71	0.37	13.49	-
	ST1	5.67	1.34	23.69	24.76	5.69	0.63	11.01	18.38
	ST2	9.69	2.11	21.74	30.96	8.80	2.59	29.40	-117.89
TGA	-	6.87	1.56	22.68	-	8.11	2.90	35.70	-
	ST1	12.90	2.37	18.45	18.65	13.50	1.86	13.79	61.37
	ST2	16.10	3.09	19.17	15.48	17.30	2.57	14.86	58.38
Hybrid	-	9.66	3.09	32.02	-	12.80	3.17	24.77	-
	ST1	36.40	17.94	49.30	-53.96	45.80	23.63	51.54	-108.07
	ST2	35.40	12.72	35.91	-12.14	46.60	13.84	29.69	-19.86

ized deviations in energy and the highest robustness gains concerning delay and energy measures.

6.3 Penalties

Overviews for metrics measurements and variability sensitivities are shown in Figs. 6.1, 6.2, 6.3, and 6.4. Since it is considered a technique where a single inverter (2 transistors) by ST1/ST2 (4/6 transistors). It is expected penalties concerning delay, energy and area metrics. For the delays, it was observed an average 30% and 97% increase

Figure 6.1: Average delay measures for nominal operation and their respective normalized deviation (variability sensitivity).

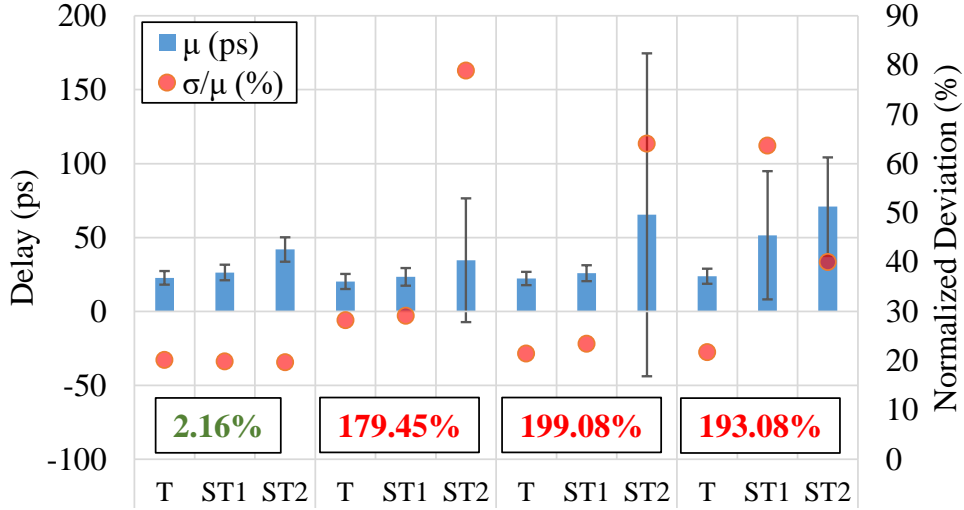
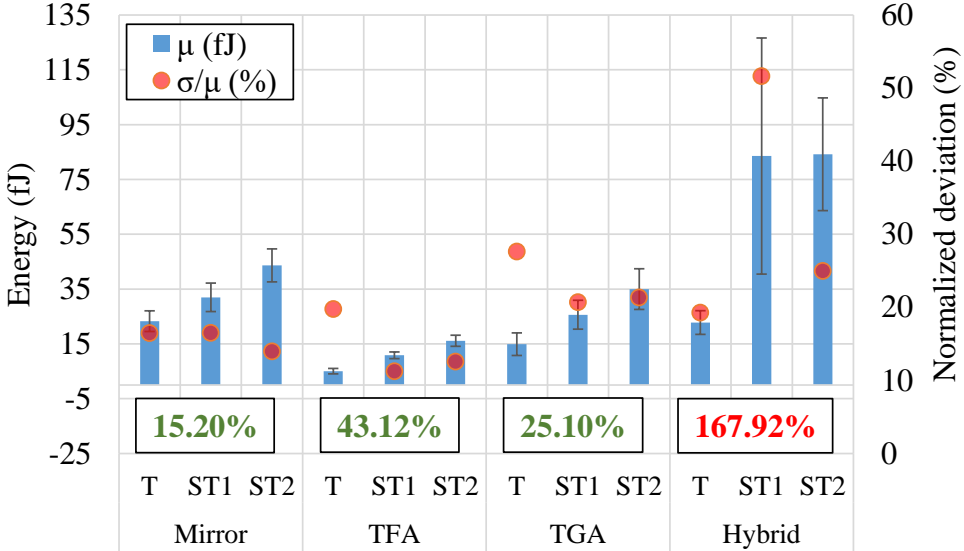


Figure 6.2: Average energy measures for nominal operation and their respective normalized deviation (variability sensitivity).

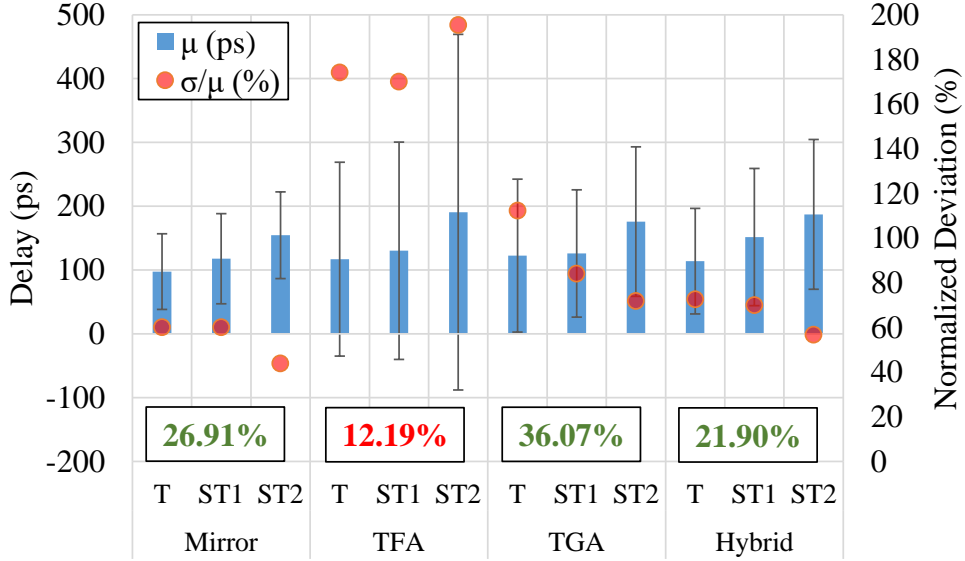


for the ST1 and ST2, respectively. Additionally, for the energy, there was a 123% and 176% average increase for the ST1 and ST2, respectively.

Concerning area penalties, the ST1 increased the FAs area by 157.71%, on average, while the ST2 increased by 52.20%. The ST1 higher increase in area is due to the necessity to use TAP-Cells, which is a technology restriction, to explicitly connect the transistor's bulk to specific points of the circuit or source/ground making the ST1 cell more prominent than expected. The ST2 does not apply specific bulk connections, although it was necessary the use of METAL3 for cell routing, increasing parasitic capacitance and resistance.

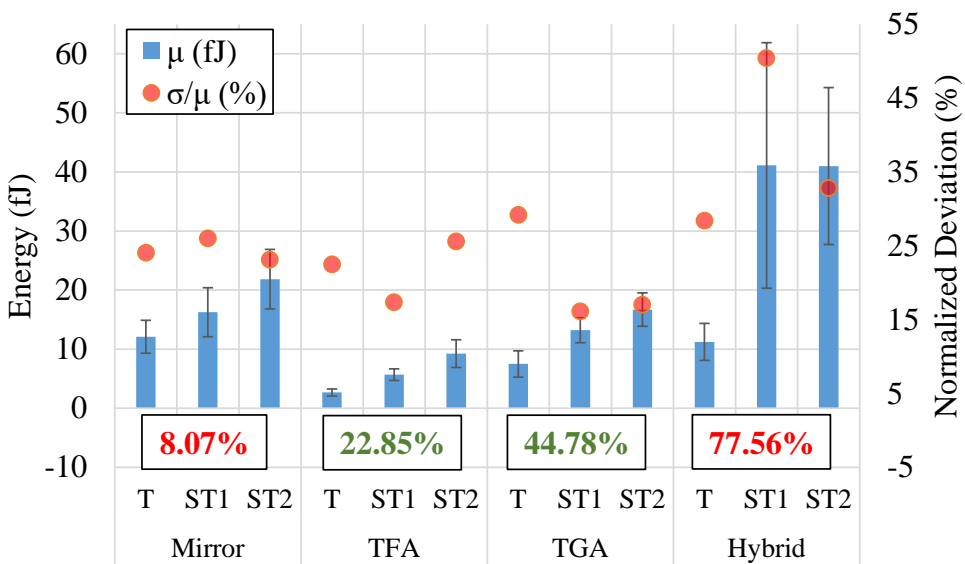
Considering all scenarios, there can be observed no delay robustness improvement

Figure 6.3: Average delay measures for near-threshold operation and their respective normalized deviation (variability sensitivity).



at nominal operation with the ST1 and ST2 showing, on average, 50% and 115.2% worsening on delay robustness, respectively. For energy robustness, at nominal operation, the ST2 presented a considerable average improvement of 11.18% while the ST1 showed an average worsening of 25%. For near-threshold operation, ST1 and ST2 showed 7.79% and 18.173% higher delay robustness. For energy robustness, the ST2 showed a 4.13% improvement while the ST1 presented a worsening of 4.5%.

Figure 6.4: Average energy measures for near-threshold operation and their respective normalized deviation (variability sensitivity).



7 CONCLUSIONS

The ongoing trend of IoT devices was enabled by two key technology improvements: battery lifetime through capacity improvement, and node scaling. Although, for specific applications, battery maintenance and charging through the power grid is not possible. Given so, IoT devices have been constrained with tight energy consumption metrics, and adapted with self-sufficient mechanisms to produce energy through external sources. The node scaling, that enabled IoT devices, comes not short of inherent challenges, with process variability being the major one. New transistor technologies have been proposed such as FinFETs, although even such devices, at deep submicron nodes (e.g. 7-nm), present considerable deviation in its metrics. Such deviations are not appropriate for such sensible devices working at narrow constraints (with energy consumption being a priority).

Given so, an analysis over multiple scenarios considering several levels of process variability, supply voltages, and transistor sizing was performed to identify the adequate fin number and supply voltage for various kinds of inverter circuits, prioritizing energy consumption and the minimization of deviations. Furthermore, the impact of the replacement of Full Adders internal inverters was analyzed considering two types of Schmitt Trigger and four types of Full Adders.

An overview for the inverter designs analysis is shown in Table 7.1, where the designs with the highest average and normalized standard deviations for each metric are presented. On performance, the inverter presented the lowest propagation times, and lowest frequency loss due to variability impact. Although, it presented the higher propagation deviations than the ST and SIG designs. The ST and SIG designs presented the lowest frequencies, but lowest propagation times deviations as well. The TIST 2:1 designs presented frequencies on average lower to the ST and SIG designs, and higher deviations, second only to the 3:1 designs which presented higher frequencies, apart from the inverter, than all of the designs. Given so, it can be observed the higher impact of variability on the TIST designs which present the lowest average frequencies (for the 2:1 TISTs) and second highest frequencies (for the 3:1 TISTs) and still presented considerable higher propagation deviations in comparison to all designs.

Trying to detect the most adequate values for the supply voltage and sizing variables for each type of application, low energy consumption, high robustness, and cost-benefit, a subset of solutions was chosen considering each level of variability. For the

Table 7.1: Overall results overview for all designs.

Metric		Average	Deviations
Delays	Highest	TIST 2:1	TIST 3:1
	Lowest	INV	SIG
Energy	Highest	TIST 2:1	TIST 2:1
	Lowest	INV	INV
SNMs	Highest	ST	-
	Lowest	TIST 2:1	-
Current Ratios	Highest	TIST 2:1	TIST 2:1
	Lowest	SIG	ST
Gain	Highest	TIST	-
	Lowest	INV/SIG	-
Slope	Highest	ST	-
	Lowest	TIST/INV/SIG	-
Hysteresis Ratio*	Highest	TIST 2:1	TIST 3:1
	Lowest	ST	ST

*The inverter and SIG designs do not present a hysteresis characteristic.

low energy applications, the inverter, ST, and SIG remained tightly together while the TIST designs presented way higher energy consumption. The high robustness application stayed favorable for the TIST designs, although not being directly comparable since it utilizes 2 to 3 times higher number of fins, and a higher supply voltage, to maintain such results. Putting the TIST designs aside, the ST design presents lower deviation, at the cost of much higher energy consumption for low variability scenarios. Therefore the SIG presents itself as an alternative, showing lower deviations and energy consumption similar to the inverter in the remaining cases. Although, it is important to highlight that the maximum energy deviation presented for this type of application was approximately 10%.

Lastly, for the cost-benefit applications, the TIST designs maintained the lowest deviations, 73% to 30% lower than the inverter, at the cost of roughly 3.5 to 4.8 times higher energy consumption in comparison to the inverter. The SIG presented similar energy consumption (20% higher) with a slight decrease on the deviations (8%) in comparison to the inverter. Therefore, the inverter and SIG designs are still good alternatives, with the TIST designs tending more to a high robustness application with no to little restraints into energy consumption. The EDP over all chosen layouts, for each considered application, is shown at Table 7.2.

When considering the current measures and deviations, the TIST designs presented the highest ratio, which is directly related to their transistor proportions. The ST

Table 7.2: EDP for each chosen design for the considered applications.

Design	EDP		
	Low Energy	High Robustness	Cost Benefit
INV	0.155	0.029	0.027
ST	0.124	0.112	0.053
SIG	0.114	0.037	0.031
TIST 2:1	0.273	0.096	0.076
TIST 3:1	0.214	0.113	0.086

presented a ratio more than two times higher than the inverter and SIG designs, while still maintaining a 1:1 transistor ratio and presenting the lowest ratio deviations. Due to the higher increase in the leakage in comparison to the dynamic current, all designs presented current ratio decreases over variability level scaling. The TIST designs presented lower decreases with the other considered designs presenting over 3x higher ratio declines. Over each specific current the ST and TIST designs presented considerably lower deviations on the dynamic current and minor improvements over leakage current deviations.

Concerning reliability over signals, the ST and TIST designs presented similar results at low supply voltages with widening differences as the supply voltage scaled up, with the ST presenting the highest noise margins and the TIST designs leveling up with the SIG and inverter designs which presented identical results through all supply voltage values. The TIST designs presented much higher gains, although presenting signal slopes comparable to the SIG and inverter designs, with the ST showing the highest signal slopes. Lastly, over the hysteresis ratios, the TIST designs presented a broad difference in comparison to the ST, although with higher deviations in most cases. Considering the hysteresis ratio scaling in comparison to the supply voltage, the TIST designs keep showing higher ratios (mainly at the lowest supply voltages), although due to higher ratios at near-threshold voltages the TIST circuits did not work properly at those specific levels of supply.

The impact of the ST1 and ST2 replacement of Full Adders internal inverters showed overall no improvement over delay deviations at nominal levels with a worsening up to 199.08%, on average. On the contrary, for the energy measures the pass-transistor logic based Full Adders presented improvements up to 43.12%, on average. At near-threshold operation, almost all designs take advantage of the gain improvement characteristic of the STs and showed a maximum of 36.07% and 44.78% lower deviations on the delays and energy metrics, respectively. Such results show that the application of the technique at near-threshold levels to be more appropriate. But also, it depends on the logic

Table 7.3: Best and worst cases considering all metrics and the two types of operation considered in the experiments.

Operation		Delay		Energy	
		Absolute	Deviation	Absolute	Deviation
Nominal	Highest	HYBRIDST2	TFAST2	HYBRIDST2	HYBRIDST1
	Lowest	TFA	MirrorST2	TFA	TFAST1
NT	Highest	TFAST2	TFAST2	HYBRIDST1	HYBRIDST1
	Lowest	Mirror	MirrorST2	TFA	TGAST1

of which the Full Adder is based, transistor count, and final layout area.

Table 7.3 shows the best and worst cases concerning the metrics, and the two levels of supply voltage considered in the experiments. It can be observed the presence of the TFA at nominal level, presenting most of the lowest measures, which comes along with the TFA also presenting the smallest transistor count of all considered designs, making it the most appropriate Full Adder at nominal operation. On the other side, the Hybrid presented the worst results and has the biggest area overall, making it not very suitable, not only for nominal operation but for near-threshold operation as well. At near-threshold the TFAST2 presents itself with the highest delays and delay variations. Although, for the energy measures, its traditional version presents the lowest energy consumption and acceptable variations, although now as low as the TGAST1. Into the performance, the Mirror presented the best results.

Additionally, since when considering just one variable much of the impact of other variables are put aside, Table 7.4 shows the layouts which presented the highest and lowest Measure Deviation Products (MDP), where the absolute value of the measures and its deviation are multiplied. This further analysis permits to consider not only one separable variable (e.g. only the absolute value or the deviation) but the impact of several measures into one index. Furthermore, to give the most overall appropriate layout, considering energy and delay measures and deviations, the MDP for energy (Energy Deviation Product - EDP) and delays (Delay Deviation Product - DDP) were multiplied as well. These results show that the original TFA presents best energy and overall results, while the Mirror Full Adder shows improved delays results. Again, the Hybrid Full Adder, with the ST1 applied on it, presented for the energy and overall the worst results, mainly due to its area and higher transistor count.

Table 7.4: Overall results considering the EDP and DPP for each metric and the product between those.

Operation		Measure Deviation Product		DDP and EDP Product
		Delay	Energy	
Nominal	Highest	TGAST2	HYBRIDST1	HYBRIDST1
	Lowest	MIRROR	TFA	TFA
NT	Highest	TFAST2	HYBRIDST1	HYBRIDST1
	Lowest	MIRROR	TFA	TFA

7.1 Future Works

For future works, it would be interesting to do a similar analysis to be made considering the TIST design at a different technology node (FD-SOI 28nm) at sub-100mV to achieve ultra low-power circuits capable of enhancing the circuits robustness to noise and to decrease the impact of process variability. Additionally, as shown in the current section of the results, the leakage currents measures and normalized deviations will exponentially scale with the WFF level. Given so, further techniques for leakage suppression and the minimization of current deviations should be investigated.

All publications - published, co-authored, book chapters, and in proceedings, are listed in Annex A.

REFERENCES

- ABBAS, Z. et al. Optimal nbt1 degradation and pvt variation resistant device sizing in a full adder cell. In: IEEE. **2015 4th International Conference on Reliability, Infocom Technologies and Optimization (ICRITO)(Trends and Future Directions)**. India, 2015. p. 1–6.
- AHMAD, S. et al. Single-ended schmitt-trigger-based robust low-power sram cell. **IEEE Transactions on Very Large Scale Integration (VLSI) Systems**, IEEE, v. 24, n. 8, p. 2634–2642, 2016.
- AHMADI, M.; ALIZADEH, B.; FOROUZANDEH, B. A hybrid time borrowing technique to improve the performance of digital circuits in the presence of variations. **IEEE Transactions on Circuits and Systems I: Regular Papers**, IEEE, v. 64, n. 1, p. 100–110, 2016.
- AL-SARAWI, S. Low power schmitt trigger circuit. **Electronics letters**, IET, v. 38, n. 18, p. 1009–1010, 2002.
- ALIOTO, M.; CONSOLI, E.; PALUMBO, G. Variations in nanometer cmos flip-flops: Part ii—energy variability and impact of other sources of variations. **IEEE Transactions on Circuits and Systems I: Regular Papers**, IEEE, v. 62, n. 3, p. 835–843, 2015.
- ALIOTO, M.; CONSOLI, E.; PALUMBO, G. Variations in nanometer cmos flip-flops: Part i—impact of process variations on timing. **IEEE Transactions on Circuits and Systems I: Regular Papers**, IEEE, v. 62, n. 8, p. 2035–2043, 2015.
- ALIOTO, M.; PALUMBO, G. Delay variability due to supply variations in transmission-gate full adders. In: IEEE. **Circuits and Systems, 2007. ISCAS 2007. IEEE International Symposium on**. University of Louisiana, New Orleans - USA, 2007. p. 3732–3735.
- AMES, S. O. et al. Investigating pvt variability effects on full adders. In: IEEE. **Power and Timing Modeling, Optimization and Simulation (PATMOS), 2016 26th International Workshop on**. [S.I.], 2016. p. 155–161.
- ASENOV, A. Random dopant induced threshold voltage lowering and fluctuations in sub 50 nm mosfets: a statistical 3datomistic’simulation study. In: . [S.I.]: IOP Publishing, 1999. v. 10, n. 2, p. 153.
- ASENOV, A. et al. Simulation of intrinsic parameter fluctuations in decanometer and nanometer-scale mosfets. **IEEE transactions on electron devices**, IEEE, v. 50, n. 9, p. 1837–1852, 2003.
- AUSTIN, T. et al. Opportunities and challenges for better than worst-case design. In: ACM. **Proceedings of the 2005 Asia and South Pacific Design Automation Conference**. [S.I.], 2005. p. 2–7.
- BAI, X.; VISWESWARIAH, C.; STRENSKI, P. N. Uncertainty-aware circuit optimization. In: ACM. **Proceedings of the 39th annual Design Automation Conference**. [S.I.], 2002. p. 58–63.

- BECKETT, P. A fine-grained reconfigurable logic array based on double gate transistors. In: **IEEE. Field-Programmable Technology, 2002.(FPT). Proceedings. 2002 IEEE International Conference on.** [S.l.], 2002. p. 260–267.
- BERNSTEIN, K. et al. High-performance cmos variability in the 65-nm regime and beyond. **IBM journal of research and development**, IBM, v. 50, n. 4.5, p. 433–449, 2006.
- BHATTACHARYA, D.; JHA, N. K. Finfets: From devices to architectures. In: . [S.l.]: Hindawi, 2014. v. 2014.
- BLEITNER, A. et al. Comparison and optimization of the minimum supply voltage of schmitt trigger gates versus cmos gates under process variations. In: **VDE. ANALOG 2018; 16th GMM/ITG-Symposium.** [S.l.], 2018. p. 1–6.
- BLISH, R. et al. Critical reliability challenges for the international technology roadmap for semiconductors (itrs). **Technology Transfer**, 2003.
- BORKAR, S. et al. Design and reliability challenges in nanometer technologies. In: **ACM. Proceedings of the 41st annual Design Automation Conference.** [S.l.], 2004. p. 75–75.
- BOSE, S.; JOHNSTON, M. L. A stacked-inverter ring oscillator for 50 mv fully-integrated cold-start of energy harvesters. In: **IEEE. 2018 IEEE International Symposium on Circuits and Systems (ISCAS).** [S.l.], 2018. p. 1–5.
- BROWN, A. R. et al. Impact of metal gate granularity on threshold voltage variability: A full-scale three-dimensional statistical simulation study. **IEEE Electron Device Letters**, IEEE, v. 31, n. 11, p. 1199–1201, 2010.
- BRUNNER, T. A. Why optical lithography will live forever. **Journal of Vacuum Science & Technology B: Microelectronics and Nanometer Structures Processing, Measurement, and Phenomena**, AVS, v. 21, n. 6, p. 2632–2637, 2003.
- CHANG, K.-L. et al. Synchronous-logic and asynchronous-logic 8051 microcontroller cores for realizing the internet of things: A comparative study on dynamic voltage scaling and variation effects. **IEEE journal on emerging and selected topics in circuits and systems**, IEEE, v. 3, n. 1, p. 23–34, 2013.
- CHAVA, B. et al. Standard cell design in n7: Euv vs. immersion. In: **INTERNATIONAL SOCIETY FOR OPTICS AND PHOTONICS. Design-Process-Technology Co-optimization for Manufacturability IX.** [S.l.], 2015. v. 9427, p. 94270E.
- CLARK, L. T. et al. Asap7: A 7-nm finfet predictive process design kit. In: . [S.l.]: Elsevier, 2016. v. 53, p. 105–115.
- COLINGE, J.-P. et al. **FinFETs and other multi-gate transistors.** [S.l.]: Springer, 2008.
- DADGOUR, H.; DE, V.; BANERJEE, K. Statistical modeling of metal-gate work-function variability in emerging device technologies and implications for circuit design. In: **IEEE. 2008 IEEE/ACM International Conference on Computer-Aided Design.** [S.l.], 2008. p. 270–277.

- DATTA, S. et al. High mobility si/sige strained channel mos transistors with hfo/sub 2//tin gate stack. In: IEEE. **IEEE International Electron Devices Meeting 2003**. [S.I.], 2003. p. 28–1.
- DEVADAS, M.; KISHORE, K. L. Design topologies for low power cmos full adder. In: IEEE. **Inventive Systems and Control (ICISC), 2017 International Conference on**. [S.I.], 2017. p. 1–4.
- DIETRICH, M.; HAASE, J. **Process Variations and Probabilistic Integrated Circuit Design**. [S.I.]: Springer Science & Business Media, 2011.
- DIGHE, S. et al. Within-die variation-aware dynamic-voltage-frequency-scaling with optimal core allocation and thread hopping for the 80-core teraflops processor. **IEEE Journal of Solid-State Circuits**, IEEE, v. 46, n. 1, p. 184–193, 2011.
- DOKANIA, V.; IMRAN, A.; ISLAM, A. Investigation of robust full adder cell in 16-nm cmos technology node. In: IEEE. **Multimedia, Signal Processing and Communication Technologies (IMPACT), 2013 International Conference on**. [S.I.], 2013. p. 207–211.
- DOKANIA, V.; ISLAM, A. Circuit-level design technique to mitigate impact of process, voltage and temperature variations in complementary metal-oxide semiconductor full adder cells. In: . [S.I.]: IET, 2015. v. 9, n. 3, p. 204–212.
- DOKI, B. L. Cmos schmitt triggers. In: IET. **IEE Proceedings G-Electronic Circuits and Systems**. [S.I.], 1984. v. 131, n. 5, p. 197–202.
- DRESLINSKI, R. G. et al. Near-threshold computing: Reclaiming moore's law through energy efficient integrated circuits. **Proceedings of the IEEE**, IEEE, v. 98, n. 2, p. 253–266, 2010.
- FARKHANI, H. et al. Comparative study of finfets versus 22nm bulk cmos technologies: Sram design perspective. In: IEEE. **2014 27th IEEE International System-on-Chip Conference (SOCC)**. [S.I.], 2014. p. 449–454.
- FEDERSPIEL, X. et al. 28nm node bulk vs fdsoi reliability comparison. In: IEEE. **Reliability Physics Symposium (IRPS), 2012 IEEE International**. [S.I.], 2012. p. 3B–1.
- FERNANDES, T. **CMOS Amplifiers and Schmitt Triggers for Ultra-Low-Voltage Applications**. [S.I.: s.n.], 2019.
- FOJTIK, M. et al. A millimeter-scale energy-autonomous sensor system with stacked battery and solar cells. **IEEE Journal of Solid-State Circuits**, IEEE, v. 48, n. 3, p. 801–813, 2013.
- FRANK, D. J. et al. Device scaling limits of si mosfets and their application dependencies. **Proceedings of the IEEE**, IEEE, v. 89, n. 3, p. 259–288, 2001.
- FRANK, D. J.; WONG, H.-S. Simulation of stochastic doping effects in si mosfets. In: IEEE. **7th International Workshop on Computational Electronics. Book of Abstracts. IWCE (Cat. No. 00EX427)**. [S.I.], 2000. p. 2–3.

- GIELEN, G. et al. Emerging yield and reliability challenges in nanometer cmos technologies. In: **Proceedings of the conference on Design, automation and test in Europe**. [S.l.: s.n.], 2008. p. 1322–1327.
- GUDURI, M.; ISLAM, A. Design of hybrid full adder in deep subthreshold region for ultralow power applications. In: **IEEE. Signal Processing and Integrated Networks (SPIN), 2015 2nd International Conference on**. [S.l.], 2015. p. 931–935.
- GUSEV, E. et al. Ultrathin high-k gate stacks for advanced cmos devices. In: **IEEE. International Electron Devices Meeting. Technical Digest (Cat. No. 01CH37224)**. [S.l.], 2001. p. 20–1.
- GUSEV, E. P.; NARAYANAN, V.; FRANK, M. M. Advanced high- κ dielectric stacks with polysi and metal gates: Recent progress and current challenges. **IBM Journal of Research and Development**, IBM, v. 50, n. 4.5, p. 387–410, 2006.
- HARRINGTON, R. C. et al. Effect of transistor variants on single-event transients at the 14/16nm bulk finfet technology generation. In: . [S.l.: s.n.], 2018. p. 1–1.
- HAYS, K. I. A 62 mv 0.13 um cmos standard-cell-based design technique using schmitt-trigger logic. 2012.
- HOBBS, C. C. et al. Fermi-level pinning at the polysilicon/metal-oxide interface-part ii. **IEEE Transactions on Electron Devices**, IEEE, v. 51, n. 6, p. 978–984, 2004.
- ISLAM, A. et al. Design and analysis of robust dual threshold cmos full adder circuit in 32nm technology. In: **IEEE. Advances in Recent Technologies in Communication and Computing (ARTCom), 2010 International Conference on**. [S.l.], 2010. p. 418–420.
- ISLAM, A.; AKRAM, M. W.; HASAN, M. Variability immune finfet-based full adder design in subthreshold region. In: **IEEE. Devices and Communications (ICDeCom), 2011 International Conference on**. [S.l.], 2011. p. 1–5.
- ISLAM, A.; HASAN, M. Design and analysis of power and variability aware digital summing circuit. In: . [S.l.: s.n.], 2011. v. 2, n. 2, p. 6–14.
- JEON, D. et al. Design methodology for voltage-overscaled ultra-low-power systems. **IEEE Transactions on Circuits and Systems II: Express Briefs**, IEEE, v. 59, n. 12, p. 952–956, 2012.
- JEONG, K.; KAHNG, A. B.; SAMADI, K. Impact of guardband reduction on design outcomes: A quantitative approach. **IEEE Transactions on Semiconductor Manufacturing**, IEEE, v. 22, n. 4, p. 552–565, 2009.
- KAHNG, A. B. et al. Slack redistribution for graceful degradation under voltage overscaling. In: **IEEE. 2010 15th Asia and South Pacific Design Automation Conference (ASP-DAC)**. [S.l.], 2010. p. 825–831.
- KAKOEE, M. R.; LOI, I.; BENINI, L. Variation-tolerant architecture for ultra low power shared-11 processor clusters. **IEEE Transactions on Circuits and Systems II: Express Briefs**, IEEE, v. 59, n. 12, p. 927–931, 2012.

- KHAN, S.; DAHIYA, R. S.; LORENZELLI, L. Flexible thermoelectric generator based on transfer printed si microwires. In: **IEEE. 2014 44th European Solid State Device Research Conference (ESSDERC)**. [S.I.], 2014. p. 86–89.
- KIM, D.; KIH, J.; KIM, W. A new waveform-reshaping circuit: an alternative approach to schmitt trigger. **IEEE journal of solid-state circuits**, IEEE, v. 28, n. 2, p. 162–164, 1993.
- KING, T.-J. Finfets for nanoscale cmos digital integrated circuits. In: **ICCAD-2005. IEEE/ACM International Conference on Computer-Aided Design, 2005**. [S.I.: s.n.], 2005. p. 207–210.
- KULKARNI, J. P.; KIM, K.; ROY, K. A 160 mv robust schmitt trigger based subthreshold sram. **IEEE Journal of Solid-State Circuits**, IEEE, v. 42, n. 10, p. 2303–2313, 2007.
- LIAO, W. et al. Investigation of reliability characteristics in nmos and pmos finfets. In: . [S.I.]: IEEE, 2008. v. 29, n. 7, p. 788–790.
- LOTZE, N.; MANOLI, Y. Ultra-sub-threshold operation of always-on digital circuits for iot applications by use of schmitt trigger gates. **IEEE Transactions on Circuits and Systems I: Regular Papers**, IEEE, v. 64, n. 11, p. 2920–2933, 2017.
- LUO, Z. et al. A sub-10 mv power converter with fully integrated self-start, mppt, and zcs control for thermoelectric energy harvesting. **IEEE Transactions on Circuits and Systems I: Regular Papers**, IEEE, v. 65, n. 5, p. 1744–1757, 2017.
- MANOJ, C. R. et al. Device optimization of bulk finfets and its comparison with soi finfets. In: **2007 International Workshop on Physics of Semiconductor Devices**. [S.I.: s.n.], 2007. p. 134–137.
- MANOLI, Y. Energy harvesting—from devices to systems. In: **IEEE. 2010 Proceedings of ESSCIRC**. [S.I.], 2010. p. 27–36.
- MEINHARDT, C.; ZIMPECK, A. L.; REIS, R. Impact of gate workfunction fluctuation on finfet standard cells. In: **IEEE. Electronics, Circuits and Systems (ICECS), 2014 21st IEEE International Conference on**. [S.I.], 2014. p. 574–577.
- MELEK, L. et al. Analysis and design of the classical cmos schmitt trigger in subthreshold operation. In: . [S.I.]: IEEE, 2017. v. 64, n. 4, p. 869–878.
- MIORANDI, D. et al. Internet of things: Vision, applications and research challenges. **Ad hoc networks**, Elsevier, v. 10, n. 7, p. 1497–1516, 2012.
- MOGHADDAM, M.; MOAIYERI, M. H.; ESHGHI, M. Design and evaluation of an efficient schmitt trigger-based hardened latch in cntfet technology. In: . [S.I.]: IEEE, 2017. v. 17, n. 1, p. 267–277.
- MORAES, L. et al. Exploring schmitt trigger circuits for process variability mitigation. In: **IEEE. 2019 17th IEEE International New Circuits and Systems Conference (NEWCAS)**. [S.I.], 2019. p. 1–4.
- MORAES, L. et al. Minimum energy finfet schmitt trigger design considering process variability. In: **IEEE. 2019 IFIP/IEEE 27th International Conference on Very Large Scale Integration (VLSI-SoC)**. [S.I.], 2019. p. 88–93.

MORAES, L. B. et al. Evaluation of variability through schmitt trigger technique on cmos full adder design. In: SBC/SBMICRO. **In Proceedings: 2018 SIM - Simpósio de Microeletrônica.** [S.I.], 2018. p. 4.

MORAES, L. B. et al. Process variability attenuation using schmitt trigger at near-threshold operation. In: SBC/SBMICRO. **In Proceedings: 2018 WCAS - Workshop on Circuits and Systems Design.** [S.I.], 2018. p. 4.

MORAES, L. B. et al. Low energy and process variability analysis over finfet schmitt trigger design. In: SBC/SBMICRO. **In Proceedings: 2019 WCAS - Workshop on Circuits and Systems Design.** [S.I.], 2019. p. 4.

MORAES, L. B. et al. Pros and cons of st and sig finfet inverters for low power designs. In: IEEE. **2020 IEEE International Symposium on Circuits and Systems (ISCAS).** [S.I.], 2020. p. 5.

MORAES, L. B. et al. Robust finfet schmitt trigger designs for low power applications. In: METZLER, C. et al. (Ed.). **VLSI-SoC: EDA, the New Technology Enabler.** [S.I.], 2020. p. 24.

MORAES, L. B. d. et al. Evaluation of variability using schmitt trigger on full adders layout. **Microelectronics Reliability**, Elsevier, v. 88, p. 116–121, 2018.

MUSTAFA, M.; BHAT, T. A.; BEIGH, M. Threshold voltage sensitivity to metal gate work-function based performance evaluation of double-gate n-finfet structures for lstp technology. Scientific Research Publishing, 2013.

NASSIF, S. Process variability at the 65nm node and beyond. In: IEEE. **Custom Integrated Circuits Conference, 2008. CICC 2008.** IEEE. [S.I.], 2008. p. 1–8.

NAVI, K. et al. A novel low-power full-adder cell for low voltage. In: . [S.I.]: Elsevier, 2009. v. 42, n. 4, p. 457–467.

NAWAZ, S. M. et al. Comparison of random dopant and gate-metal workfunction variability between junctionless and conventional finfets. **IEEE electron device letters**, IEEE, v. 35, n. 6, p. 663–665, 2014.

NEUBERGER, G.; WIRTH, G.; REIS, R. **Protecting chips against hold time violations due to variability.** [S.I.]: Springer, 2014.

PAL, I.; ISLAM, A. Circuit-level technique to design variation-and noise-aware reliable dynamic logic gates. **IEEE Trans. on Device and Materials Reliability**, IEEE, v. 18, n. 2, p. 224–239, 2018.

PAWLOWSKI, R. et al. A 530mv 10-lane simd processor with variation resiliency in 45nm soi. In: IEEE. **2012 IEEE International Solid-State Circuits Conference.** [S.I.], 2012. p. 492–494.

PEDRONI, V. Low-voltage high-speed schmitt trigger and compact window comparator. **Electronics Letters**, IET, v. 41, n. 22, p. 1213–1214, 2005.

PFISTER, A. Novel cmos schmitt trigger with controllable hysteresis. **Electronics Letters**, IET, v. 28, n. 7, p. 639–641, 1992.

- POSSE, G.; SAPATNEKAR, S. S.; REIS, R. **Electromigration Inside Logic Cells: Modeling, Analyzing and Mitigating Signal Electromigration in NanoCMOS.** [S.l.]: Springer, 2016.
- QIAN, K. **Variability modeling and statistical parameter extraction for CMOS devices.** Thesis (PhD) — UC Berkeley, 2015.
- RABAEEY, J.; CHANDRAKASAN, A.; NIKOLIC, B. **Digital integrated circuits.** [S.l.]: Prentice hall Englewood Cliffs, 2002.
- RAHIMI, A.; BENINI, L.; GUPTA, R. K. Variability mitigation in nanometer cmos integrated systems: A survey of techniques from circuits to software. In: . [S.l.]: IEEE, 2016. v. 104, n. 7, p. 1410–1448.
- REIS, R. et al. Circuit level design methods to mitigate soft errors. In: IEEE. **2020 IEEE Latin-American Test Symposium (LATS).** [S.l.], 2020. p. 1–3.
- REN, P. et al. New insights into the hci degradation of pass-gate transistor in advanced finfet technology. In: **2018 IEEE International Reliability Physics Symposium (IRPS).** [S.l.: s.n.], 2018. p. P-CR.3-1–P-CR.3-4.
- RITHE, R. et al. The effect of random dopant fluctuations on logic timing at low voltage. **IEEE Transactions on Very Large Scale Integration (VLSI) Systems**, IEEE, v. 20, n. 5, p. 911–924, 2011.
- SCHROM, G.; DE, V.; SELBERHERR, S. Vlsi performance metric based on minimum tcad simulations. In: IEEE. **SISPAD'97. 1997 International Conference on Simulation of Semiconductor Processes and Devices. Technical Digest.** [S.l.], 1997. p. 25–28.
- SHAH, A. P. et al. Soft error hardening enhancement analysis of nbti tolerant schmitt trigger circuit. **Microelectronics Reliability**, Elsevier, v. 107, p. 113617, 2020.
- SHAMS, A. M.; BAYOUMI, M. A. A novel high-performance cmos 1-bit full-adder cell. In: . [S.l.]: IEEE, 2000. v. 47, n. 5, p. 478–481.
- STEYAERT, M.; SANSEN, W. Novel cmos schmitt trigger. **Electronics Letters**, IET, v. 22, n. 4, p. 203–204, 1986.
- STINE, B. E.; BONING, D. S.; CHUNG, J. E. Analysis and decomposition of spatial variation in integrated circuit processes and devices. **IEEE Transactions on Semiconductor Manufacturing**, IEEE, v. 10, n. 1, p. 24–41, 1997.
- TACHE, M. et al. Reliability and performance of optimised schmitt trigger gates. **The Journal of Engineering**, IET, v. 2018, n. 8, p. 735–744, 2018.
- TAKEDA, E.; SUZUKI, N. An empirical model for device degradation due to hot-carrier injection. **IEEE electron device letters**, IEEE, v. 4, n. 4, p. 111–113, 1983.
- TAUR, Y.; NING, T. H. **Fundamentals of modern VLSI devices.** [S.l.]: Cambridge university press, 2013.
- TOLEDO, S. P.; ZIMPECK, A. L.; MEINHARDT, C. Impact of schmitt trigger inverters on process variability robustness of 1-bit full adders. In: IEEE. **Conference on Electronics, Circuits and Systems (ICECS).** [S.l.], 2016.

- TOLEDO, S. P. et al. Pros and cons of schmitt trigger inverters to mitigate pvt variability on full adders. In: IEEE. **2018 IEEE International Symposium on Circuits and Systems (ISCAS)**. [S.I.], 2018. p. 1–5.
- TSCHANZ, J. W. et al. Adaptive body bias for reducing impacts of die-to-die and within-die parameter variations on microprocessor frequency and leakage. **IEEE Journal of Solid-State Circuits**, IEEE, v. 37, n. 11, p. 1396–1402, 2002.
- WANG, W. et al. Statistical prediction of circuit aging under process variations. In: IEEE. **2008 IEEE Custom Integrated Circuits Conference**. [S.I.], 2008. p. 13–16.
- WANG, X. et al. Statistical threshold-voltage variability in scaled decanometer bulk hkmg mosfets: A full-scale 3-d simulation scaling study. In: . [S.I.]: IEEE, 2011. v. 58, n. 8, p. 2293–2301.
- WESTE, N. H. E.; ESHRAGHIAN, K. **Principles of CMOS VLSI design**. [S.I.]: Addison-Wesley New York, 1985.
- WONG, H.-S. et al. Nanoscale cmos. **Proceedings of the IEEE**, IEEE, v. 87, n. 4, p. 537–570, 1999.
- XIONG, S.; BOKOR, J. Sensitivity of double-gate and finfetdevices to process variations. In: . [S.I.: s.n.], 2003. v. 50, n. 11, p. 2255–2261.
- YOUNG, D.; CHRISTOU, A. Failure mechanism models for electromigration. **IEEE Transactions on Reliability**, IEEE, v. 43, n. 2, p. 186–192, 1994.
- ZEGHBROECK, B. V. Principles of semiconductor devices. **Colarado University**, v. 34, 2004.
- ZHANG, C.; SRIVASTAVA, A.; AJMERA, P. K. Low voltage cmos schmitt trigger circuits. In: . [S.I.]: IET, 2003. v. 39, n. 24, p. 1696–1698.
- ZHANG, R. et al. Modeling of the reliability degradation of a finfet-based sram due to bias temperature instability, hot carrier injection, and gate oxide breakdown. In: **2017 IEEE International Integrated Reliability Workshop (IIRW)**. [S.I.: s.n.], 2017. p. 1–4.
- ZIMPECK, A. L. et al. Finfet cells with different transistor sizing techniques against pvt variations. In: IEEE. **Circuits and Systems (ISCAS), 2016 IEEE International Symposium on**. [S.I.], 2016. p. 45–48.

ANNEX A — PUBLICATIONS

A.1 Published

MORAES, L. B. d. et al. Evaluation of variability using schmitt trigger on full adders layout. **Microelectronics Reliability**, Elsevier, v. 88, p. 116–121, 2018.

MORAES, L. et al. Exploring schmitt trigger circuits for process variability mitigation. In: IEEE. **2019 17th IEEE International New Circuits and Systems Conference (NEWCAS)**. [S.I.], 2019. p. 1–4.

MORAES, L. et al. Minimum energy finfet schmitt trigger design considering process variability. In: IEEE. **2019 IFIP/IEEE 27th International Conference on Very Large Scale Integration (VLSI-SoC)**. [S.I.], 2019. p. 88–93.

A.2 Co-author

REIS, R. et al. Circuit level design methods to mitigate soft errors. In: IEEE. **2020 IEEE Latin-American Test Symposium (LATS)**. [S.I.], 2020. p. 1–3.

A.3 Submitted and Accepted

MORAES, L. B. et al. Pros and cons of st and sig finfet inverters for low power designs. In: IEEE. **2020 IEEE International Symposium on Circuits and Systems (ISCAS)**. [S.I.], 2020. p. 5.

A.4 Book Chapter (to be published)

MORAES, L. B. et al. Robust finfet schmitt trigger designs for low power applications. In: METZLER, C. et al. (Ed.). **VLSI-SoC: EDA, the New Technology Enabler**. [S.I.], 2020. p. 24.

A.5 In Proceedings

MORAES, L. B. et al. Low energy and process variability analysis over finfet schmitt trigger design. In: SBC/SBMICRO. **In Proceedings: 2019 WCAS - Workshop on Circuits and Systems Design.** [S.I.], 2019. p. 4.

MORAES, L. B. et al. Process variability attenuation using schmitt trigger at near-threshold operation. In: SBC/SBMICRO. **In Proceedings: 2018 WCAS - Workshop on Circuits and Systems Design.** [S.I.], 2018. p. 4.

MORAES, L. B. et al. Evaluation of variability through schmitt trigger technique on cmos full adder design. In: SBC/SBMICRO. **In Proceedings: 2018 SIM - Simpósio de Microeletrônica.** [S.I.], 2018. p. 4.

ANNEX B — INVERTER DESIGNS LAYOUTS

Figure B.1: 1 fin inverter layout. Height (H): 270nm, Width (W): 162nm, Area (A): 43,740nm².

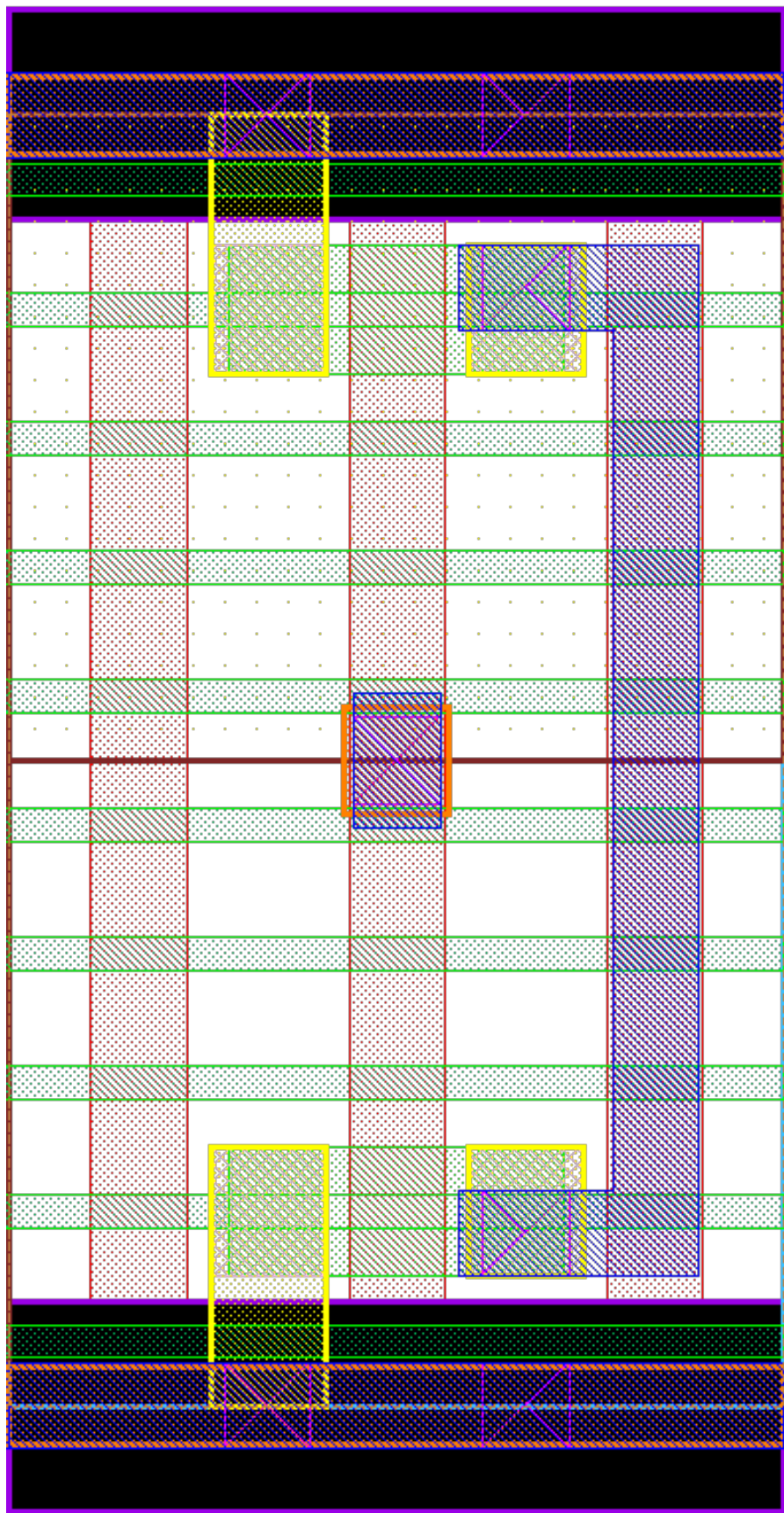
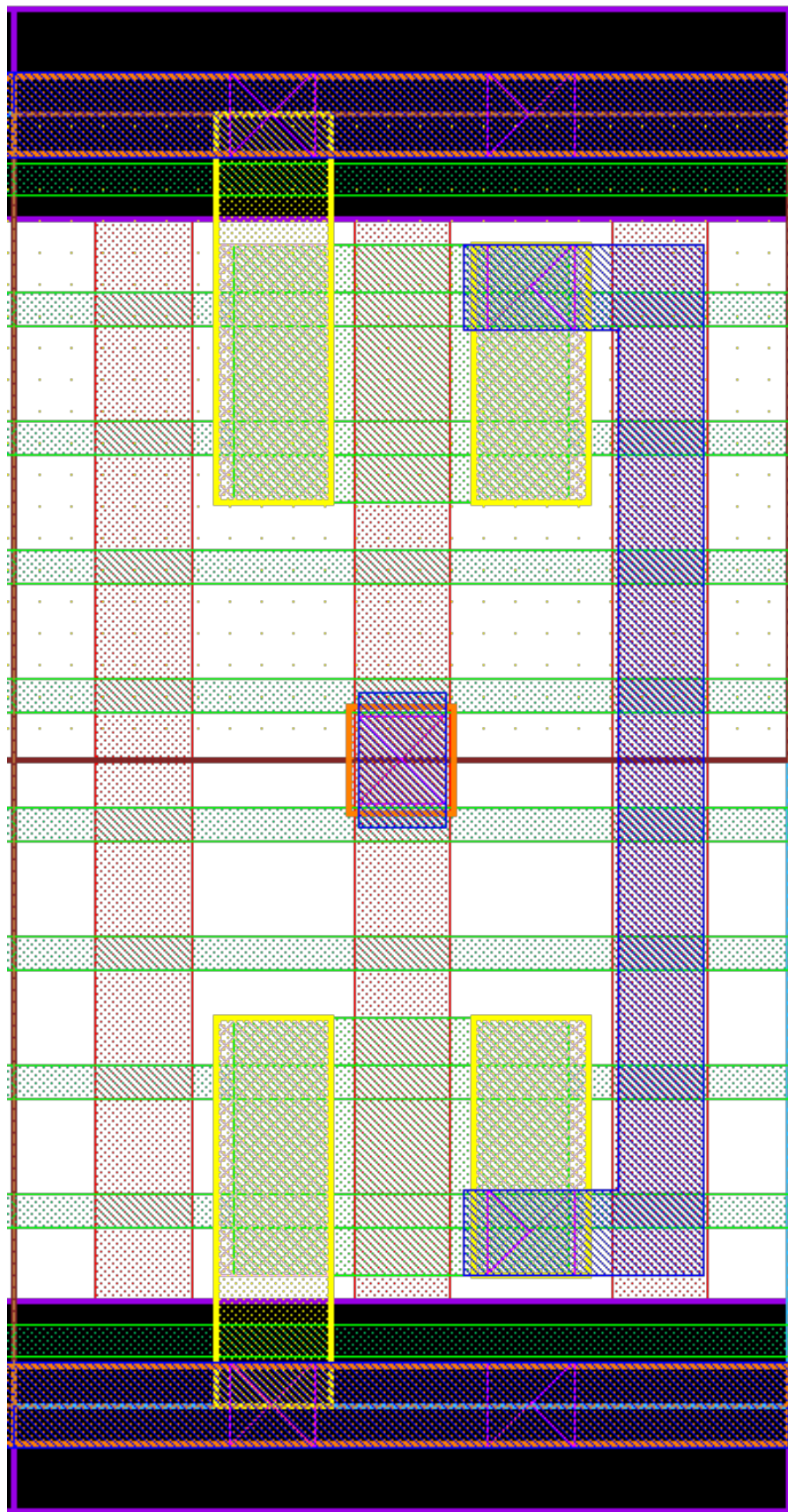
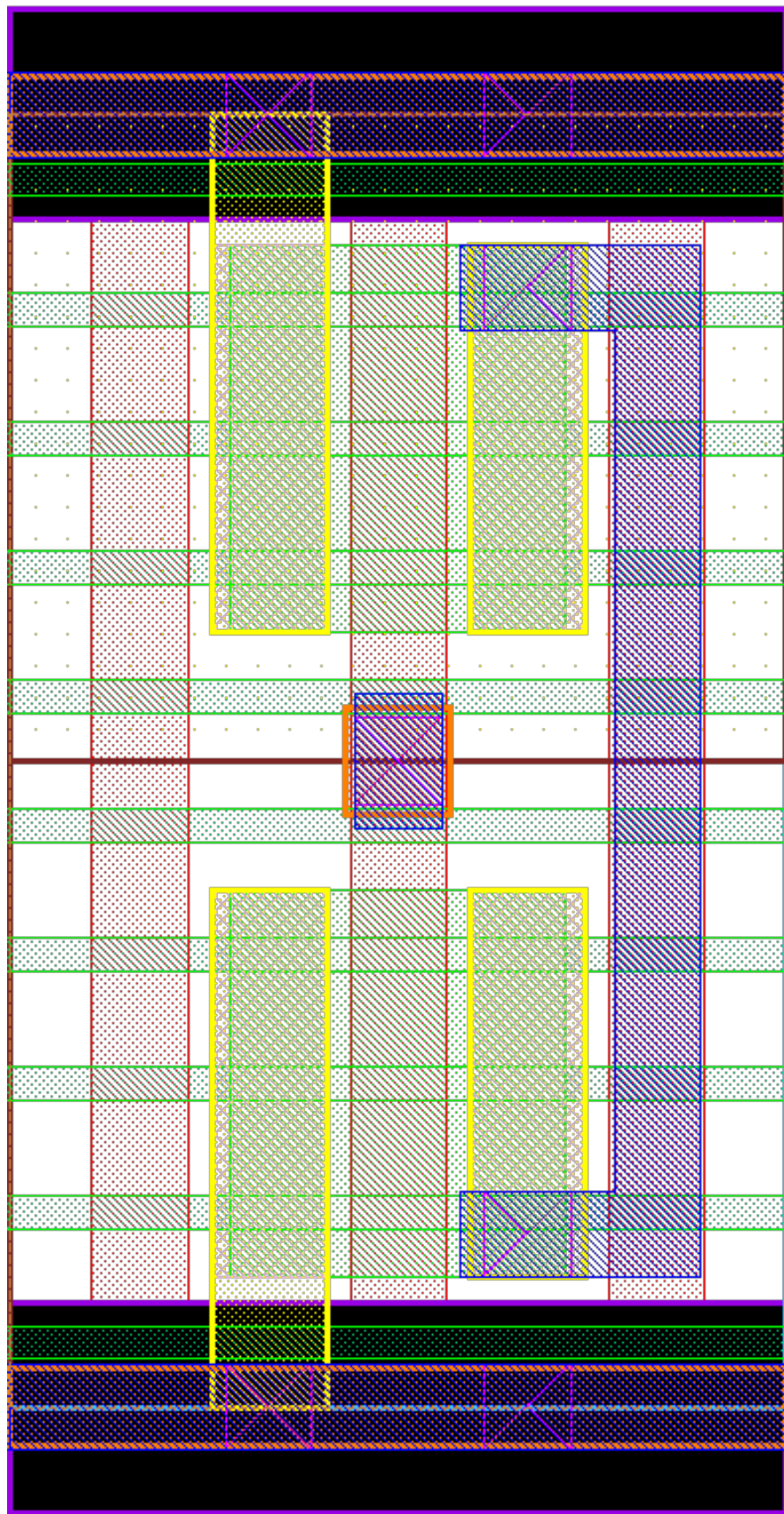


Figure B.2: 2 fins inverter layout. H: 270nm, W: 162nm, A: 43,740nm².



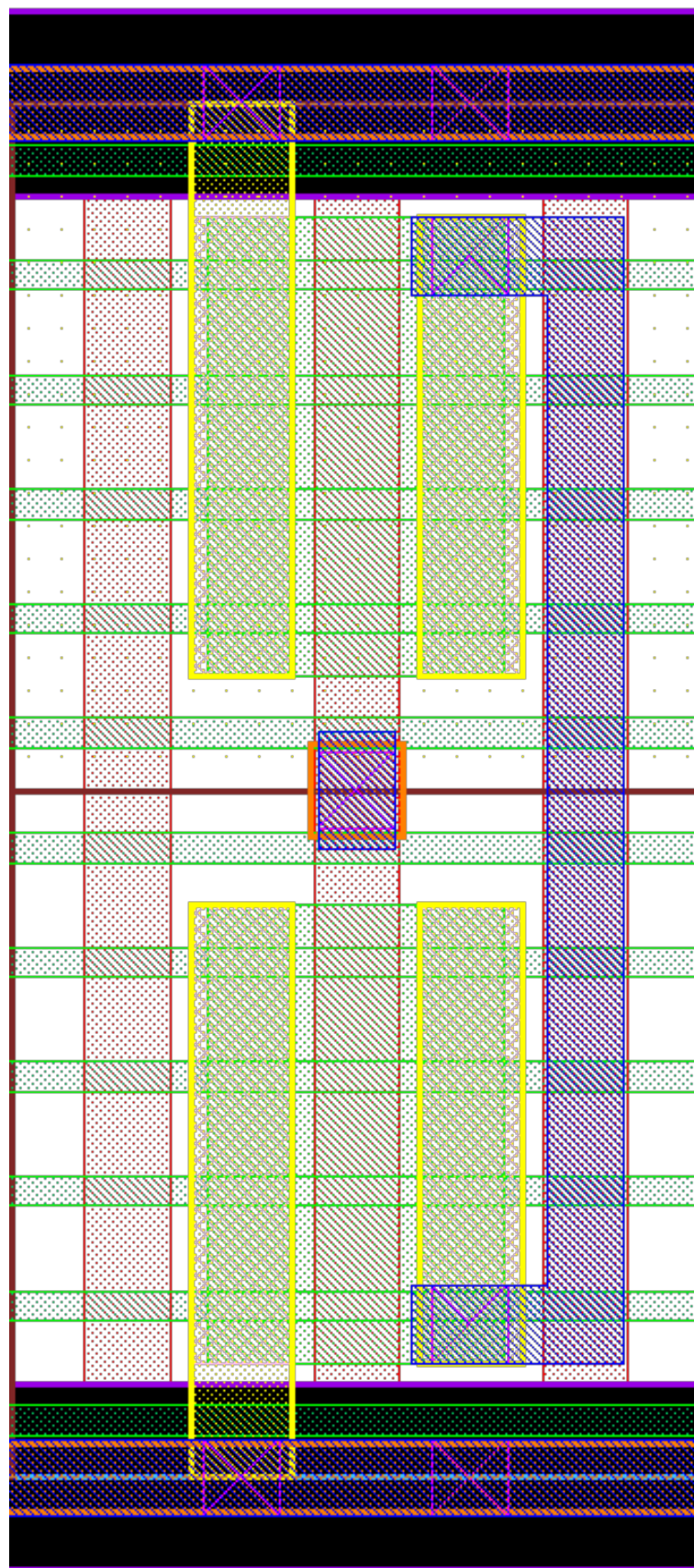
Source: From the author.

Figure B.3: 3 fins inverter layout. H: 270nm, W: 162nm, A: 43,740nm².



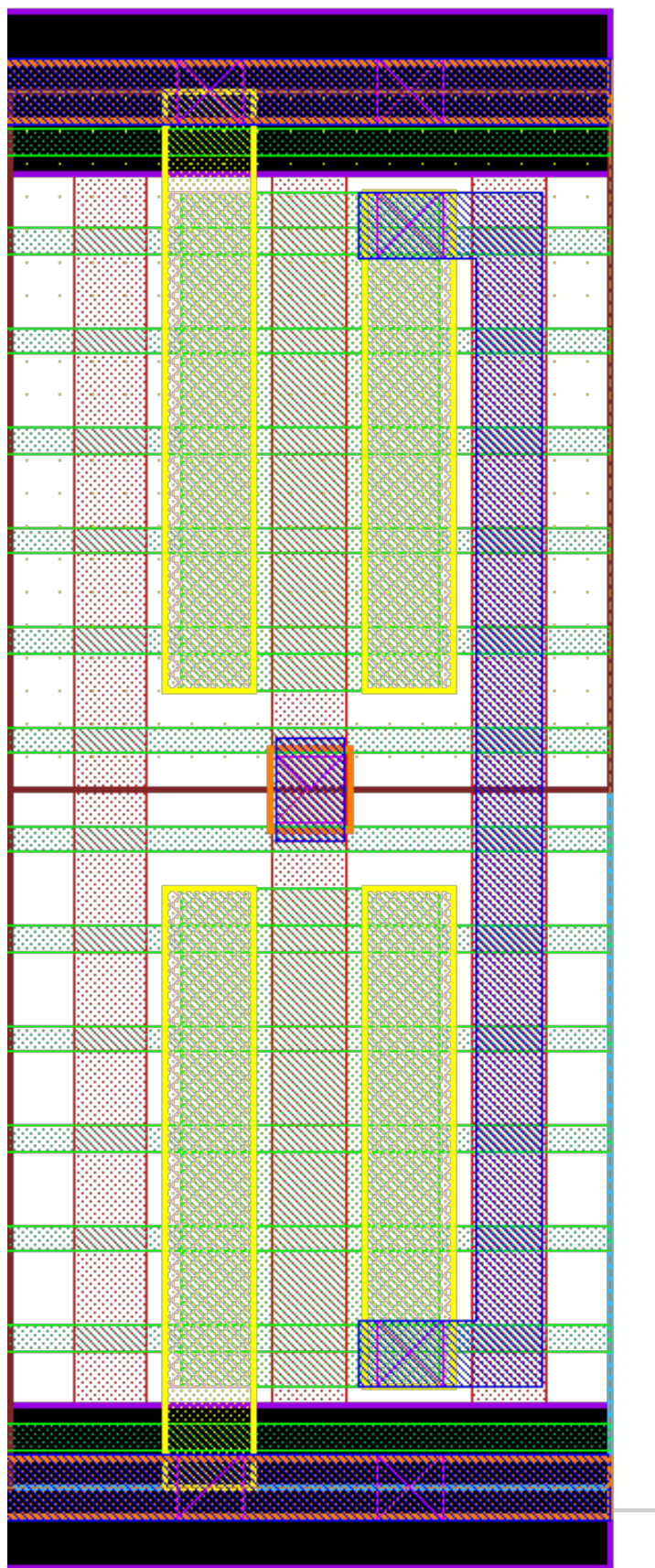
Source: From the author.

Figure B.4: 4 fins inverter layout. H: 324nm, W: 162nm, A: 52,488nm².



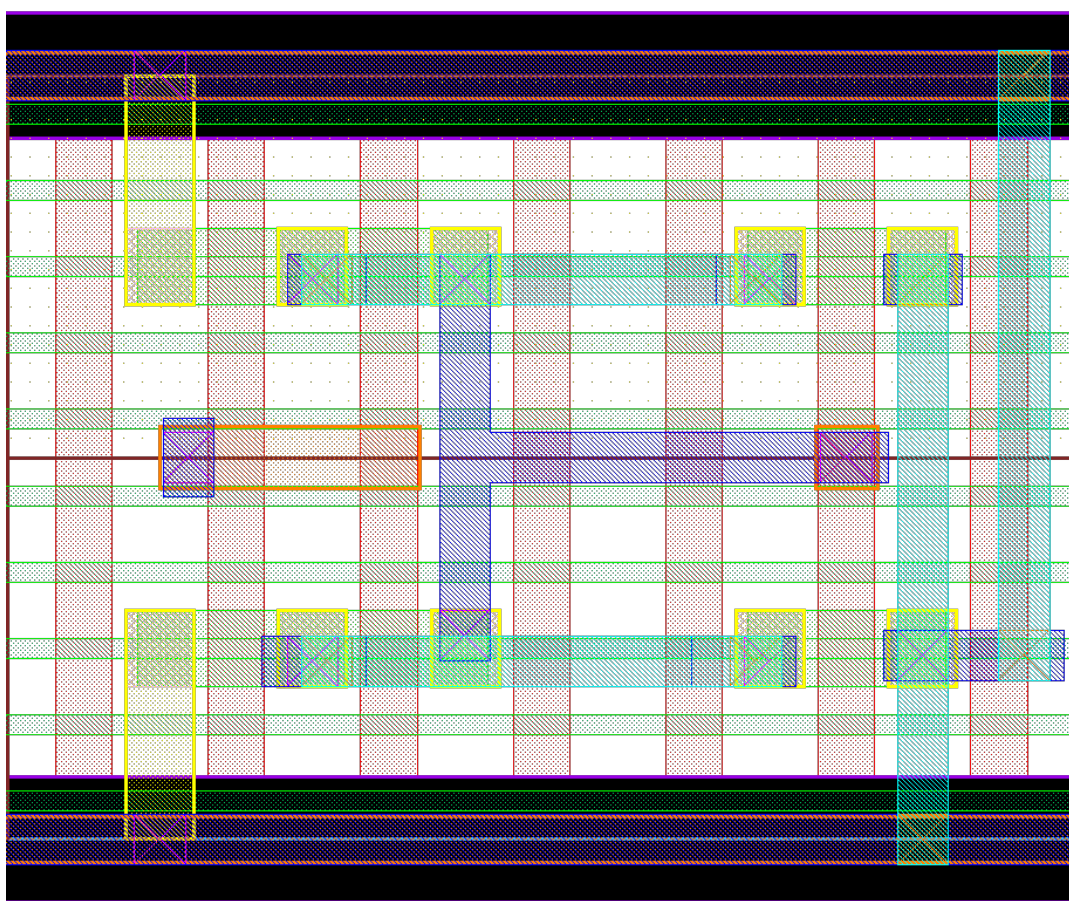
Source: From the author.

Figure B.5: 5 fins inverter layout. H: 378nm, W: 162nm, A: 61,236nm².



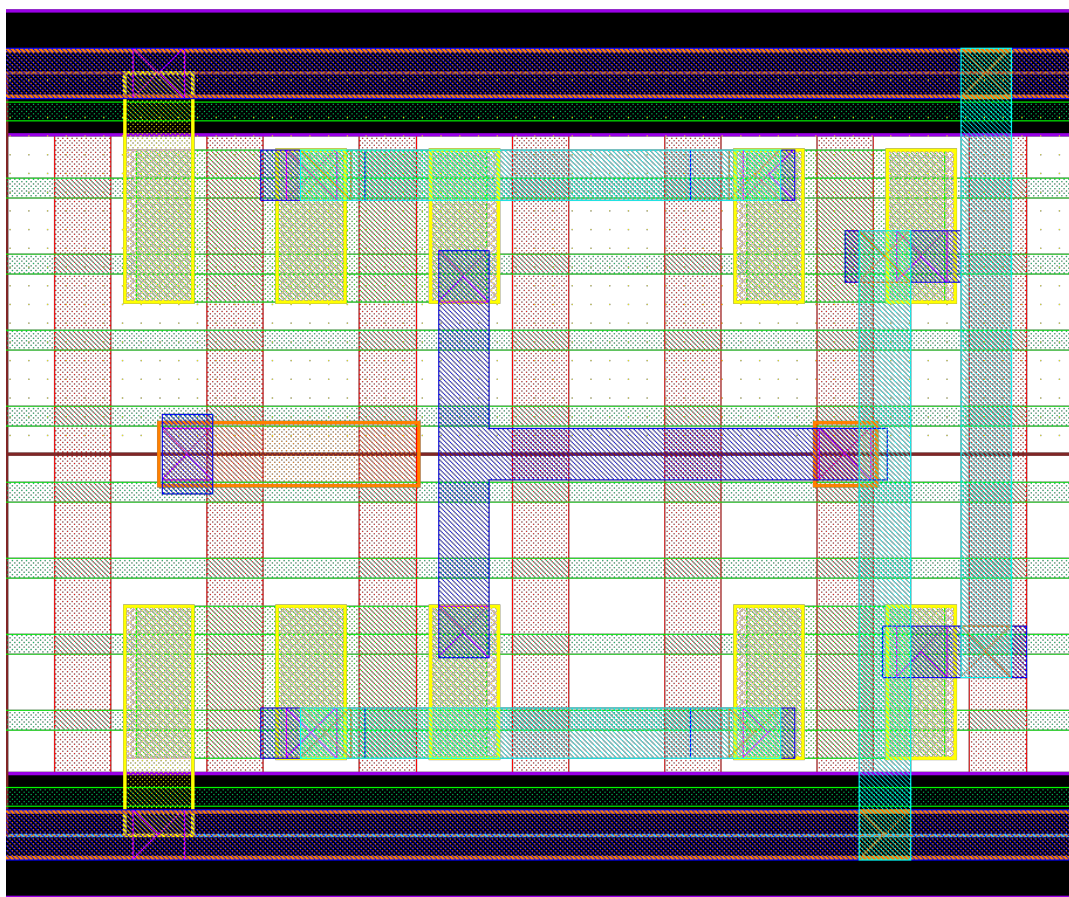
Source: From the author.

Figure B.6: 1 fin ST layout. H: 270nm, W: 378nm, A: 102,060nm².



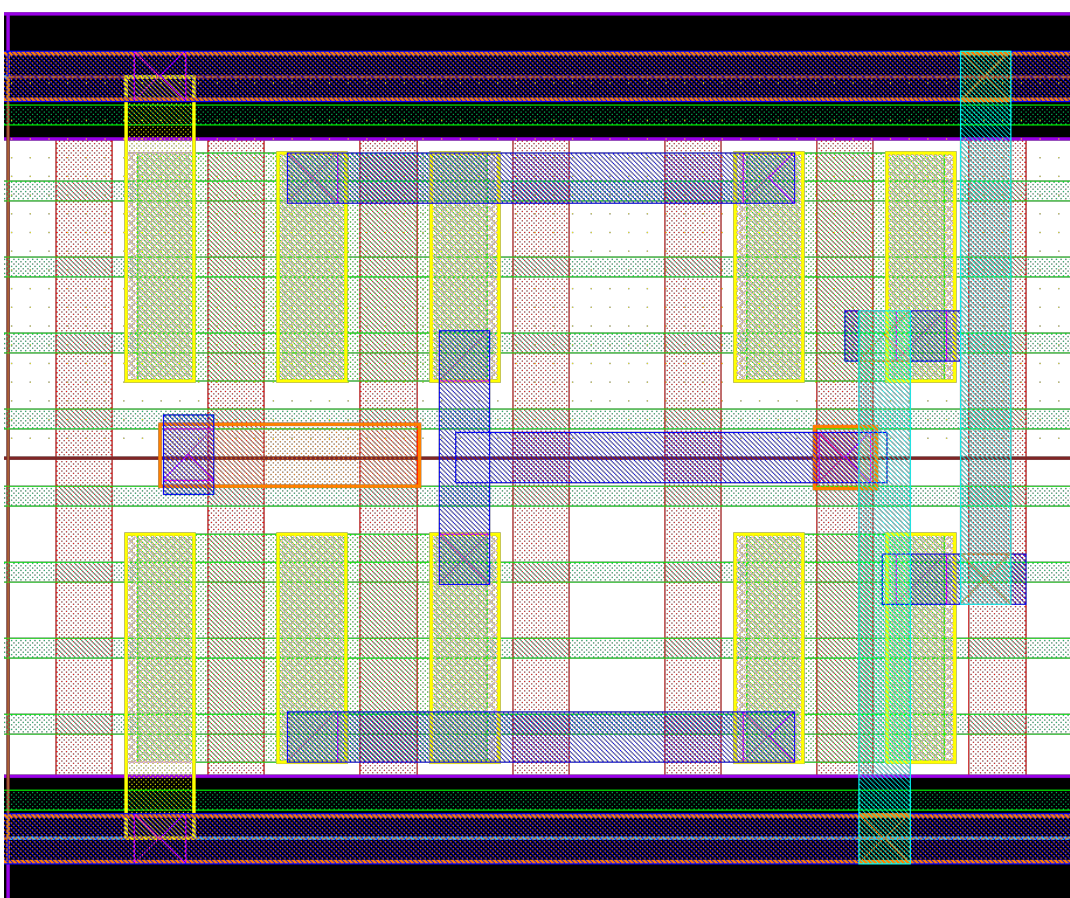
Source: From the author.

Figure B.7: 2 fins ST layout. H: 270nm, W: 378nm, A: 102,060nm².



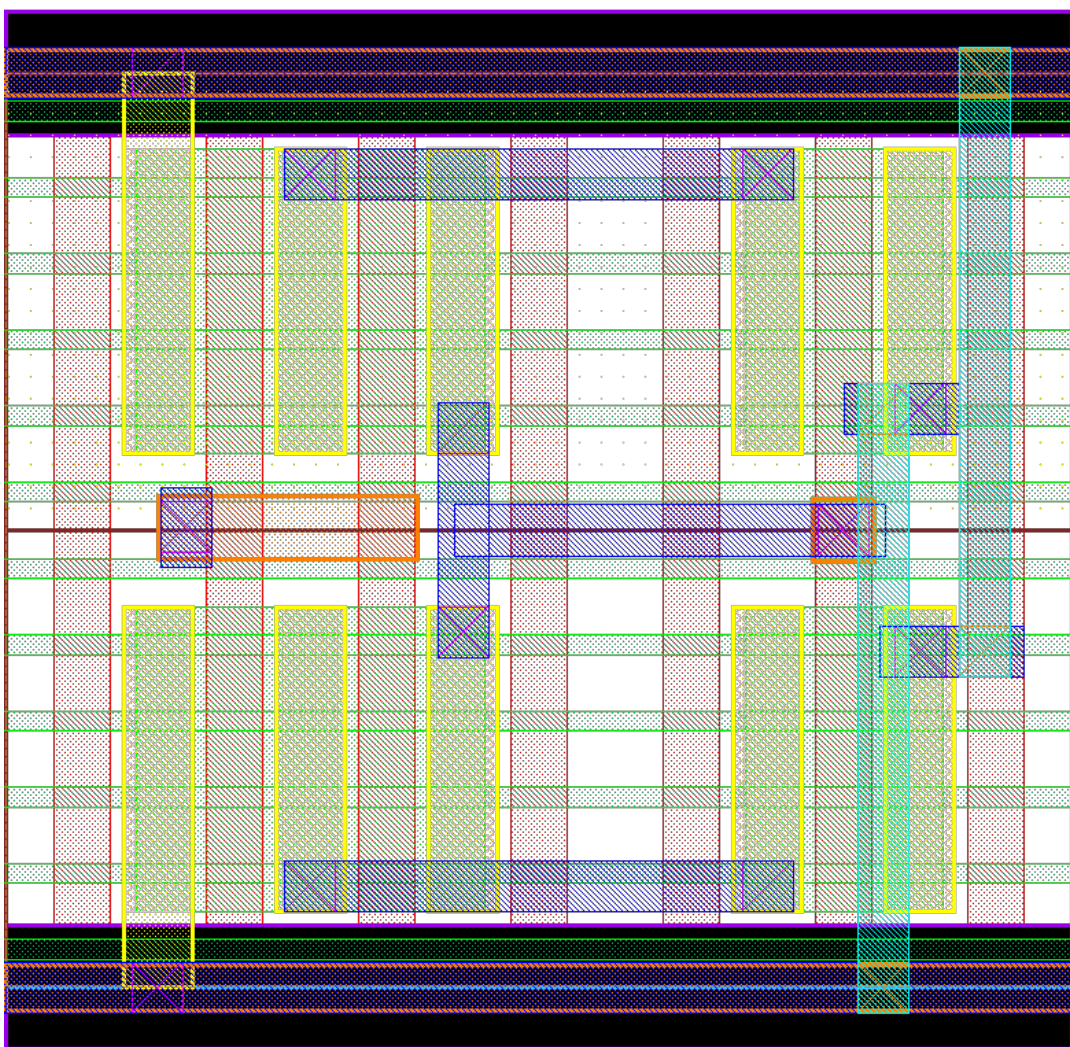
Source: From the author.

Figure B.8: 3 fins ST layout. H: 270nm, W: 378nm, A: 102,060nm².



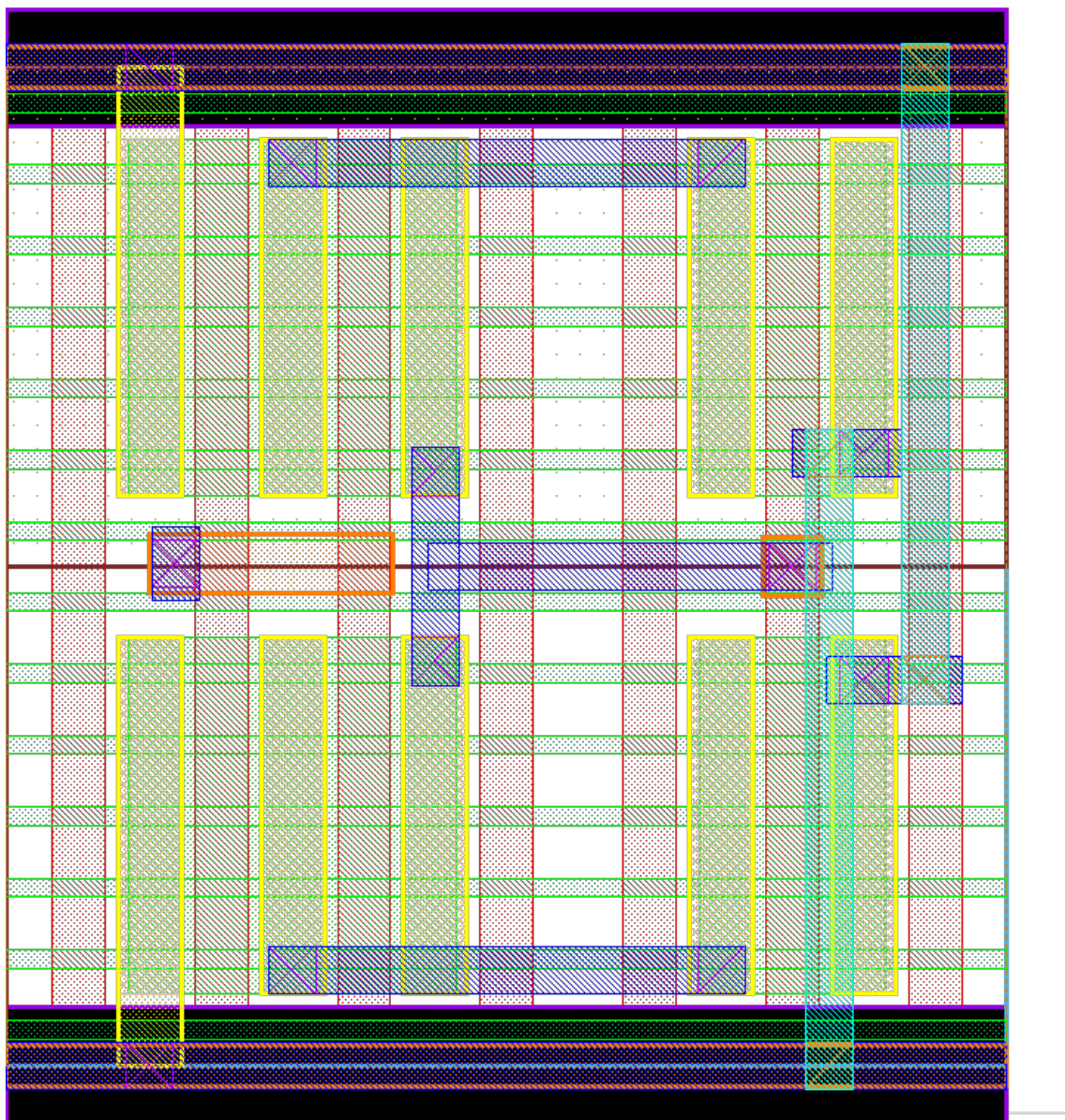
Source: From the author.

Figure B.9: 4 fins ST layout. H: 324nm, W: 378nm, A: 122,472nm².



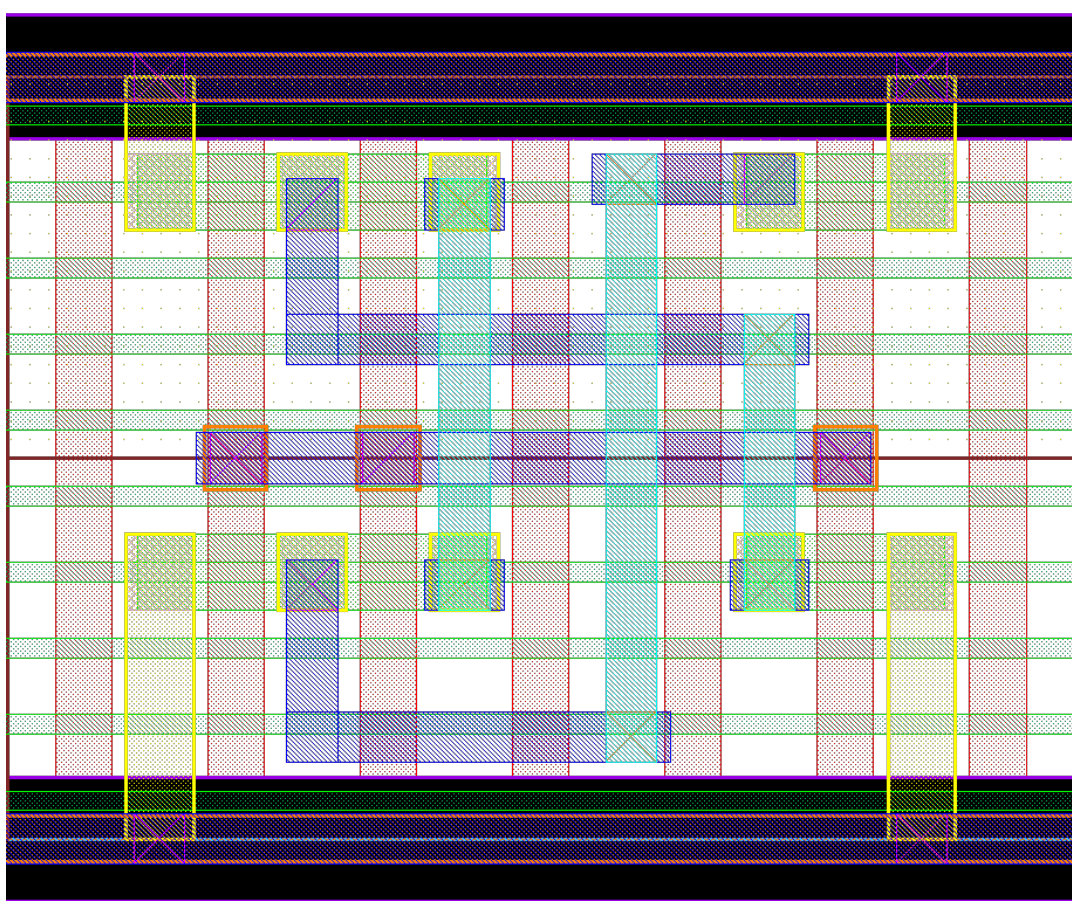
Source: From the author.

Figure B.10: 5 fins ST layout. H: 378nm, W: 378nm, A: 142,884nm².



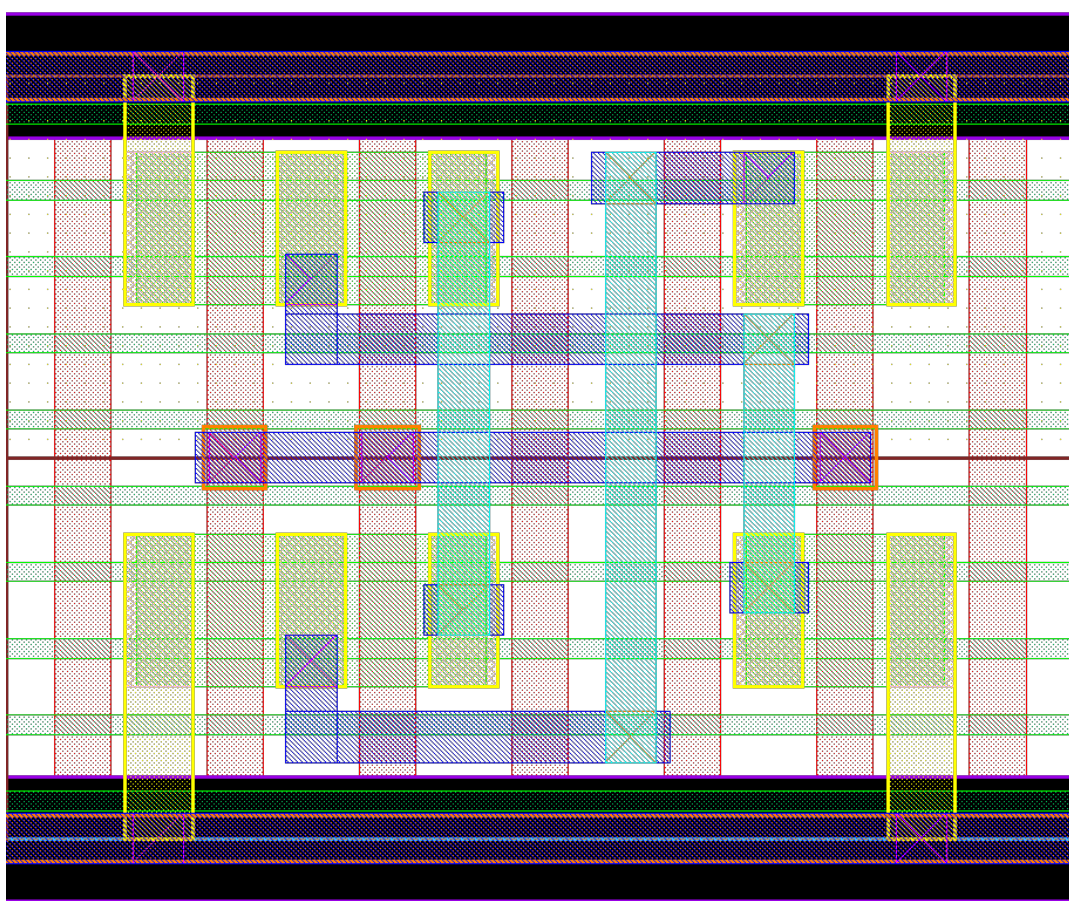
Source: From the author.

Figure B.11: 1 fin SIG layout. H: 270nm, W: 378nm, A: 102,060nm².



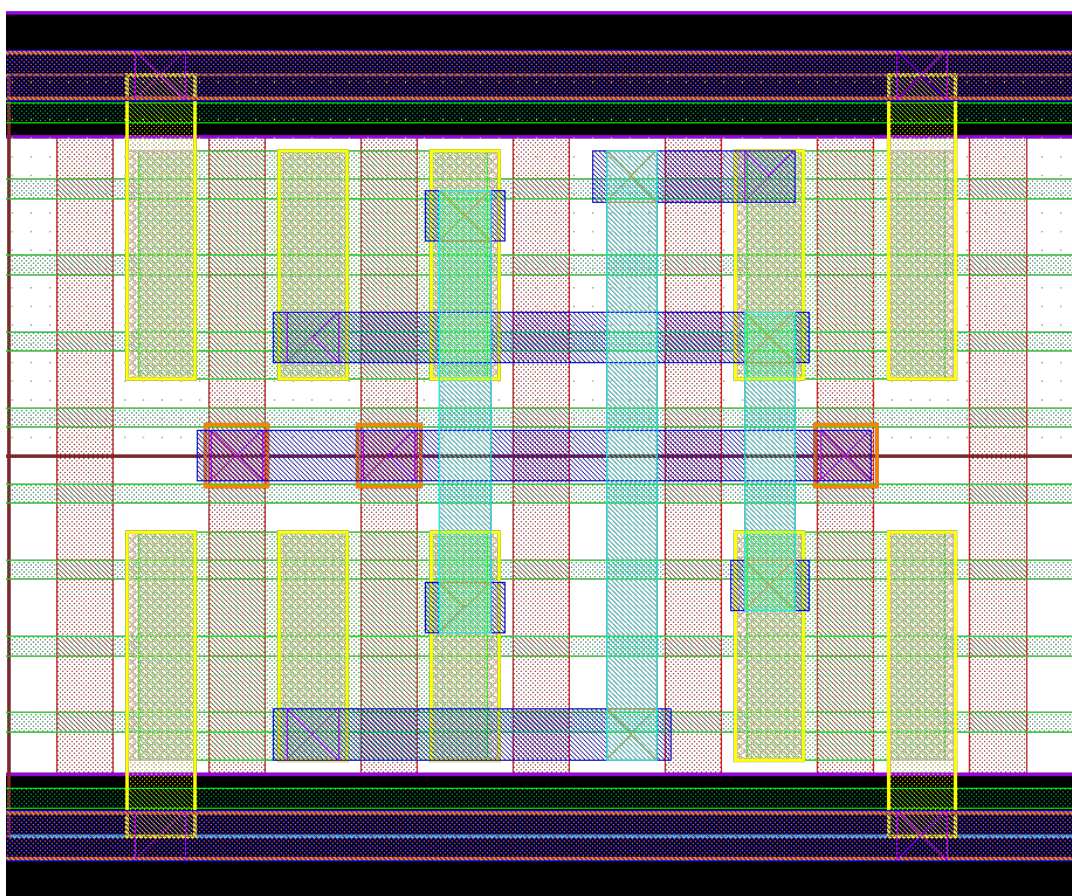
Source: From the author.

Figure B.12: 2 fins SIG layout. H: 270nm, W: 378nm, A: 102,060nm².



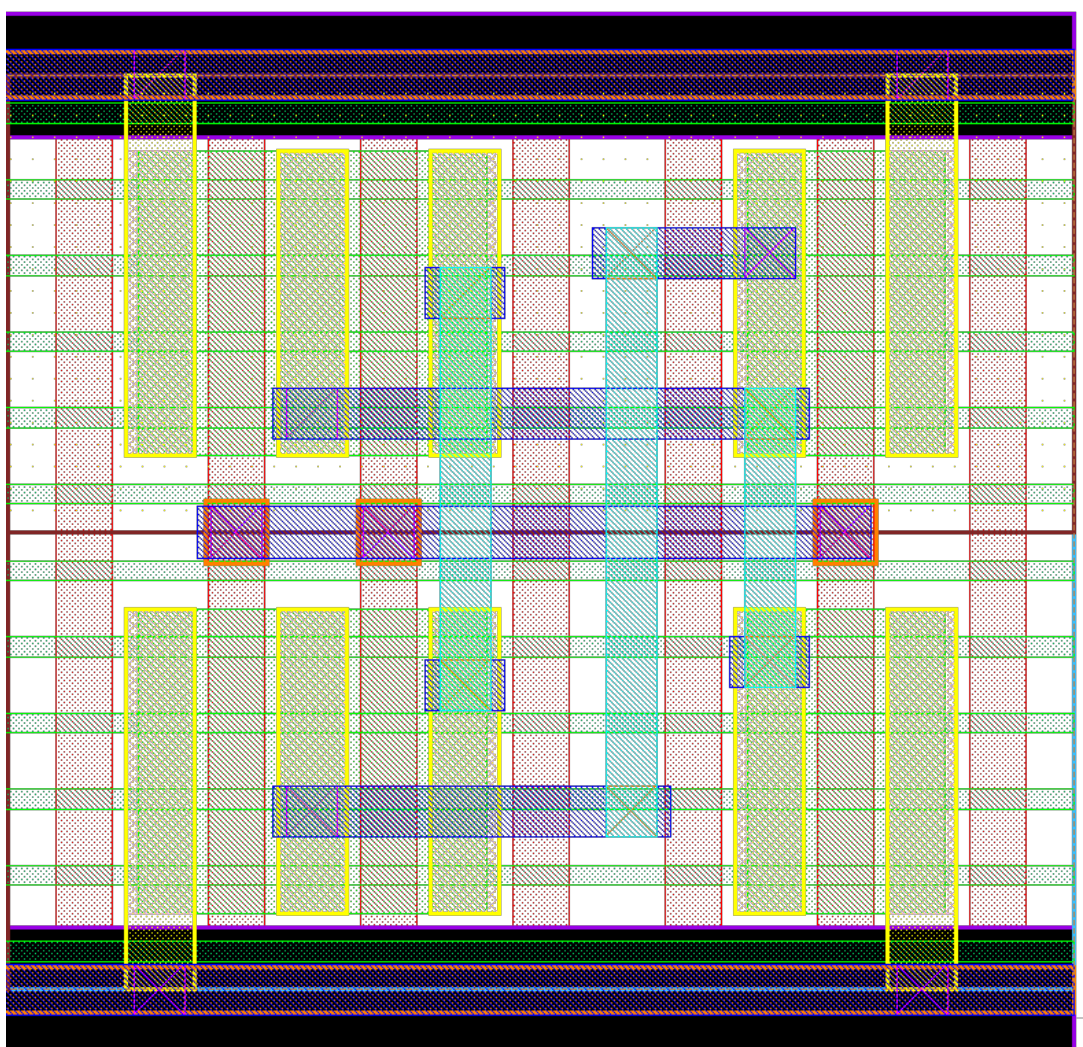
Source: From the author.

Figure B.13: 3 fins SIG layout. H: 270nm, W: 378nm, A: 102,060nm².



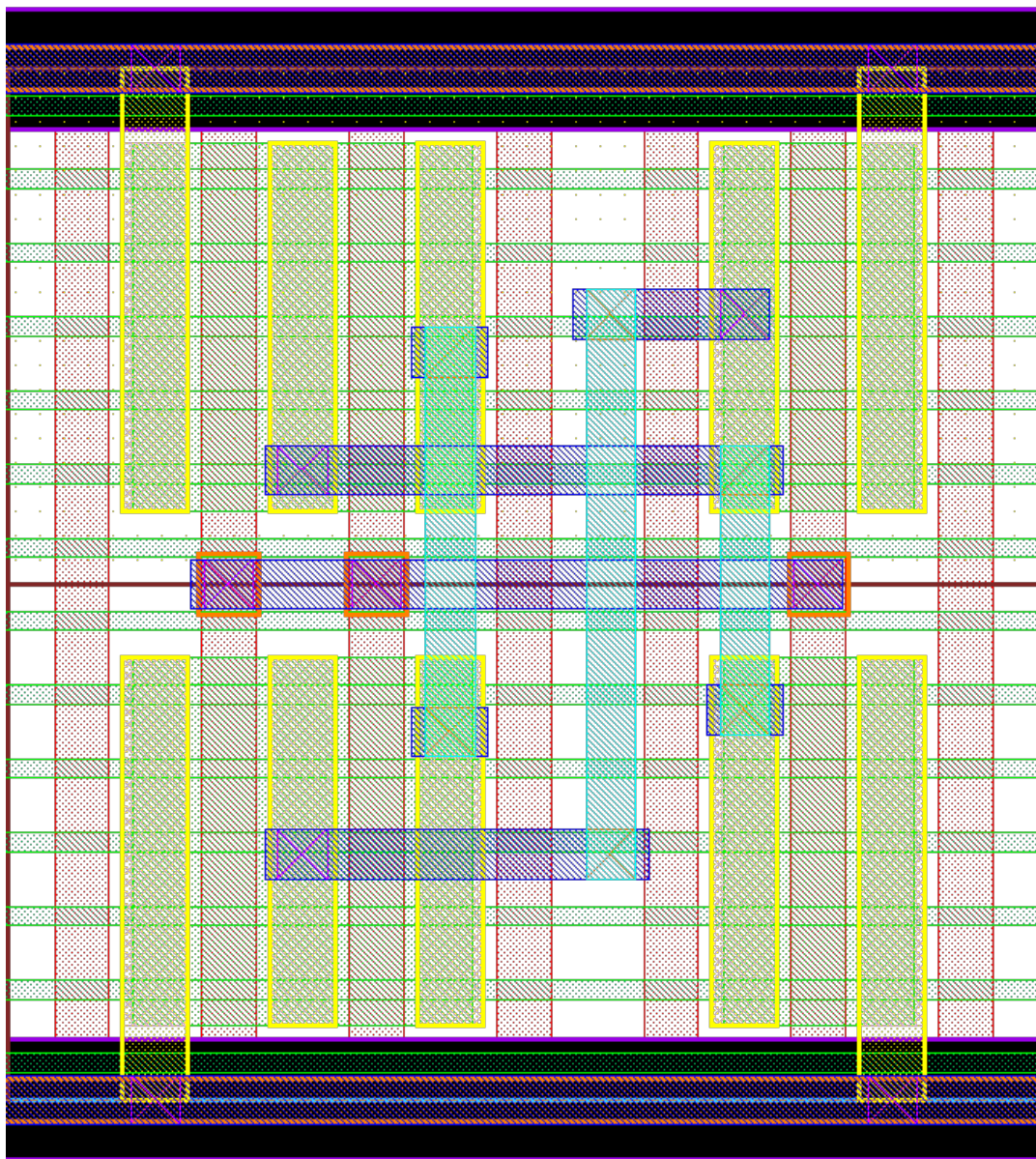
Source: From the author.

Figure B.14: 4 fins SIG layout. H: 324nm, W: 378nm, A: 122,472nm².



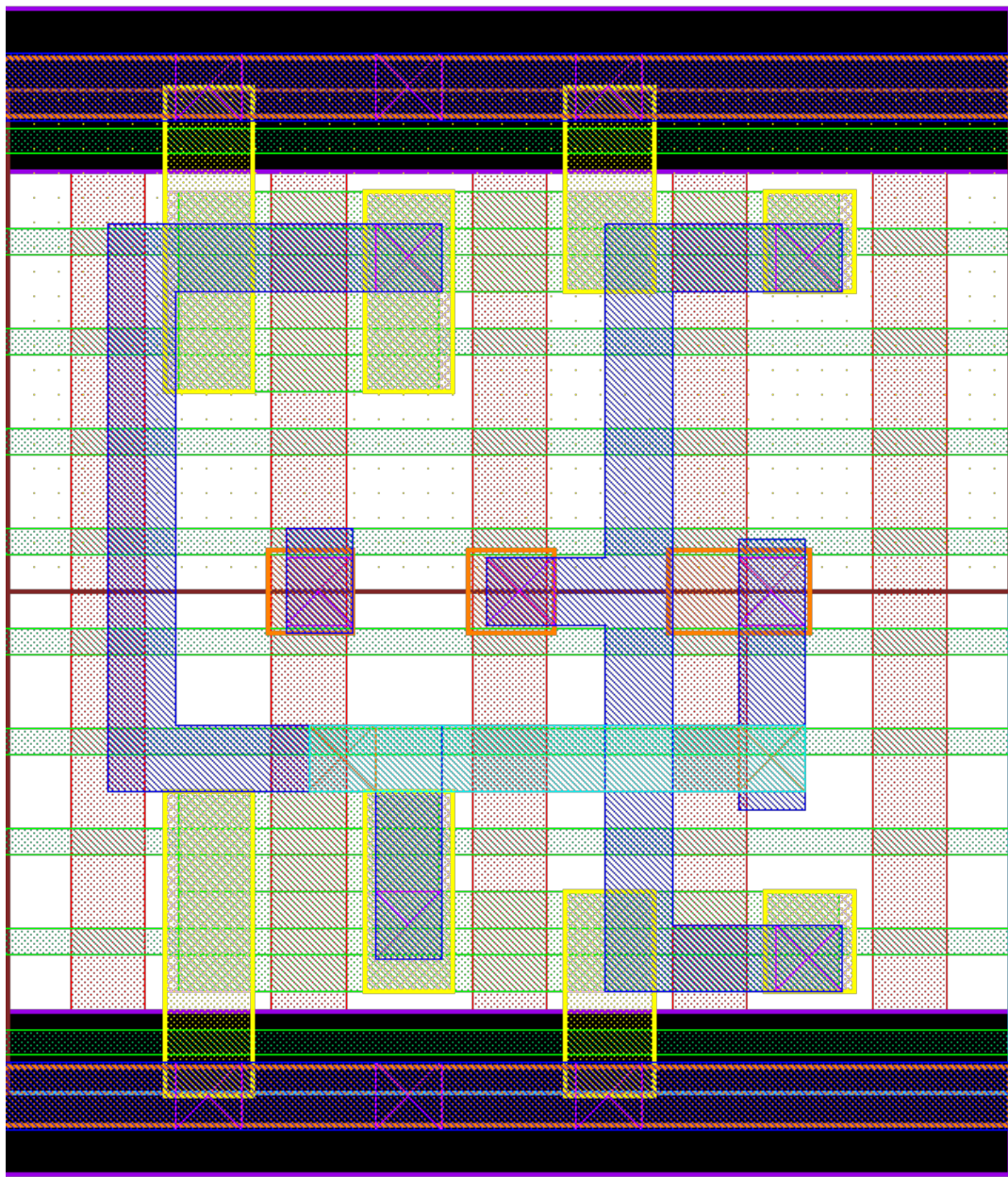
Source: From the author.

Figure B.15: 5 fins SIG layout. H: 378nm, W: 378nm, A: 142,884nm².



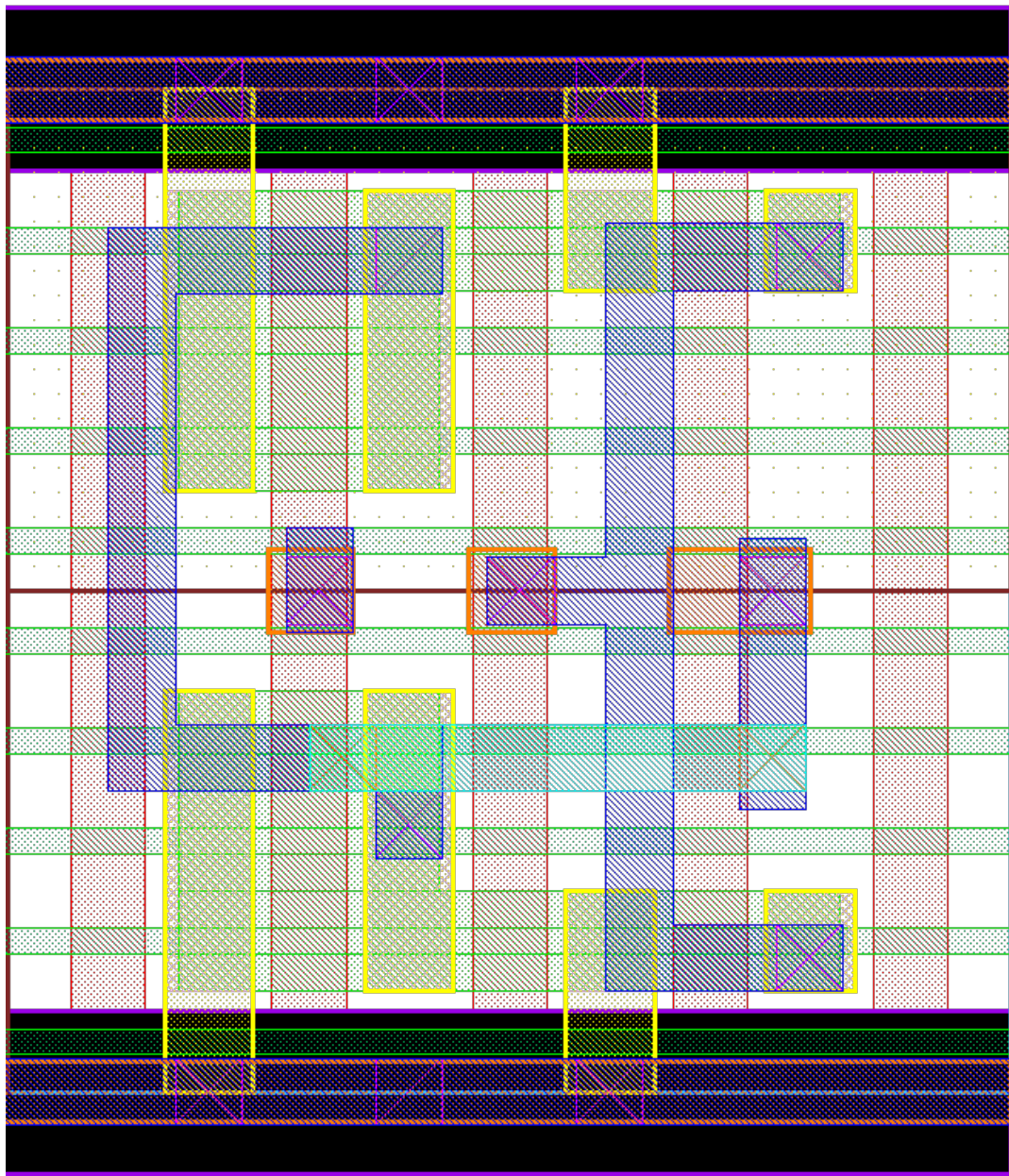
Source: From the author.

Figure B.16: 2 fin max., proportion 2:1 TIST layout. H: 270nm, W: 270nm, A: 72,900nm².



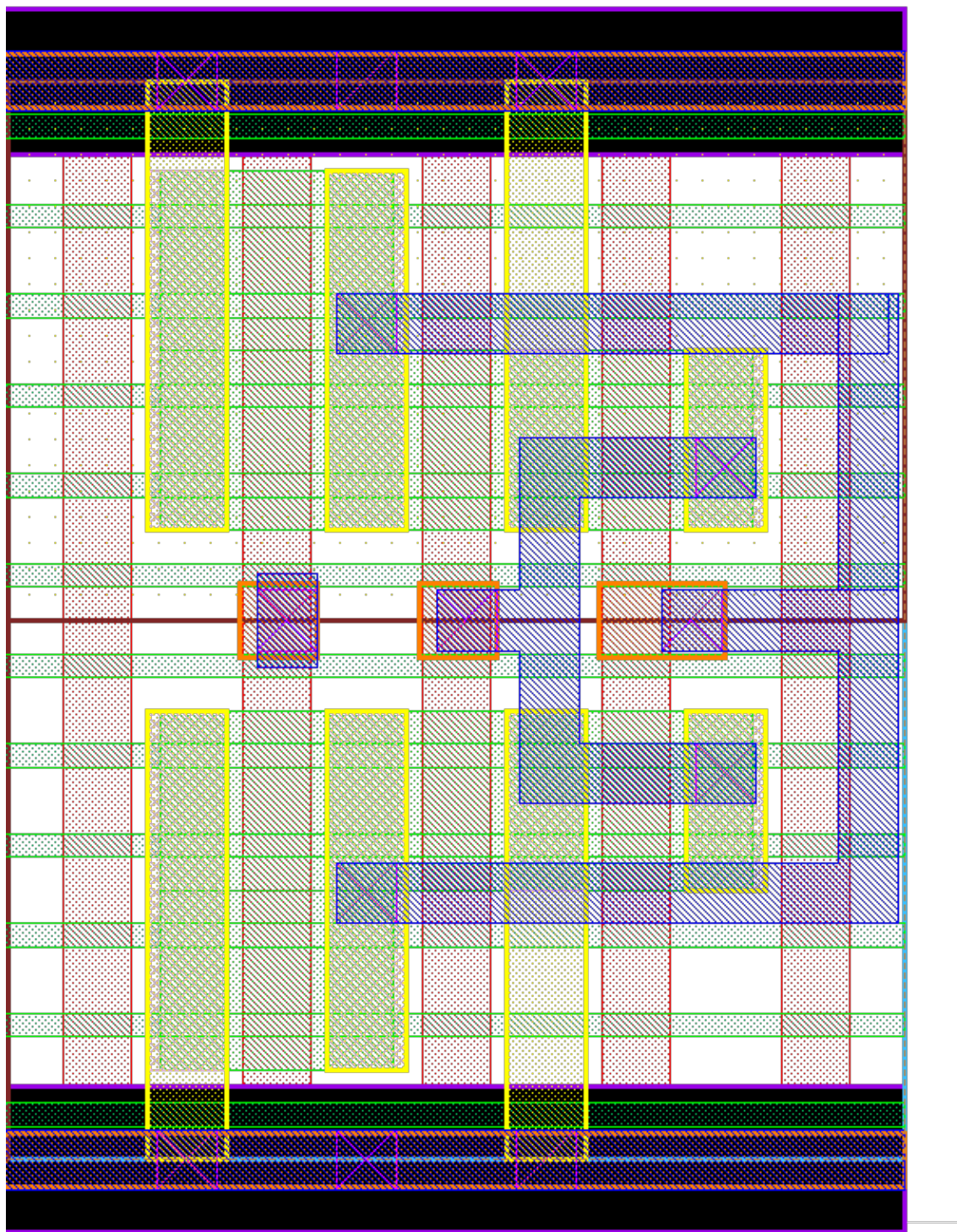
Source: From the author.

Figure B.17: 3 fin max., proportion 3:1 TIST layout. H: 270nm, W: 270nm, A: 72,900nm².



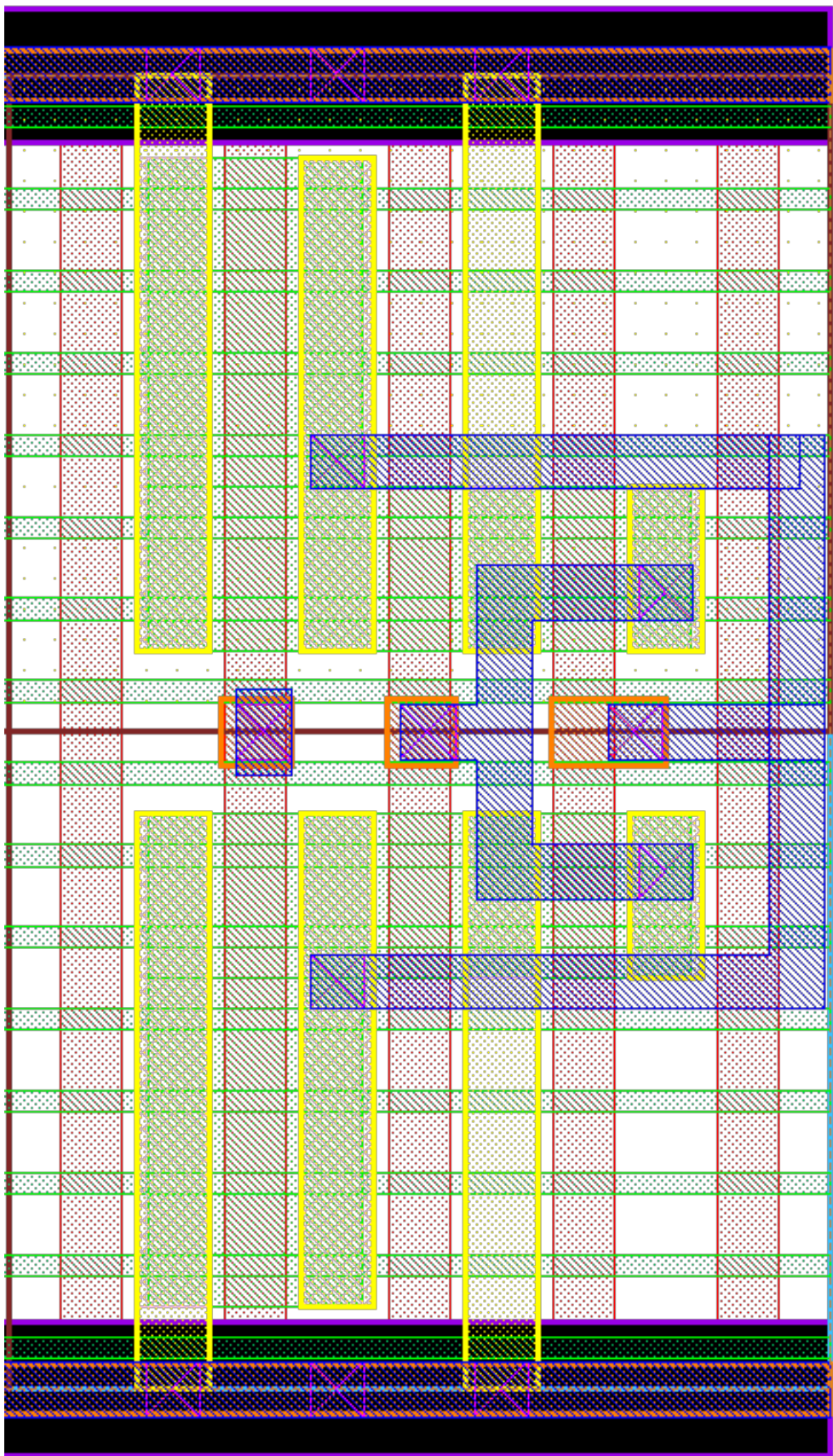
Source: From the author.

Figure B.18: 4 fin max., proportion 2:1 TIST layout. H: 324nm, W: 270nm, A: 87,480nm².



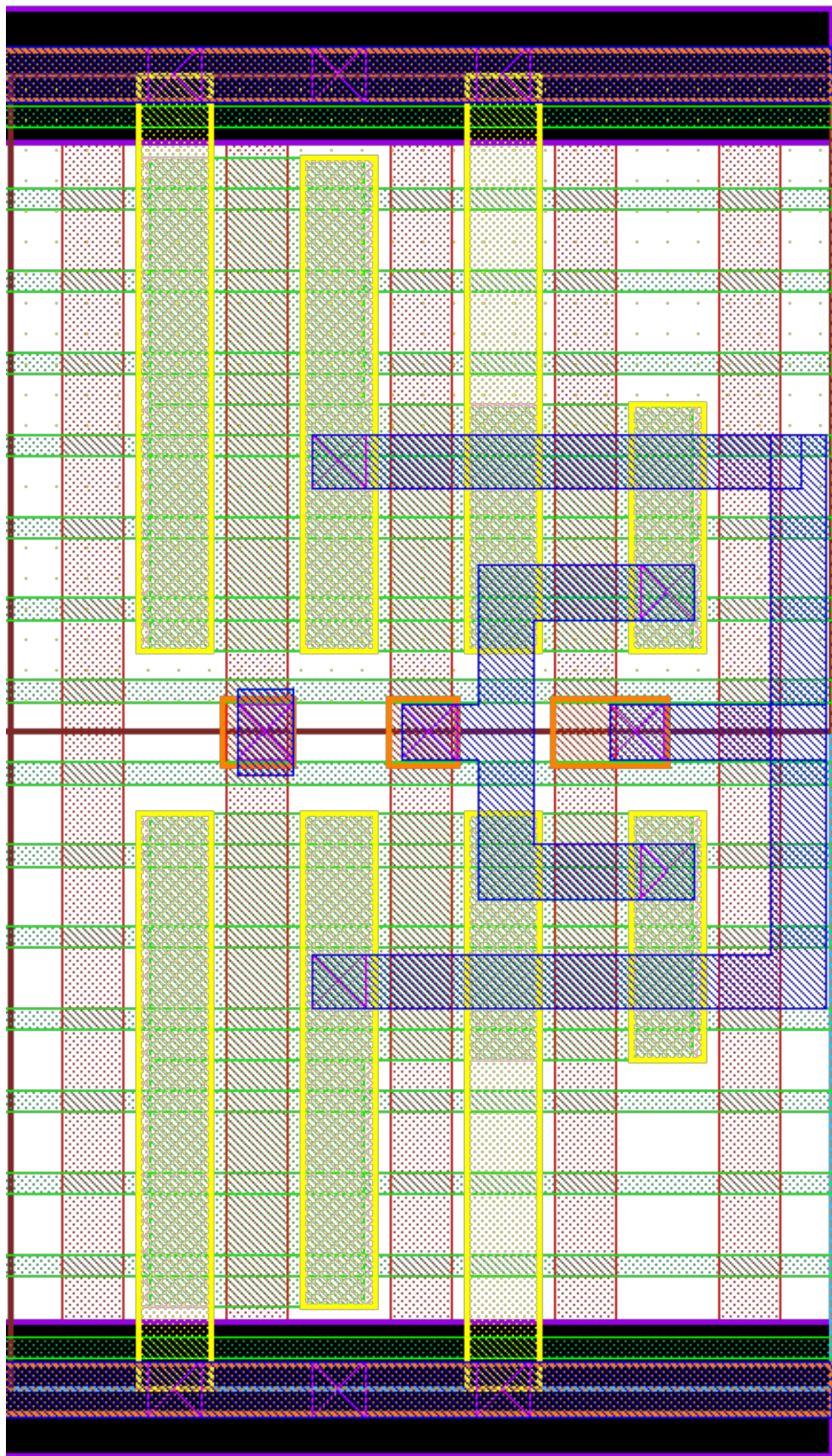
Source: From the author.

Figure B.19: 6 fin max., proportion 3:1 TIST layout. H: 432nm, W: 270nm, A: 116,640nm².



Source: From the author.

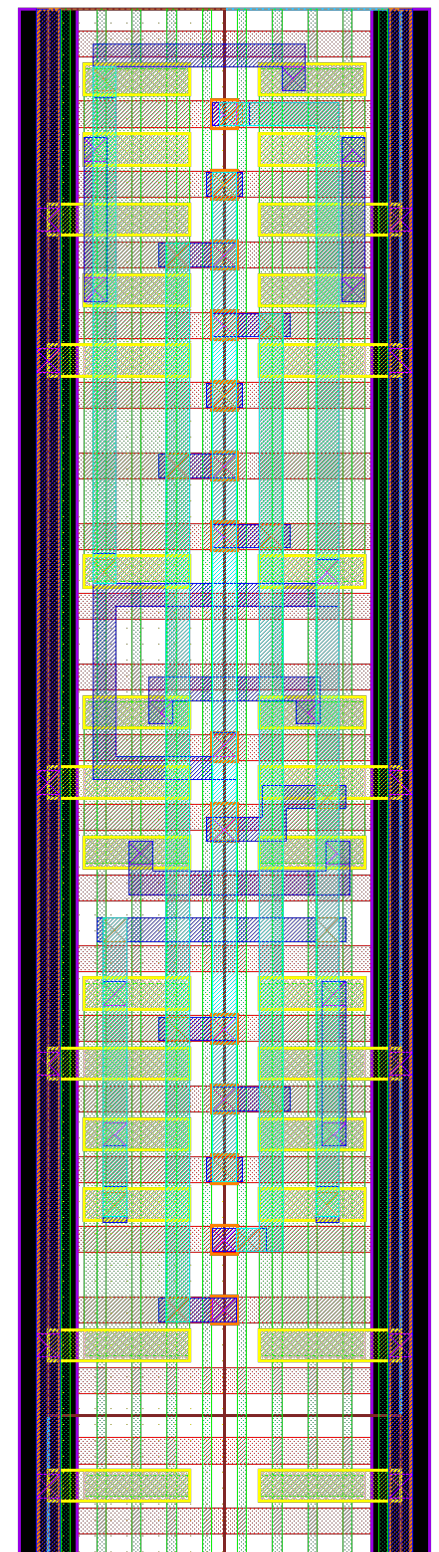
Figure B.20: 6 fin max., proportion 2:1 TIST layout. H: 432nm, W: 270nm, A: 116,640nm².



Source: From the author.

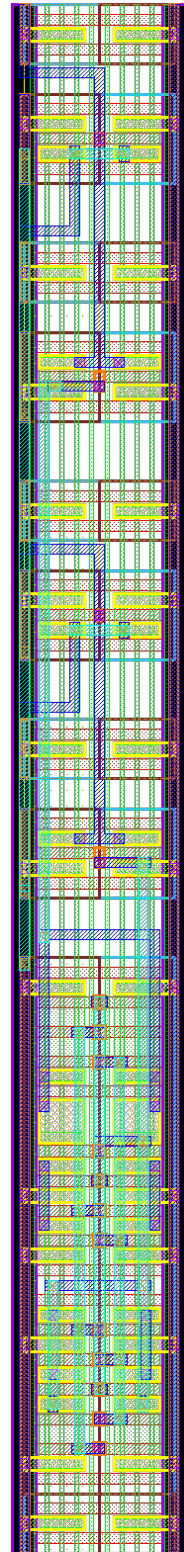
ANNEX C — FULL ADDERS

Figure C.1: Traditional Mirror Full Adder layout. The image is rotated 90° anti-clockwise.



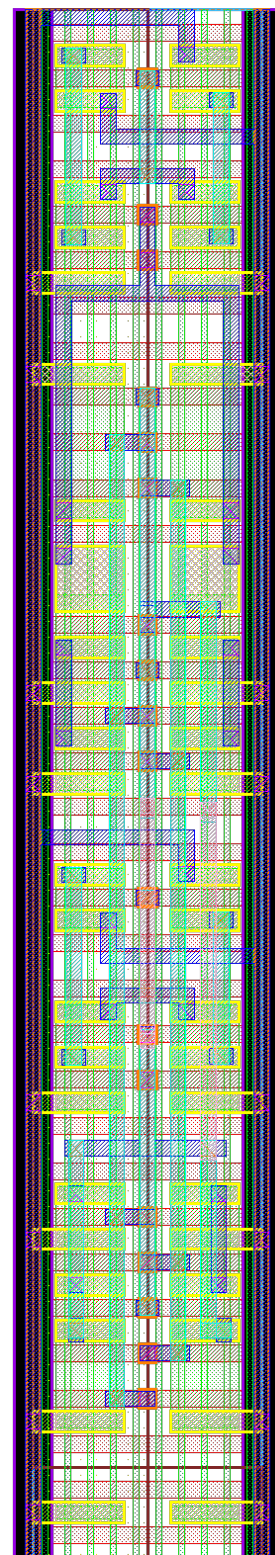
Source: From the author.

Figure C.2: Mirror Full Adder layout with internal inverters replaced by ST1. The image is rotated 90° anti-clockwise.



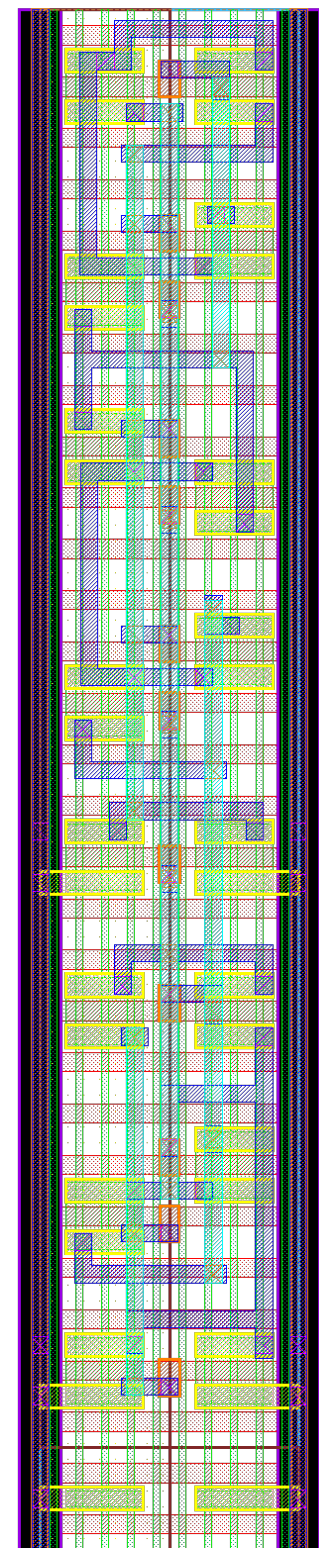
Source: From the author.

Figure C.3: Mirror Full Adder layout with internal inverters replaced by ST2. The image is rotated 90° anti-clockwise.



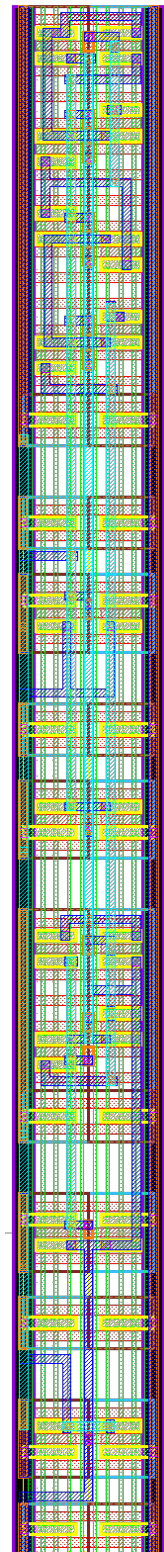
Source: From the author.

Figure C.4: Traditional Transmission Full Adder layout. The image is rotated 90° anti-clockwise.



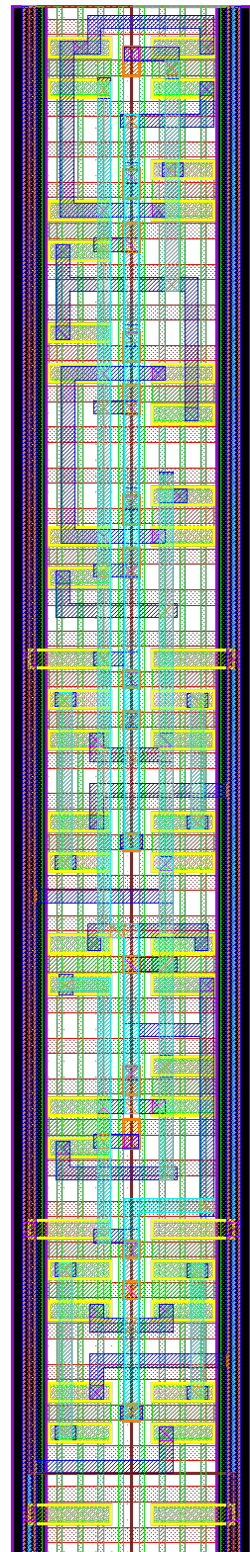
Source: From the author.

Figure C.5: Transmission Full Adder layout with internal inverters replaced by ST1. The image is rotated 90° anti-clockwise.



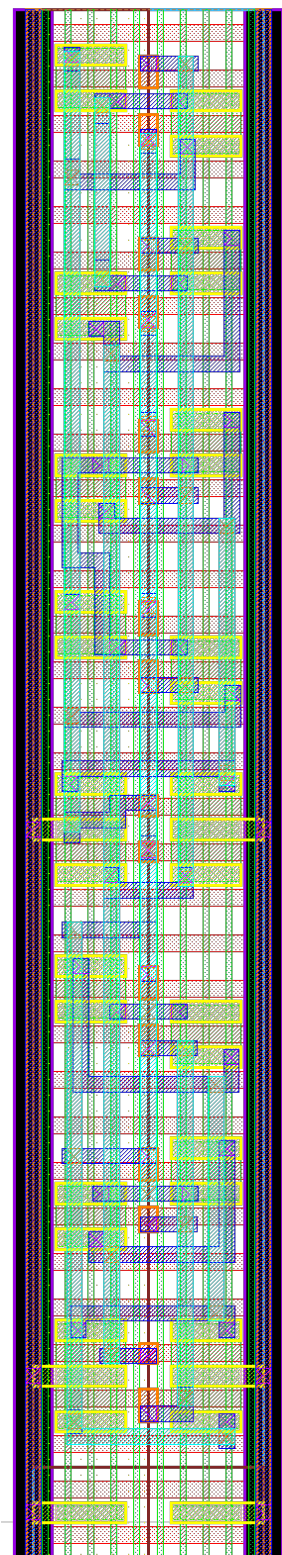
Source: From the author.

Figure C.6: Transmission Full Adder layout with internal inverters replaced by ST2. The image is rotated 90° anti-clockwise.



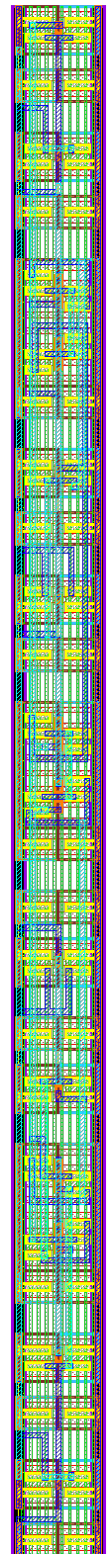
Source: From the author.

Figure C.7: Traditional Transmission Gate Adder layout. The image is rotated 90° anti-clockwise.



Source: From the author.

Figure C.8: Transmission Gate Adder layout with internal inverters replaced by ST1. The image is rotated 90° anti-clockwise.



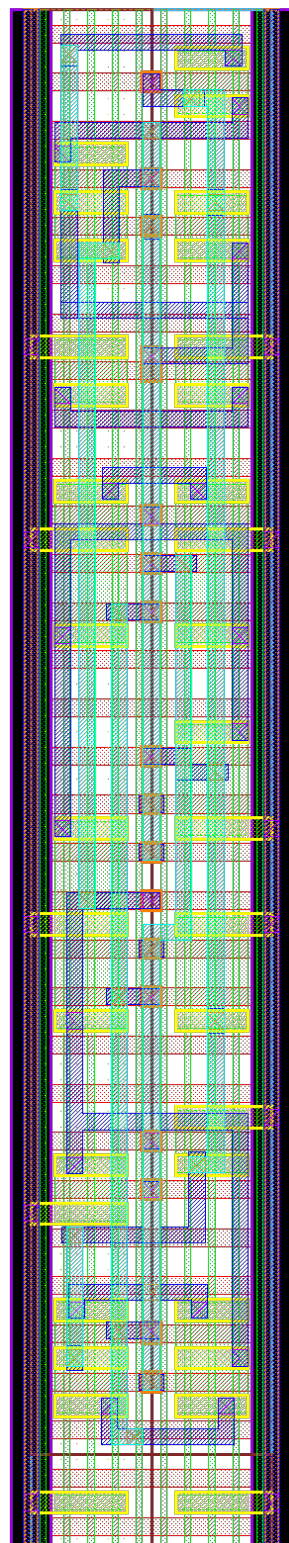
Source: From the author.

Figure C.9: Transmission Gate Adder layout with internal inverters replaced by ST2. The image is rotated 90° anti-clockwise.



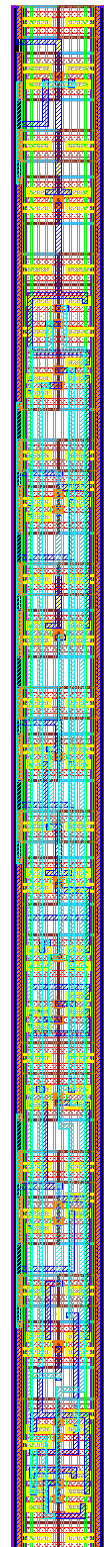
Source: From the author.

Figure C.10: Traditional Hybrid Full Adder layout. The image is rotated 90° anti-clockwise.



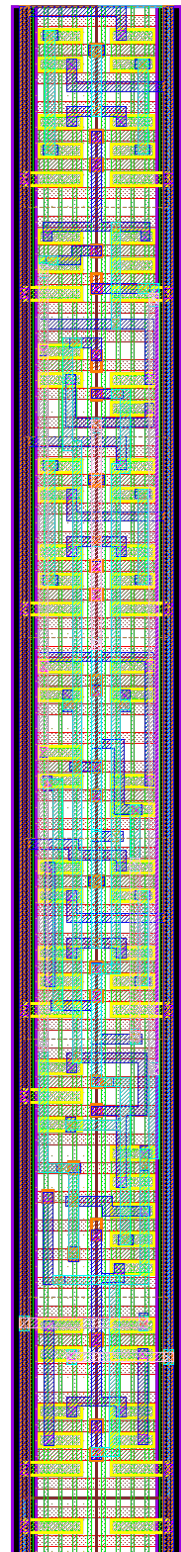
Source: From the author.

Figure C.11: Hybrid Full Adder layout with internal inverters replaced by ST1. The image is rotated 90° anti-clockwise.



Source: From the author.

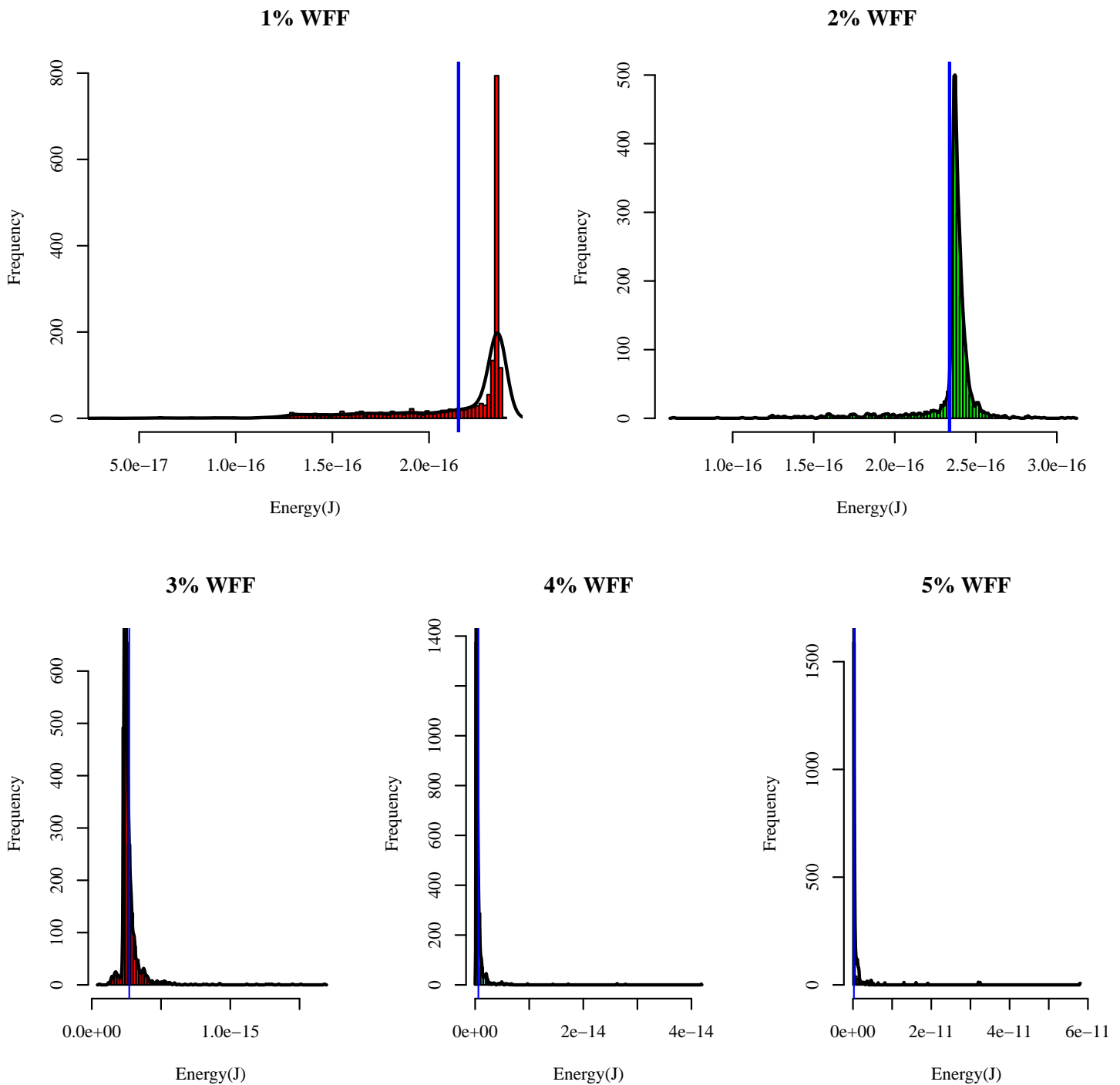
Figure C.12: Hybrid Full Adder layout with internal inverters replaced by ST2. The image is rotated 90° anti-clockwise.



Source: From the author.

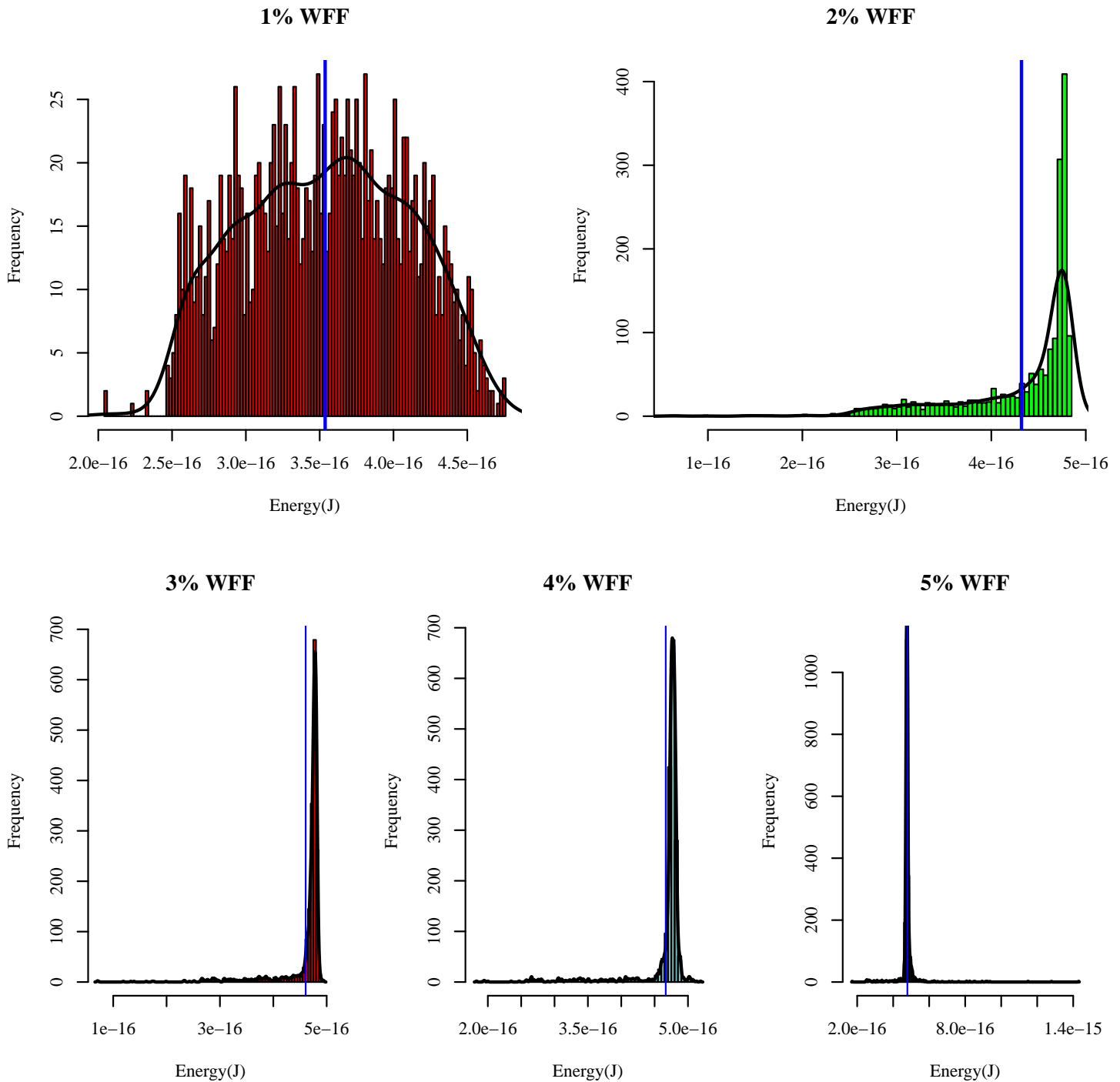
ANNEX D — ENERGY MEASURES DISTRIBUTIONS

Figure D.1: Inverter energy measures distribution operating at 0.2V.



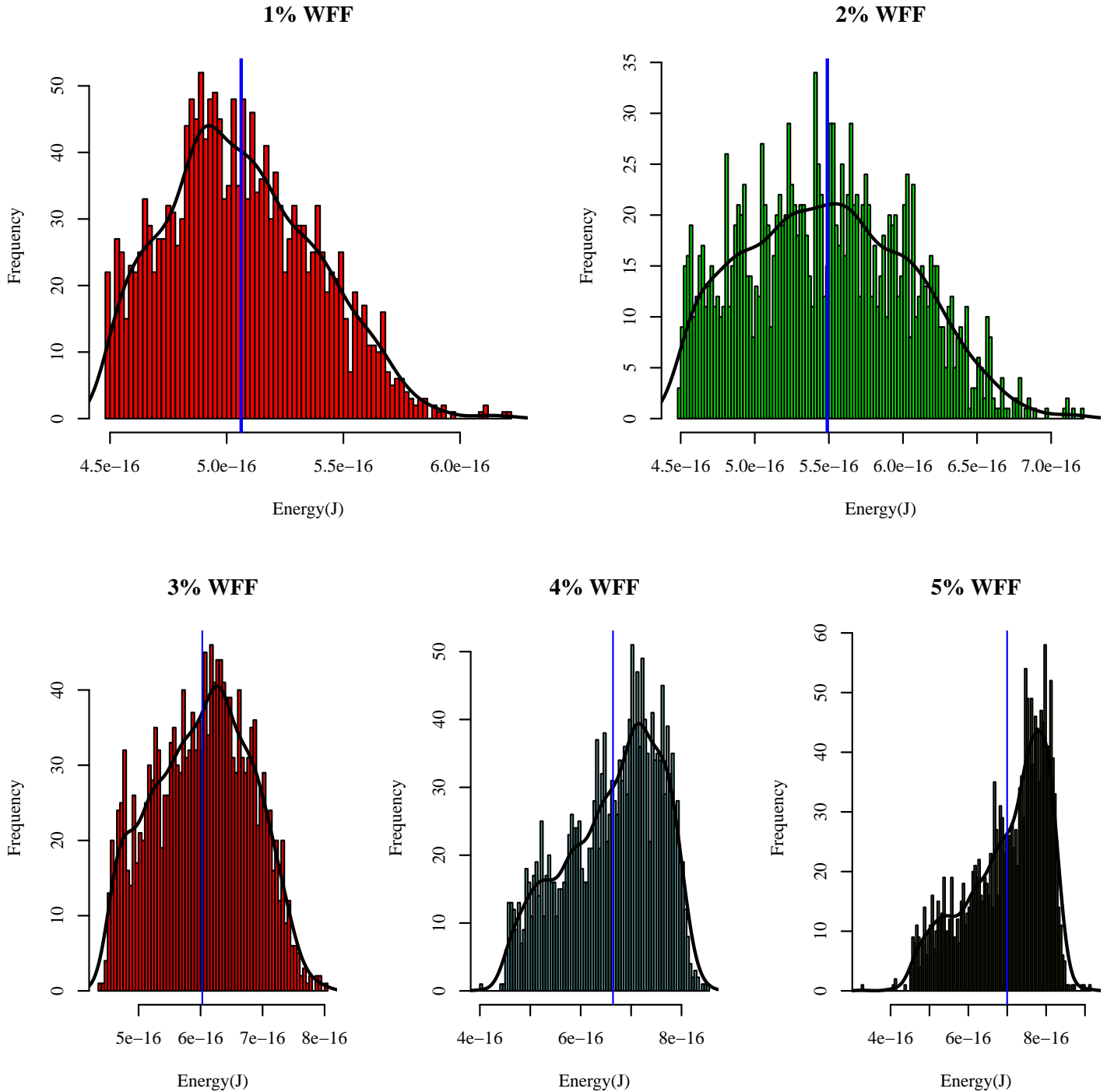
Source: From the author.

Figure D.2: Inverter energy measures distribution operating at 0.4V.



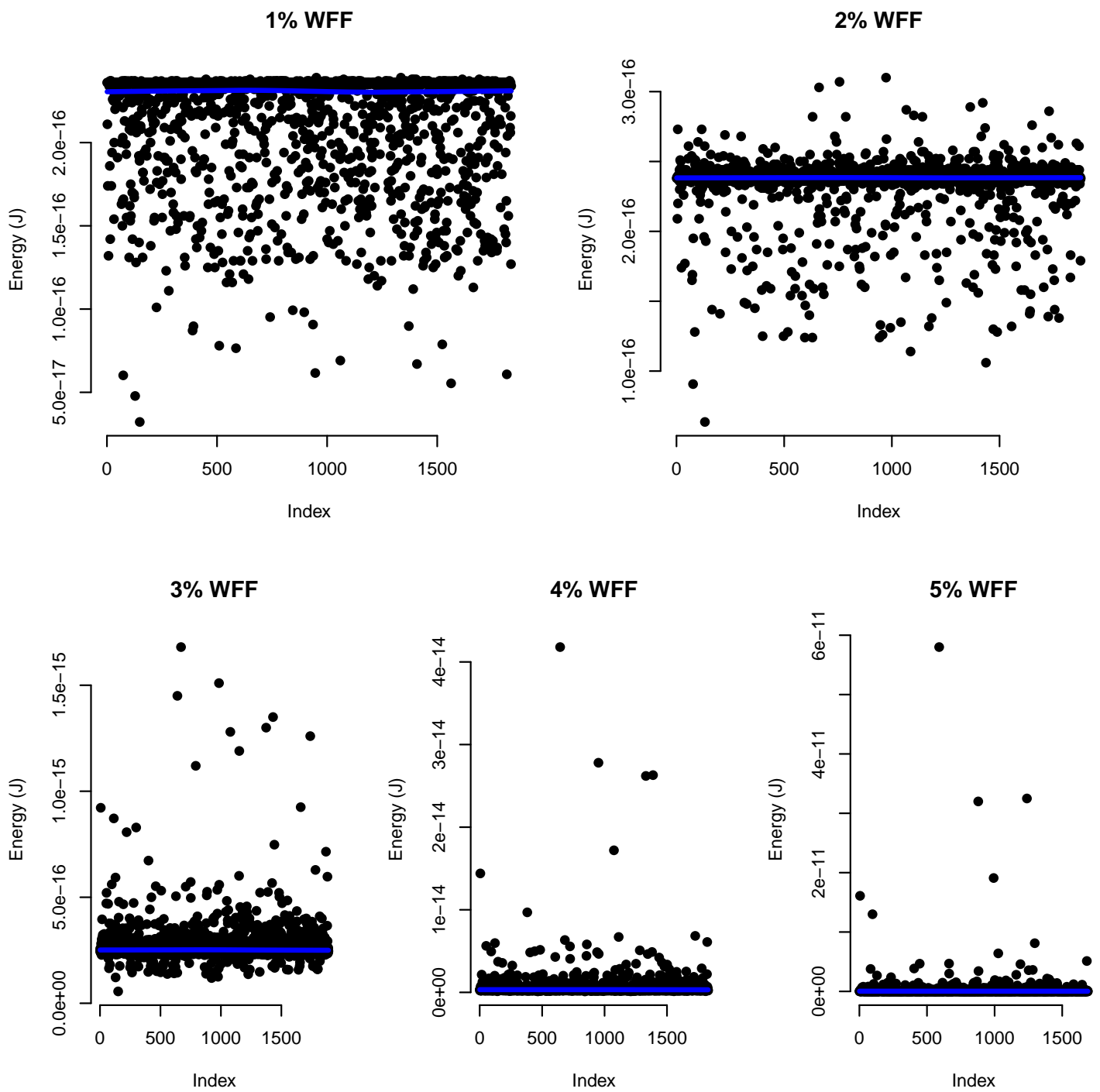
Source: From the author.

Figure D.3: Inverter energy measures distribution operating at 0.7V.



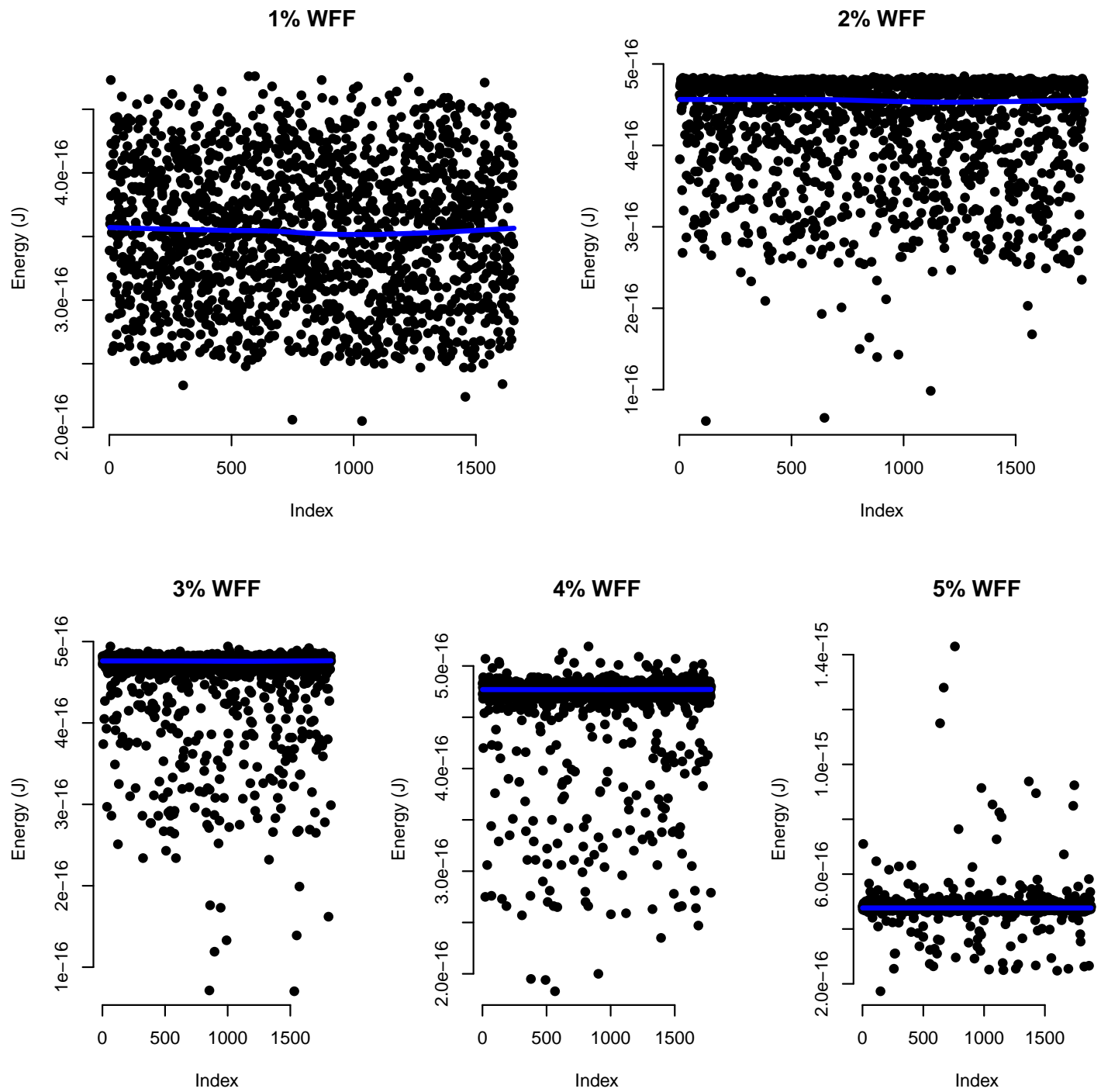
Source: From the author.

Figure D.4: Inverter energy measures dispersion operating at 0.2V.



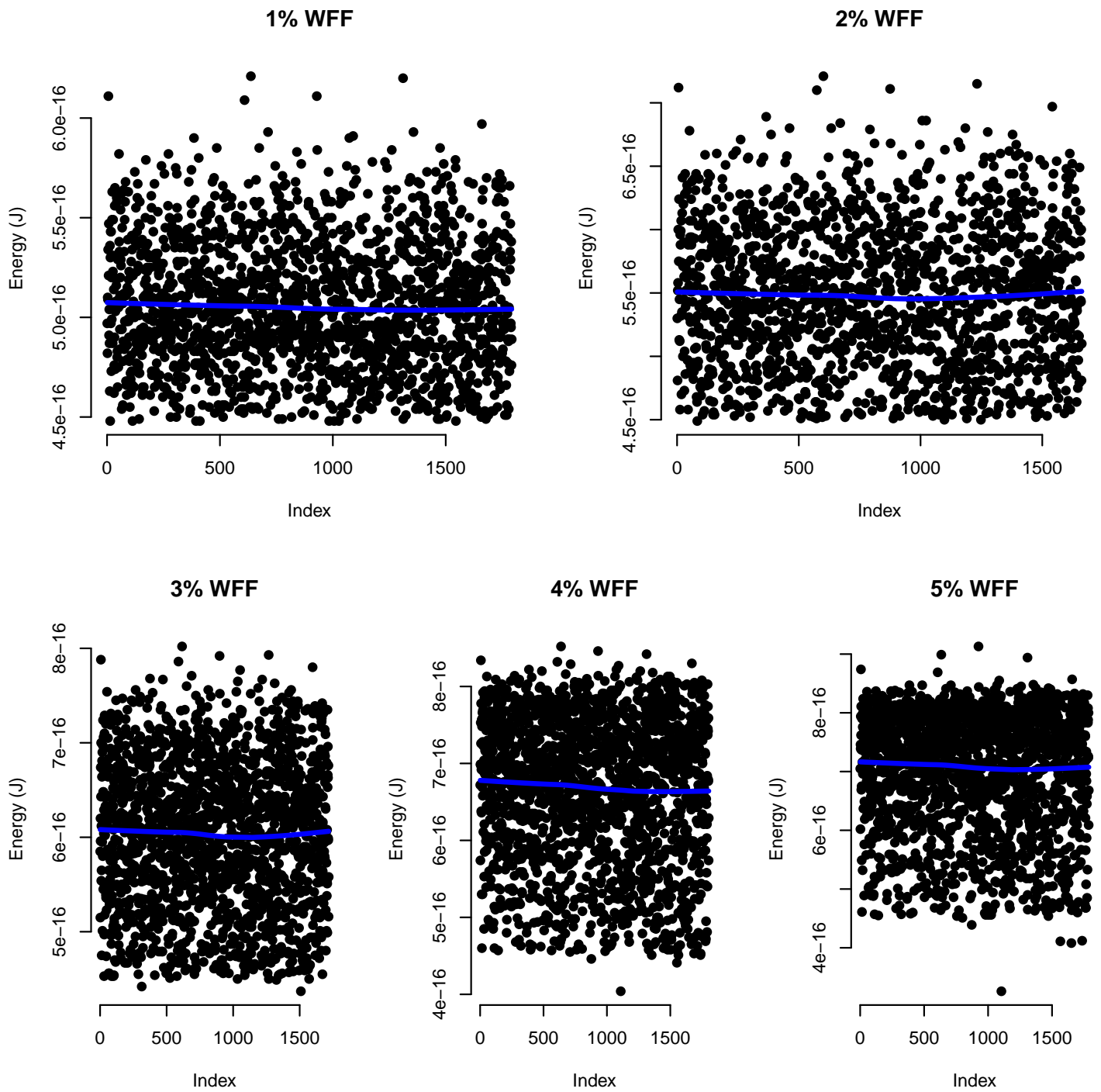
Source: From the author.

Figure D.5: Inverter energy measures dispersion operating at 0.4V.



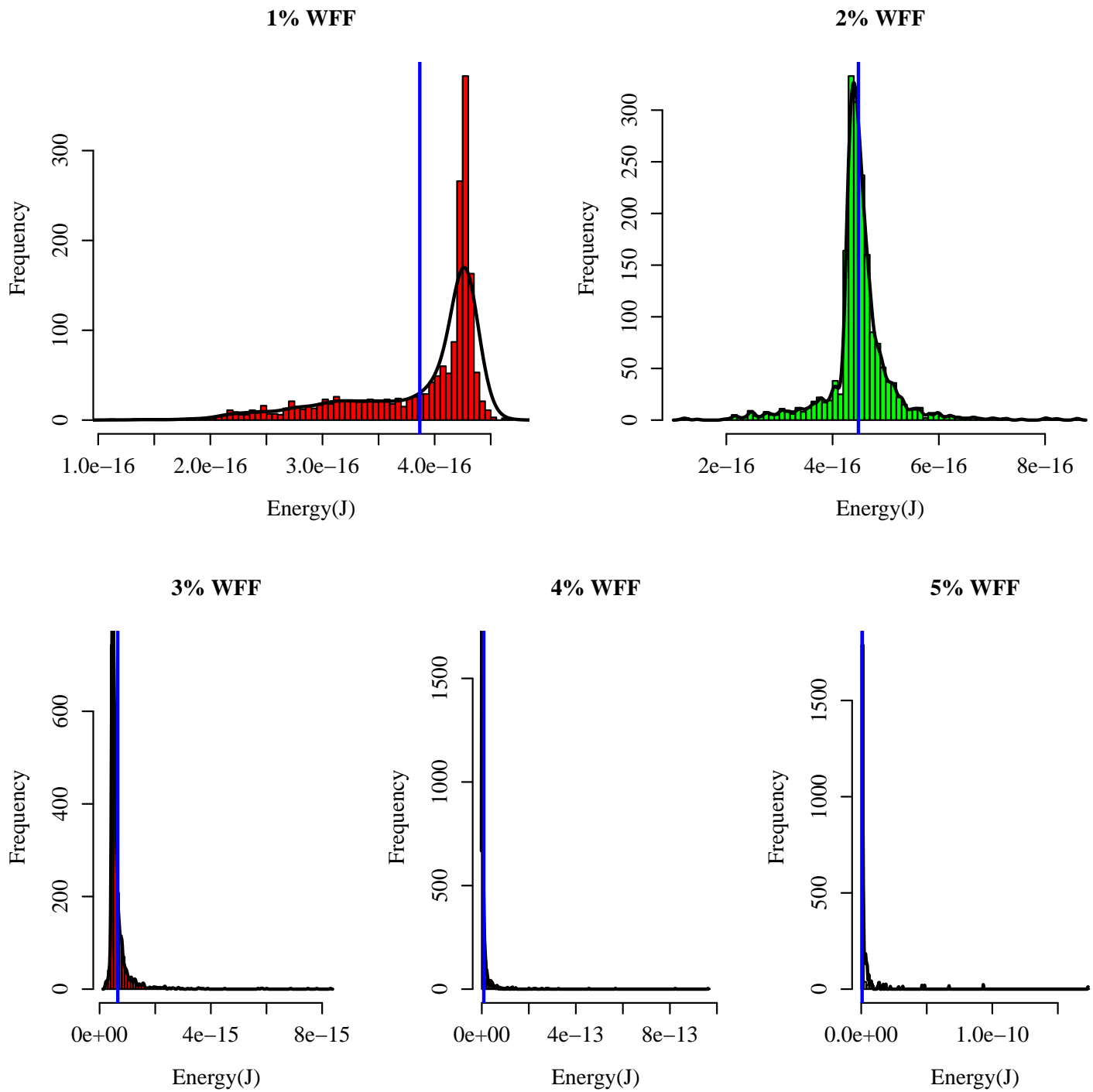
Source: From the author.

Figure D.6: Inverter energy measures dispersion operating at 0.7V.



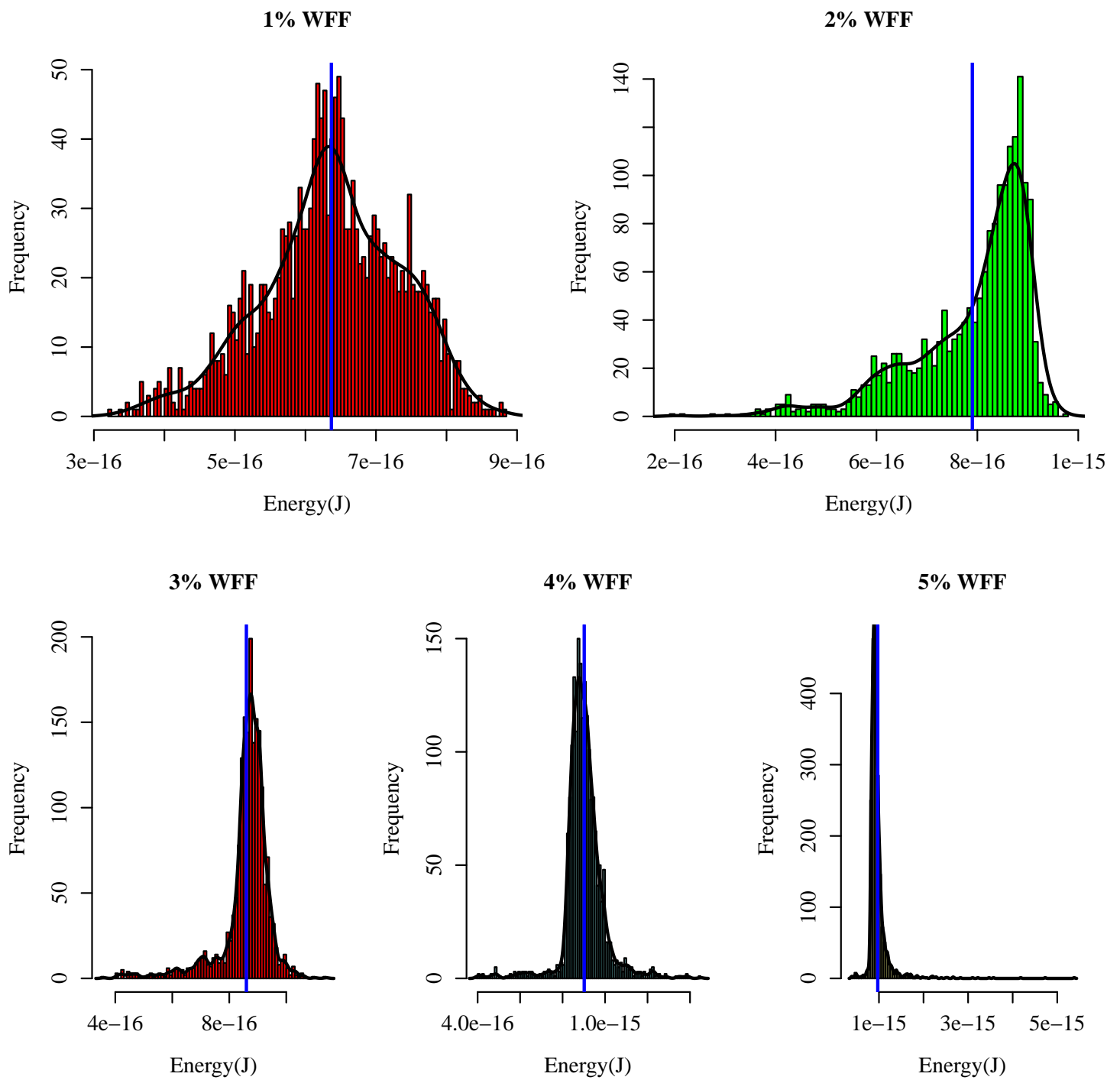
Source: From the author.

Figure D.7: ST energy measures distribution operating at 0.2V.



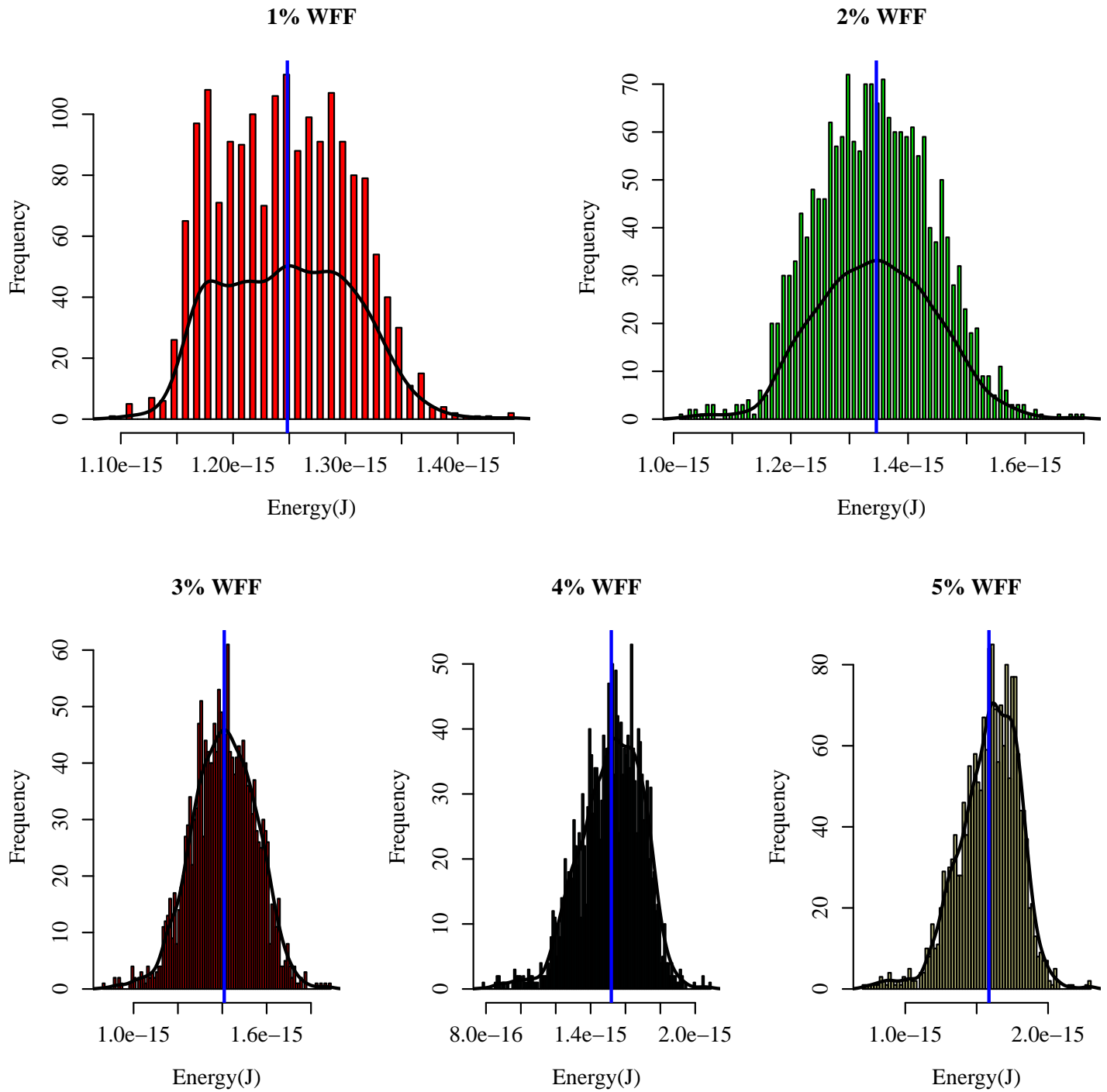
Source: From the author.

Figure D.8: ST energy measures distribution operating at 0.4V.



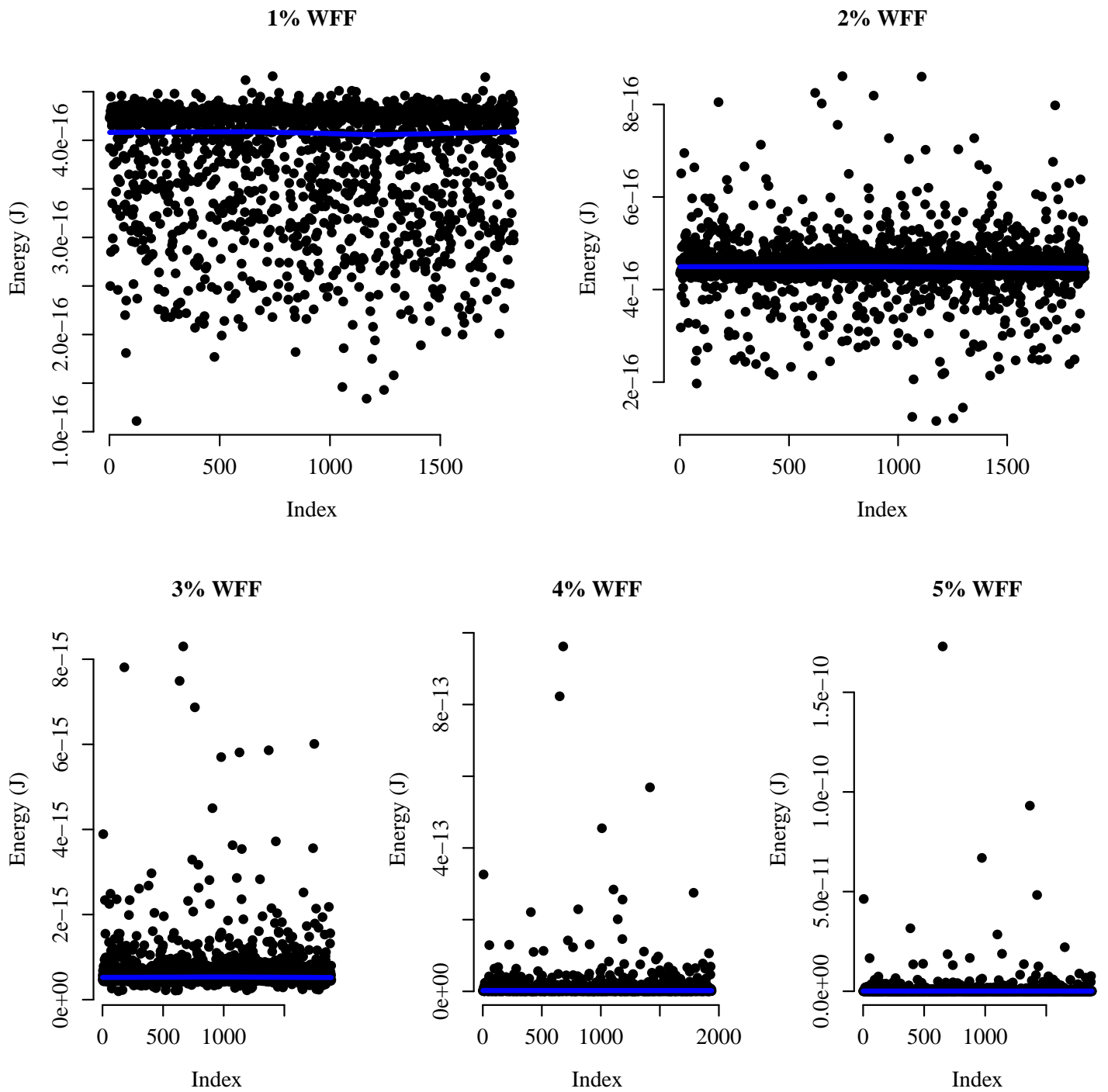
Source: From the author.

Figure D.9: ST energy measures distribution operating at 0.7V.



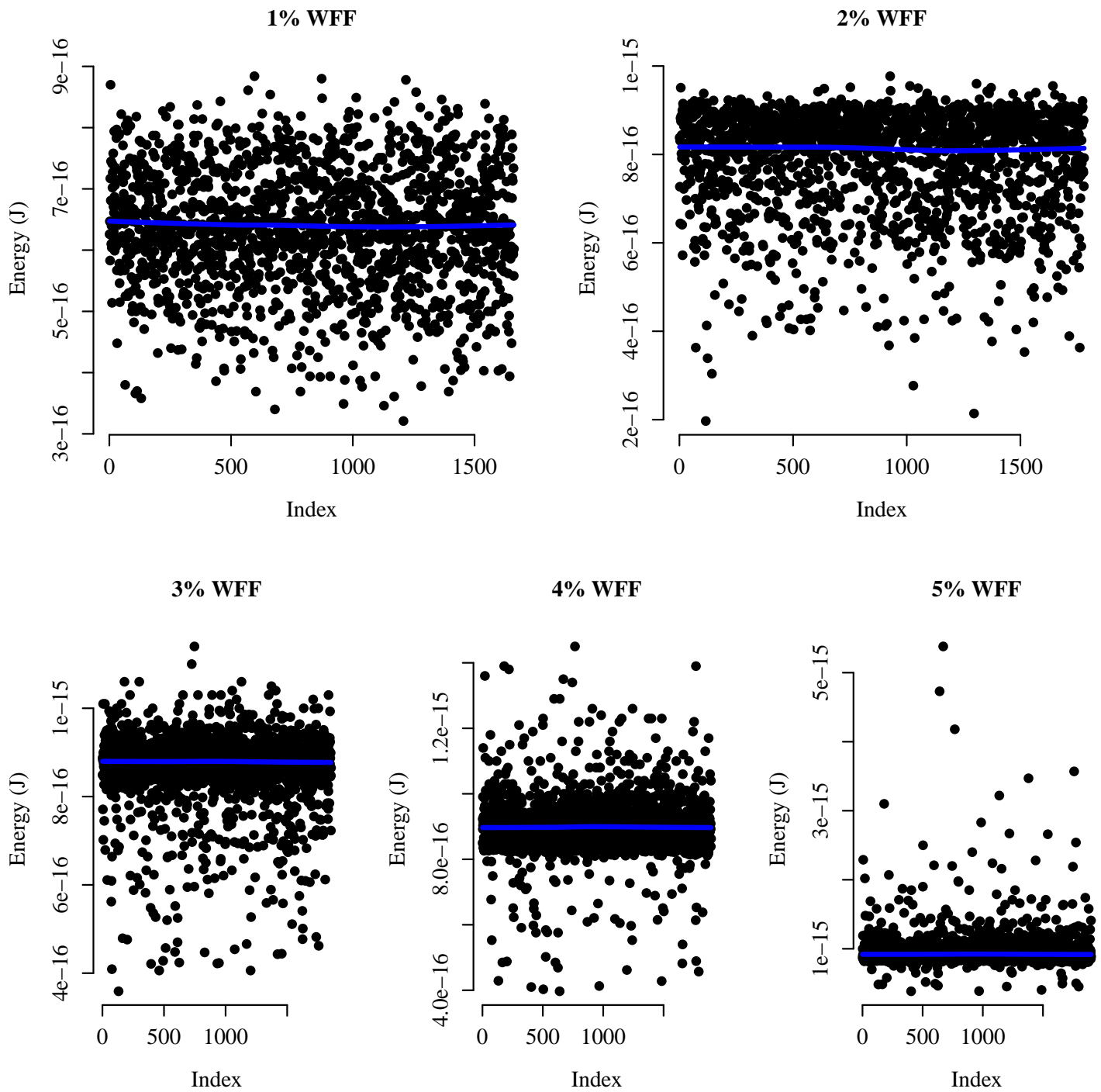
Source: From the author.

Figure D.10: ST energy measures dispersion operating at 0.2V.



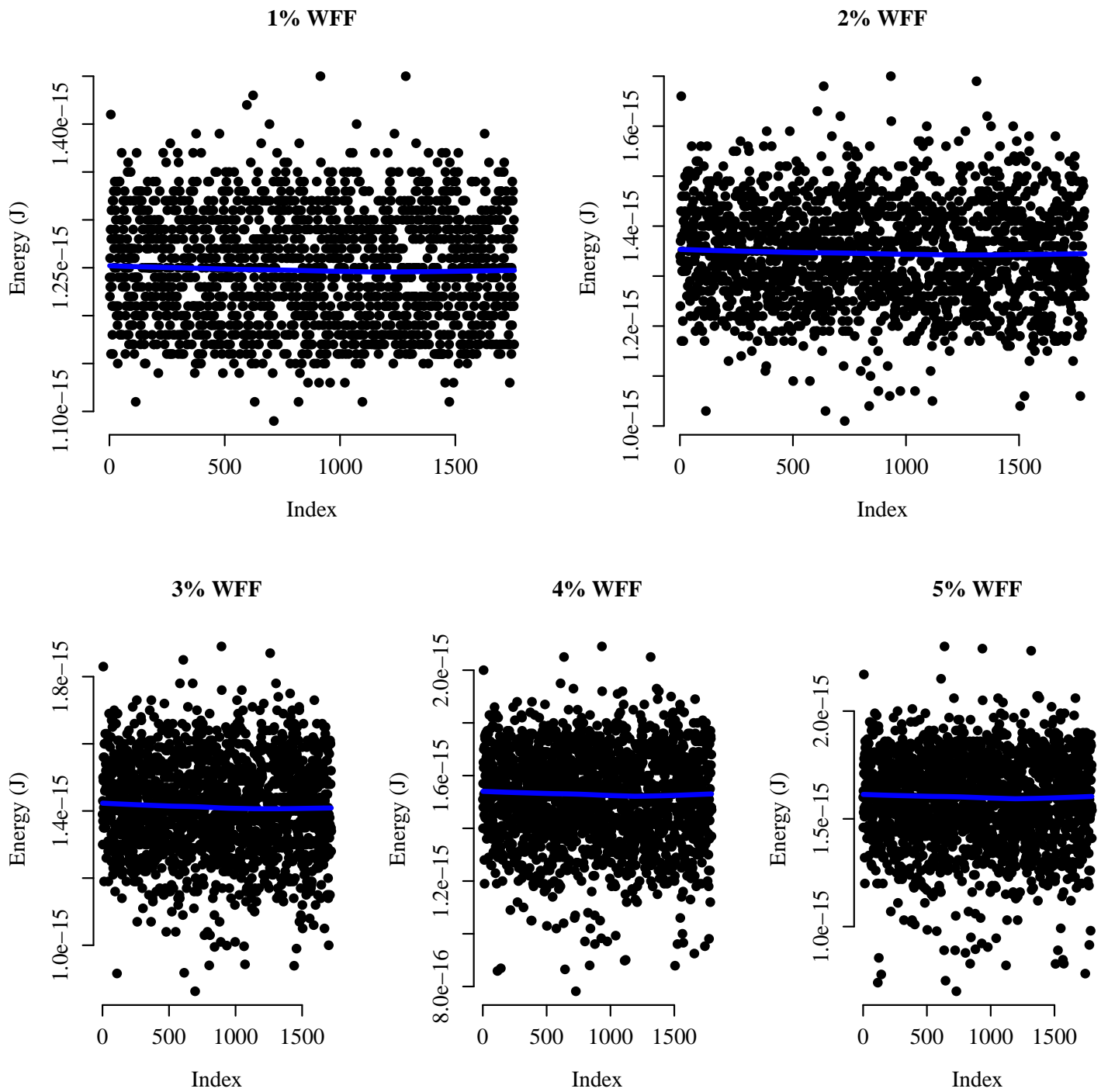
Source: From the author.

Figure D.11: ST energy measures dispersion operating at 0.4V.



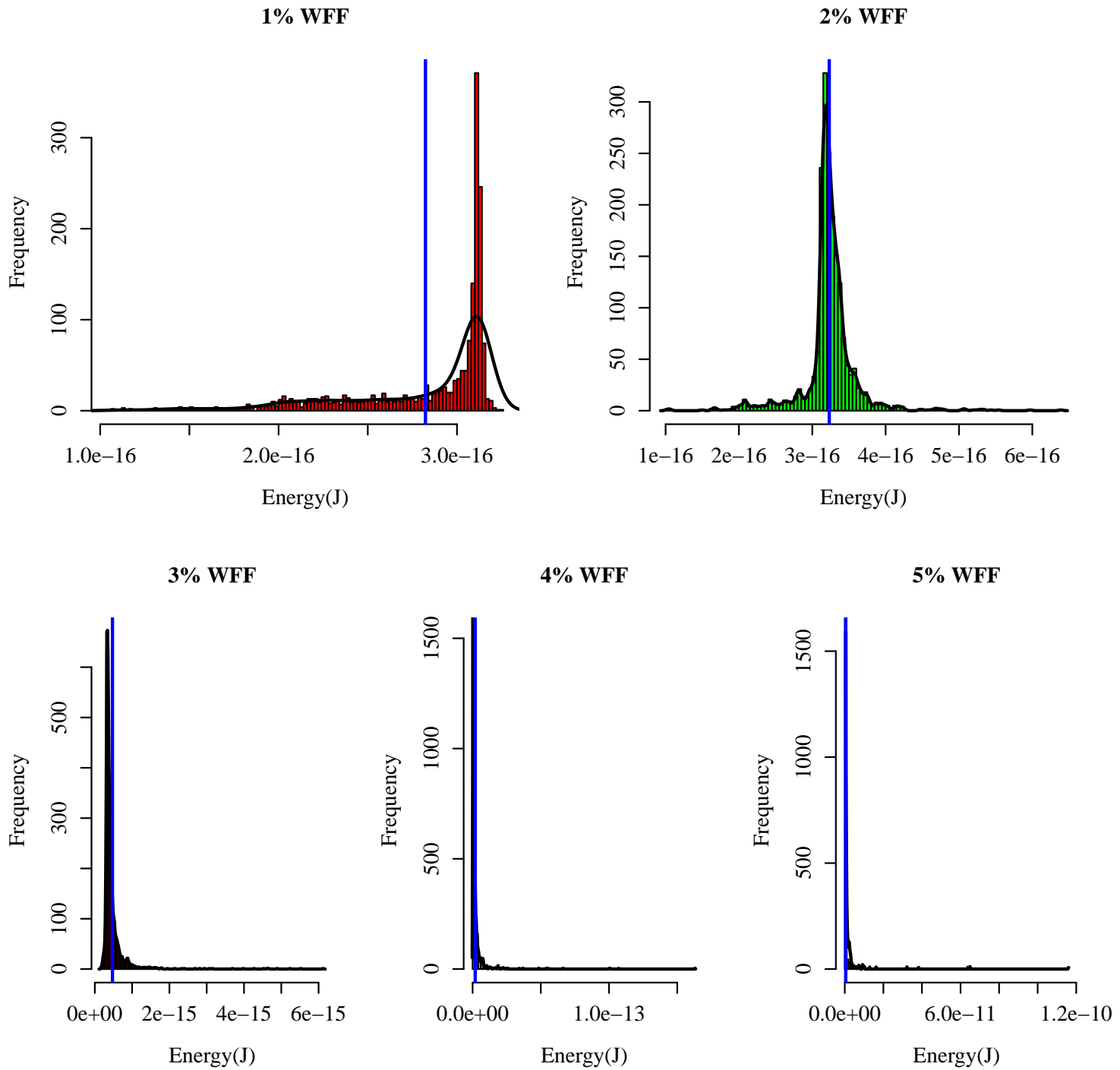
Source: From the author.

Figure D.12: ST energy measures dispersion operating at 0.7V.



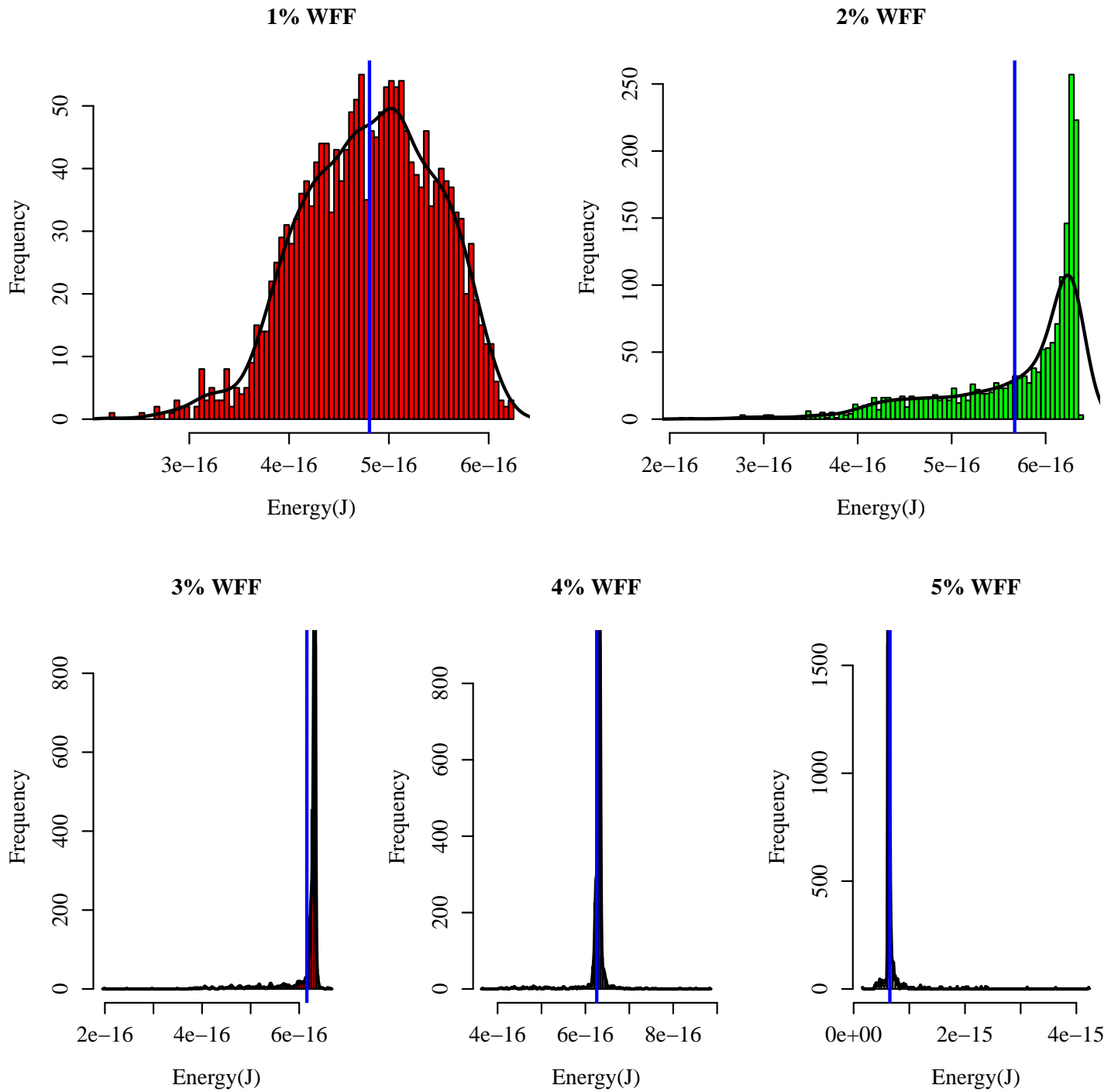
Source: From the author.

Figure D.13: SIG energy measures distribution operating at 0.2V.



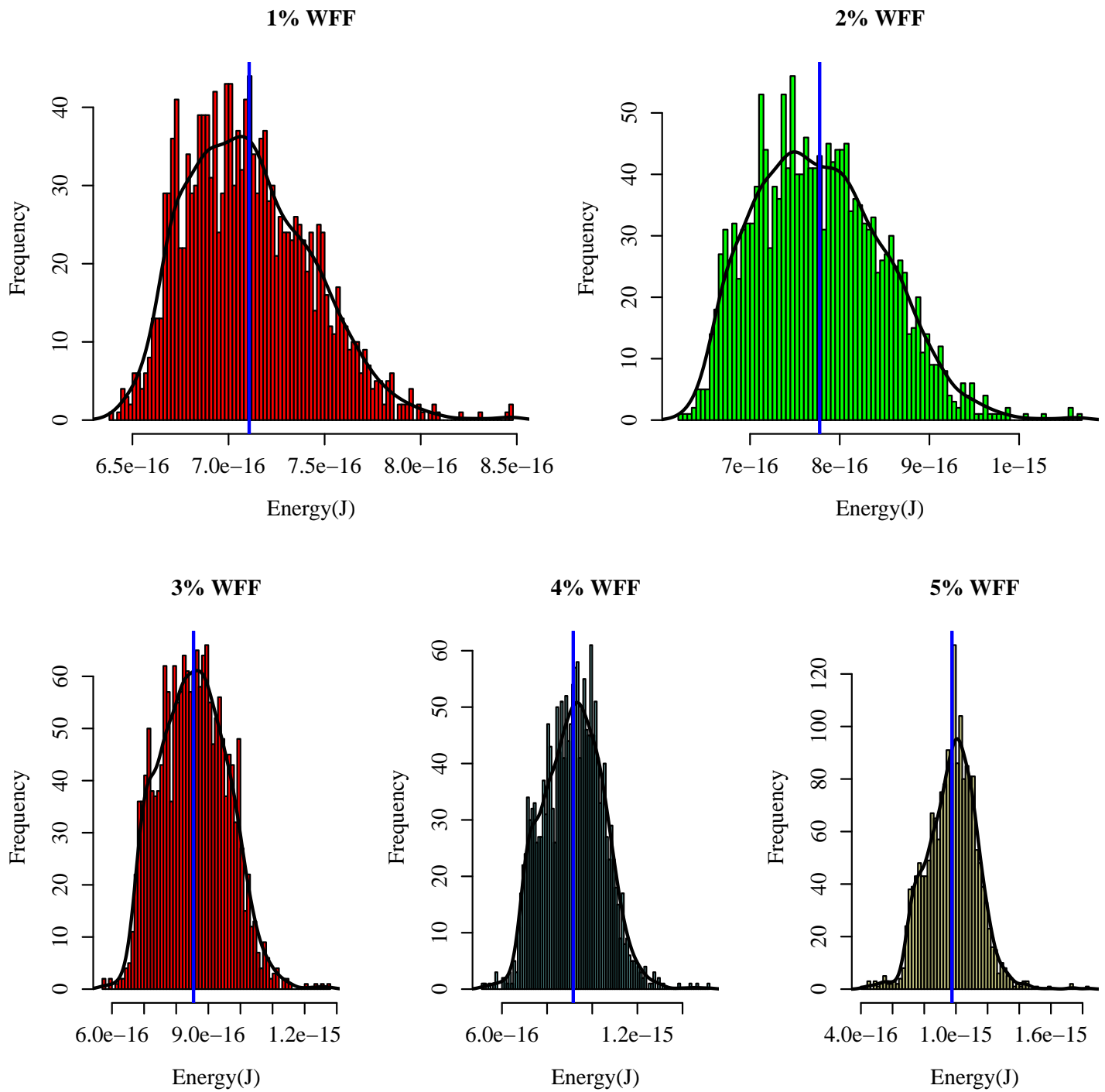
Source: From the author.

Figure D.14: SIG energy measures distribution operating at 0.4V.



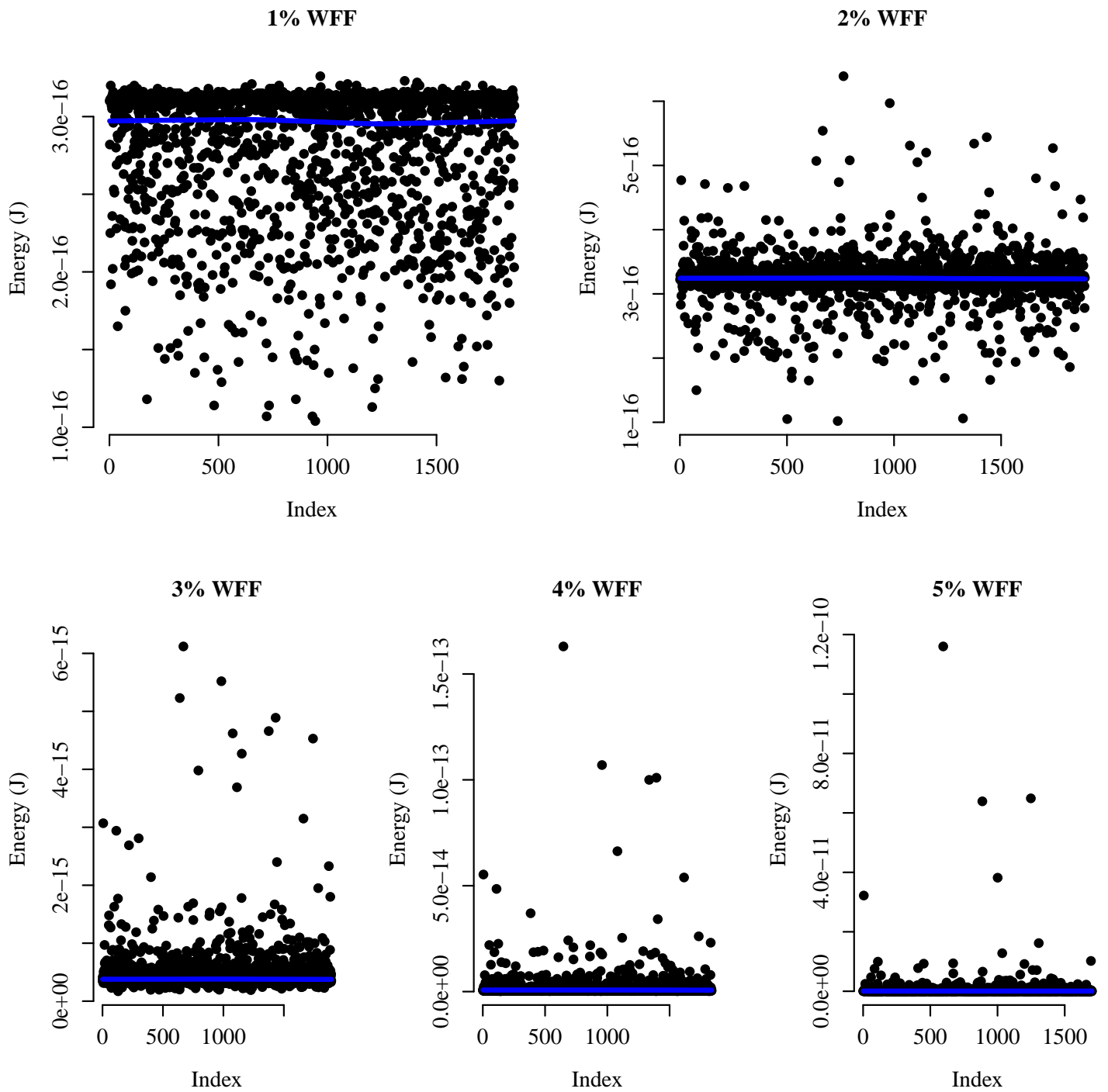
Source: From the author.

Figure D.15: SIG energy measures distribution operating at 0.7V.



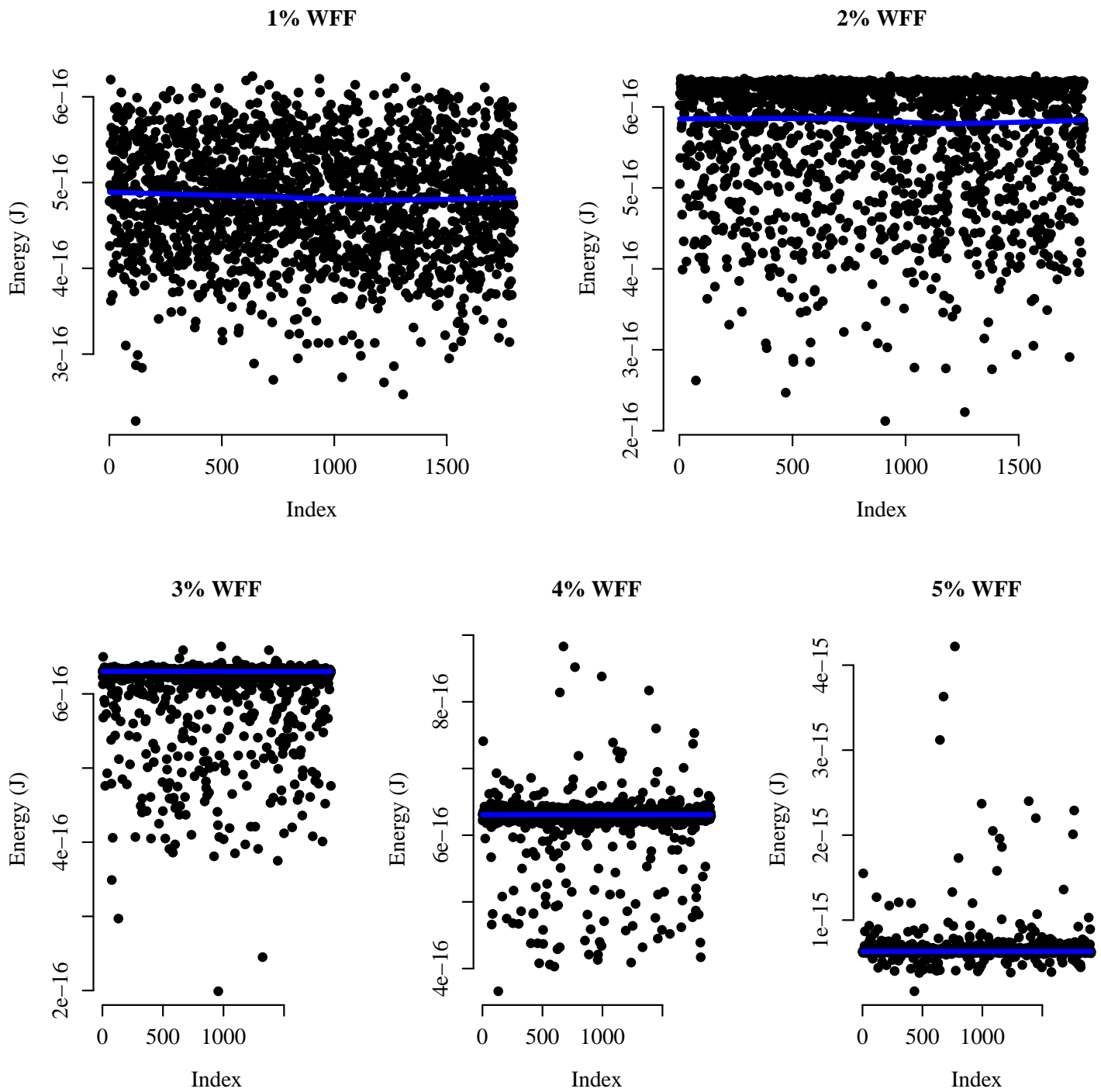
Source: From the author.

Figure D.16: SIG energy measures dispersion operating at 0.2V.



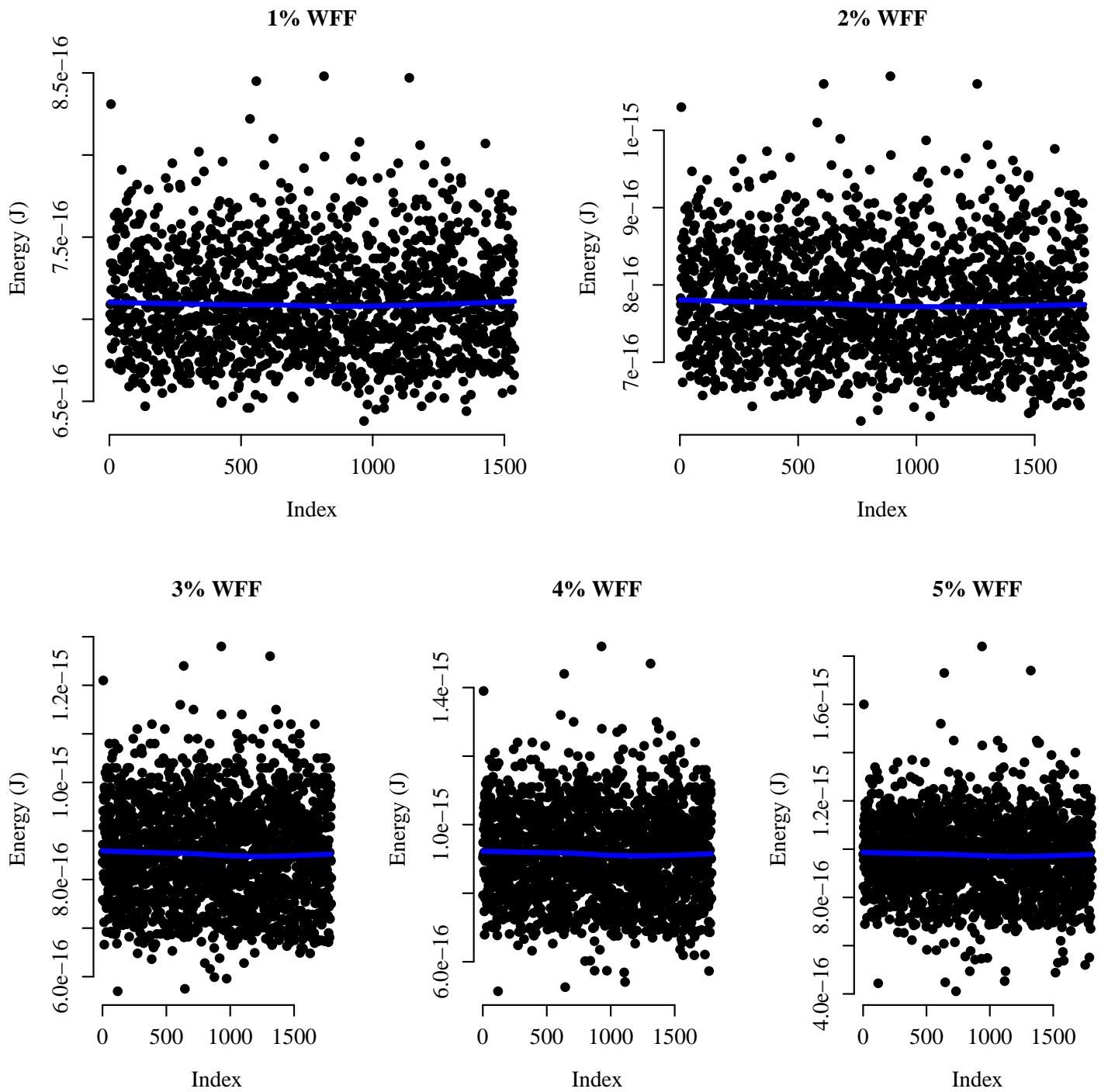
Source: From the author.

Figure D.17: SIG energy measures dispersion operating at 0.4V.



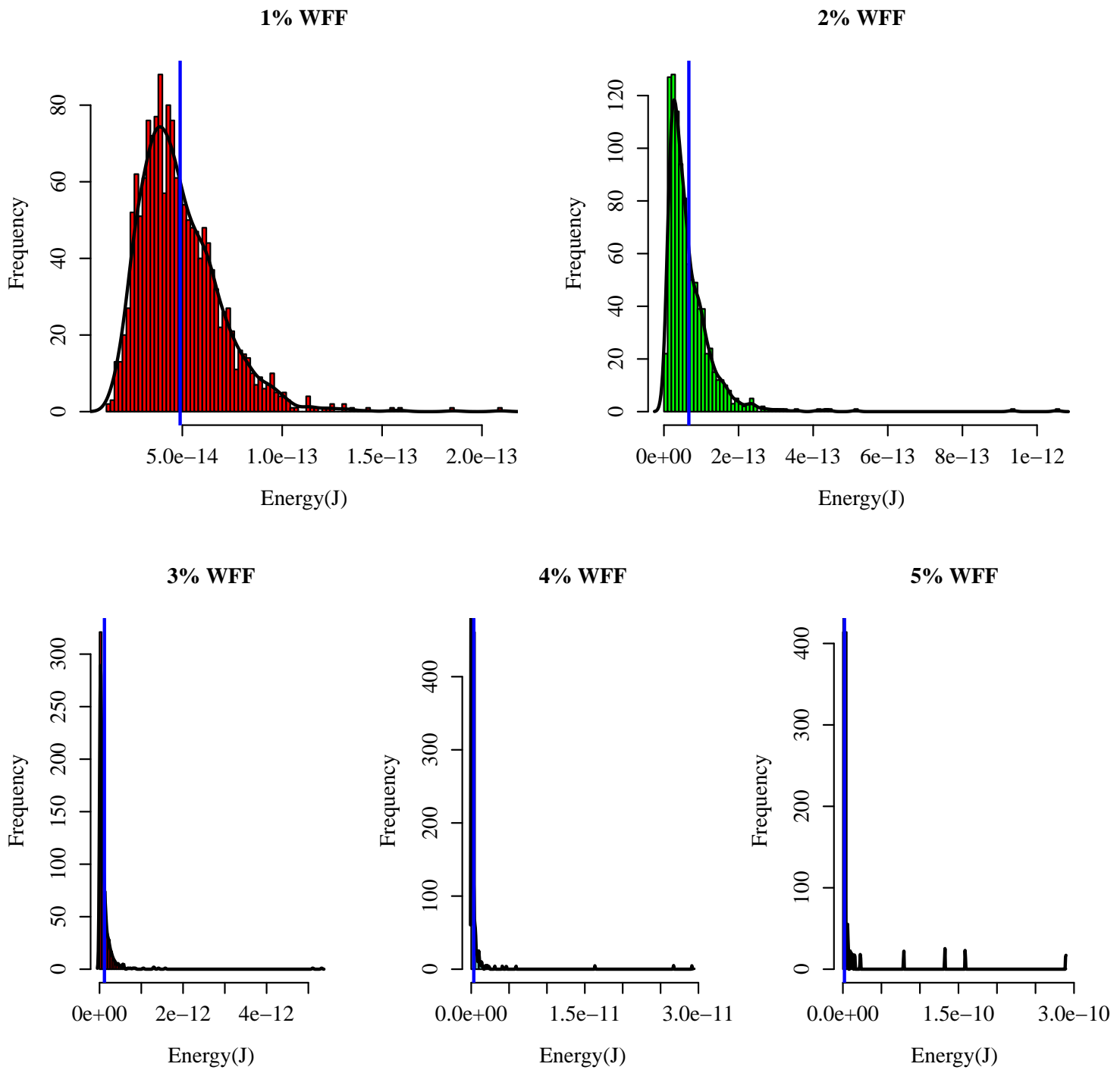
Source: From the author.

Figure D.18: SIG energy measures dispersion operating at 0.7V.



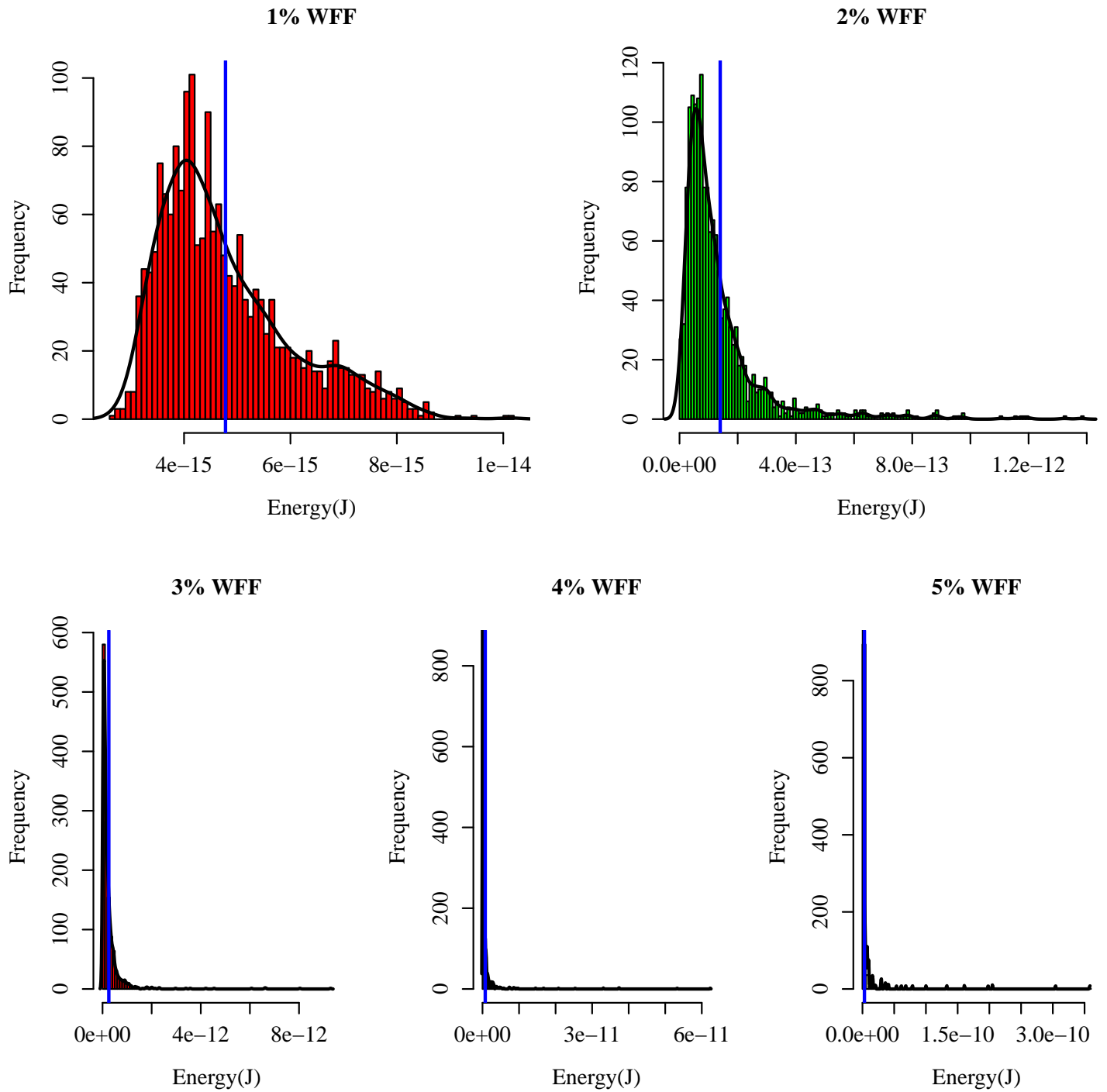
Source: From the author.

Figure D.19: TIST 2:1 energy measures distribution operating at 0.2V.



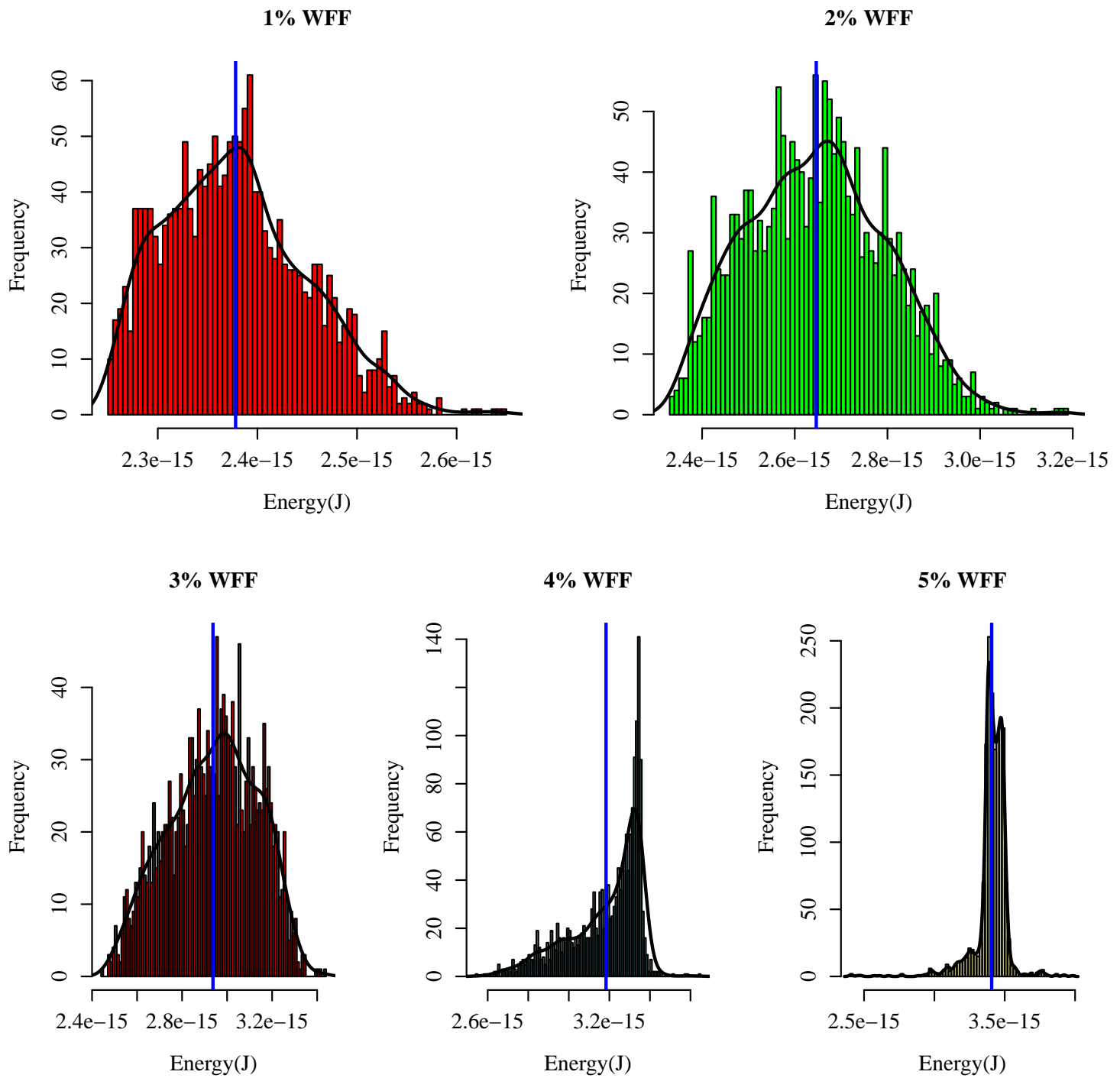
Source: From the author.

Figure D.20: TIST 2:1 energy measures distribution operating at 0.4V.



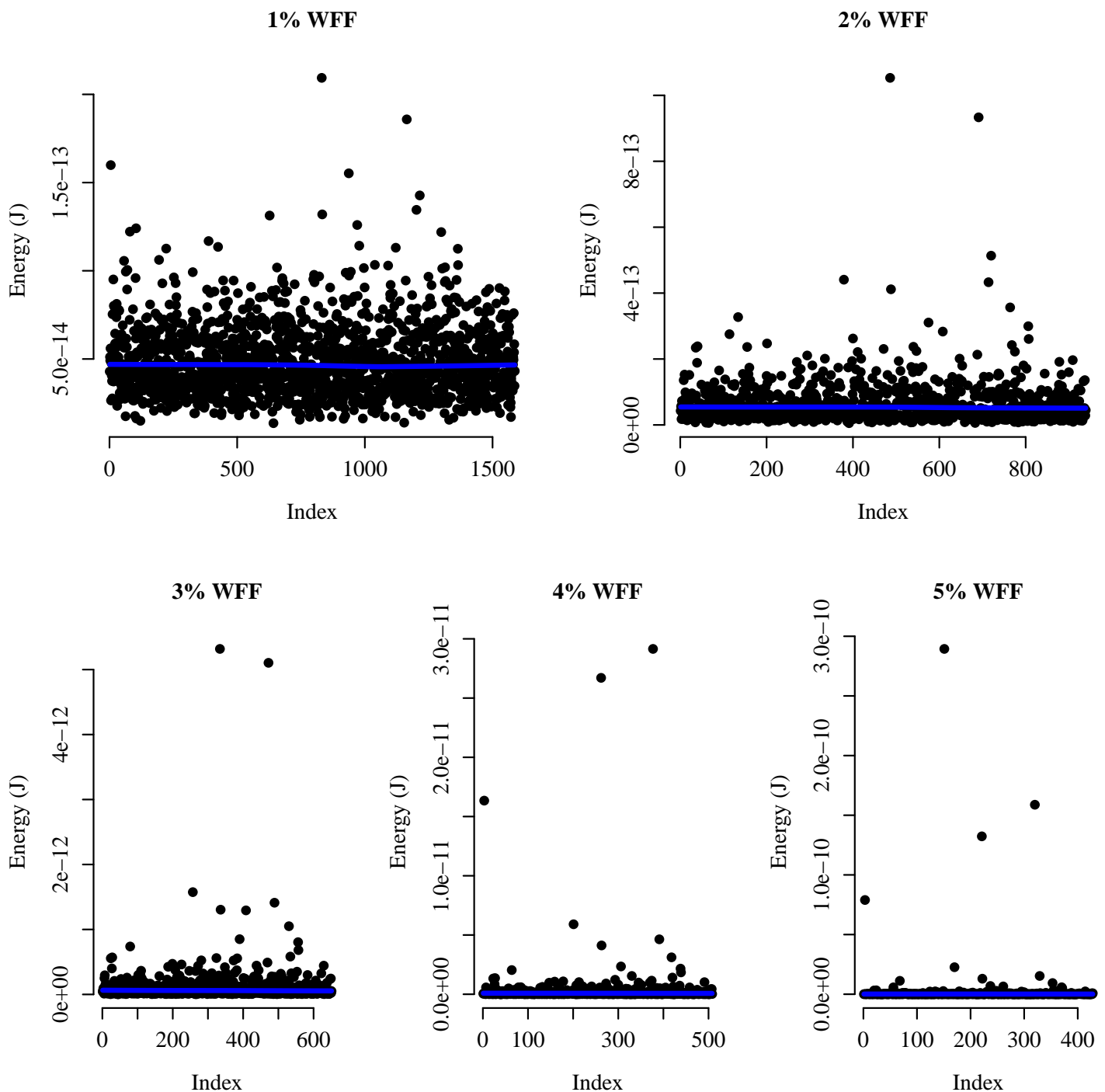
Source: From the author.

Figure D.21: TIST 2:1 energy measures distribution operating at 0.7V.



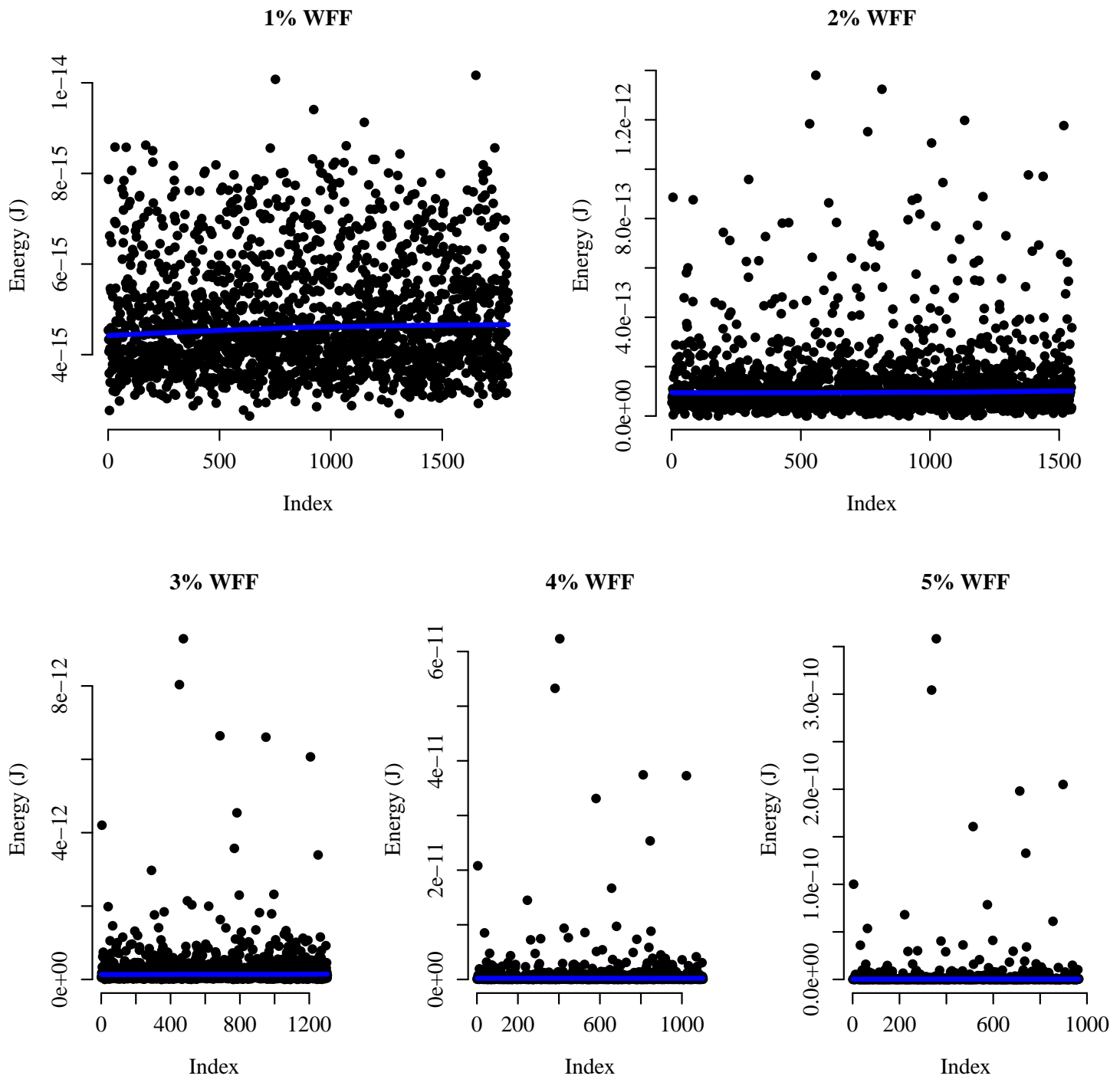
Source: From the author.

Figure D.22: TIST 2:1 energy measures dispersion operating at 0.2V.



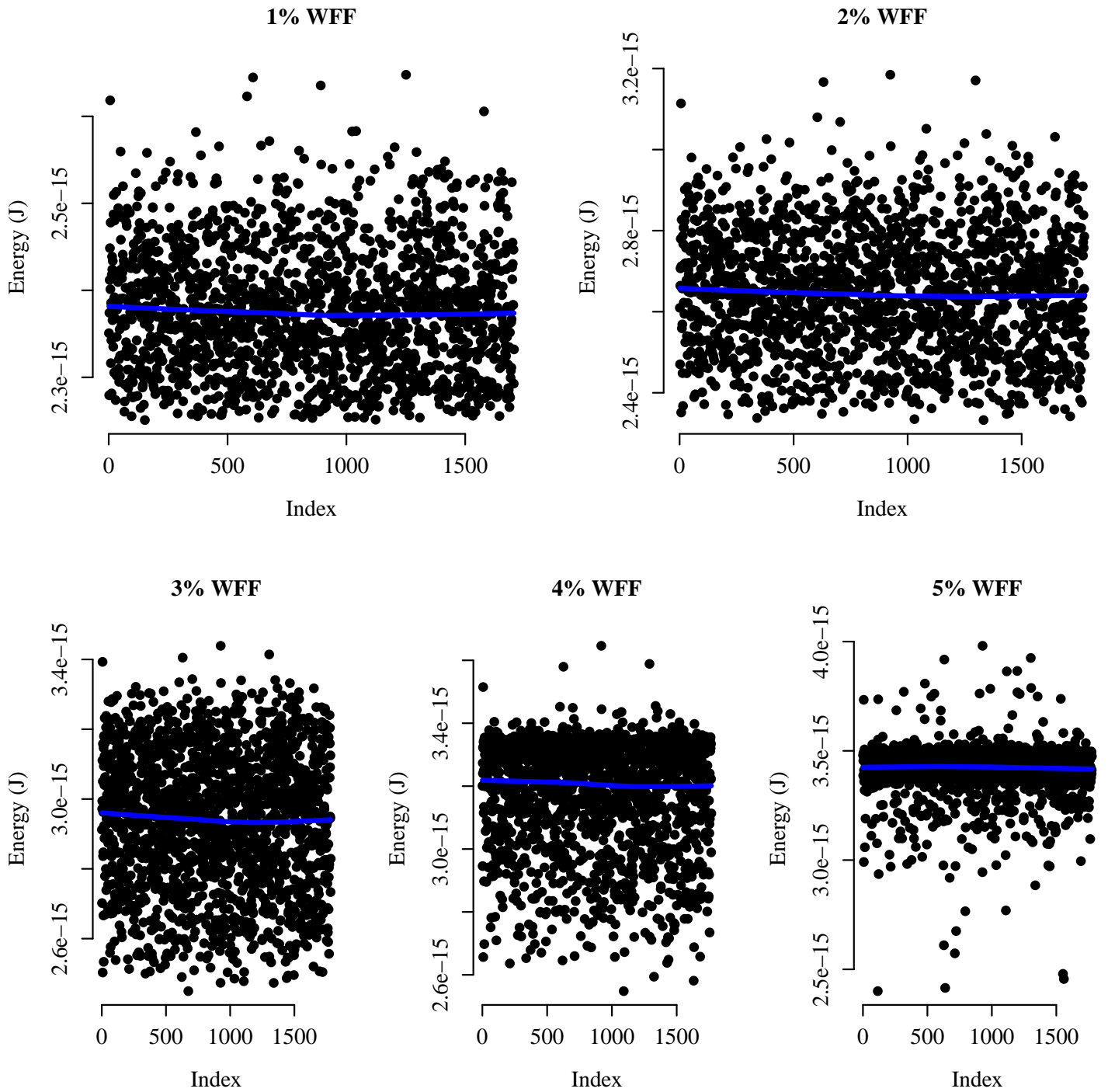
Source: From the author.

Figure D.23: TIST 2:1 energy measures dispersion operating at 0.4V.



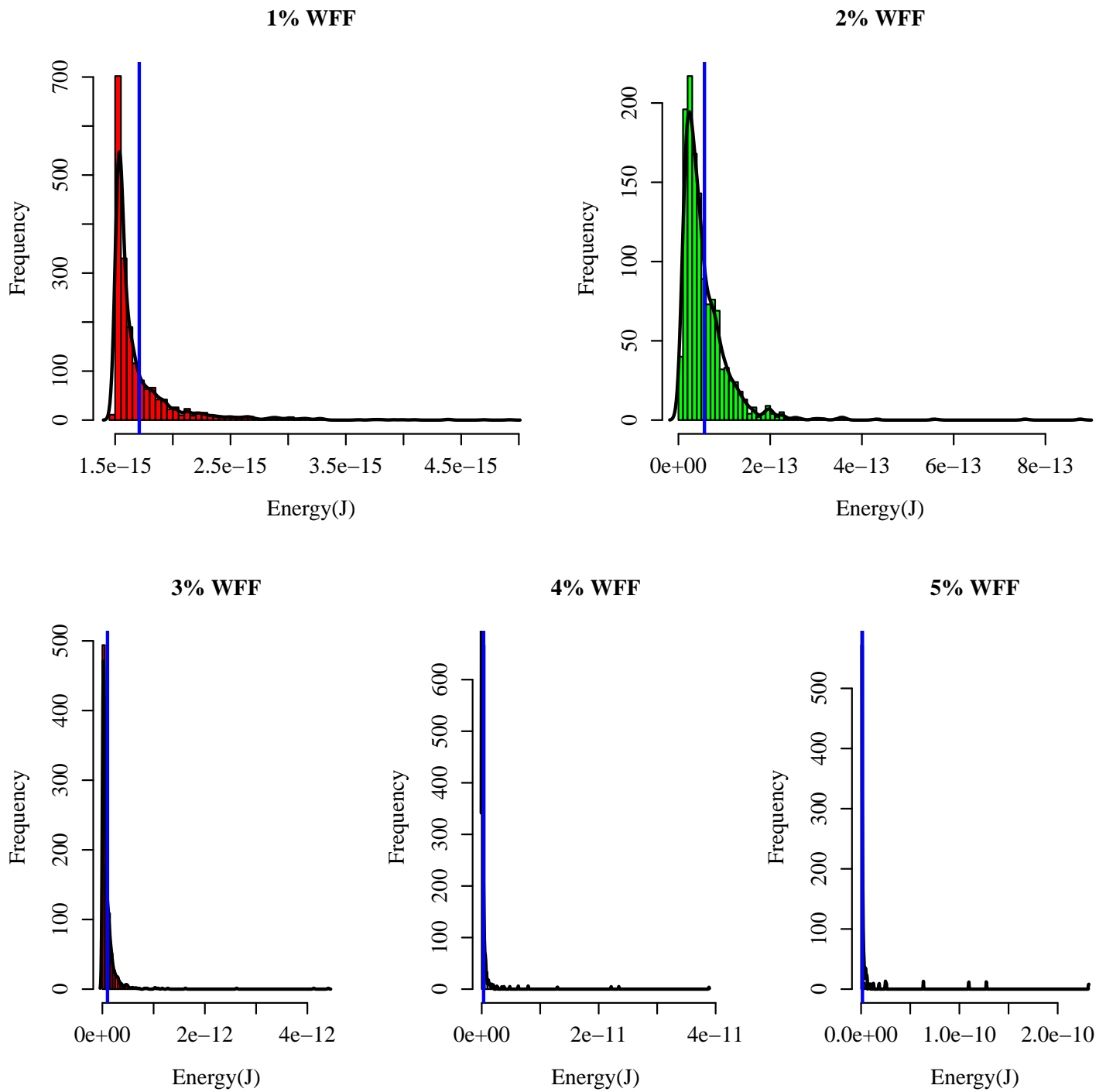
Source: From the author.

Figure D.24: TIST 2:1 energy measures dispersion operating at 0.7V.



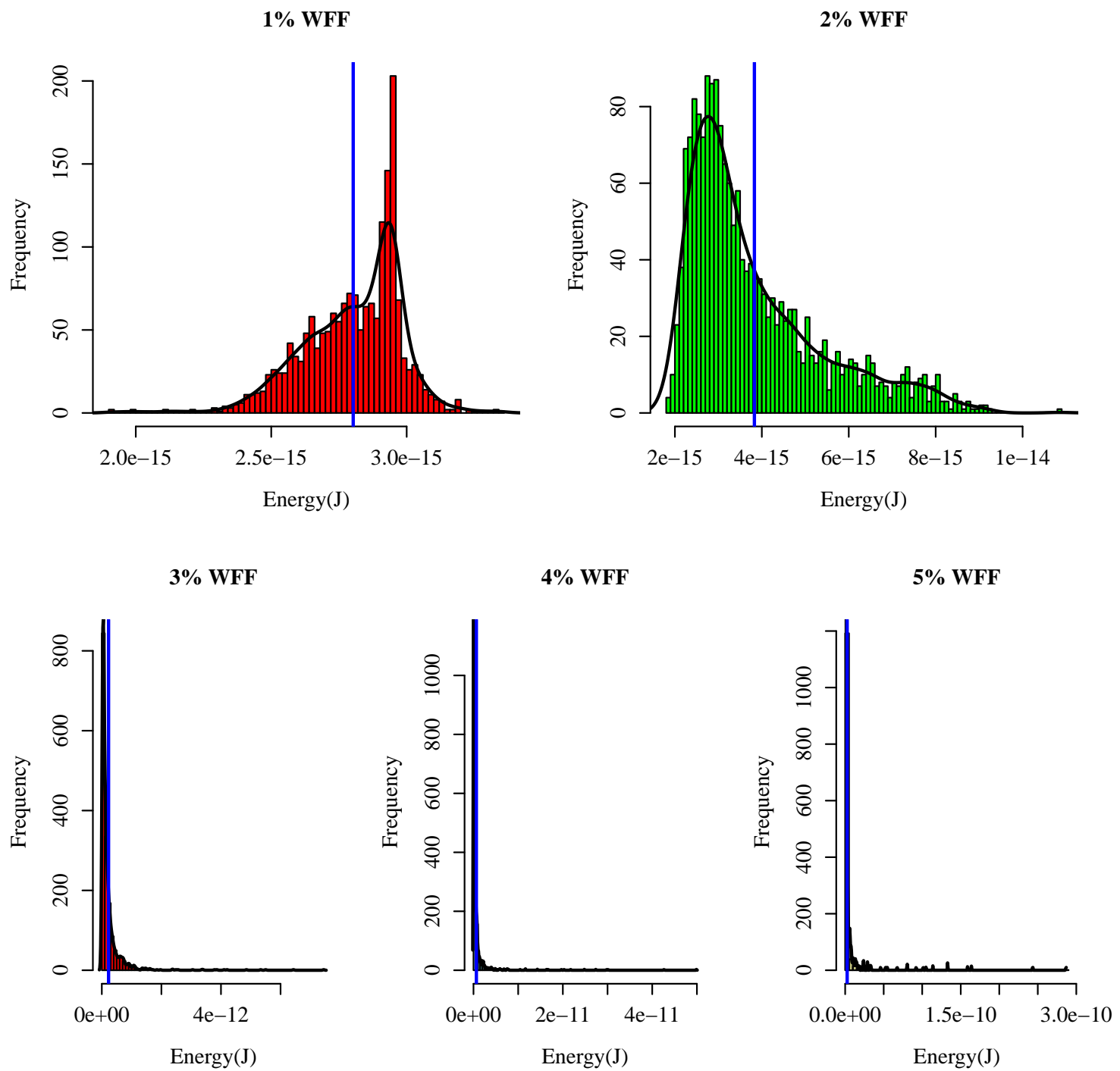
Source: From the author.

Figure D.25: TIST 3:1 energy measures distribution operating at 0.2V.



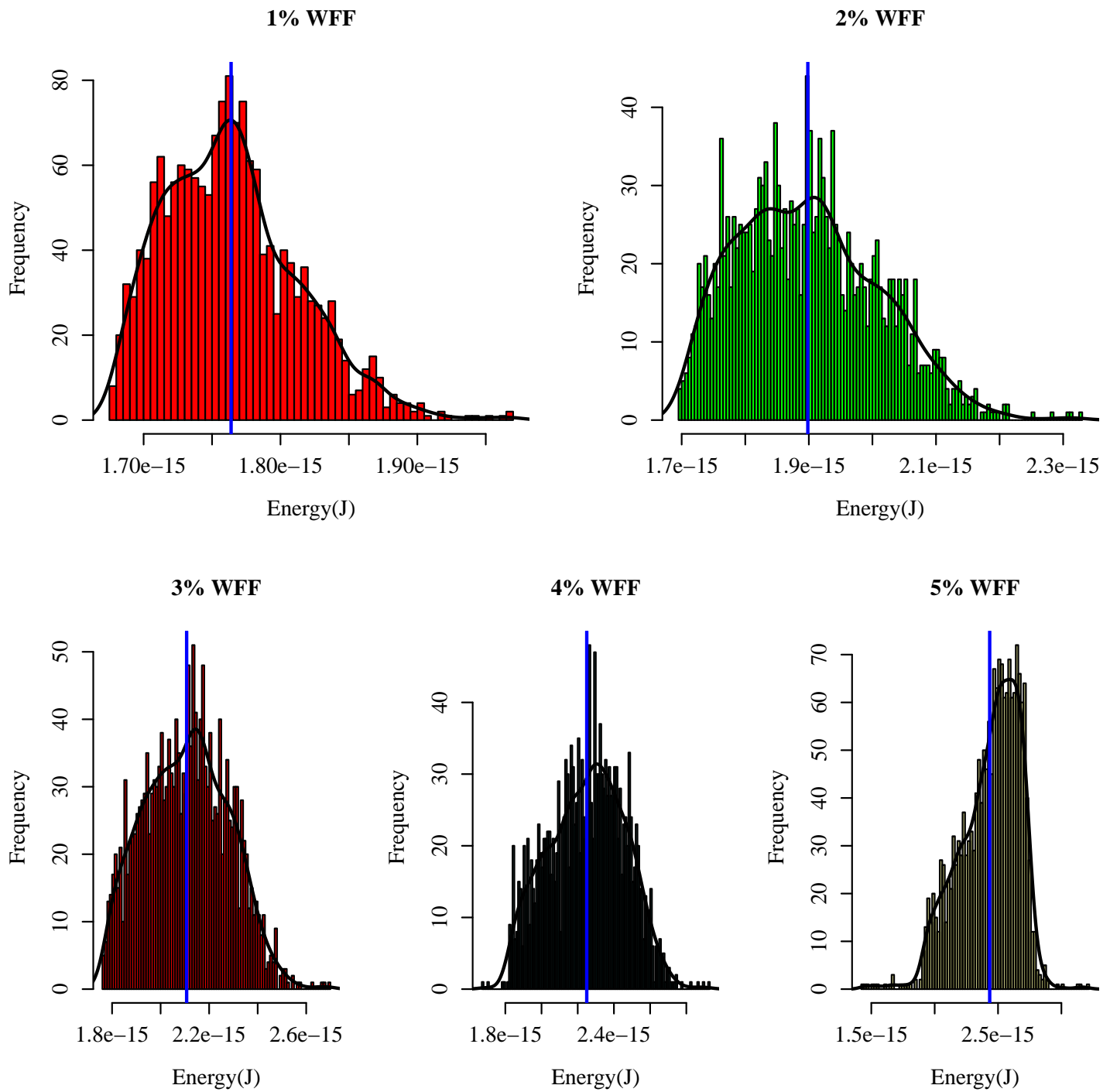
Source: From the author.

Figure D.26: TIST 3:1 energy measures distribution operating at 0.4V.



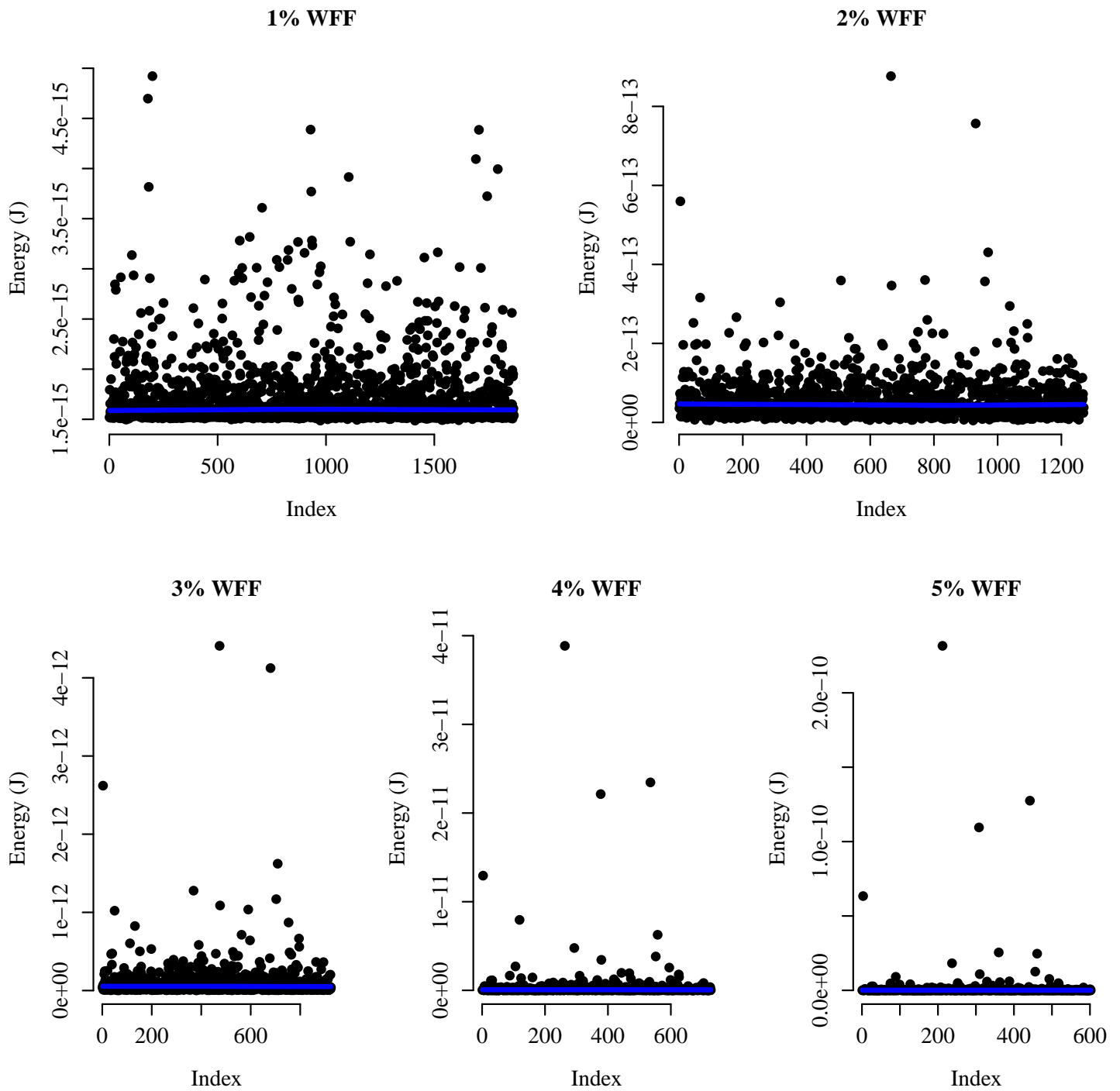
Source: From the author.

Figure D.27: TIST 3:1 energy measures distribution operating at 0.7V.



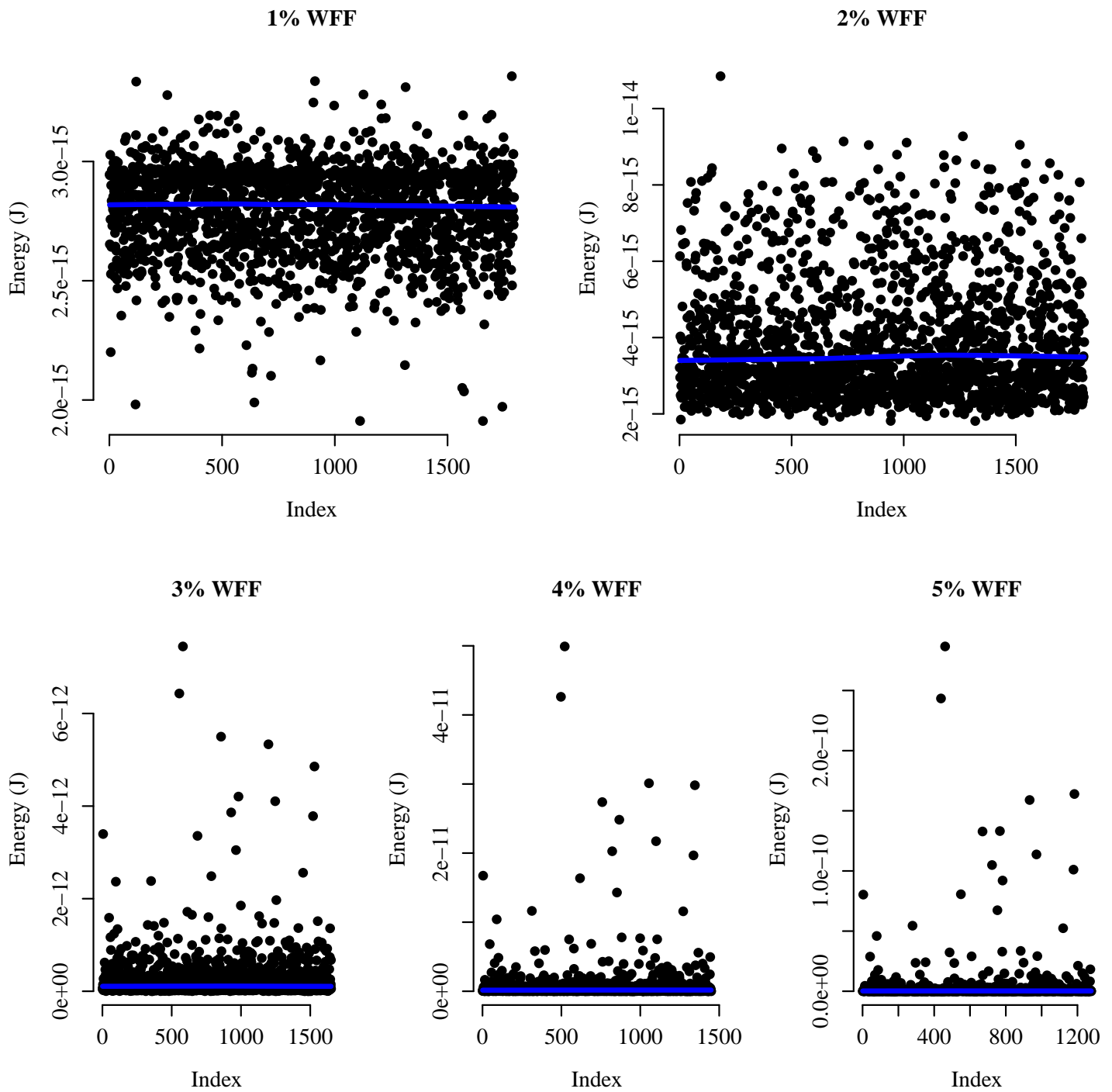
Source: From the author.

Figure D.28: TIST 3:1 energy measures dispersion operating at 0.2V.



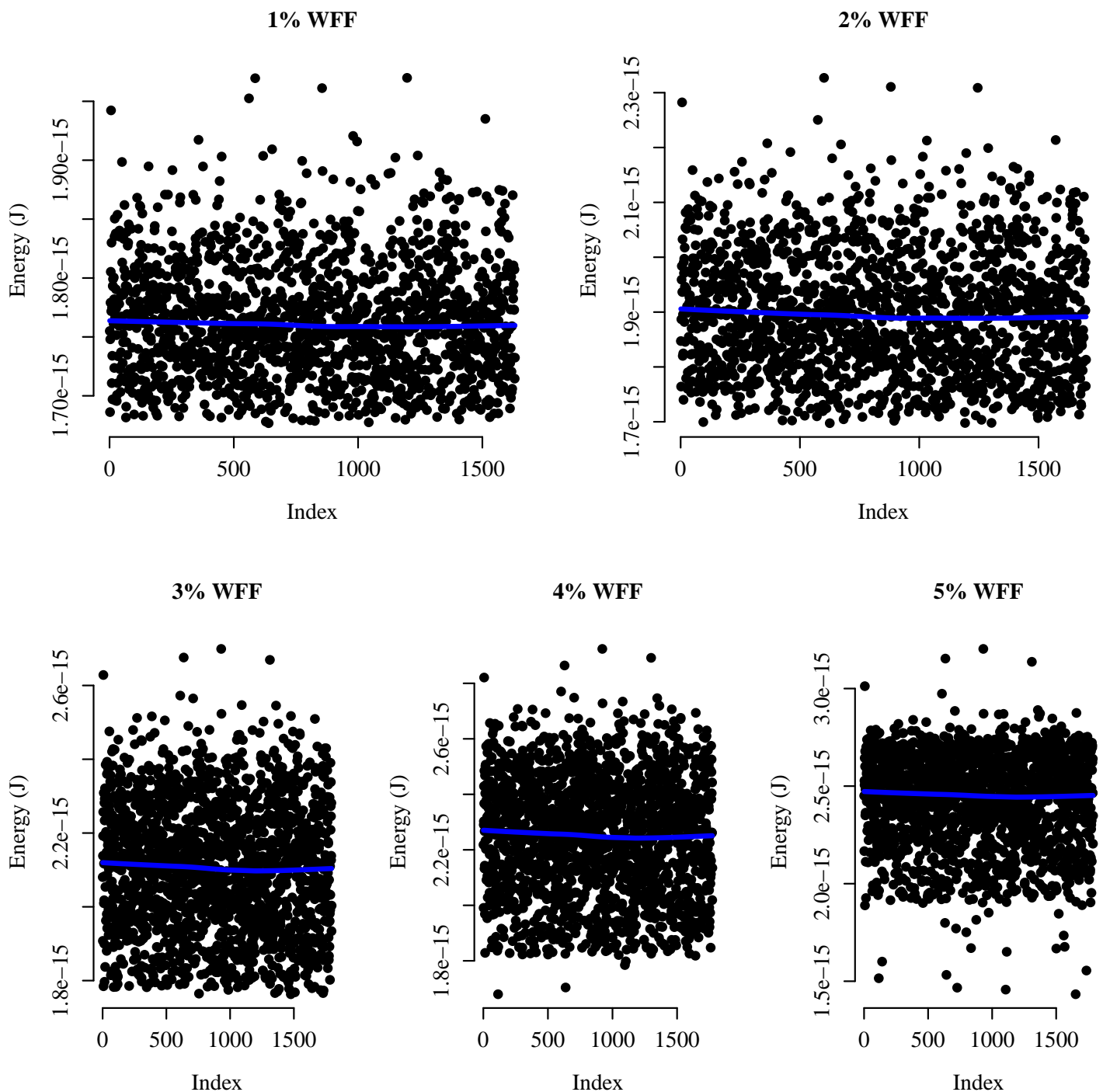
Source: From the author.

Figure D.29: TIST 3:1 energy measures dispersion operating at 0.4V.



Source: From the author.

Figure D.30: TIST 3:1 energy measures dispersion operating at 0.7V.



Source: From the author.